

Developing Tools to Evaluate Structure-Function of c-Src Kinase

by

Kristin Ko

**A dissertation submitted in partial fulfillment
of the requirements for the degree of
Doctor of Philosophy
(Chemistry)
in the University of Michigan
2016**

Doctoral Committee:

**Assistant Professor Matthew B. Soellner, Chair
Professor Carol A. Fierke
Professor Anna K. Mapp
Professor Shaomeng Wang**

© **Kristin Ko 2016**

Dedication

To my parents, Mei and Ming

Acknowledgements

First and foremost, I owe a tremendous amount of gratitude to my amazing family, my parents, Mei and Ming, and my brother Kevin. They are my entire world and, to be honest, where would I be without them? My parents gave up their lives, the comfort of their friends and family to come halfway across the world to America to start a new life in a new world. And boy have they come far. Especially my mom, who began her journey from a rural village right by the Pacific Ocean, growing up as a fisherman's daughter and having to endure unfathomably difficult childhood life. I know my mom would berate me for mentioning these things here because despite these hardships, she doesn't want anyone's pity. To this day, both of my parents are still working away, now at a small carry out restaurant they own. As a graduate student who works long hours and weekends, they still put me to shame the amount of hours they work. And despite all those hours, they manage to still find the time to taxi me around to all the soccer, softball, and tennis matches, violin lessons, and after school activities. I will never forget the sacrifices you made so that I could be where I am today. Both are the strongest people I know and the source of my inspiration and motivation. I am truly honored and blessed to be your daughter.

To Kevin, forever the little baby in the family, sorry I stole all your toys when we were younger. I wouldn't forget all the us vs the parents, times where we tag teamed and plotted on how we can play all the Dota in Starcraft and Warcraft without getting caught. You are also the hardest working, thoughtful and most diligent person I know. Despite being the older sister, you have, at times, also been like an older brother to me that's how mature and wise beyond your years you are.

It is true that it takes a village to raise a person, and to my village of people, I wouldn't be the person I'm here today if it weren't for your kindness, generosity,

and big heart. You were there to help, offer friendship and give advice when I couldn't offer anything in return, especially in the earliest stages of my life where I needed all the help I could get. As a result you have all had the most powerful and lasting impact in my life as you helped shaped the foundation of which I am standing on today. I can't thank you all enough, I will never forget. Shout out to those first villagers, Don and Louise Amlin and Ted and Gloria Guest of Dayton, Ohio. You were there right in the beginning. When my parents first came over with absolutely nothing, you taught them English and took care of us like family. You are all truly gracious and the best people I know, our guardian angels.

To Mrs. Vance (sorry it still feels weird calling you Peggy!), whom I knew since I was five, and the most patient and loving piano teacher ever. You introduced me to my first love, music and over the years, the piano lessons became more than just piano lessons, and lessons about life.

To Jan Groshoff, for telling me to relax and enjoy life more as high schooler. I wasn't a big fan of high school counselor meetings but I didn't realize how much my perception in life would change afterwards, and now I always look forwards to our meetings. You were the very first person to believe in me.

To Dr. Sandra Craig, and Prof. Irene Lee of CWRU. To Sandra, who saw me wandering around aimlessly in lab and slapped some sense into me, literally. She took me under her wing and taught me all the organic synthesis that I know, and then as an award, had to put up with my constant 24/7 pestering. Thanks for being the best sugar momma ever! And to Irene Lee, the most intimidating "British American" undergraduate research advisor that I was incredibly blessed to work with. You were the definition of tough love, always brutally honest in your comments and advice. Under all that loud, scary, façade of yours, was a big heart, you truly and genuinely cared for each and every one of your students, even me, a nobody undergrad and went out of your way to help. And yes, now everyone can know now that it is in print.

To my best high school friends, Stephanie LaCount and Jenny Albertz now both Drs.! Boy, have we come along way, since AP Chem class, throwing lemon warheads at each other and getting yelled at by Mrs. Keep, "planning" AP history class for Mr. Fuller, trying not to fall asleep (or maybe that was just me?) in AP Calc

with Mr. Ellis, amongst other things, things that hopefully will not keep getting mentioned ok?

To my best undergrad friends, the girls of Michelson, Elise Vickery, Marika Laino and Dr. Rebekah Stafford who are all married now, whom it has been an absolute blessing to be friends with and pure coincidence that we ended up living together all the way up those darn elephant stairs. To Drs. Cynthia Chu and Marta Worwag, the most dedicated, funny, and wise tennis players that I know, never forget the fun on court and off courts sessions together. To Chen-san and Torio-San, Japanese class wouldn't be the same without you, and thanks Chen-san for being awesome! And the fellowship group of Koinonia, thank you for making me feel at home, the home cooked meals and the heart to heart fellowship meetings where for the first time, I could be myself.

To the villagers of Ann Arbor. Over my time here, I have been extremely fortunate and honored to meet and to work with incredibly talented people. My friends, who I first came into the chemistry program with, Dr. Wendi Hale and Amy Speelman. Wendi, when we first met in the summer of 2010 for driving me around half asleep to show me the campus. Thank you for being so understanding and for your friendship thru thick and thin, I will miss our monthly long dinners at Applebees! To Amy, not sure what I would have done without you, I would just be constantly hungry! Thanks for being a sci fi nut like me, bonding first over Game of Thrones and watching marathons of Battlestar Galactica and then surviving together the lab of terror, and all (ALL) the movie fun times.

To the special friends I have made in the Ann Arbor tennis community, whom you are all very dear to me, Dr. Chiquita Berg, Sherry (Jerry) Walker, Dr. Marie Vantubbergen, Sheryl (Jerry) Leicher, Carly Eckert, Prof. Diane Fingar, Dr. Egor Alekseev, Ann-Marie Kim, Terri Baily, Margaret Krebsbach, Mary Beth Putnam and Aleli Alcala. Thank you for taking a flier out on me and welcoming me with open arms into your tennis family. I wouldn't forget all the Sun. and Sat. morning doubles/singles matches, Tues night Varsity, our trip to Saddlebrook, third place finish at Nationals, Red Robin for dough rings and Bailey's ice cream shake, and most importantly BEATING MONROE (twice!).

And last but not least, my lab mates in Chem 3606-3614, whom I have spent the last waking hours of my life with and whom I have learned so much from. To the past Soellner Lab members, Dr. Shana Santos, Dr. Steve Bremmer, Dr. Meghan Breen, Dr. Kris Brandvold, Christel Fox, and Mike Steffey, a huge thank you for making the lab a great collaborative environment to work in and for allowing me to pester you for help.

Special thanks to Shana, my first cubby mate, who kept me from going insane, had to put up with rantings of a newbie grad student, and the first pioneer of the coffee runs. I'm not sure what I would have done without you, especially in those first difficult year that I had. Chris Fox, who taught me everything about protein purification and had to put up with all my pestering, and for being the most thoughtful and caring person in lab.

And to the current lab members, Dr. Sameer Phadke, Mike Agius, Eric Lachacz, Frank Kwarczynski, and Taylor Johnson. This past year has been an absolute blast, I didn't think graduate school could be so much fun. Special shout out to my current cubby buddy, Mike Agius who is responsible for collaborating with for the work done in Chapter 2. I'm not sure if I would have been able to make it the last few years in grad school without such an incredible labmate and friend, who kept grad school life enjoyable and fun with various adventures to 7-11, Chipotle, Sadako, Sat. lunch Ahmos runs, Espresso ICED coffee runs, and \$1 Walgreens sodas. I will sorely miss our philosophical discussions, day dreaming of starting a company, and weightlifting workouts at the butt crack of dawn at CCRB.

And last but not least, my adviser, Matt Soellner. I appreciate how available you were to discuss anything and I have learned much from those discussions. Huge thanks for your support over the years.

Table of Contents

Dedication	ii
Acknowledgements	iii
List of Figures	x
List of Tables	xvi
List of Abbreviations	xvii
Abstract	xix
Chapter 1	1
Introduction	
1.1 Kinase Background	1
1.2 c-Src Structure	2
1.3 Conformational Selective Ligands	7
1.4 Global Conformation of c-Src	8
1.5 References	20
Chapter 2	23
Exploring Global Conformations of c-Src: Clinical and Non-Clinical Mutations	
2.1 Introduction	23
2.2 Designing an Assay to Identify Global Conformation	28
2.3 Assay Results and Discussion	32
2.4 Activity Assay Results and Discussion	39

2.5	Investigating pY419-pY530	40
2.6	Non-Clinical Mutation: W263A	44
2.7	Exploring R163W and W121R	45
2.8	Exploring Conformational Effects on Phosphorylation State	48
2.9	Conclusions	51
2.10	Experimental Section	54
2.11	References	79
Chapter 3		
Development of a chimeric c-Src kinase and HDAC inhibitor		
3.1	Abstract	81
3.2	Introduction	81
3.3	Results and Discussion	83
3.4	Conclusion	93
3.5	Experimental Section	95
3.6	References	148
Chapter 4		
Development of a dual p38 β /c-Src Inhibitor for Triple Negative Breast Cancer		
4.1	Introduction	150
4.2	Rational Design in Improving Dasatinib Efficacy in TNBC	151
4.3	Biochemical Evaluation of 4.1 using BODIPY	153
4.4	Cellular Evaluation of 4.1	153
4.5	Metabolic Stability of 4.1	155
4.6	Analogs of 4.1	156
4.7	Evaluation of 4.4 Analog	158
4.8	Conclusions	161

4.9	Experimental Section	163
4.10	References	195
Chapter 5		197
Conclusions and Future Outlook		
Appendix A		203
A.1	Introduction: Developing a Truly Selective c-Src Inhibitor	203
A.2	Probing the Validity of the Docking Model of Compound A1	205
A.3	SAR of Compound A1 and A2	207
A.4	Results and Discussion	208
A.5	Introduction: Gatekeeper c-Src Inhibitors and DFG-out Conformation	211
A.6	Results and Discussion	214
A.7:	References	217

List of Figures

- Figure 1.1: c-Src signaling pathway 2
- Figure 1.2: A. c-Src kinase domain. Highlighted in yellow is N-terminus lobe. c-terminus is shown in white. Activation loop is shown in blue and c-helix is in purple. Space filled model of ligand bound depicts the ATP-pocket/active site. PDB: 2Src. B. c-Src kinase domain overlaid to demonstrate c-helix movement. c-helix-in is marked in purple and c-helix-out is marked in green. The glutamic acid residue, color denoted purple or green depending on c-helix position, is a crucial residue necessary for catalysis. PDB: 2Src and 3G5D. 3
- Figure 1.3: A. Crystal structure of ligand stabilized conformations of c-Src. From left to right, DFG-in (Type I Inhibitor, PDB: 3G5D), DFG-out (Type II Inhibitor, PDB: 3EL8), c-helix-out (c-helix-out inhibitor, PDB: 4DGG). B. The DFG flip. Depending on the conformations of c-Src, the DFG can be flipped in or out, which specifically refers to the position of the phenylalanine shown in green. The phenylalanine moves nearly 10 Å and rotates nearly 180° between the two positions. 4
- Figure 1.4: A simplified cartoon with ATP bound depicting the most common binding pockets of Type I and Type II inhibitors. 6
- Figure 1.5: 3D wt-Src crystal structure of global conformational changes from more open to closed. Kinase domain is shown in white, SH2 domain in orange, and SH3 domain in magenta. From left to right PDB code: 1Y57 and 2Src 9
- Figure 1.6: A cartoon representation of the stabilized global conformations observed in 3D c-Src kinase, open, apo, and closed. 10
- Figure 1.7: c-Abl full length structure. On the left, is the closed/inactive form of c-Abl with the blue denoting the SH3 domain and the red is the SH2 domain. On the right is the active/open/"top hat" conformation. Only the SH2 and kinase domain were crystallized. Left, PDB: 2FO0 and Right, PDB: 1OPL. 11
- Figure 1.8: c-Abl kinase overlaid demonstrating the large dynamic movement and distance the the activation loop travels between DFG-in (blue) and DFG-out (red) conformation. Highlighted in green is the tyrosine residue that is phosphorylated. Top hat conformation of c-Abl could result in autophosphorylation at this tyrosine residue because it forces the activation loop into the DFG-in conformation

- (blue), allowing the tyrosine to be accessible. PDB: 2GQG (blue), 1IEP (red) 12
- Figure 1.9: Redrawn from Lamontanara et. al.⁴⁰ Depicts the SH2 domain conformation is important in dictating activation loop conformation for phosphorylation of Y412. SH2-Abl kinase dead (D382N) was shown to be phosphorylated at Y412, demonstrating that the SH2 top hat conformation is necessary to force the activation loop into the correct conformation for phosphorylation by the added wt-Abl kinase domain. I164E-D382N, kinase dead mutation that destabilizes the top hat conformation displays no pY412, which reinforces the notion that the top hat conformation is necessary for the correct activation loop conformation for pY419. 13
- Figure 1.10: Redrawn from Lamontanara et. al.⁴⁰ Diagram shows that DFG-in (dasatinib) and DFG-out (imatinib) inhibitors can affect the conformation of the activation loop as shown thru the amount of phosphorylation at Y412. Dasatinib, DFG-in inhibitors prime the activation loop in the correct conformation for phosphorylation at Y412 and the DFG-out imatinib does not. 14
- Figure 2.1: The only two known crystal structures of 3D Src. Kinase domain is in white, SH2 is in orange, and SH3 is in magenta. The structure on the left is bound to a Type I ligand and is in the more open conformation than the structure on the right, which is bound with ATP γ S, is in the closed inactive configuration. Left PDB: 1Y57 and Right PDB: 2Src. 25
- Figure 2.2: Cartoon diagram depicting c-Src regulatory mechanism involving c-Src's open/closed conformations resulting from different phosphorylation states. Inactive c-Src is usually found in the cytosol and is a result of phosphorylation at Y530 from Csk. This causes the clamping down of both SH3 and SH2 domains which configures c-Src in a closed conformation. Dephosphorylation of Y530 and/or phosphorylation of Y419 on the activation loop targets c-Src to the membrane resulting in a fully activated kinase, where it can interact with its protein binding partners thru scaffolding effects and/or phosphorylate its other substrates. 27
- Figure 2.3: Chart of three main regulation mechanism of c-Src, localization, phosphorylation state, and conformational state. Black arrows indicates an effect that directly contributes as a result. Hexagons shows a secondary effect and the green circle is the final aggregate effect which is usually the signal transduction pathway that c-Src is involved in gets turned on/off. The red arrows are effects that will be investigated in this chapter as we are interested in whether or not mutations effect conformational state and thereby disrupts c-Src's regulation mechanism. 28
- Figure 2.4: Diagram of thermolysin protease assay. c-Src mutations were incubated with thermolysin at various time points and then loaded and ran on an SDS-PAGE gel for analysis. An example gel is

- shown. As incubation time is increased (starting from left 0min to right), depending on the conformational state, either 3D Src band starts to decrease (open) or stays the same (closed). A more close conformation would show a slower rate of cleavage (dashed red line) as oppose to a more open conformation, which would have a faster rate of cleavage. 29
- Figure 2.5: Cut site is shown to be between G257 and L258 and confirmed by mass spec. The cut site residues are shown in yellow and the linker is highlighted in red. PDB: 1Y57 30
- Figure 2.6: Thermolysin Half-Life of clinical and non-clinical mutations. All values were normalized to w-Src and depicted on a log scale. Negative values typify more open conformations whereas positive values signal more closed. 35
- Figure 2.7: FITC-SH2 Fluorescence Polarization Assay on select c-Src mutation constructs. Kd were taken and normalized to wt-Src (apo conformation) which is set to 1. Half lives from thermolysin assay is shown above the bars for each mutation. 37
- Figure 2.8: Vmax (RFU/sec) evaluated for those mutations with catalytic activity. Values were normalized to wt-Src which was set to 0. Higher catalytic activity compared to wt-Src are positive numbers and lower activity than wt-Src are negative numbers. Half lives from thermolysin assay added for each mutation and shown in colored bar graphs. Blue: closed, Black: Apo, and Orange: open. 42
- Figure 2.9: Top Left: c-helix-in crystal structure, 1Y57, c-helix and W263 is highlighted in blue. Top Right: c-helix-out crystal structure, 2Src, c-helix and W263 is highlighted in red. Bottom left is overlay of both crystal structure (blue is 1Y57, c-helix in; red is 2Src, c-helix-out) depicting the movement of the c-helix with regard to W263 position. Bottom right is same overlaid, view is from the side, depicting W263 in a space filled model. The positioning of W263 triggers the positioning of the c-helix as well as the SH2/SH3 domains. The SH2 linker is to show where the SH2/SH3 domains (not pictured) would be orientated. In 1Y57, a more open conformation, W263 is wedged in forcing the c-helix in, resulting in SH2/SH3 domain positioned in a more linear open conformation as shown in this picture, with the SH2 linker position coming toward the reader. In 2Src, a closed conformation, W263 is swung out resulting in a c-helix-out, resulting in SH2/SH3 domain to be clamped down alongside the back of the kinase domain, as depicted with the SH2-linker position going away from the reader, in a closed conformation. 46
- Figure 2.10: From PDB 2Src. Picture on left shows full length c-Src, SH3 (magenta), SH2 (orange), and kinase domain (white). R163 residue is highlighted in blue and the surrounding residues, N400, E160, D368, and Q372 are in green. Picture on right is a close up view, with red dotted lines from R163 that show the potential salt bridge/H-bonding that upon disruption by substitution to a

- tryptophan, might explain the more open conformation that results. 47
- Figure 2.11: PDB 2Src. Top picture, depicts a close up of W121 lone H-bond partner to the backbone of G257. Bottom left is W121 in blue and G257 in green of the entire protein and bottom right depicts space filled image of W121 (blue) within the transient pocket formed by K260, A259, L258, G257, and Q256 of the SH2-linker 47
- Figure 2.12: The percent phosphorylation of Y419 on Y530F, T341R-Y530F, and D120N-Y530F. 50
- Figure 3.1: (A) Structure of highly selective c-Src inhibitor 3.1 (B) Kinome dendrogram for selectivity profiling of 3.1 at 10 μ M. c-Src is colored blue, and off-target kinases of 3.1 are colored red. Dendrogram was generated using TREEspot software tool with 10% cutoff. Green circles denote kinases included in panel that show no binding below cutoff. 82
- Figure 3.2: Synergy studies of selective c-Src inhibitor 3.1 (2 μ M), panobinostat (HDACi, 10 nM), and combination (3.1 + HDACi, 2 μ M 3.1, 10 nM panobinostat) in SK-BR-3 cell line. Red line denotes predicted additivity of 3.1+ panobinostat. The higher level of inhibition than the predicted additivity indicated synergism between 3.1 and panobinostat. Work done by Mike Steffey. 83
- Figure 3.3: Structure of PP2~Alkyne (3.2) and chimeric inhibitors 3.3 and 3.4 85
- Figure 3.4: c-Src inhibitor 3.10 and HDAC inhibitor 3.9 88
- Figure 3.5: PDB 3G5D of c-Src bound dasatinib (green). The arrows indicate the ideal groups that can be substituted with the HDAC pharmacophore without disrupting binding to c-Src. 91
- Figure 3.6: Structure of the new dual c-Src/HDAC inhibitor that utilizes the dasatinib scaffold as the c-Src pharmacophore, replacing the pyrazolo-pyrimidine core while maintaining the same phenyl triazole hydroxamic acid as the HDAC warhead. Replacement of the 4-methyl group off of the pyrimidine results in compound 3.12 using a morpholine instead of the hydroxyethyl piperazine to help decrease MW. Replacing the hydroxyethyl piperazine results in compound 3.11. 93
- Figure 4.1: From PDB 3G5D (c-Src and dasatinib) and 2HYY (c-Abl and imatinib). Picture on the left depicts an overlay of both c-Src and c-Abl crystal structures, shown in white, and both dasatinib (magenta) and imatinib (green) ligands. The picture on the right shows the ligands alone. From the ligand overlay, the methyl phenyl ring (red arrow) are almost perfectly aligned, giving the rationale that using the dasatinib scaffold and adding the phenyl methyl piperazine of imatinib (the DFG-out portion) would create a DFG-out ligand that would bind c-Src. 152
- Figure 4.2: Western Blot data in MDA-MB-231 cells of increasing concentration (0, 50, 100, 250, 500, 1000 nM) of compound 4.1. From selectivity data, p38 MAPK kinases were potently inhibited

- and thus it was of interest to see if it had any cellular activity. At 50 nM, both phosphorylated p38 MAPK (P-p38 MAPK) and phosphorylated Src (pY419) were completely absent suggesting both Src and p38 MAPK are inhibited. 155
- Figure 4.3: Compound 4.3 and 4.2. Similar to 4.1, however there is an additional chlorine on the CF₃ phenyl ring which was installed in hopes of increasing metabolic stability due to increased residency times as well as substituting the hydroxyethyl piperazine, as the major metabolite of 4.1 was oxidation of the piperazine. 156
- Figure 4.4: Major metabolite of 4.1, which is oxidation of the N off of the hydroxyethyl end of piperazine. 157
- Figure 4.5: Top picture depicts how compound 4.4 is derived from 4.1 and BIRB-796. Bottom picture: PDB 3G5D (c-Src + dasatinib) and 1KV2 (p38 + BIRB 796) with dasatinib shown in magenta and BIRB-796 in green overlaid within the kinase (left) and ligand only overlay on the right. 159
- Figure A1: PP2, PP2-alkyne, A2, and A1. 205
- Figure A2: KINOMEScan of PP2 and A1. The red circles represent the kinase inhibited and the larger the radius of the circle correlates with increasing potency. (Taken from Brandvold et. al)¹ 205
- Figure A3: c-Src is colored light green with P-loop of c-Src highlighted yellow. c-Abl is colored light blue with P-loop of c-Abl highlighted red. (Taken from Brandvold et.al)¹ 206
- Figure A4: Left is compound A1 docking model in c-Src. Right is docking model of compound A1 showing the *S* conformation. Note in the picture on the right, compound is not in optimized conformation. 207
- Figure A5: Biochemical assay and chemical structure of compounds A1-A5 in c-Src 207
- Figure A6: BRAF binding assay of compounds 1, A4, A5, and A18 (3-OMe) 208
- Figure A7: Biochemical assay of compounds A6-A13 in c-Src 210
- Figure A8: Biochemical assay of compounds 13-28 in c-Src and parent biphenyl compound 1. 211
- Figure A9: A simplified cartoon with ATP bound depicting the most common binding pockets of Type I and Type II inhibitors. 212
- Figure A10: A: Crystal structure of T341M c-Src, DFG-out (PDB: 3F3W) aligned with wt-Src DFG-in (PDB: 3G5D) demonstrating the DFG-flip, shown in yellow. The orange residues show the GK methionine and the xDFG residue, alanine. B: Same crystal structure as above instead Compound A27 (T341M) and Dasatinib (wt-Src) are shown. Compound A27 is split into three different colors signifying the binding pockets. Green = ATP pocket, red = GK pocket, blue = hydrophobic pocket. Dasatinib is shown in white and visualizes how a bulky GK can prevent access into the hydrophobic pocket and GK pocket. The yellow curved line demonstrates one design strategy to evade the GK by avoiding binding directly through the GK pocket (as shown by the phenyl

ring of Dasatinib and red portion of compound A27) which all current Type II binding follows.

213

Figure A11: Lead compounds of the 37 compounds tested are shown. Compounds marked in red are commercially available. Compounds in blue were provided by Prof. Dustin Maly, and compounds in black were synthesized. Out of the synthesized compounds A28 was the most potent against wt-Src.

215

List of Tables

Table 2.1: List of mutations. Ones on the left are somatic clinical mutations found from Catalogue of Somatic Mutations in Cancers (COSMIC) and Cancer Cell Line Encyclopedia (CCLE) and ones on the right are non-clinical mutations.	31
Table 2.2: c-Src constructs from literature used as controls to correlate thermolysin half-lives to conformational state. Cartoon picture of what past literature has depicted as open, apo, and closed. ⁴⁵	34
Table 2.3: Thermolysin assay half-life values grouped around the three control c-Src constructs, wt-Src, pY419, and pY530 (highlighted in red).	36
Table 2.4: Select mutations representing open/apo/closed conformation were used in FP assay to evaluate SH2 domain accessibility. Binding affinity is in Kd (nM). Half lives from thermolysin assay shown in second column.	38
Table 2.5: Vmax, ATP and peptide substrate K _M values for the three control c-Src constructs, pY419 (open), wt-Src (apo), and pY530 (closed)	39
Table 2.6: ATP and substrate peptide K _M and Vmax values of all active mutations	41
Table 3.1: Cellular efficacy of selective c-Src inhibitor 3.1, vorinostat, 3.1:vorinostat (1:1), and chimera 3.4. Work by Mike Steffey	84
Table 3.2: SAR of Linker	87
Table 3.3: HDAC Profiling of Chimera 4 and Vorinostat	89
Table 3.4: NCI-60 Panel Data for Chimera 3.4, Vorinostat, and Dasatinib against Select Cell Lines	90
Table 3.5: Biochemical evaluation of compound 3.12 and 3.11 against c-Src and HDAC1	93
Table 4.1: GI ₅₀ (nM) of dasatinib and 2.1 in MDA-MB-231 and HMEC cells	155
Table 4.2: Fluorescence assay, Kd values from BODIPY version of compounds dasatinib, 4.1, and 4.4	158
Table 4.3: Microsomal half-life in minutes of dasatinib, 4.1, 4.2, 4.3, and 4.4	158
Table 4.4: The nine kinases that differed in the Luceome selectivity panel between 4.2 and 4.4. Compound 4.1 is shown as well but was done in a separate Luceome panel which is why LOK was not tested.	160
Table 4.5: MDA-MB-231 GI ₅₀ values for compounds 4.1, 4.2, 4.3, and 4.4.	161

List of Abbreviations

3D Src: Three domain c-Src

ADP: Adenosine Diphosphate

ATP: Adenosine triphosphate

BCR-Abl: Break point cluster Abl Kinase

COSMIC: Catalogue of Somatic Mutations

CSK: C-terminal Src Kinase

DDI: Drug-drug interaction

EGFR: Epidermal growth factor

FAK: Focal adhesion kinase

FP Assay: Fluorescence polarization assay

GPCR: G-protein-coupled receptor

HAT: Histone acetylase

HDAC: Histone Deacetylase

HDACi: Histone Deacetylase inhibitor

IC₅₀: Half maximal inhibitory concentration

KD: Kinase Domain

K_M: The concentration of substrate required to observe the reaction rate at one half V_{max}

PDGFR: Platelet-derived growth factor receptor

PI3K: Phosphoinositide-3-kinase

PPI: Protein-protein interaction

PTK: Protein tyrosine kinase

pY419: Phosphorylated tyrosine 419

pY530: Phosphorylated tyrosine 530

RTK: Receptor tyrosine kinase

SAR: Structure-activity relationship

SH2: Src Homology Domain 2

SH3: Src Homology Domain 3

TNBC: Triple negative breast cancer

Abstract

Despite being the first proto-oncogene discovered, c-Src's role in cancer remains poorly understood. The usual implication of kinase involvement in oncogenesis is generally due to mutations leading to over-activity and thus dysregulation of those signal transduction pathways. However, c-Src is unusual in that it is frequently observed to be overexpressed and implicated in cancer, and yet cases of overactive c-Src mutations are rare. With the advancement of sequencing technology, additional somatic mutations of c-Src have been found in cancer tumors and human cancer cell lines. These clinical mutations have never been previously characterized. Whether or not these mutations are transformative, involved in cancer progression, development, or maintenance remains to be seen. Given that overactive mutants are rare, we hypothesized that mutations could dysregulate c-Src function by disrupting its native conformational state. The work in Chapter 2 is our beginning effort in characterizing these new clinical mutations of c-Src.

In order to explore whether or not mutations affect conformations, a new assay, based on the principles of limited proteolytic assay, was developed using the protease thermolysin. This new assay is superior to previously established literature methods to analyze conformations as it was necessary to develop an assay that is high throughput to enable analysis of 29 c-Src mutations. Using our proteolytic assay, we found that mutations do indeed affect the global conformations of c-Src, displaying a wide range of conformational states from closed, apo, and open. Non-clinical mutations were part of the analysis as well, due to the fact that many of these mutants were often utilized in chemical genetic studies as substitution for wt-Src. It is assumed that these mutations retain all the same features of wt-Src, but from our assay, we have found that this is not true, as native conformations of wt-Src are disrupted.

Catalytic activity was also evaluated and three mutations, W121R, V140M, and P171Q demonstrated at least a two-fold increase in catalytic activity compared to wt-Src, suggesting that these three mutations could be transformative due to their higher activity. Also, an interesting correlation was observed between catalytic activity and conformational states. In general, it appears the more open the conformation, the higher the catalytic activity and the more closed conformations have lower activity. Lastly, due to mutant-disrupted conformational states, protein-protein interactions were found to be affected.

Chapter 3 and 4 takes on more of an application approach. Since there are studies throughout literature that implicates c-Src in cancer progression, we aimed to explore methods to make targeting c-Src more efficacious. The approach in Chapter 3 takes a selective c-Src inhibitor, designed in our lab, to look for inhibiting other protein targets which would work in synergy with c-Src inhibition. We found HDAC inhibitors to work in synergy, and with that information, we explored the design process for the first dual acting HDAC/c-Src inhibitor, compound **3.1** (c-Src $K_i = 138$ nM, HDAC1 $K_i = 0.26$ nM), which also demonstrated excellent potency against SK-BR3 breast cancer cell lines (0.2 μ M) as well against 60 varying cancer cell lines in a National Cancer Institute screen (NCI-60).

The goals of Chapter 4 are along the same lines except the approach was to improve the efficacy of dasatinib in triple negative breast cancer. The resulting inhibitor was a DFG-out dasatinib/imatinib hybrid, compound **4.1** which had unprecedented activity in triple negative breast cancer cell line MDA-MB-231 ($GI_{50} = 6$ nM) and low toxicity profile (HMEC $GI_{50} = 1800$ nM) compared to FDA approved c-Src inhibitor Dasatinib (MDA-MB-231, $GI_{50} = 830$ nM). This led us to find the increased in potency over dasatinib was the result of the new inhibitor acting as a dual p38 β /c-Src inhibitor and we describe the process of further improving this new dual acting inhibitor.

Chapter 1

Introduction

1.1 Kinase Background

The life system of a cell is driven by thousands, perhaps millions of reactions that happen per second. These reactions are necessary to keep the cells properly functioning and serves as a method of cellular communication allowing the cells to turn on or off important cellular functions such as growth, differentiation, transcription, mitogenesis, and apoptosis.¹ One form of this communication is done through phosphorylation of proteins, which is one of the most crucial post-translational modification in cell signaling.^{1,2} This simple phosphorylation step is facilitated by protein kinases which serves as a molecular switch to turn on/off those signal transduction pathways. The resulting response is reliant upon the protein substrate and in some cases the specific phosphorylation site. In most instances, phosphorylation of the protein substrate leads to an increase of catalytic activity which serves as a mechanism to amplify the signal towards all downstream protein targets.^{3,4} Phosphorylation can also effect structural changes which itself can have subsidiary side effects in signal transduction pathways such as protein-protein interactions.^{5,6} There are currently 518 known protein kinases and even though they only comprise 2% of the human genome, it has been estimated that they phosphorylate at least half of the proteins expressed.⁷

Due to its importance as a key regulator in the signal transduction pathway, kinases are tightly regulated. Though when dysregulation occurs, either due to overexpression or mutations, aberrant activity results, and can lead to a myriad of diseases including cancer.⁸⁻¹⁰ As such, it is the number two target for drug development behind GPCRs.^{11,12}

Our laboratory is interested in elucidating the structure and function of the non-receptor protein kinase c-Src, specifically its effect in oncogenesis. Discovered in 1978, c-Src, was the first identified protein tyrosine kinase (PTK) which was later implicated as a proto-oncogene. c-Src is believed to associate with a number of receptor tyrosine kinases (RTK) such as EGFR and PDGF, which serves in part as their regulator and also as a co-transducer of their originating signals.¹³ This activation of c-Src results in the phosphorylation of downstream targets such as focal adhesion kinase (FAK), Ras, Stat3, and phosphoinositide 3-kinase (PI3K) which play an integral role in cell

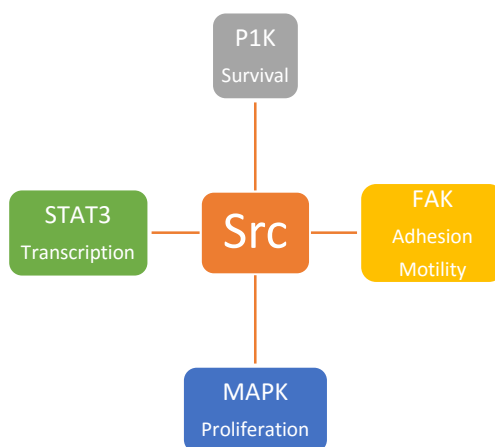


Figure 1.1: c-Src signaling pathway

proliferation, division, and survival, as well as cell motility and adhesion as shown in Figure 1.1.^{14,15} As such, the dysregulation of c-Src has been implicated in cancers including breast, colon, pancreatic, and lung cancer and consequently, multiple studies conducted have validated c-Src as a target for the treatment of such cancers.¹⁵

However, despite the wealth of research involved in c-Src, it is still poorly misunderstood, especially its role in oncogenesis. Therefore, the focus of my research that will be described here is involved in developing chemical tools that can be used to study c-Src kinase.

1.2 c-Src Structure

The challenge of studying c-Src kinase lies in its structural protein fold, which is conserved and shared across the kinome.^{11,16} All protein kinases have a catalytic domain which can be categorized into two lobes. The N-terminus lobe consists of β -strands connected by flexible linkers and a C-terminus lobe composed of mainly α -helices as shown in Figure 1.2. Both lobes are connected by a hinge linker which also marks the location of the active site/ATP binding pocket.

Two important structural motifs that will be mentioned throughout are the activation loop and the c-helix (Figure 1.2). Both elements have the most dynamic movement on the kinase structure as they are involved in catalysis as well as stabilization of conformational states which will be discussed in more detail later. The activation loop is a flexible polypeptide and resides in between the ATP pocket and solvent

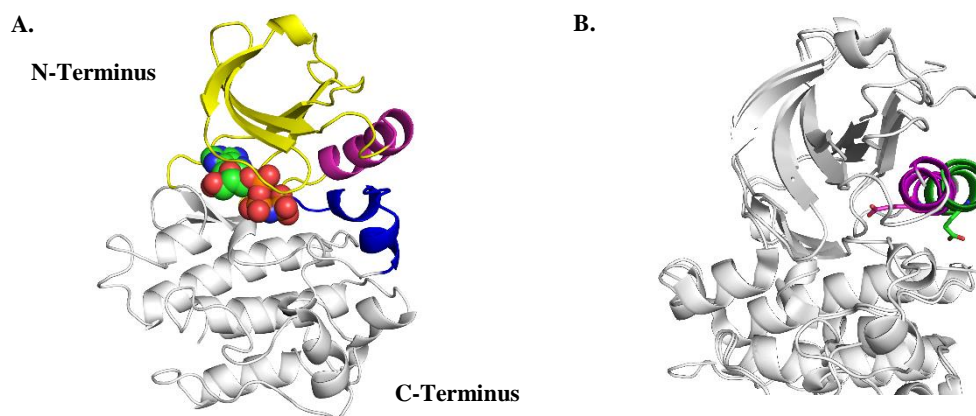


Figure 1.2: A. c-Src kinase domain. Highlighted in yellow is N-terminus lobe. C-terminus is shown in white. Activation loop is shown in blue and c-helix is in purple. Space filled model of ligand bound depicts the ATP-pocket/active site. PDB: 2Src. B. c-Src kinase domain overlaid to demonstrate c-helix movement. C-helix-in is marked in purple and c-helix-out is marked in green. The glutamic acid residue, color denoted purple or green depending on c-helix position, is a crucial residue necessary for catalysis. PDB: 2Src and 3G5D.

exposed substrate pocket. Threonine, serine, or tyrosine residues are often found on the activation loop as they can be subject to phosphorylation. It also contains a highly conserved Asp-Phe-Gly (DFG) amino acid residues that participates in catalysis as well being an identifying marker for two conformational states that bear its name. In general, phosphorylation of the activation loop leads to greater catalytic kinase activity.¹⁷ The c-helix motif (highlighted in purple, Figure 1.2) is located in the N-

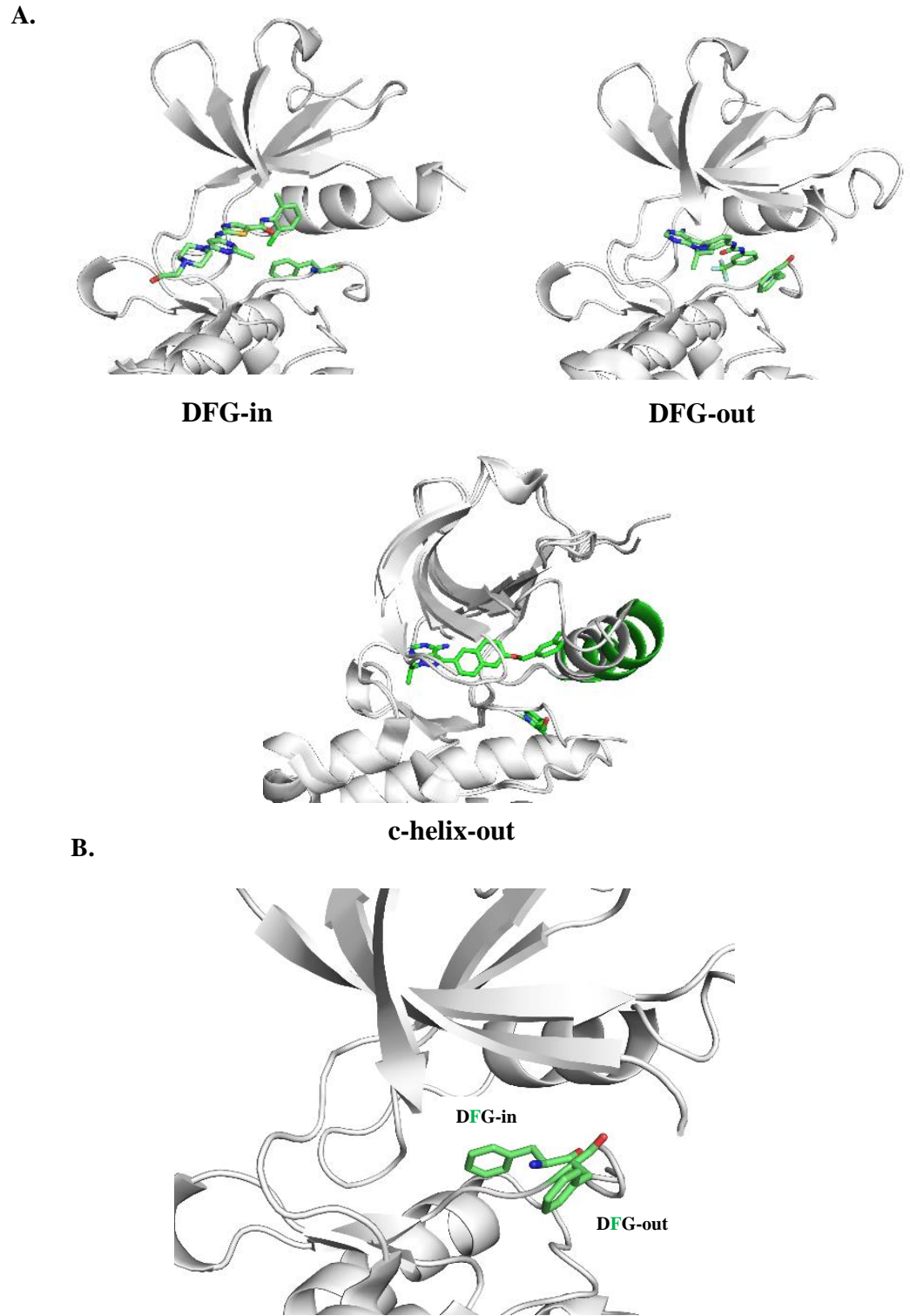


Figure 1.3: **A.** Crystal structure of ligand stabilized conformations of c-Src. From left to right, DFG-in (Type I Inhibitor, PDB: 3G5D), DFG-out (Type II Inhibitor, PDB: 3EL8), c-helix-out (c-helix-out inhibitor, PDB: 4DGG). **B.** The DFG flip. Depending on the conformations of c-Src, the DFG can be flipped in or out, which specifically refers to the position of the phenylalanine shown in green. The phenylalanine moves nearly 10 Å and rotates nearly 180° between the two positions.

Terminus lobe and is situated behind the ATP binding pocket. It contains a critical glutamic acid residue which is necessary for kinase activity. Depending on the conformational state of the kinase, the c-helix can either be swung inwards towards the active site (Figure 1.2B), which positions the glutamic acid for catalysis, or outward, resulting in an inactive kinase as the glutamic acid is flipped out. The dynamism of the c-helix and activation loop has been a studied topic as it appears that their concerted movement is responsible for either activating or deactivating kinase activity.¹⁸⁻²¹ How this movement occurs is still unknown but it has been suggested that an allosteric network is involved. Whether or not the activation loop movement is the cause of c-helical movement or vice versa is still a contentiously debated topic.²²

Because kinases and c-Src in general are a loosely held protein structure with various moving parts, it is flexible. This inherent flexibility suggest the existence of many transient conformational states.¹⁷ However, three main conformations of c-Src has been identified due in part to ligand stabilization that have been captured by crystallography (Figure 1.3A). Two of these structural conformations revolve around the DFG residues, and so are aptly termed DFG-in and DFG-out. The DFG refers to the aspartic acid, phenylalanine, and glycine residues on the activation loop. DFG-out/in (Figure 1.3B) refers to the position of the phenylalanine, which moves almost 10 Å and rotates nearly 180° to reside either in the hydrophobic pocket (an active DFG-in) or a solvent exposed region adjacent to the ATP pocket in a flipped out (an inactive DFG-out) conformation.²³ This structural feature has been widely studied in a variety of kinases and has only recently become a popular topic to pursue due to the accidental discovery of the DFG-out conformation discovered between imatinib (Gleevec) binding to c-Abl kinase.²⁴

These conformations are thought to be compound dependent however, it is unknown if the DFG-out is stable enough to exist in sufficient numbers without ligand bound; as to how or where the compounds bind can stabilize or force the kinase into either the DFG-in (Type I binding) or DFG-out conformation (Type II binding). Less than 10% of kinases have been found to adopt the DFG-out

conformation.¹⁴ Whether this is due to the lack of an appropriate ligand that can favorably force the DFG-out remains to be seen, however, this does suggest that Type II ligands could be exploited as a means to increase ligand selectivity as evidenced by imatinib (Type II), which displays impressive selectivity against the kinome. The reduction of kinase off-targets can help decrease the toxicity of a drug as well as aiding the design of selective chemical probes, which are crucial to interrogate individual kinase functions.

On a side note, recent discoveries in our lab could dispel this notion that Type II inhibitors are more selective than Type I inhibitors. This demonstrates that more kinases can assume the DFG-out conformation than previously reported. The key to proving those statements are correlated in the Type II inhibitor design. A great number of kinases have a large bulky gatekeeper, which is an amino acid

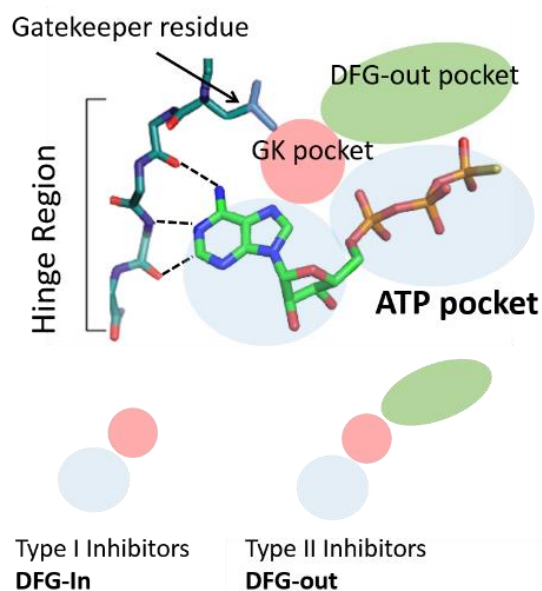


Figure 1.4: A simplified cartoon with ATP bound depicting the most common binding pockets of Type I and Type II inhibitors.

residue that divides the active site into two sub pockets, the front adenine pocket and the back DFG pocket (Figure 1.4). Type I inhibitors generally only bind within the adenine pocket whereas Type II inhibitors spans both sub pockets. Type II ligands requires access to the back DFG pocket as the additional moiety that resides there is a characteristic identifier of a Type II inhibitor. Therefore, the size of the gatekeeper

residue can sterically block Type II inhibitors from binding. As a result, if the Type II inhibitors aren't designed to avoid bulky gatekeeper residues (as most Type II inhibitors are not), then it might appear that the kinases it does not bind cannot assume DFG-out. In reality, the poor inhibition is a direct consequence of a large gatekeeper. Our lab has synthesized a Type II inhibitor designed to evade large bulky gatekeepers and its selectivity has been profiled against 518 kinases (Data not shown). Unsurprisingly, this type II inhibitor is quite unselective and perhaps is the most promiscuous inhibitor to date.

The third structural conformation is termed c-helix-out. Stabilized by "c-helix-out ligands", the defining structural trait is the c-helix moiety rotated outward causing the catalytically important glutamic acid to flip out of the active site (Figure 1.2B). The DFG moiety remains flipped in (DFG-in). The c-helix-out conformation, unlike DFG-out, has been observed natively without ligand stabilization.²⁵ natural occurrence is believed to serve as an auto-inhibitory mechanism because this conformational state results in an inactive kinase. The c-helix-out state has also been observed in many other kinases.²⁶⁻³⁰

1.3 Conformational Selective Ligands

From an inhibition standpoint, questions have been raised concerning the importance of developing different categories of ligands. Are there any advantages conferred because of the ligand type and does ligand type really matter? As a therapeutic agent, it would appear that this question is moot. For all intents and purposes, the three ligand types (Type I, Type II, c-helix-out) all block access to the ATP-binding pocket and stops all catalytic activity. However, recent developments do suggest ligand types are important and therefore, is a necessary component to consider before its use. As mentioned earlier and discussed, ligand types can confer different benefits such as selectivity. However, one crucial detail that is often overlooked is the particular conformation that the ligands induce. And those different conformational structures have been seen to influence the function/localization of the kinase, in what is being defined as the modulation of non-catalytic activity.¹⁸

This non-catalytic effect has been recently observed in a few kinases, but it demonstrates that different conformations effect how the kinase participates in protein-protein interactions (PPIs).³¹ Consequently, different ligand types have ancillary side effects besides turning off kinase activity and are not due to selectivity differences. This modulation of non-catalytic activity has been observed in the kinase IRE1 α and its RNase domain.³¹ The RNase domain is only active upon oligomerization of IRE1 α . Type I ligands that inhibit the kinase domain of IRE1 α was shown to not effect oligomerization and therefore, the activity of RNase remains unchanged. However, Type II inhibitors disrupted IRE1 α 's ability to oligomerize, resulting in an inactive RNase domain. Thus, the ability of these ligand types to modulate the non-catalytic activity of kinases through conformationally stabilized states suggest the relevance of developing different categories of inhibitors. Further investigation into how each conformational selective inhibitor modulates non-catalytic activity of other kinase is warranted. Chapter 2 investigates how these conformational structures might influence the non-catalytic activity of c-Src and could lead to a possible explanation of a c-Src role in oncogenesis.

1.4 Global Conformation of c-Src

One important structural feature that wasn't mentioned earlier about c-Src is that in addition to its catalytic kinase domain, it has four additional domains, SH2, SH3, and SH4. Most structural studies of c-Src have been focused on the kinase domain, as it expresses well and is easier to handle than full length c-Src, which is only expressed in its three domain (3D, SH2/SH3/kinase domain) version.³² However, recent literature have begun to utilize 3D c-Src in more studies as it is a closer mimic to its natural form.

The SH2 and SH3 domains appear to act as a regulatory element of c-Src activity.^{20,21,25} As such, these additional domains participate in various conformational structures, in what is aptly termed global conformations. Conformational changes in the kinase domain are transmitted to the SH2 and SH3 domains causing a rearrangement in their positions and thus, forces a transformation in the global conformation.^{1,20,25} Two previous crystal structures (shown in Figure

1.5) captures these global conformations.²⁵ The first exhibits the SH2 and SH3 domains in a more "open" conformation wherein both domains are unorganized and laid out in a line. The second presents a more organized "closed" conformation, where the SH2 and SH3 domains are clamped down together along the side of the kinase domain. *In cellulo*, the C-terminus tail of c-Src can be phosphorylated (at residue Y530) by a C-terminus Src kinase (Csk). The SH2 domain has a small hydrophobic pocket wherein the phosphorylated tyrosine residue of the tail can bind tightly and initiates the closed conformation of c-Src. This acts as a regulatory

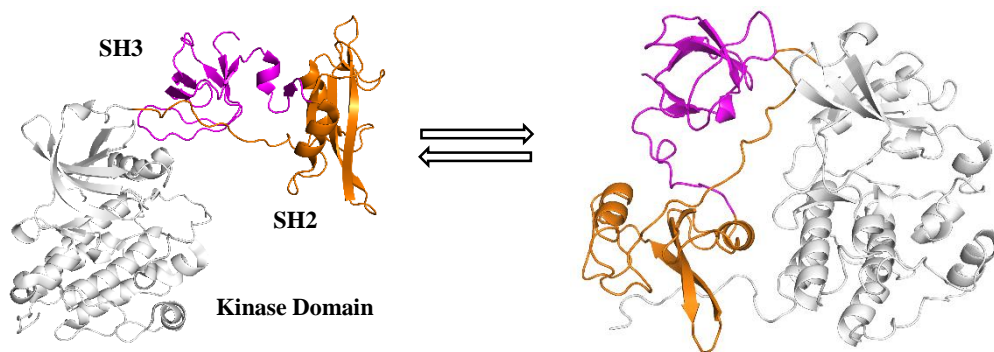


Figure 1.5: 3D wt-Src crystal structure of global conformational changes from more open to closed. Kinase domain is shown in white, SH2 domain in orange, and SH3 domain in magenta. From left to right PDB code: 1Y57 and 2Src

mechanism of c-Src activity as the closed version of c-Src has drastically decreased catalytic activity compared to the open version.^{13,25,33-35}

c-Src is known to have PPIs, specifically ones that interact with its SH2 and SH3 domains. Therefore, these open and closed global conformations can affect PPIs and thus, modulate its non-catalytic activity.³⁶⁻³⁸ One example is focal adhesion kinase (FAK). FAK is a known substrate of c-Src and binds to the SH2 and SH3 domains. Therefore, an open conformation of c-Src would not affect FAK binding whereas the closed conformation could abolish its interaction. As such, both the SH2 and SH3 domain act as method of regulation for not only c-Src kinase activity but its non-catalytic activity through structural conformational states.

Consequently, different types of ligands were found to affect global conformations. A pulldown assay was utilized to assess these distinct global conformational changes. A SH2 peptide was linked to a bead and incubated with 3D Src and either a Type I, Type II, or c-helix-out inhibitor. The accessibility of the SH2 domain which is dependent upon whether c-Src is open (SH2 accessible) or closed (SH2 inaccessible) dictated the amount of protein that was pulled down which can then be directly correlated to differences in the global conformation. A type II ligand appears to force c-Src into an open conformation, type I, an apo conformation,

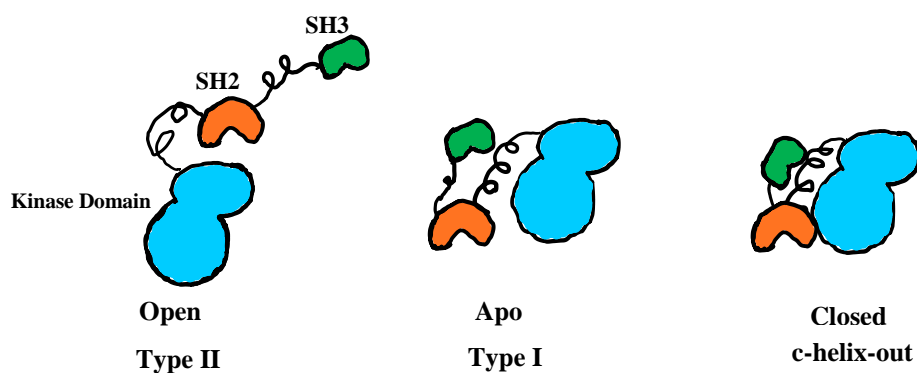


Figure 1.6: A cartoon representation of the stabilized global conformations observed in 3D c-Src kinase, open, apo, and closed.

and c-helix-out into a closed conformation (Figure 1.6). The results from this study suggest that through these stabilized structural changes, conformational selective inhibitors can modulate the non-catalytic activity of c-Src. The remaining questions then becomes does global conformations of c-Src influence non-catalytic activity and if so how. Answers to these queries could lead to a possible explanation to the role of c-Src and further our understanding of its participation in cancer progression.

In regards to the proposed query, c-Abl kinase might provide some insight into how global conformational changes could affect non-catalytic activity. Like c-Src, c-Abl is a protein tyrosine kinase that consist of a SH2 and SH3 domain that also act as a regulatory mechanism for its catalytic activity. However, more is known

about c-Abl's role in driving oncogenesis as well as examples of its structural conformational affecting this change.

Its auto inhibited state resembles the closed conformation of c-Src (Figure 1.7). It is the loss of this closed conformational state, a direct consequence of fusing with the breakpoint cluster region (Bcr) protein to form Bcr-Abl that drives chronic myeloid leukemia. c-Abl's "open conformation" though takes on a different shape than c- Src's version and is a more organized structure. NMR has shown that c-Abl

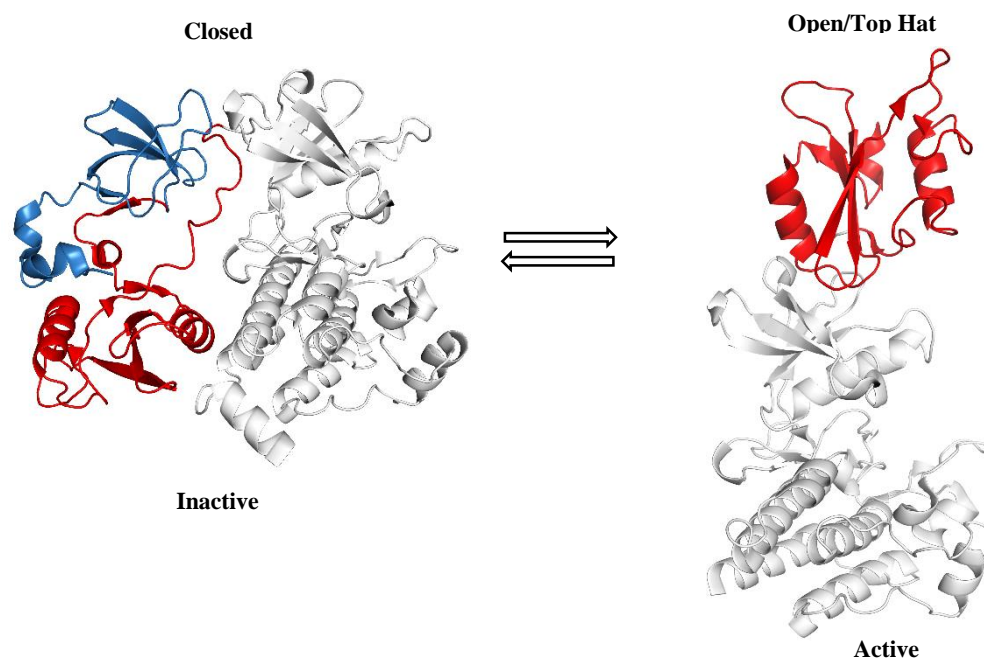


Figure 1.7: c-Abl full length structure. On the left, is the closed/inactive form of c-Abl with the blue denoting the SH3 domain and the red is the SH2 domain. On the right is the active/open/"top hat" conformation. Only the SH2 and kinase domain were crystallized. Left, PDB: 2FO0 and Right, PDB: 1OPL.

Adopts a "top hat" conformation, where the SH2 domain engages the kinase domain by sitting "on top", and this conformation is found to be responsible for activating c-Abl activity (Figure 1.7).³⁹ As such, this SH2-kinase domain engagement is necessary to sustain in vitro and cellular activities and can be directly related to causing leukemogenesis. Specifically, it has been demonstrated that disrupting SH2 from docking to the kinase domain inhibits Bcr-Abl kinase activity and transformation, leading to the loss of leukemogenesis. A previous literature study

further examined the global conformation of c-Abl, specifically this SH2-kinase domain "top hat" conformation.⁴⁰ First, they found that the SH2-kinase domain interaction was crucial for c-Abl autophosphorylation. Similar to c-Src, c-Abl also has a tyrosine residue that can be phosphorylated/autophosphorylated on its activation loop, Figure 1.8. This leads to two possible conclusions, the top hat conformation, being "open" affords better binding for c-Abl to bind itself or the top hat conformation forces the activation loop to be accessible for autophosphorylation.

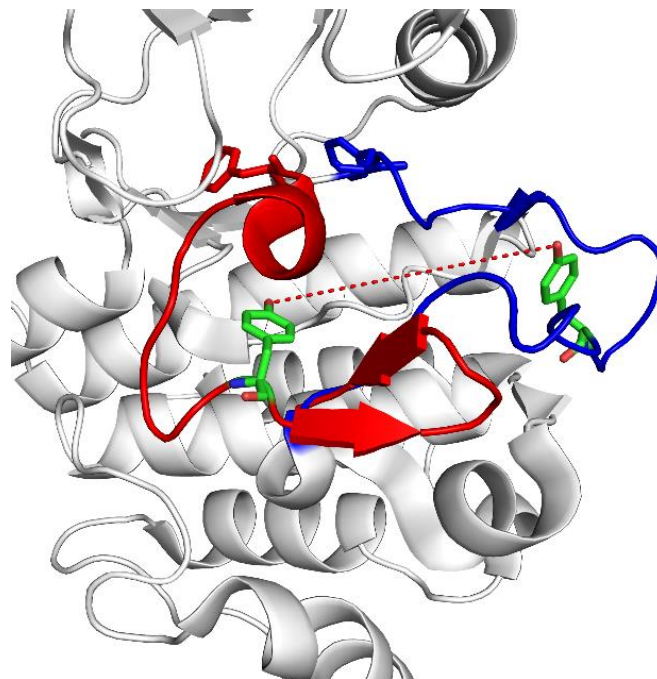


Figure 1.8: c-Abl kinase overlaid demonstrating the large dynamic movement and distance the the activation loop travels between DFG-in (blue) and DFG-out (red) conformation. Highlighted in green is the tyrosine residue that is phosphorylated. Top hat conformation of c-Abl could result in autophosphorylation at this tyrosine residue because it forces the activation loop into the DFG-in conformation (blue), allowing the tyrosine to be accessible. PDB: 2GQG (blue), 1IEP (red)

In a series of mutations found to stabilize and destabilize the top hat conformation, they were able to depict that it was indeed the activation loop accessibility being affected. In a catalytically dead SH2-kinase domain c-Abl where the top hat conformation can be stabilized, the activation loop was able to be phosphorylated by kinase domain (KD) c-Abl whereas in a top hat destabilized conformation, the activation loop was not phosphorylated (Figure 1.9).

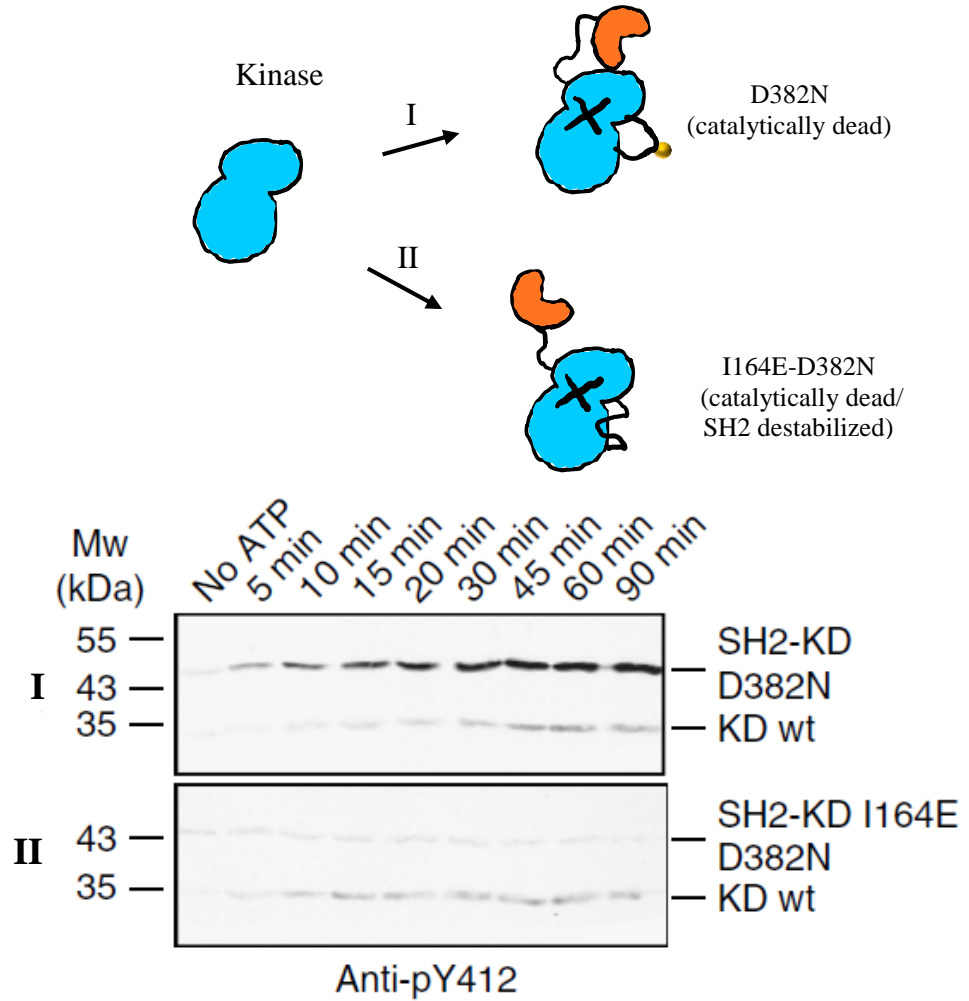


Figure 1.9: Redrawn from Lamontanara et. al.⁴⁰ Depicts the SH2 domain conformation is important in dictating activation loop conformation for phosphorylation of Y412. SH2-Abl kinase dead (D382N) was shown to be phosphorylated at Y412, demonstrating that the SH2 top hat conformation is necessary to force the activation loop into the correct conformation for phosphorylation by the added wt-Abl kinase domain. I164E-D382N, kinase dead mutation that destabilizes the top hat conformation displays no pY412, which reinforces the notion that the top hat conformation is necessary for the correct activation loop conformation for pY419.

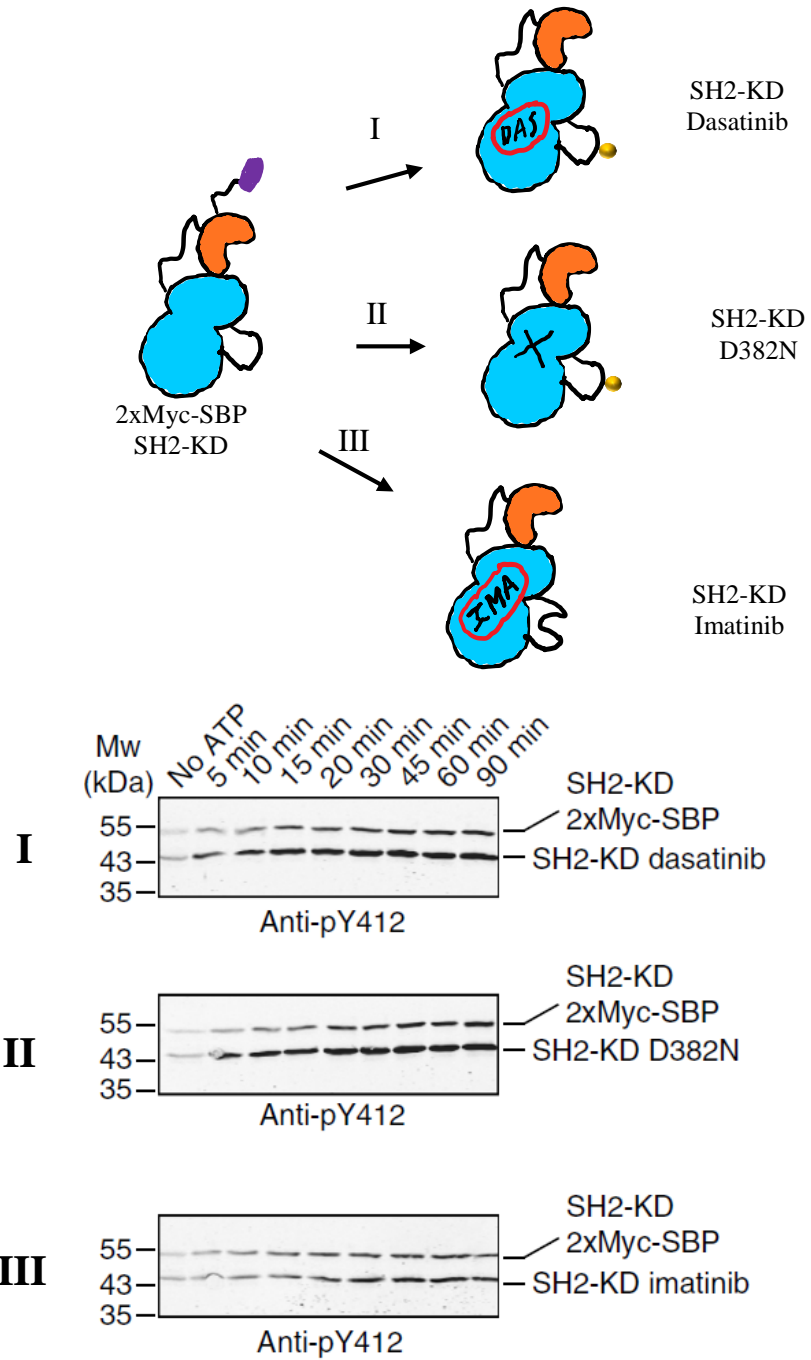


Figure 1.10: Redrawn from Lamontanara et. al.⁴⁰ Diagram shows that DFG-in (dasatinib) and DFG-out (imatinib) inhibitors can affect the conformation of the activation loop as shown thru the amount of phosphorylation at Y412. Dasatinib, DFG-in inhibitors prime the activation loop in the correct conformation for phosphorylation at Y412 and the DFG-out imatinib does not.

Interestingly, different types of ligands were found to perturb the phosphorylation state, though this result is not entirely without precedence. Crystal structures of c-Abl with the activation loop resolved shows its dynamic movement between two configurations (Figure 1.8). Each stabilized by a different ligand type, it demonstrates how a Type I or Type II ligand can influence the activation loop conformation and thus possibly affecting its phosphorylation state. Lamontanara et al was able to prove this in a biochemical setting (Figure 1.10).⁴⁰

On the KD of c-Abl, Type I inhibitor dasatinib was found to increase phosphorylation of the activation loop, whereas apo and Type II inhibitor imatinib was not phosphorylated. With a SH2-KD c-Abl construct, which alone was able to rescue phosphorylation to the apo c-Abl version, the Type I inhibitor dasatinib was still phosphorylated whereas the Type II imatinib was not.

The resulting findings suggest that the top hat conformation is not only important for catalytic activity but for the phosphorylation state of c-Abl, which further serves to increase kinase activity. Conformational selective ligands appears to have the ability to override the top hat accessible activation loop and thus can modulate the non-catalytic activity of c-Abl in this manner. Therefore, these examples here for c-Abl conformations provide an explanation of how it impacts phosphorylation state and thus how structure can affect its function. Given c-Abl's structural similarity to c-Src, it offers an insight into how c-Src's structural state can influence its own function. Chapter 2 describes these global conformational changes that occurs in c-Src, particularly those stabilized by clinical mutations. Perhaps these studies can lend some clarity into a possible role of c-Src in oncogenesis.

Whereas Chapter 2 deals with understanding c-Src's role in cancer progression, Chapter 3 and 4 is more application based and focuses on utilizing past knowledge of c-Src in combating cancer. The premise of these chapters revolves around purposely exploiting the use of synergy in targeting cancer cells. Specifically, cancer cells that possess an overexpression of c-Src. Moreover, each of these chapters detail two separate approaches. Chapter 3 is a designed method to investigate the possibility of synergy with c-Src amongst other protein targets. Using

the resulting information, an inhibitor was chimerically designed to hit both targets. Chapter 4 details a more serendipitous approach to synergy, wherein c-Src was the original target of inhibition, but the surprisingly pronounced potency could not be explained by c-Src inhibition alone. Thus, another possible synergistic target was found upon closer examination of the inhibitor's off target.

Although its role in oncogenesis hasn't been fully elucidated, it has long been thought that the inhibition of c-Src alone isn't sufficient enough to halt and/or reverse the growth of cancer in patients.¹⁴ Using compound **3.1**, a selective c-Src inhibitor developed in our lab, it was found that the selective inhibition of c-Src alone is not potent enough in killing cancer cells.⁴¹ Therefore, while the inhibition of c-Src itself may aid in disrupting the ability of cancers to progress and thereby, help prevent metastasis, it is more likely that its full therapeutic potential will be realized in combination with the inhibition of another anti-cancer target.²³ We decided to explore combination therapy to determine if it could be a successful method in taking advantage of the effects that inhibition of c-Src could provide while being able to effectively kill cancer cells *in cellulo*.

One particular secondary target of interest are histone deacetylases (HDACs). HDACs are a current popular target for combination therapy, as the first HDAC inhibitor, Vorinostat (SAHA), was recently FDA approved in 2006. Targeting HDACs alone have proven to be a successful anti-cancer target, as the onset of aberrant activity has been associated with cancer.^{42,43} Evaluation of HDAC inhibitors alone has shown promising induction of growth arrest, differentiation, and apoptosis *in vivo* and *in vitro*, however when paired with other anti-cancer drugs, the results demonstrate an increase in efficacy and potency.⁴⁴ Current studies show that HDAC inhibitors have promising synergistic effects with other anti-cancer agents on the market and thus fueling interest in the exploration of its use in combination therapies for increased efficacy against a variety of cancers. Notably, it has been effective when utilized in combination therapy towards cancers that have developed drug resistance, such as in the tyrosine kinase inhibitor imatinib (Gleevec) resistant chronic myeloid leukemia.⁴⁵ Finding an ideal synergism with c-Src *in cellulo* has been the drive for our work as there are previous literature studies

suggesting that HDAC inhibitors directly repress the SRC gene transcription and thereby down regulating c-Src.⁴⁶

The deacetylation and acetylation of the lysine side chain of proteins are mediated by histone acetyltransferases (HATs) and histone deacetylases (HDACs) respectively. These enzymes are involved in the post-translational modification of mainly histones, their known primary target, as well as other non-histone proteins such as the oncosuppressor p53.^{42,43} A balance between substrate acetylation and deacetylation is thought to be an on and off switch that is in part responsible for the regulation of transcription and other nuclear events as well as managing several other cytoplasmic proteins.⁴⁷ As such, the onset of aberrant activity or imbalance between HDAC and HAT has been associated with cancer.^{42,43,48} Most notably, the functional inactivation of HATs or overexpression of HDACs are found to mediate tumor cell proliferation.^{42,49} Initial evaluation of histone deacetylase inhibitors (HDACi) has shown promising induction of growth arrest, differentiation, or apoptosis *in vivo* and *in vitro* without affecting healthy cells, making it an attractive target in cancer.⁵⁰⁻⁵² Because of these successful results against tumor cell proliferation, HDACi are currently under study in combination with other cancer drugs to evaluate any positive synergistic effects.

Despite some success of using a combination drug therapy, there are disadvantages with this approach such as patient compliance, cost, increased side effects, and drug-drug interactions (DDI).⁵³ A new strategy to circumvent these issues is the design of dual inhibitor drugs. Such inhibitors are designed to possess two pharmacophore for two drug targets.⁵⁴ Not only is the dual inhibitor inherently more efficacious (targeting two different cancer pathways), but also lowers the likelihood of resistance, has better pharmacokinetics, no DDI, and less side effects. The successful synergism shown in combining a PTK inhibitor, imatinib, and Vorinostat, holds promise in the design of a dual ligand for both HDAC and PTK that shows similar if not better response.⁴⁵ Recently, there has been a successful attempt of a dual HER2/EGFR and HDAC inhibitor which is at present in clinical trials.⁵⁵ Therefore, in an attempt to take advantage of both combination drug therapy

and the budding success of a dual ligand, Chapter 3 entails a chimeric design of a c-Src/HDAC inhibitor.

Metastasis is not a term a patient wants to hear in regards to their cancer. It is an extremely aggressive stage of cancer with nearly a 90% fatality rate.⁵⁶ One of the most commonly known cancers associated with metastasis is breast cancer mainly due to its consistent repeat as the second leading cause of death of women in the United States.⁵⁷⁻⁶⁰ The three most prevalent types of breast cancers are ER+/PR+, HER2+, and ER+/PR+/HER2+. ER+ stands for estrogen receptor, PR+ as progesterone receptor, and HER2+ refers to EGFR kinase. In these types of cancers, those particular hormone receptors are overexpressed and as such, are the driving force for those breast cancers. Hence the specific targeting of these overabundant species have proven to be an effective treatment. However, a fourth category of breast cancer, triple negative breast cancer (TNBC), aptly named because of the lack of ER/PR/HER2 hormone receptor expression, has no known driving force and thus, no known target. This is particularly disconcerting as TNBCs are notoriously lethal due to their high risk of metastasis and proclivity to rapidly reoccur.⁶¹⁻⁶⁵ Unfortunately, 10-15% of breast cancers fall into this subcategory and the lack of treatment target for these patients often results in a poor prognosis. There are no FDA-approved targeted therapies.⁶⁶ Treatment is entirely dependent upon cytotoxic agents, but even such methods are not effective as non-metastatic TNBC reoccurs in about 40% of the patients, a much higher rate than in HER2+ breast cancer, which is less than 25% reoccurrence. There is evident need for a specific therapeutic against TNBCs. Chapter 4 addresses this issue and proposes c-Src as a target of choice.

A previous *in vitro* study involving gene expression profiling had identified dasatinib, a c-Src tyrosine kinase inhibitor, to be sensitized to TNBC tumors and was demonstrated to reduce cell proliferation. As such, the results from the study validated c-Src as a viable target for TNBC. As mentioned (*vide supra*), c-Src is a ubiquitously expressed membrane-associated non-receptor kinase. c-Src participates in signaling pathways for adhesion, migration, and invasion, which are all characteristic functions hacked by TNBC. Thus, c-Src, with high expression levels

found in TNBCs, has been implicated in a role in cancer progression of TNBC cancer cell lines, making it an attractive therapeutic target.⁶⁷⁻⁷⁰

Unfortunately, targeting of c-Src using existing FDA approved inhibitors for c-Src have not translated successfully to the clinical setting. Patients with advanced or metastatic TNBC showed little improvement while on dasatinib or bosutinib in a recent phase II trial.⁷¹⁻⁷³ These results are puzzling as in vitro studies have proven targeted c-Src inhibition to be effective against TNBCs. In an effort to understand this perplexing issue, our lab has decided to design our own c-Src ligand. It is possible that the promiscuous nature of dasatinib and bosutinib for other kinases besides c-Src could have negated any beneficial effects it demonstrated in in vitro studies.

1.5 References

- (1) Hunter, T. *Cell* **1995**, *80*, 225.
- (2) Marshall, C. J. *Cell* **1995**, *80*, 179.
- (3) Manning G, Whyte DB, Martinez R, Hunter T, S. S. *Science (80-.)*. **2002**, *298*, 1912.
- (4) Marshall, C. J. *Cell* **2015**, *80* (2), 179.
- (5) Lawrence, D. S.; Niu, J. *Pharmacol. Ther.* **1998**, *77* (2), 81.
- (6) Hunter, T. *Cell* **2000**, *100*, 113.
- (7) Sickmann, A. R. J. *Proteomics* **2005**, *5* (16), 4052.
- (8) Roberts, P. J.; Der, C. J. *Oncogene* **2007**, *26* (22), 3291.
- (9) Bartek, J.; Lukas, J. *Cancer Cell* **2003**, *3* (5), 421.
- (10) Andreas Gschwind, O. M. F. & A. U. *Nat. Rev. Cancer* **2004**, *4*, 361.
- (11) Knight, Z. a; Lin, H.; Shokat, K. M. *Nat. Rev. Cancer* **2010**, *10* (2), 130.
- (12) Cohen, P. *Nat. Rev. Drug Discov.* **2002**, *4*, 309.
- (13) Brown, M. T.; Cooper, J. A. *Biochim. Biophys. Acta - Rev. Cancer* **1996**, *1287* (2–3), 121.
- (14) Roskoski Jr., R. *Biochem. Biophys. Res. Commun.* **2005**, *331* (1), 1.
- (15) Biscardi, J. S.; Tice, D. A.; Parsons, S. J. In *Advances in Cancer Research*; 1999; Vol. 76, pp 61–119.
- (16) Knight, Z. A.; Shokat, K. M. *Chem. Biol.* **2005**, *12* (6), 621.
- (17) Jura, N.; Zhang, X.; Endres, N. F.; Seeliger, M. A.; Schindler, T.; Kuriyan, J. *Mol. Cell* **2011**, *42* (1), 9.
- (18) Gonfloni, S.; Weijland, A.; Kretzschmar, J.; Superti-Furga, G. *Nat Struct Mol Biol* **2000**, *7* (4), 281.
- (19) Yadav, S. S.; Miller, W. T. *Cancer Lett.* **2007**, *257* (1), 116.
- (20) Irtegun, S.; Wood, R. J.; Ormsby, A. R.; Mulhern, T. D.; Hatters, D. M. *PLoS One* **2013**, *8* (7), e71035.
- (21) Chong, Y.-P.; Ia, K. K.; Mulhern, T. D.; Cheng, H.-C. *Biochim. Biophys. Acta - Proteins Proteomics* **2005**, *1754* (1–2), 210.
- (22) Ozkirimli, E.; Post, C. B. *Protein Sci.* **2006**, *15* (5), 1051.
- (23) Seeliger, M. A.; Nagar, B.; Frank, F.; Cao, X.; Henderson, M. N.; Kuriyan, J. *Structure* **2007**, *15* (3), 299.
- (24) Schindler, T.; Bornmann, W.; Pellicena, P.; Miller, W. T.; Clarkson, B.; Kuriyan, J. *Sci.* **2000**, *289* (5486), 1938.
- (25) Xu, W.; Doshi, A.; Lei, M.; Eck, M. J.; Harrison, S. C. *Mol. Cell* **1999**, *3* (5), 629.
- (26) Levinson, N. M.; Seeliger, M. A.; Cole, P. A.; Kuriyan, J. *Cell* **2008**, *134* (1), 124.
- (27) Deindl, S.; Kadlecsek, T. A.; Brdicka, T.; Cao, X.; Weiss, A.; Kuriyan, J. *Cell* **2007**, *129* (4), 735.
- (28) Min, X.; Lee, B.-H.; Cobb, M. H.; Goldsmith, E. J. *Structure* **2004**, *12* (7), 1303.
- (29) Rellos, P.; Ivins, F. J.; Baxter, J. E.; Pike, A.; Nott, T. J.; Parkinson, D.-M.; Das, S.; Howell, S.; Fedorov, O.; Shen, Q. Y.; Fry, A. M.; Knapp, S.;

Smerdon, S. J. *J. Biol. Chem.* **2007**, 282 (9), 6833.

- (30) Wang, W.; Marimuthu, A.; Tsai, J.; Kumar, A.; Krupka, H. I.; Zhang, C.; Powell, B.; Suzuki, Y.; Nguyen, H.; Tabrizizad, M.; Luu, C.; West, B. L. *Proc. Natl. Acad. Sci. United States Am.* **2006**, 103 (10), 3563.
- (31) Wang, L.; Perera, B. G. K.; Hari, S. B.; Bhatarai, B.; Backes, B. J.; Seeliger, M. A.; Schürer, S. C.; Oakes, S. A.; Papa, F. R.; Maly, D. J. *Nat. Chem. Biol.* **2012**, 8 (12), 982.
- (32) Cowan-Jacob, S. W.; Fendrich, G.; Manley, P. W.; Jahnke, W.; Fabbro, D.; Liebetanz, J.; Meyer, T. *Structure* **2005**, 13 (6), 861.
- (33) Hunter, T. *Cell* **1987**, 49 (1), 1.
- (34) Superti-Furga, G.; Courtneidge, S. A. *BioEssays* **1995**, 17 (4), 321.
- (35) Matsuda, M.; Mayer, B. J.; Fukui, Y.; Hanafusa, H. *Science* **1990**, 248 (4962), 1537.
- (36) Thomas, J. W.; Ellis, B.; Boerner, R. J.; Knight, W. B.; White, G. C.; Schaller, M. D. *J. Biol. Chem.* **1998**, 273 (1), 577.
- (37) Mamidipudi, V.; Zhang, J.; Lee, K. C.; Cartwright, C. A. *Mol. Cell. Biol.* **2004**, 24 (15), 6788.
- (38) Li, S.; Couet, J.; Lisanti, M. P. *J. Biol. Chem.* **1996**, 271 (46), 29182.
- (39) Iacob, R. E.; Pene-Dumitrescu, T.; Zhang, J.; Gray, N. S.; Smithgall, T. E.; Engen, J. R. *Proc. Natl. Acad. Sci.* **2009**, 106 (5), 1386.
- (40) Lamontanara, A. J.; Georgeon, S.; Tria, G.; Svergun, D. I.; Hantschel, O. *Nat. Commun.* **2014**, 5, 5470.
- (41) Brandvold, R.; Ste, M. E.; Fox, C. C.; Soellner, M. B. *ACS Chem. Biol.* **2012**, 7, 1393.
- (42) Bolden, J. E.; Peart, M. J.; Johnstone, R. W. *Nat Rev Drug Discov* **2006**, 5 (9), 769.
- (43) Glaser, K. B. *Biochem. Pharmacol.* **2007**, 74 (5), 659.
- (44) Carew, J. S.; Giles, F. J.; Nawrocki, S. T. *Cancer Lett.* **2008**, 269 (1), 7.
- (45) Yu, C.; Rahmani, M.; Almenara, J.; Subler, M.; Krystal, G.; Conrad, D.; Varticovski, L.; Dent, P.; Grant, S. *Cancer Res.* **2003**, 63 (9), 2118.
- (46) C., K. K.; S., D.; D., B.; Bonham. *Oncogene* **2002**, 21 (41), 6340.
- (47) Minucci, S.; Pelicci, P. G. *Nat Rev Cancer* **2006**, 6 (1), 38.
- (48) Shen, J.; Woodward, R.; Kedenburg, J. P.; Liu, X.; Chen, M.; Fang, L.; Sun, D.; Wang, P. G. *J. Med. Chem.* **2008**, 51 (23), 7417.
- (49) Kouzarides, T. *Curr. Opin. Genet. Dev.* **1999**, 9 (1), 40.
- (50) Marks, P. A.; Breslow, R. *Nat Biotech* **2007**, 25 (1), 84.
- (51) Marks, P. A.; Rifkind, R. A.; Richon, V. M.; Breslow, R.; Miller, T.; Kelly, W. K. *Nat Rev Cancer* **2001**, 1 (3), 194.
- (52) Johnstone, R. W. *Nat Rev Drug Discov* **2002**, 1 (4), 287.
- (53) Morphy, R. *J. Med. Chem.* **2010**, 53 (4), 1413.
- (54) Morphy, R.; Rankovic, Z. *J. Med. Chem.* **2005**, 48 (21), 6523.
- (55) Cai, X.; Zhai, H. X.; Wang, J.; Forrester, J.; Qu, H.; Yin, L.; Lai, C. J.; Bao, R.; Qian, C. *J. Med. Chem.* **2010**, 53 (5), 2000.
- (56) Weigelt, B.; Peterse, J. L.; van 't Veer, L. J. *Nat. Rev. Cancer* **2005**, 5 (8), 591.

- (57) Perou, C. M.; Sorlie, T.; Eisen, M. B.; van de Rijn, M.; Jeffrey, S. S.; Rees, C. A.; Pollack, J. R.; Ross, D. T.; Johnsen, H.; Akslen, L. A.; Fluge, O.; Pergamenschikov, A.; Williams, C.; Zhu, S. X.; Lonning, P. E.; Borresen-Dale, A.-L.; Brown, P. O.; Botstein, D. *Nature* **2000**, *406* (6797), 747.
- (58) Sorlie, T.; Tibshirani, R.; Parker, J.; Hastie, T.; Marron, J. S.; Nobel, A.; Deng, S.; Johnsen, H.; Pesich, R.; Geisler, S.; Demeter, J.; Perou, C. M.; Lonning, P. E.; Brown, P. O.; Borresen-Dale, A.-L.; Botstein, D. *Proc. Natl. Acad. Sci. U. S. A.* **2003**, *100* (14), 8418.
- (59) Sørli, T.; Perou, C. M.; Tibshirani, R.; Aas, T.; Geisler, S.; Johnsen, H.; Hastie, T.; Eisen, M. B.; van de Rijn, M.; Jeffrey, S. S.; Thorsen, T.; Quist, H.; Matese, J. C.; Brown, P. O.; Botstein, D.; Lønning, P. E.; Børresen-Dale, A.-L. *Proc. Natl. Acad. Sci.* **2001**, *98* (19), 10869.
- (60) Jemal, A.; Siegel, R.; Xu, J.; Ward, E. *CA. Cancer J. Clin.* **2010**, *60* (5), 277.
- (61) Finnegan, T. J.; Carey, L. A. *Future Oncol.* **2007**, *3* (1), 55.
- (62) Schneider, B. P.; Winer, E. P.; Foulkes, W. D.; Garber, J.; Perou, C. M.; Richardson, A.; Sledge, G. W.; Carey, L. A. *Clin. Cancer Res.* **2008**, *14* (24), 8010.
- (63) Anders, C. K.; Carey, L. A. *Clin. Breast Cancer* **2009**, *9* (Suppl 2), S73.
- (64) Carey, L.; Winer, E.; Viale, G.; Cameron, D.; Gianni, L. *Nat. Rev. Clin. Oncol.* **2010**, *7* (12), 683.
- (65) Foulkes, W. D.; Smith, I. E.; Reis-Filho, J. S. *N. Engl. J. Med.* **2010**, *363* (20), 1938.
- (66) Bayraktar, S.; Gluck, S. *Breast Cancer Res. Treat.* **2013**, *138* (1), 21.
- (67) Aleshin, A.; Finn, R. S. *Neoplasia* **2010**, *12* (8), 599.
- (68) Mayer, E. L.; Krop, I. E. *Clin. Cancer Res.* **2010**, *16* (14), 3526.
- (69) Tryfonopoulos, D.; Walsh, S.; Collins, D. M.; Flanagan, L.; Quinn, C.; Corkery, B.; McDermott, E. W.; Evoy, D.; Pierce, A.; O'Donovan, N.; Crown, J.; Duffy, M. J. *Ann. Oncol.* **2011**, *22* (10), 2234.
- (70) Sánchez-Bailón, M. P.; Calcabrini, A.; Gómez-Domínguez, D.; Morte, B.; Martín-Forero, E.; Gómez-López, G.; Molinari, A.; Wagner, K.-U.; Martín-Pérez, J. *Cell. Signal.* **2012**, *24* (6), 1276.
- (71) Finn, R. S.; Bengala, C.; Ibrahim, N.; Roche, H.; Sparano, J.; Strauss, L. C.; Fairchild, J.; Sy, O.; Goldstein, L. J. *Clin. Cancer Res.* **2011**, *17* (21), 6905.
- (72) Gucalp, A.; Sparano, J. A.; Caravelli, J.; Santamauro, J.; Patil, S.; Abbruzzi, A.; Pellegrino, C.; Bromberg, J.; Dang, C.; Theodoulou, M.; Massague, J.; Norton, L.; Hudis, C.; Traina, T. A. *Clin. Breast Cancer* **2011**, *11* (5), 306.
- (73) Campone, M.; Bondarenko, I.; Brincat, S.; Hotko, Y.; Munster, P. N.; Chmielowska, E.; Fumoleau, P.; Ward, R.; Bardy-Bouxin, N.; Leip, E.; Turnbull, K.; Zacharchuk, C.; Epstein, R. J. *Ann. Oncol.* **2012**, *23* (3), 610.

Chapter 2

Exploring Global Conformations of c-Src: Clinical and Non-Clinical Mutations

2.1 Introduction

Our laboratory is interested in elucidating the structure and function of protein kinase c-Src, specifically its effect in oncogenesis. Discovered in 1978, c-Src, was the first identified protein tyrosine kinase (PTK) which was later implicated as a proto-oncogene. c-Src is believed to associate with a number of receptor tyrosine kinases (RTK) such as EGFR and PDGF, which serves in part as their regulator and also as a co-transducer of their originating signals.¹ This activation of c-Src results in the regulation of normal and oncogenic processes by affecting its downstream targets such as focal adhesion kinase (FAK), Ras, Stat3, and phosphoinositide 3-kinase (PI3K) and plays an integral role in cell proliferation, differentiation, division, and survival, as well as cell motility and adhesion.^{2,3} As such, the dysregulation of c-Src has been implicated in cancers including breast, colon, pancreatic, and lung cancer and consequently, multiple studies conducted have validated c-Src as a target for the treatment of such cancers.³

However, despite the wealth of research involved in c-Src, it is still poorly misunderstood, especially its role in oncogenesis.^{4,5} Its overexpression is frequently observed in various cancers and is usually correlated with increased malignancy and metastasis resulting in poorer patient prognosis.^{4,6,7} Though when this overexpression is replicated in *in vitro* experiments, the results confusingly demonstrates that the overabundance of c-Src alone is only weakly oncogenic.⁸ Furthermore, clinical mutations of c-Src are rarely overactive which is usually

prototypical for the transformation into cancerous cells.⁹⁻¹³ Herein lies the disconnect, c-Src is crucial in regulating important normal cellular functions which then rationally correlates with observations of its implication and maintenance of several human cancers, yet displays a poor innate ability as a transformative key towards cancer. The following assumes that c-Src is not a dominant/lone transforming factor.¹⁴ It is more likely that overexpression of c-Src leads to the dysregulation of other signaling pathways in which another target is the true dominant transformative switch or it's a combination of deregulated targets resulting in a transformative affect to cancer.¹⁴ In this regard, the question becomes how is c-Src involved in influencing those pathways? Could this help explain a role c-Src plays and its frequent observation in affecting oncogenesis?

The existence of clinical c-Src mutations were identified in the Catalogue of Somatic Mutations in Cancers (COSMIC) database which encompasses over 542,000 cancer tumors and 947 human cancer cell lines.¹⁵ Why are there mutated forms of c-Src if not to participate in cancer maintenance and/or progression? Overactive c-Src mutants that have been previously found to be involved in colon cancer are rare.⁹ However these clinical mutations of c-Src from the COSMIC database have not been characterized, and so the reason for their existence, whether or not they are transformative or occur randomly is unknown.^{15,16} If these mutants do not result in over activity, perhaps there are other aspects of c-Src dysregulation they affect and could lead to a deeper understanding in the role that c-Src plays in oncogenesis. This chapter will explore these clinical mutations and look to explain their possible role in c-Src dysregulation.

c-Src native structure *in cellulo* contains 4 domains, SH4, SH3, and SH2 domain with a long polypeptide linker connected to the catalytic kinase domain (SH1). The SH2 and SH3 domains will be the main focus in this chapter as c-Src is only biochemically expressed in its 3 domain (3D) form.¹⁷ The SH2 and SH3 domains act as a regulatory element of c-Src by assuming different configurations in relation to the kinase domain in what is described as its global conformation.¹⁸⁻²⁰ There are two main conformations of c-Src, an open/active conformation, in which the SH2, SH3, and kinase domain are disorganized in space and a closed/inactive

conformation, where the SH2 and SH3 domains are held clamped down alongside the kinase domain (Figure 2.1).

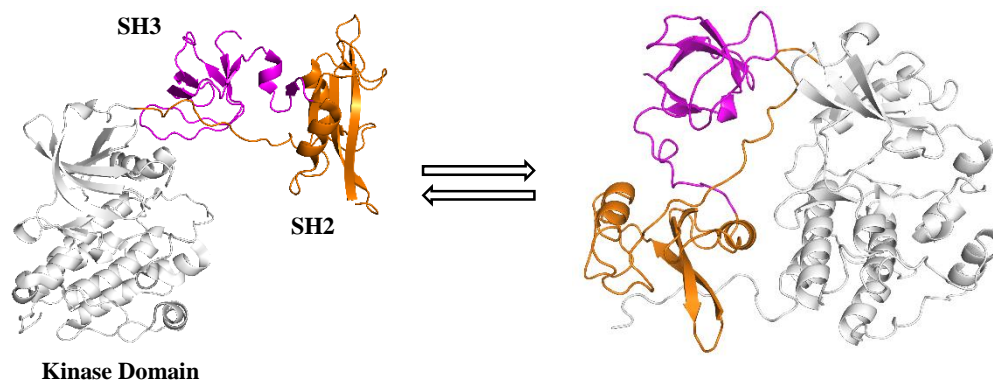


Figure 2.1: The only two known crystal structures of 3D Src. Kinase domain is in white, SH2 is in orange, and SH3 is in magenta. The structure on the left is bound to a Type I ligand and is in the more open conformation than the structure on the right, which is bound with ATP γ S, is in the closed inactive configuration. Left PDB: 1Y57 and Right PDB: 2Src.

c-Src is normally maintained in an inactive/closed state, but transitions into the active/open configuration during cellular events.² This switch between open and close is one method in regulating c-Src functions (as this not only affects catalytic activity but protein-protein interaction).^{19,20} The most well-known event controlling this switch is the phosphorylation state. The classic sites of phosphorylation on c-Src are Y419 on the activation loop and Y530 on the C-terminus tail. Phosphorylation either by itself or other kinases at Y419 results in an open and fully catalytically active c-Src whereas phosphorylation at Y530 by Csk leads to the close/inactive conformation.^{1,20-22} Tail phosphorylation at Y530 allows the SH2 domain, which contains a shallow phosphate pocket, to bind tightly, collapsing the domains together.²³ Consequently, the opposite effects occur upon dephosphorylation by phosphatases at both sites. The balance between phosphorylation and dephosphorylation is the regulatory mechanism turning c-Src catalytic function on or off.^{1,21}

As such, disruption in this balance leads to dysregulation of the kinase and has been observed in cancer.⁹ Downregulated Csk and upregulated phosphatases for the tail pY530 have been found in cancer which could prevent c-Src from being

turned off.²⁴⁻²⁶ There is also an abnormal mutation where the tail phosphorylation site is entirely truncated resulting in a constitutively active kinase form known as v-Src.⁴ First, found to affect chickens, it is a retroviral oncogene which triggers uncontrolled cell growth leading to cancer (Rous sarcoma virus). The truncated tail mutation was later identified to happen in c-Src as well and found to be activating, transformative, and tumorigenic in some cases of advanced human colon cancer.⁹ All of these dysregulated form above describes how phosphorylation states at these classic sites affect conformation and thereby catalytic activity precipitating into oncogenesis.

Phosphorylation states not only regulate catalytic activity but dictate different conformational states, thereby affecting intramolecular activity or protein-protein interactions (PPIs).²⁷⁻³⁰ Both the SH3 and SH2 domains serve as binding sites for other c-Src partners such as FAK, RACK1, PDGFR.^{31,32} Therefore, the accessibility to these domains facilitated by global conformational changes directly influences these PPIs and thereby signaling pathways that c-Src binding partners control. As such, a bidirectional regulatory mechanism has been proposed, in which the regulation of catalytic conformation also regulates PPI activity (non-catalytic activity) and vice versa wherein the regulation of PPI modulates catalytic activity.^{33,34}

A third aspect, often overlooked in c-Src regulation is how these conformations alter its location in the cell. Many of c-Src's protein partners exist in various locations and as a result, how c-Src signals other pathways is based on its proximity to its substrates/protein binding partners. Natively, c-Src remains in its closed form in the cytosol, specifically at perinuclear sites of the cell.⁴ Upon its activation, by the dephosphorylation of the tail Y530 and then phosphorylation at Y419, causes a more open/fully activated c-Src. It is subsequently transported and attached to the plasma membrane allowing it to interact with its protein partners, such as membrane bound receptor tyrosine kinases and integrins, either through catalysis or PPIs leading to the start of a signaling cascade.

In short, the entire story discussed thus far about c-Src's regulation mechanism can be summarized around three main factors, location, phosphorylation state, and conformational state. Each one of these facets participates in how c-Src is regulated in the cell, Figure 2.3. In Figure 2.3, the arrows indicate a direct causation effect, hexagons are the resulting secondary effect, and the green circle is the final end result. The location of c-Src influences its proximity to substrates which dictates what substrates c-Src interacts with, ultimately resulting in what pathways get turn on and off. The localization of c-Src is determined by its phosphorylation state which directly affects conformational state, a physical switch earmarking c-Src's destination in the cell. Phosphorylation state also affects catalytic activity. In turn, conformational state can affect how other protein binding partners can interact with it as well as indirectly affecting catalytic activity.

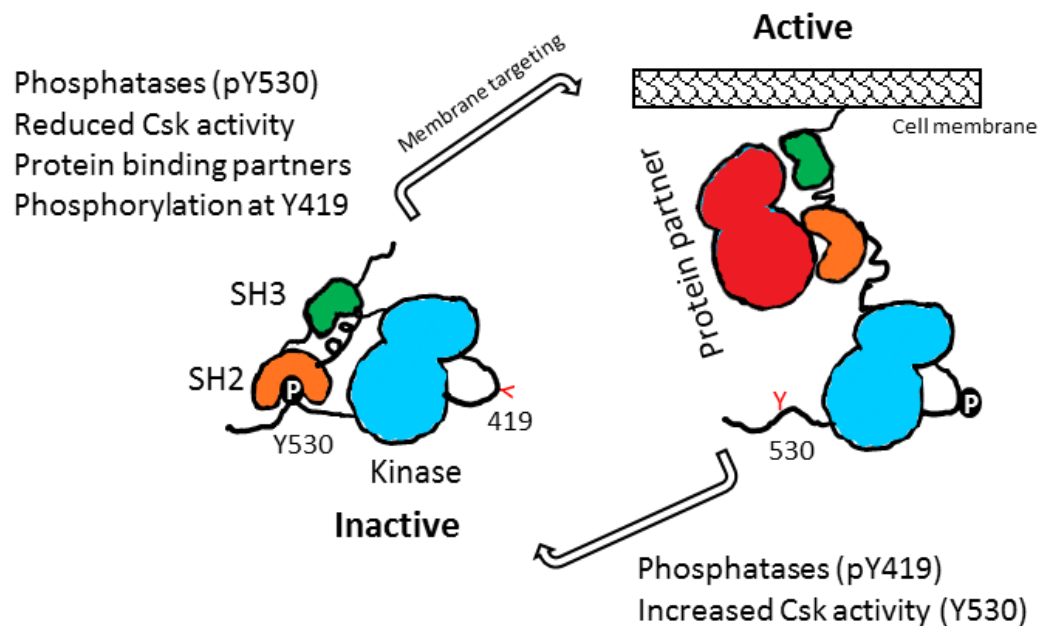


Figure 2.2: Cartoon diagram depicting c-Src regulatory mechanism involving c-Src's open/closed conformations resulting from different phosphorylation states. Inactive c-Src is usually found in the cytosol and is a result of phosphorylation at Y530 from Csk. This causes the clamping down of both SH3 and SH2 domains which configures c-Src in a closed conformation. Dephosphorylation of Y530 and/or phosphorylation of Y419 on the activation loop targets c-Src to the membrane resulting in a fully activated kinase, where it can interact with its protein binding partners through scaffolding effects and/or phosphorylate its other substrates.

In terms of clinical mutations, the over-activity of c-Src is rarely seen to be responsible for oncogenesis, and thus not the main contributing factor in its development. However, from this regulation map, it appears that one other possibility is left in regards to how clinical mutations could be disrupting the regulation mechanism. We speculate that these clinical mutations can disrupt conformational states and in doing so, bypass the cell's ability to directly dictate

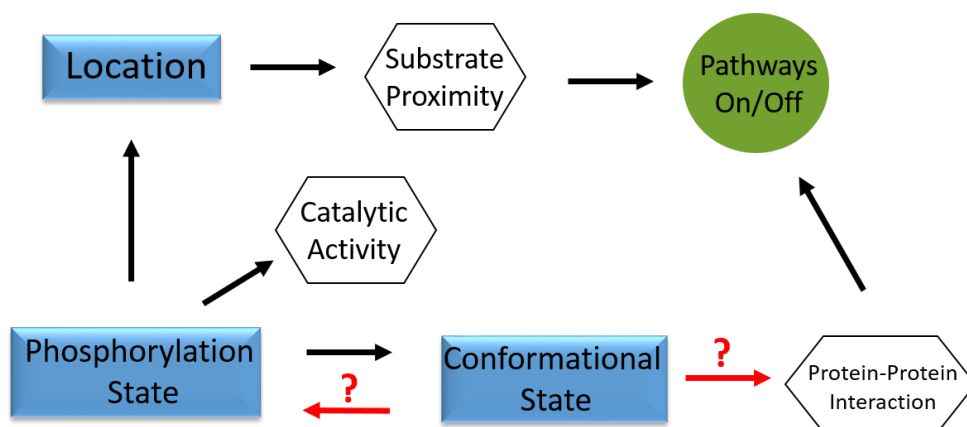
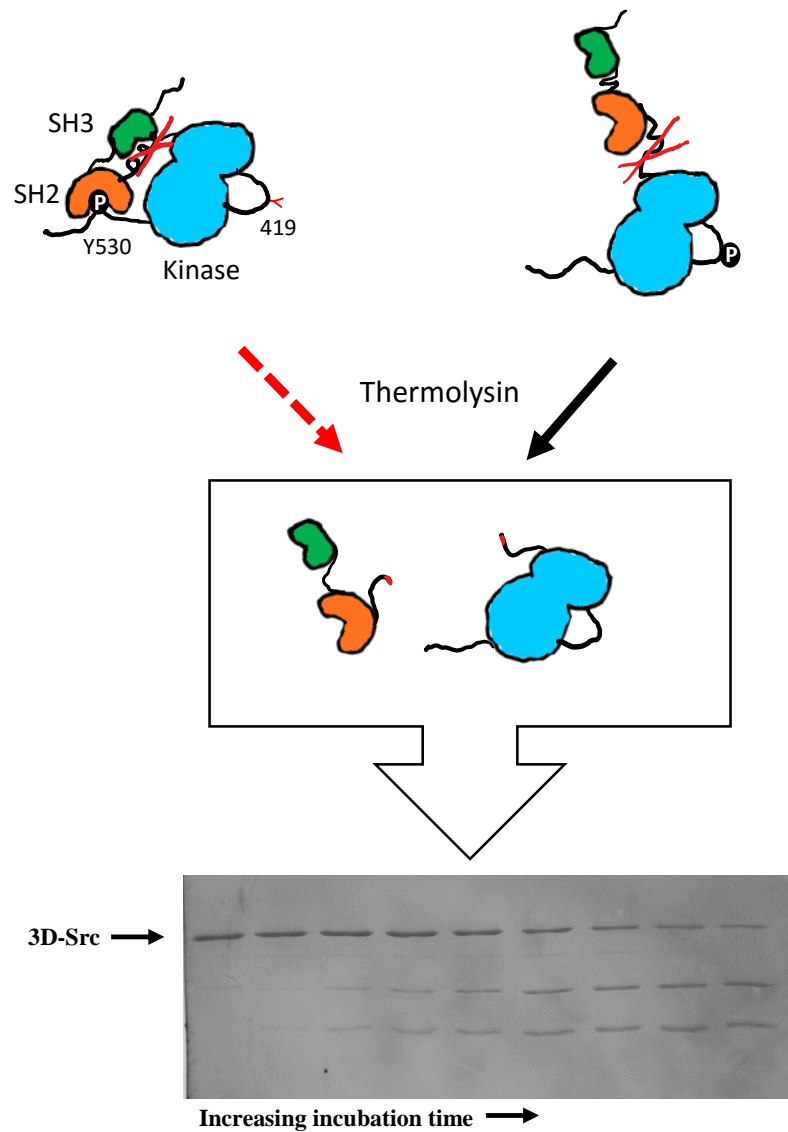


Figure 2.3: Chart of three main regulation mechanism of c-Src, localization, phosphorylation state, and conformational state. Black arrows indicates an effect that directly contributes as a result. Hexagons shows a secondary effect and the green circle is the final aggregate effect which is usually the signal transduction pathway that c-Src is involved in gets turned on/off. The red arrows are effects that will be investigated in this chapter as we are interested in whether or not mutations effect conformational state and thereby disrupts c-Src's regulation mechanism.

localization, catalytic activity, and PPIs by interrupting the native phosphorylation state balance. This is indicated in red arrows in Figure 2.3 and is what this chapter will attempt to explore. However, for this theory to be possible, the first fundamental issue needs to be addressed, do mutations affect global conformations?

2.2 Designing an Assay to Identify Global Conformation

From the COSMIC database was characterized 19 somatic mutations of the SRC gene, Table 2.1. We also looked at 16 other non-clinical mutations of c-Src. These mutations have been utilized in various structure-function studies of c-Src kinase domain. We were curious if these kinase domain mutations had a distant



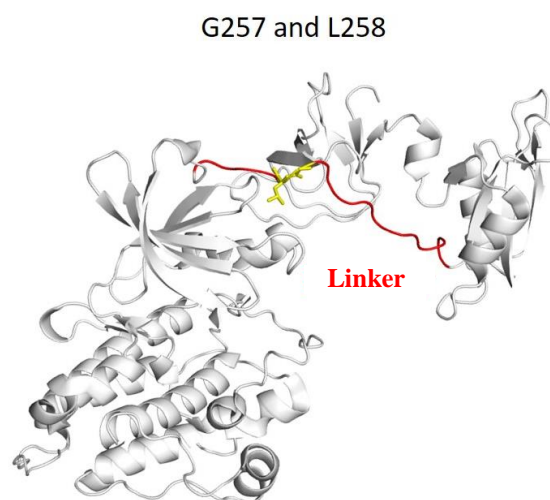
Open constructs = Faster cleavage
 Closed constructs = Slower cleavage

Figure 2.4: Diagram of thermolysin protease assay. c-Src mutations were incubated with thermolysin at various time points and then loaded and ran on an SDS-PAGE gel for analysis. An example gel is shown. As incubation time is increased (starting from left 0min to right), depending on the conformational state, either 3D Src band starts to decrease (open) or stays the same (closed). A more close conformation would show a slower rate of cleavage (dashed red line) as oppose to a more open conformation, which would have a faster rate of cleavage.

effect on global conformations. If this holds true, it might hold unsuspecting implications for c-Src studies *in cellulo*, specifically in cases where these kinase domain mutations have been substituted in place of wt-Src. To evaluate these

mutational effects on conformation, we modified an existing assay previously developed to explore the conformational state of 3D c-Src.

Back before any crystal structure of 3D c-Src was solved and knowledge of global configuration was known, MacAuley et. al designed a protease assay to probe the conformations.³⁵ They thought the catalytic activity of c-Src is regulated through conformational changes, and thus wanted to investigate. The structure of 3D Src possesses polypeptide linker regions to connect all three domains together and accessibility to these linkers, specifically the SH2 linker (the longest linker, which



Mass Spec.

Calculated: 19952.25 & 31946.13

Found: 19953.0 & 31950.0

Figure 2.5: Cut site is shown to be between G257 and L258 and confirmed by mass spec. The cut site residues are shown in yellow and the linker is highlighted in red. PDB: 1Y57

connects the kinase domain and SH2 domain, (shown in red in Figure 2.5) they reasoned, depended on the changes in conformation. Therefore, they utilized proteases, which cleave peptide bonds, as a tool to evaluate linker exposure and correlated the cleavage pattern to conformations. They assessed three different forms of 3D Src, phosphorylated Y530 (pY530), Y530F, and wt-Src (Y530 dephosphorylated) using mainly trypsin and then thermolysin and pronase E. pY530 appeared less receptive to proteolysis than either Y530F and wt-Src which were both similar, suggesting there were two different conformations between inactive

CLINICAL	NON-CLINICAL
D407H	I339W
R483W	K298M
R163W	L320I
K298E	F408G
T341M	T341I
T341R	F408A
D521N	A406S
I113F	T341M-A406S
P307R	T341G
P171Q	Y530F
V140M	Y419F
E527K	D407N
Q529H	W263A
D120N	
K298R	
R98W	

Table 2.1: List of mutations. Ones on the left are somatic clinical mutations found from Catalogue of Somatic Mutations in Cancers (COSMIC) and Cancer Cell Line Encyclopedia (CCLE) and ones on the right are non-clinical mutations.

(pY530) and active (wt-Src and Y530F) c-Src. Both thermolysin and pronase E displayed similar results compared to trypsin. The varying cleavage products are due to disparate cut sites (Cut site at C-terminus tail (thermolysin and pronase E) instead of the linker between SH2 and kinase domain (trypsin)). As such, they concluded that pY530 inhibits kinase activity by exhibiting a configuration in which the C-terminus tail was hidden as neither thermolysin or pronase E could access the cleavage site.

We wanted to take this similar concept using thermolysin to evaluate how clinical mutations affected c-Src conformation. Instead of looking at substrate products, we measured the rate of cleavage, quantified by SDS-PAGE over a period

of 4 hours into half-lives (Figure 2.4). Thru numerous optimizations, we found the concentration of thermolysin which only cuts at the SH2 linker where the SH3 domain binds and was confirmed by mass spec (Figure 2.5). Therefore, by taking advantage of the SH3 linker accessibility, which should be different depending on the conformation, as a faster rate of cleavage, and thus smaller half-life would indicate an open conformation as the linker is more exposed and vice versa. Using three known control c-Src constructs, pY419, apo wt-Src, and pY530, the method was validated and demonstrated correlation between half-life and three different conformations (Table 2.2) that corresponds to open/closed/apo.

2.3 Assay Results and Discussion

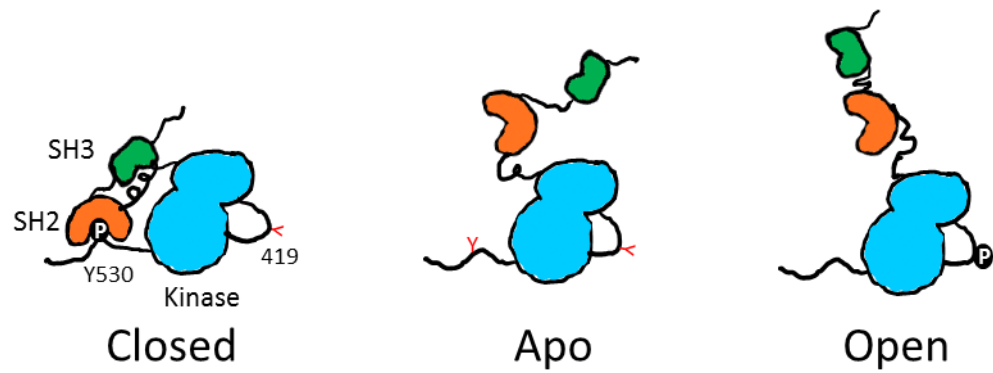
Next, we evaluated all 29 mutations in the thermolysin assay and results are shown in Figure 2.6 and Table 2.3. Gratifyingly, mutations do stabilize different global conformations and exhibits a gradient from fully open to closed and various degrees of openness and closeness in between. Altogether, it can be rationalized that given the flexibility of c-Src, it must inherently lead to a myriad of transient conformational states.

As a secondary assay to further confirm the results seen from the thermolysin assay, we decided to use a fluorescence polarization (FP) assay using a FITC labeled SH2 optimal peptide (EPQpYEEIPIYL). The FITC-SH2 peptide binds to the phosphotyrosine pocket of the SH2 domain of c-Src. Similar in concept to the thermolysin assay, the accessibility to this SH2 pocket would allow us to infer the global conformation of c-Src. For instance, tighter binding of the FITC-SH2 peptide would indicate an open conformation as the SH2 domain should be fully accessible and a close conformation would be a decrease in binding. To validate the FP assay and allow us to establish a correlation between K_d values and open/closed conformations, the three known control c-Src constructs, pY419, apo wt-Src, and SH2-Eng was utilized. The results are shown in

Table 2.4. Both K_d values for wt-Src and SH2-Eng correlated well with their conformational state. The closed conformation did not show any binding compared to wt-Src (729 nM). However, results for pY419 were surprising, with a K_d value

~10 μM (a full K_d curve could not be generated due to limited kinase concentration). In theory, binding of the SH2-peptide should be better than wt-Src because of the increased SH2 accessibility of a more open conformation. We hypothesized that the large concentration of pY419 c-Src causes aggregation/dimerization thru a possible interaction of the SH2-domain of c-Src with the pY419 of another c-Src. We also had difficulty in preparing pY419 thru autophosphorylation, due to precipitation of the kinase, which lends further credence to the aggregation theory. It wasn't until the addition of triton that we could successfully generate useable amount of pY419. In literature, Irtegun et. al. had also proposed that the open state of c-Src tends to dimerize upon autophosphorylation at Y419.¹⁸ Therefore, despite an open conformation, the dimerization/aggregation of pY419 would prevent the FITC-SH2 peptide from binding tightly, explaining the ~10 μM K_d of an open state c-Src construct.

Due to the limited amount of protein available, we were only able to measure the K_d value of some mutations, though there are examples from each open/apo/closed (identified thru thermolysin assay) category, which we believed were sufficient to back up the thermolysin assay. The results are shown in Figure 2.7 and Table 2.4. Surprisingly, it appears that outside of some exceptions, the K_d of the FITC-SH2 peptide appear to vary with mutations, but do not correlate with half-life. These results lead us to conclude that the FP assay using the FITC-SH2 peptide cannot be used to identify conformational states. For the most part, K_d values are nearly similar between open and closed conformation with an exception with T341R and K298M, which think could be attributed to mutational effects on the SH2 binding pocket. Therefore, the K_d values which would indicate SH2 accessibility, cannot be correlated to an open/closed configuration. Upon further investigation of the literature, an experiment done by Maly et. al. is possibly better at showing whether or not SH2 domain accessibility can be correlated to open/closed conformation. It appears to indicate that despite the various open/closed configuration generated by conformationally selective inhibitors, access to the SH2 domain is not affected. Taken together, the global conformation of c-Src isn't affecting SH2 domain accessibility. In other words, the SH2 domain is in a



c-Src constructs	Half Life (min)	Conformation
pY419	12.21	Open
Wt-Src	32.96	Apo
Src-SH2-Eng	356.4	Closed
pY530	240.9	Closed

Table 2.2: c-Src constructs from literature used as controls to correlate thermolysin half-lives to conformational state. Cartoon picture of what past literature has depicted as open, apo, and closed.⁴⁵

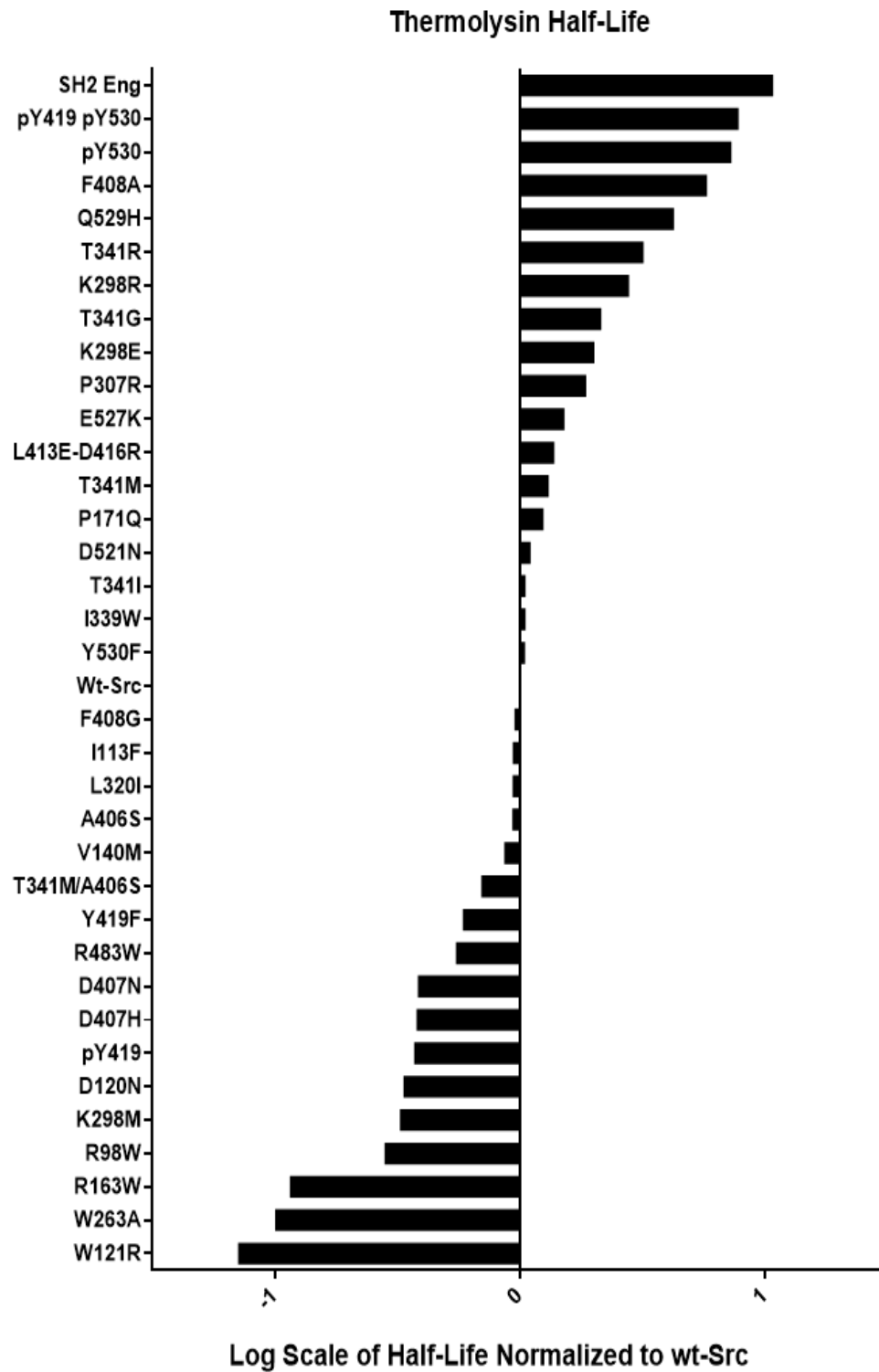


Figure 2.6: Thermolysin Half-Life of clinical and non-clinical mutations. All values were normalized to w-Src and depicted on a log scale. Negative values typify more open conformations whereas positive values signal more closed.

<i>Mutation</i>	<i>Half-Life (min)</i>	<i>Mutation</i>	<i>Half-Life (min)</i>
<i>W121R</i>	2.3	D407H	12.5
<i>W263A</i>	3.3	D407N	12.7
<i>R163W</i>	3.8	R483W	18.1
<i>R98W</i>	9.3	Y419F	19.3
<i>K298M</i>	10.7	T341M-A406S	22.9
<i>D120N</i>	11.1		
<i>pY419</i>	12.2		
<i>V140M</i>	28.5	Y530F	34.7
<i>A406S</i>	30.7	I339W	34.8
<i>L320I</i>	30.8	T341I	34.8
<i>I113F</i>	30.9	D521N	36.5
<i>F408G</i>	31.4	P171Q	41.19
<i>Wt-Src</i>	32.9	T341M	43.3
<i>E527K</i>	50.2	Q529H	141
<i>P307R</i>	61.6	F408A	191.6
<i>K298E</i>	66.5	pY530	241
<i>T341G</i>	71	pY419-pY530	258
<i>K298R</i>	92	SH2-Eng	356.4
<i>T341R</i>	105.7		

Table 2.3: Thermolysin assay half-life values grouped around the three control c-Src constructs, wt-Src, pY419, and pY530 (highlighted in red).

configuration that allows the pocket to be accessed, regardless of the conformation.

Despite the FP assay not being able to be used to indicate open/closed conformation, the thermolysin data still indicates that mutations, both clinical and non-clinical, were able to affect the global conformation of c-Src. Next, we decided

to further characterize these mutations and look at ways in how conformations could affect c-Src function.

Since the thermolysin assay still indicates that mutations, both clinical and non-clinical, were able to affect the global conformation of c-Src, which addresses our first fundamental issue, we decided to further characterize these mutations and look at ways in how conformations could affect c-Src function. Going back to Figure 2.2, if conformations were to dysregulate c-Src function, it could do so thru catalytic

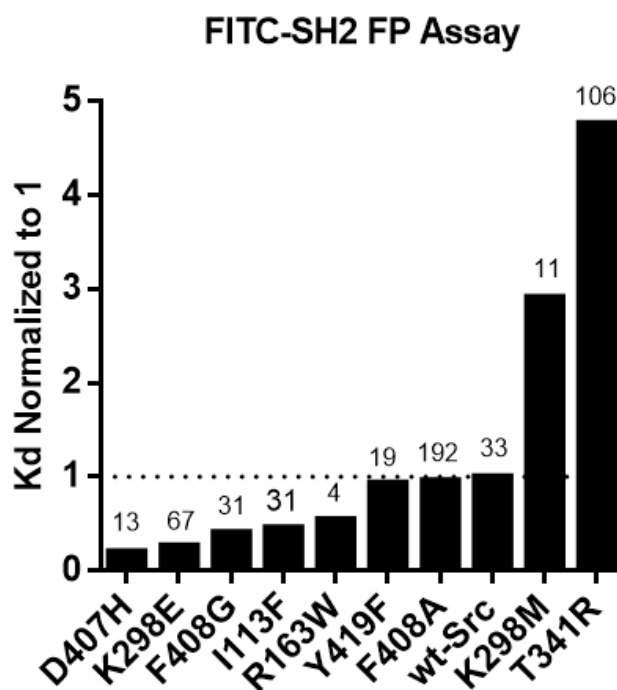


Figure 2.7: FITC-SH2 Fluorescence Polarization Assay on select c-Src mutation constructs. Kd were taken and normalized to wt-Src (apo conformation) which is set to 1. Half lives from thermolysin assay is shown above the bars for each mutation.

c-Src Constructs	Kd (nM)	Half Life (min)
Wt-Src	729 ± 87	33
pY419	~10,000	12.2
T341R	3472	105
SH2-Eng	Does not bind	356.4
K298M	2100 ± 340	10.7
D407H	146 ± 12	12.5
Y419F	682 ± 47	19.33
R163W	397 ± 89	3.8
I113F	332 ± 18	30.8
F408G	297 ± 51	31.4
K298E	192 ± 21	66.5
F408A	699 ± 32	191.6

Table 2.4: Select mutations representing open/apo/closed conformation were used in FP assay to evaluate SH2 domain accessibility. Binding affinity is in Kd (nM). Half lives from thermolysin assay shown in second column.

activity, PPI's and native phosphorylation state balance, which would ultimately affect localization. We speculate that these clinical mutations can disrupt conformational states and in doing so, bypass the cell's ability to directly dictate localization, catalytic activity, and PPIs by interrupting the native phosphorylation state balance. We were curious if in general, different conformational states had an effect on catalytic activity. The catalytic activity of c-Src can be regulated thru phosphorylation states. It has been found that phosphorylation at Y419 on the activation loop leads to a fully catalytically active c-Src whereas phosphorylation at Y530 on the C-terminus tail greatly decreases the activity. Coincidentally, pY419 results in an open conformation and pY530 stabilizes a closed conformation which has led many to believe that the changes in conformational states, triggered by phosphorylation, plays a role in affecting catalytic activity. As such, we were interested to see if our mutation stabilized conformations would have a similar effect on catalytic activity, which would allow us to explore if catalytic activity could be effected by conformations alone. The relative catalytic activity was measured using Vmax values and Km of both ATP and peptide substrate were assessed as well. Our

three control constructs, pY419, wt-Src, and pY530 were measured first and agrees with previous literature results.^{36,37} pY419 Src, which is a known open construct, displays 4.3-fold higher activity than wt-Src which is 2.2-fold active than pY530 Src (closed) and results shown in Table 2.5. It is also possible that open conformations have increased affinity for ATP and/or substrate peptide over the closed form, explaining the higher activity. The controls for open (pY419), apo (wt-Src), and closed (SH2-Eng and pY530) having varying affinity for ATP that does correlate with their conformational state. pY419 has ~2-fold increase binding to ATP than wt-Src whereas SH2-Eng and pY530 display ~3-fold and nearly ~6-fold decrease binding to ATP respectively.

2.4 Activity Assay Results and Discussion

Next, mutant c-src was evaluated and the results are compiled in Table 2.6. Not all mutations could be tested as some mutations happened to abolish catalytically important amino acid residues. Unfortunately, there were no noticeable trends associated with conformational states. Open state mutations did not bind

Kinase	Wt-Src	pY419	pY530
<i>V_{max}</i>	56 ± 6	239 ± 8	25 ± 6
<i>ATP K_M</i> (μM)	51 ± 14	28 ± 5	340 ± 99
<i>Substrate K_M</i> (μM)	43 ± 2	169 ± 19	108 ± 28

Table 2.5: *V_{max}*, ATP and peptide substrate *K_M* values for the three control c-Src constructs, pY419 (open), wt-Src (apo), and pY530 (closed)

ATP or peptide substrate tighter than apo state mutations or closed states. *V_{max}* values also show no correlation in open conformation being more active than their apo and closed counterparts, Figure 2.8. Upon further examination though, discrepancies between the control c-Src constructs and mutations can be explained. We believe the differences in ATP/peptide substrate and *V_{max}* values are due to the individual mutations itself and therefore cannot be correlated to their open/apo/closed conformations. Oftentimes, these affects are seen in mutations on just the kinase domain alone. Our control c-Src construct's conformations are stabilized through their post-translational modifications and do not contain any

mutated residues. As such, their V_{max} and affinity values can be correlated to their configured states. Unfortunately, we were unable to evaluate global conformational effects alone on catalytic activity since decoupling mutation and phosphorylation effects were not possible.

A couple of other mutations of interest are V140M, P307R, and W121R. These clinical mutations display nearly 2-3 fold increase in catalytic activity and slightly better binding affinity to ATP compared to wt-Src. It would be of interest to see if these catalytically more active mutants are transformative since the hyperactive v-Src mutation leads to cancer.

2.5 Investigating pY419-pY530

However, there appears to be an interesting case, hinted throughout several literature articles, that phosphorylation states can indeed "override" most conformational effects on catalytic activity.^{18,33} Here, pY530 is demonstrated to have little catalytic activity, and thru thermolysin assay, assessed to be in a closed conformation. Therefore, the assumption has been that a closed conformation, for the most part equals inactivated kinase. As previously observed, however, an additional phosphorylation at Y419 on pY530, which has been found in a cellular study, retains activity despite its closed state.¹⁸ We decided to evaluate this biochemically and generated a pY530-pY419 c-Src construct. pY419 does indeed "rescue" activity, with a nearly 5-fold increase in V_{max} compared to pY530 alone and surprisingly, a 2-fold increase above wt-Src. Activity of the double phosphorylation still remains less active than pY419 alone.

A couple studies by Gonfloni et. al. and Irtegun et al. took a closer look at why a "closed" conformation would still be active despite other literature articles describing that the closed conformation, involving the clamping down effect of SH2 and SH3 domains, actually results in a physical distortion of the ATP pocket, thereby prohibiting ATP binding and ADP release.^{18,33,36} In observations from their expt.

<i>Mutation</i>	<i>ATP K_M (μM)</i>	<i>Substrate K_M (μM)</i>	<i>V_{max}</i>
<i>pY419</i>	28 ± 5	215 ± 47	239 ± 8
<i>R483W</i>	62 ± 14	55 ± 15	35 ± 6
<i>R163W</i>	31 ± 4	102 ± 7	50 ± 5
<i>W121R</i>	20 ± 4	101 ± 26	128 ± 21
<i>R98W</i>	34 ± 5	42 ± 4	74 ± 7
<i>W263A</i>	7 ± 3.5	65 ± 14	16 ± 2
<i>Y419F</i>	46 ± 1	99 ± 12	126 ± 14
<i>Wt-Src</i>	51 ± 14	43 ± 2	56 ± 6
<i>I113F</i>	111 ± 12	24 ± 4	30 ± 5
<i>V140M</i>	38 ± 3	104 ± 8	152 ± 1
<i>Y530F</i>	54 ± 4	155 ± 14	106 ± 8
<i>T341I</i>	33 ± 4	106 ± 17	58 ± 7
<i>D521N</i>	81 ± 9	83 ± 8	29 ± 1
<i>P171Q</i>	22 ± 6	142 ± 29	115 ± 28
<i>T341M</i>	17 ± 3	53 ± 7	54 ± 5
<i>E527K</i>	95 ± 5	78 ± 24	28 ± 10
<i>P307R</i>	17 ± 5	222 ± 23 μM	23 ± 2
<i>SH2-Eng</i>	150 ± 4	58 ± 10	6.5 ± 0.5
<i>pY530</i>	340 ± 99	108 ± 28	25 ± 6
<i>Q529H</i>	14 ± 4	89 ± 9	49 ± 11
<i>T341R</i>	5.5 ± 0.9	48 ± 6	17 ± 1.4
<i>pY419-pY530</i>	79 ± 17	96 ± 6	118 ± 24
<i>pY530-pY530-R163W</i>	74 ± 4	82 ± 11	169 ± 13

Table 2.6: ATP and substrate peptide K_M and V_{max} values of all active mutations

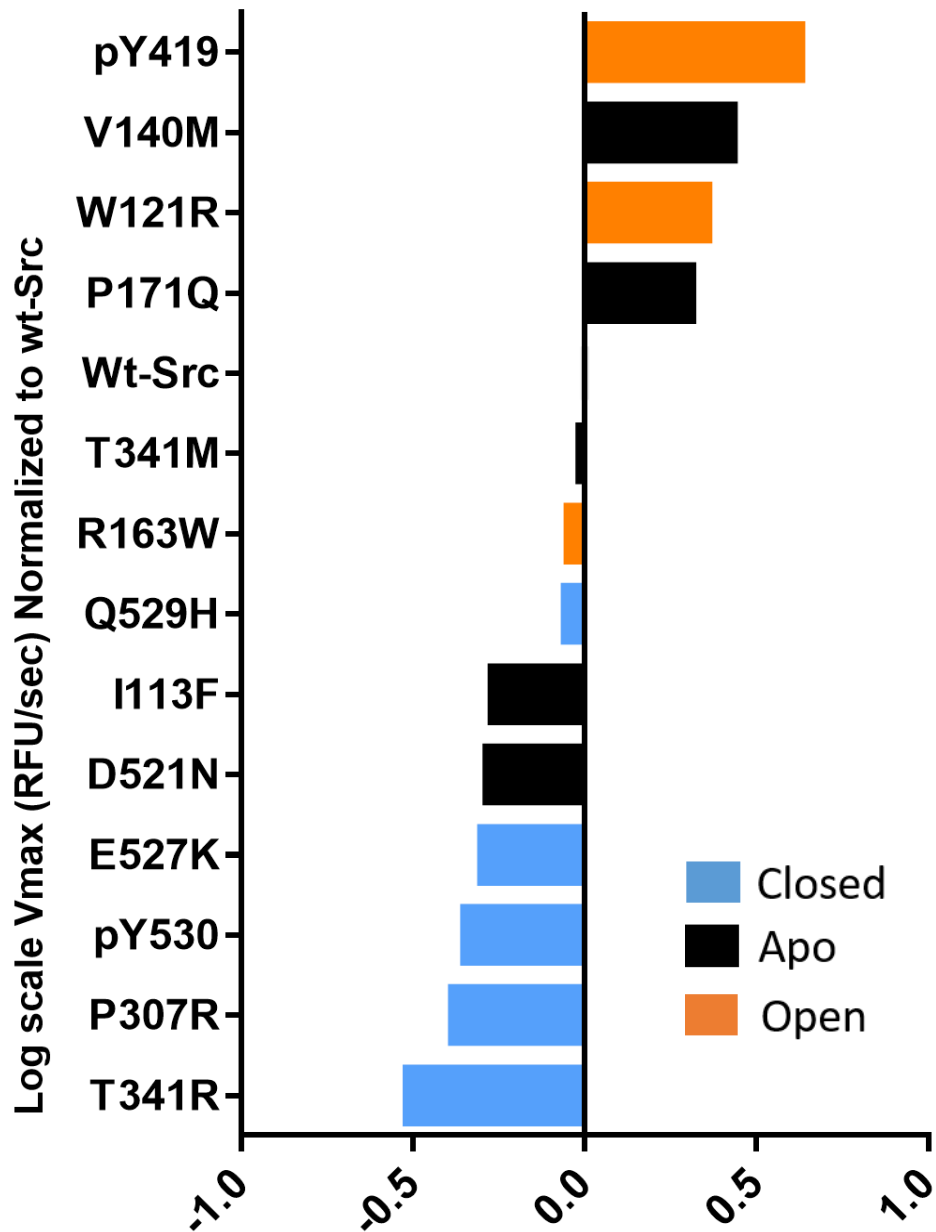


Figure 2.8: Vmax (RFU/sec) evaluated for those mutations with catalytic activity. Values were normalized to wt-Src which was set to 0. Higher catalytic activity compared to wt-Src are positive numbers and lower activity than wt-Src are negative numbers. Half lives from thermolysin assay added for each mutation and shown in colored bar graphs. Blue: closed, Black: Apo, and Orange: open.

Irtegun et. al. concluded, however, that c-Src might have a complex multi-state conformational states that regulate activity instead of the traditional "open" and "closed" states. Their conclusion arises from other studies of another Src family

kinase, Hck, which is shown to be activated by two different mechanisms.^{38,39} The first involving displacement of the SH3 domain by high-affinity SH3 ligands such as the Nef protein without, most interestingly, displacing the SH2 domain interaction with the C-terminal tail. Therefore, in this supposedly "closed" inactive conformation, which they suggest is most likely an intermediate conformation between fully open and fully closed, Hck is actually active. The second, is a reverse role of the domains, whereby the displacement of the SH2 domain with the SH3 domain still bound results in Hck activation. Taken together, this suggested that the proposed regulation mechanism of an open and closed conformation correlating to an active and inactive kinase respectively, is too simple of a model to encompass what has been observed.¹⁸ Also, this suggest that the different "new" conformations that have been found in Hck could happen in c-Src as well. Not surprisingly then, according to Gonfloni et al., these conformations do exist in c-Src.³³ In their pulldown experiments using a resin coupled SH3 optimal peptide, they found a higher amount of pulldown pY530-pY419 compared to pY530 c-Src. This suggested an increased accessibility of the SH3 domain of the doubly phosphorylated c-Src and hence this supposedly "closed" conformation is actually more like the intermediate conformational state described in Hck-Nef activation.³⁸

Interestingly, and perhaps rather confusingly, our thermolysin assay data of pY530-pY419, which should have shown a faster half-life due to the increased accessibility of the SH3 domain and thus indicating an open conformation, instead showed an extremely long half-life similar to pY530 and SH2-Eng, two closed c-Src constructs (Table 2.3). These results suggest a few things. Data from the thermolysin assay can actually give a crude physical image of global conformation, similar to SAXS and Hydrogen/Deuterium exchange MS techniques. Because thermolysin is a protease, it requires less steric hindrance to access the cleavage site on the SH2-linker and therefore cannot efficiently compete off a bound SH3-domain. Therefore, the long half-life of pY530-pY419 is an actual reflection of a still bound SH3-domain correlating to a closed global conformation.

The previous assumption that pY530-pY419 is most likely an intermediate state and not an actual closed state results from using a resin-bound SH3 optimal

peptide to look at SH3 domain accessibility. Because the resin bound SH3 peptide is small, it has the ability to compete with the SH2-linker for binding to the SH3 domain, thus making pY419-pY530 look artificially more open. In short, just because changes to the kinase domain, like phosphorylation of Y419 on pY530 can certainly make the SH3 domain bind worse, this does not indicate that the conformation is supposed to be more open. Instead, it is the pulldown assay using the resin bound SH3-peptide that makes the conformation look artificially more open.

In summary, pY419-pY530 is a closed c-Src conformation with catalytic activity. Phosphorylation at Y419 can indeed override conformational effects on activity suggesting activation loop phosphorylation plays a key role in orientating the kinase domain into a catalytically ready conformation but can also influence SH3 domain from binding as tightly as normal as shown in the resin-SH3 peptide pulldown assay.

2.6 Non-Clinical Mutation: W263A

How all this could happen is thru an H-bond network mechanism that starts with the activation loop conformation. Once positioned to perform catalysis (like the effect from pY419), this triggers a domino effect thru H-bond networks that causes the c-helix to swing inwards, forcing tryptophan 263 to dislodge, which could cause a change in the SH2-linker configuration to decrease binding of the SH3 domain, Figure 2.9. As such, this whole network system is how the activity of c-Src is regulated and has been explored before.⁴⁰ The vice versa could happen as well, where the tight binding of the SH3 domain to the SH2-linker causes tryptophan 263 to wedge itself into the c-helix, pushing the c-helix outwards, and simultaneously forcing the activation loop into a position that prevents catalysis.

We explored a part of this network by looking at W263, a conserved residue throughout protein tyrosine kinases, thru its mutation to alanine. There have been literature studies suggesting the tryptophan, in the regulation model explained above, is an important residue involved in catalysis by propagating "signals" from the catalytic kinase domain to the SH2/SH3 domains, triggering a conformational

change.^{36,41} LaFevre-Bernt et. al., tested this by mutating the tryptophan to an alanine in Hck and found a few things; 1.) Hck W263A is more active than wt Hck; 2.) autophosphorylation rates are higher; 3.) accessibility to the SH2 and SH3 domains are changed.⁴¹ Gonfloni et al, has also showed that W263A in c-Src in *S. pombe* assay can partly escape downregulation by Csk.⁴² Our thermolysin data for W263A shows an open conformation which agrees with LaFevre-Bernt et. al. finding in Hck that the SH2/SH3 domain is more accessible. In terms of activity however, W236A c-Src is 3.5 times less active but does bind increase ATP binding by 7-fold compared to wt-Src, Table 2.5. Perhaps, W263A mutation does not necessarily affect c-Src activity as much as it does Hck but the increase binding to ATP does correlate with previous speculation that W263, thru its rearrangement, causes changes in the catalytic ATP pocket.⁴³ It would be interesting to see the overall conformation of W263A-pY530 and its activity as this form of W263A was seen to escape regulation by Csk in the *S. pombe* assay, as well as its autophosphorylation rates at Y419.

2.7 Exploring R163W and W121R

Adding to the thermolysin assay, upon further inspection, some mutations and the conformations they stabilized can be logically explained. For example, the substitution of a bulkier side chain could prevent the domains from closing properly, the added positive/negative charge could lead to a repulsion (open) or a salt bridge/H-bond that would help keep c-Src closed, and etc. Mutations such as R163W and W121R (both open conformations) fits in this category. R163 located on the SH2 domain (but when c-Src is closed, at the interface between the kinase domain and SH2 domain) removes multiple salt bridge interactions with residues Q372, N400, E160, and D368 disrupting the native c-Src closed conformation, Figure 2.10. W121 sits in the SH3 domain and appears to fit in a small transient pocket created by the SH2-linker residues K260, A259, L258, G257, and Q256. Substituting tryptophan to arginine can disrupt this pocket along with the addition of a positive charge, which might lead to repulsive affects forcing c-Src to open (Figure 2.11). In short, both these mutations, R163W and W121R, prevents the closed conformation

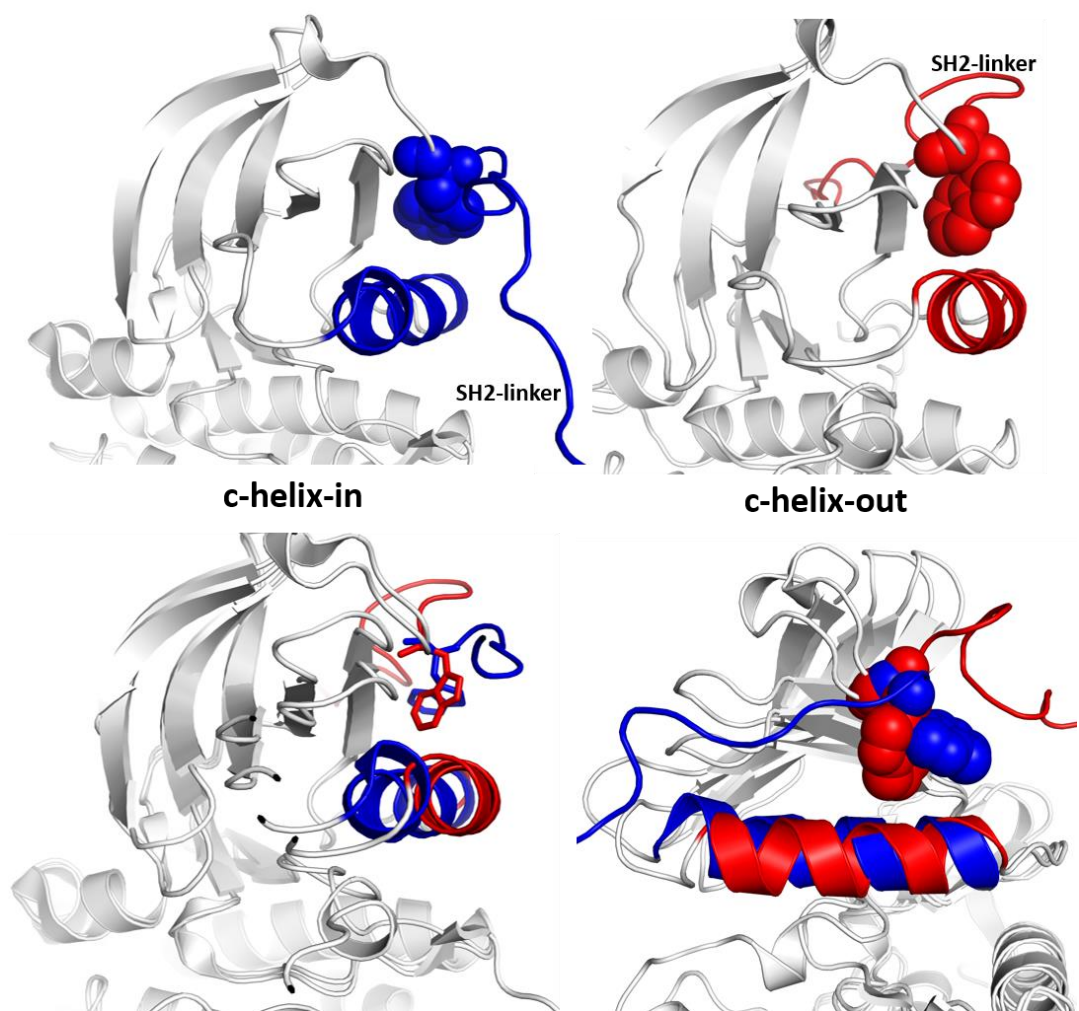


Figure 2.9: Top Left: c-helix-in crystal structure, 1Y57, c-helix and W263 is highlighted in blue. Top Right: c-helix-out crystal structure, 2Src, c-helix and W263 is highlighted in red. Bottom left is overlay of both crystal structure (blue is 1Y57, c-helix in; red is 2Src, c-helix-out) depicting the movement of the c-helix with regard to W263 position. Bottom right is same overlaid, view is from the side, depicting W263 in a space filled model. The positioning of W263 triggers the positioning of the c-helix as well as the SH2/SH3 domains. The SH2 linker is to show where the SH2/SH3 domains (not pictured) would be orientated. In 1Y57, a more open conformation, W263 is wedged in forcing the c-helix in, resulting in SH2/SH3 domain positioned in a more linear open conformation as shown in this picture, with the SH2 linker position coming toward the reader. In 2Src, a closed conformation, W263 is swung out resulting in a c-helix-out, resulting in SH2/SH3 domain to be clamped down alongside the back of the kinase domain, as depicted with the SH2-linker position going away from the reader, in a closed conformation.

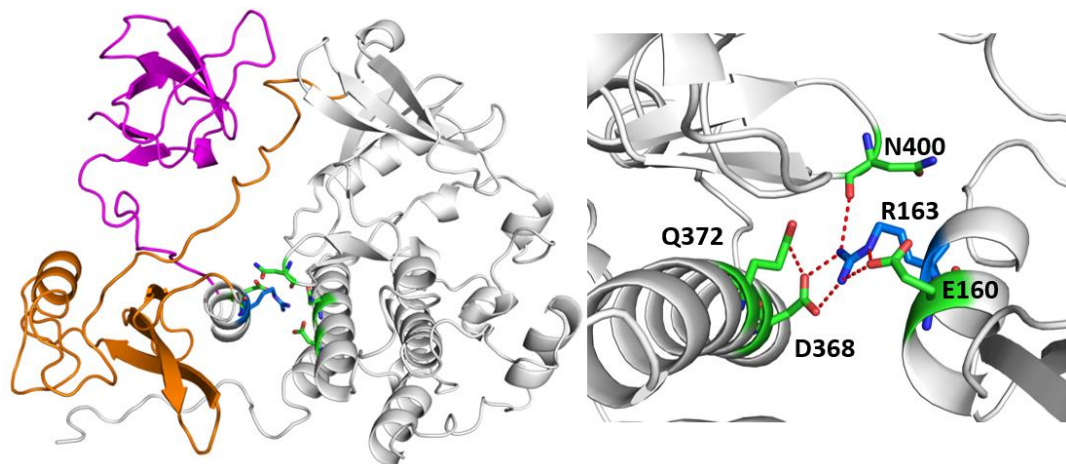


Figure 2.10: From PDB 2Src. Picture on left shows full length c-Src, SH3 (magenta), SH2 (orange), and kinase domain (white). R163 residue is highlighted in blue and the surrounding residues, N400, E160, D368, and Q372 are in green. Picture on right is a close up view, with red dotted lines from R163 that show the potential salt bridge/H-bonding that upon disruption by substitution to a tryptophan, might explain the more open conformation that results.

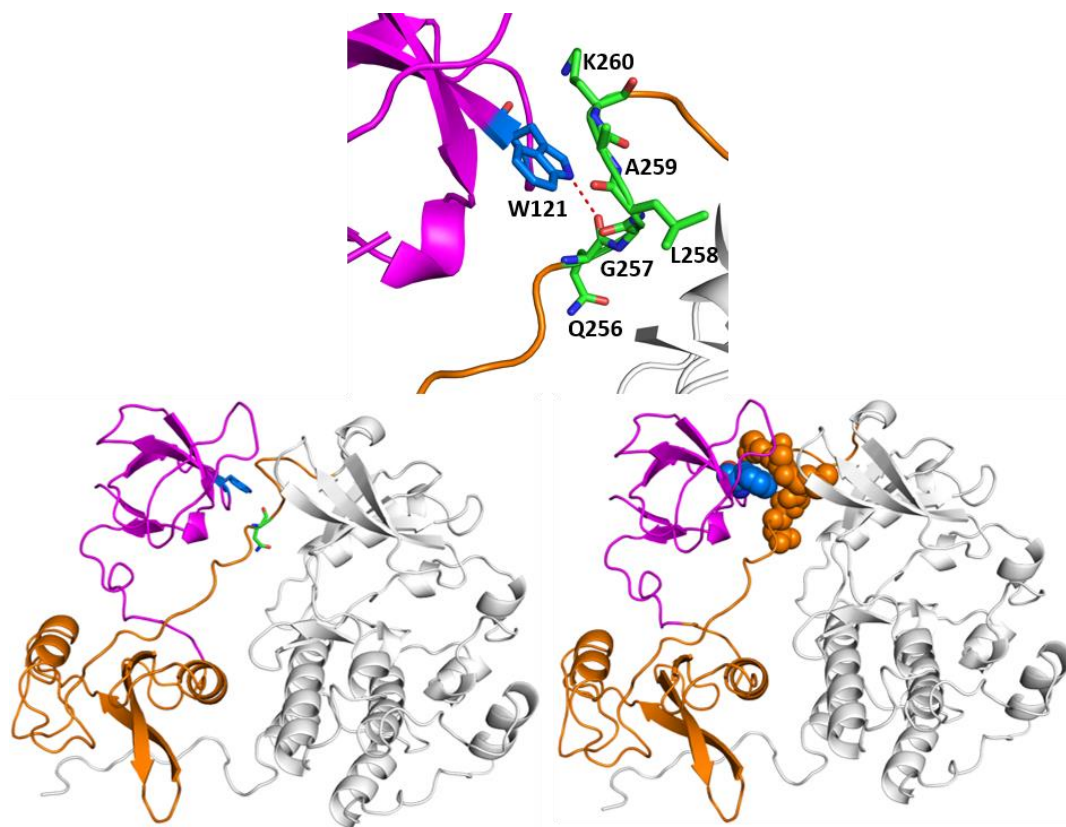


Figure 2.11: PDB 2Src. Top picture, depicts a close up of W121 lone H-bond partner to the backbone of G257. Bottom left is W121 in blue and G257 in green of the entire protein and bottom right depicts space filled image of W121 (blue) within the transient pocket formed by K260, A259, L258, G257, and Q256 of the SH2-linker

of c-Src from being stabilized, thus shifting the equilibrium state of c-Src towards more open conformations. Hence, the thermolysin assay demonstrates that these mutations are more open.

An argument could also be made for those mutations that don't contribute to any significant conformational changes compare to apo-wt Src because those substitutions neither add nor subtract an effect compared to the original amino acid. However upon a cursory glance, most other mutations don't make much sense in terms of how they are stabilizing their conformation. It is possible these mutations are involved with either stabilizing/disrupting a hydrogen bond network or hydrophobic spine within c-Src, contributing to the resulting conformation observed. Further mutagenesis studies would have to be performed to ascertain these answers.

2.8 Exploring Conformational Effects on Phosphorylation State

Since catalytic activity is found, in general, not to be directly dictated by conformations, we were curious to explore whether or not conformations could affect the phosphorylation state. Phosphorylation states can dictate the conformation of c-Src which influences its location in cells. As mentioned *vide supra*, c-Src can only signal other pathways when it is in close proximity to its substrates/protein binding partners and thus its localization in the cell is important. Localization of c-Src is dependent on its conformation which is mainly influenced by its phosphorylation states. Therefore, mutations that disturb this native phosphorylation balance by stabilizing conformations that are either more prone to activation by phosphorylation at Y419 or less prone to inactivation by escaping phosphorylation at Y530 can disrupt native c-Src localization. Since phosphorylation at Y419 is found to be an autophosphorylation event, different conformations may influence how well c-Src can associate with itself and hence how well it can autophosphorylate itself at Y419 on the activation loop. It has been found in c-Abl kinase (described in Chapter 1) that conformations of its SH2 domain does modulate the conformation of the activation loop and thus the phosphorylation state at that residue.⁴⁴ Naturally, we were curious if c-Src kinase, which is similar to c-Abl in structure, had an

activation loop that was similarly affected by the configuration of the SH2/SH3 domains. It is possible that open/apo/closed conformations allow different accessibility to Y419, leading to different phosphorylation states, and thus influencing its location in cells.

To demonstrate if these mutations affect phosphorylation states on Y419, three c-Src constructs were chosen. It was previously shown that c-Src can autophosphorylate itself at Y530 and thus to prevent this reaction from interfering, an additional Y530F mutation was introduced.^{18,33} The control apo construct is Y530F. Fully open mutation R163W-Y530F, D120N-Y530F (partly open) and closed mutation T341R-Y530F are the two conformational mutations used. These three constructs would allow us to assess if a mutation stabilized open/closed conformation would affect phosphorylation state at Y419. Over 1.5 hours, the c-Src constructs were incubated with 1mM ATP to autophosphorylate and the reaction was quenched at various time points. An SDS-PAGE gel was run and stained first with a phosphostain, which would fluoresce in the presence of phosphorylated proteins.

To assess the total amount of protein at each time point, the gel was stained afterwards with Sypro Ruby, which fluoresces in the presence of protein. With data of both total amount of protein and phosphorylated protein, we can calculate the percent conversion of phosphorylation at each time point and obtain a rate. The results are shown in Figure 2.12. It appears that there is no difference between the phosphorylation rates of apo Y530F and open D120N-Y530F as both are nearly 100% autophosphorylated in about 1 min. However, the close conformation, T341R-Y530F is much slower to autophosphorylate and does not even reach 100% phosphorylation. This does suggest that closed conformations are slower to autophosphorylate than more open conformations. The mutation-stabilized closed conformation decreases phosphorylation at Y419 probably due to decrease protein-protein interactions as it is necessary for c-Src to bind to itself first before it can autophosphorylate.

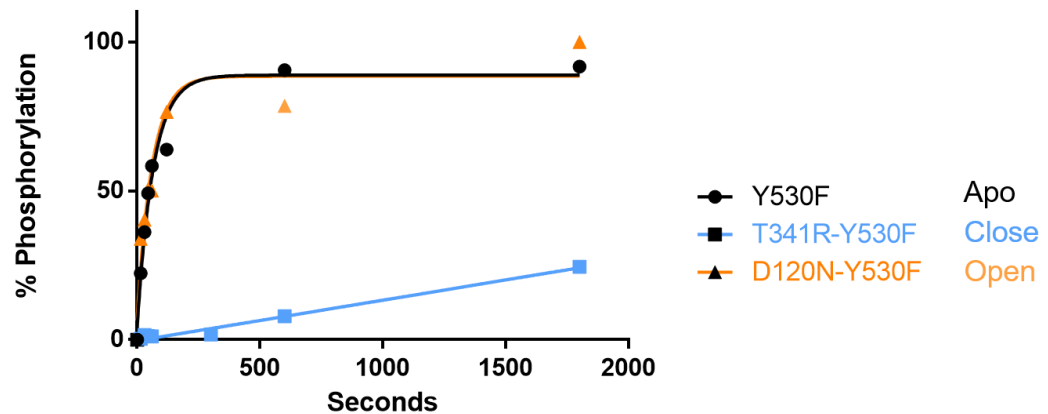


Figure 2.12: The percent phosphorylation of Y419 on Y530F, T341R-Y530F, and D120N-Y530F.

As mentioned above, phosphorylation states can affect conformational state of wt-Src but one aspect of this relationship we were curious about is whether or not phosphorylation states could affect mutation stabilized conformations. In other words, do phosphorylation at either Y419 and/or Y530 override the conformational states dictated by mutations? This is especially relevant *in cellulo* where c-Src has only ever been found in either a single phospho or double phospho state. To evaluate the effects of pY419 on an open/closed constructs, the pY419 versions of R163W-Y530F, D120N-Y530F, and T341R-Y530F were assessed in thermolysin assay. Given that R163W is already a mutation that is open, we were curious to see if given a slightly less open mutation, D120N, if pY419 was able to fully open the mutation to the same extent as R163W. Likewise, pY419-T341R-Y530F was also of particular interest and given its closed state, we were interested if pY419 could allow for a fully open conformation.

Phosphorylation at Y530 will most likely result in a closed conformation but we decided to see if this is true for an open stabilized mutation, R163W. To prevent autophosphorylation at Y419, the Y419F mutation was introduced and thereby it was R163W-Y419F that was assessed alongside Y419F, which was used as the

control apo construct. Thermolysin assay was used and unfortunately, at the time of this writing, the experiments have not been finished.

Next we explored the double phosphorylation state of c-Src in terms of mutations, where both Y419 and Y530 are phosphorylated. Previous studies have found double phosphorylation state in cells¹⁸, but not quite sure what the function serves. In our thermolysin assay as described above, pY530-pY419 is a closed state with greater catalytic activity than wt-Src but lower than pY419 alone. We were curious if an open stabilized mutation like R163W, upon phosphorylation at both Y419 and Y530, would be able to maintain a more open conformation and if it would be more active compared to wt-Src pY530-pY419.

Also, there were some mutations that were found to affect the $\beta 3/\alpha$ -C loop and activation loop which happened to escape Csk downregulation effects. Specifically in *S. pombe* assays, P302E-P307E mutation was found to be active and phosphorylated at Y419 which is shown as a decrease in *S. pombe* growth. Surprisingly, upon expression of P302E-P307E with Csk, growth of *S. pombe* was still effectively arrested. This happened with a few other mutations as well. The interesting result from their *S. pombe* assay is that pY530-pY419, while active in our activity assay, did not stop yeast growth. What is the difference between pY530-pY419 wt-Src and P302E-P307E-pY530-pY419? We decided to make P302E-P307E as well as L410A c-Src and look at both activity and conformational state. Is it possible that these mutations cannot be regulated by pY530 because these mutations stabilize a conformation that escapes regulation by Csk or their double phosphorylation state is far more active than pY530-pY419 wt-Src? At the time of this writing, the experiments have not yet been completed.

2.9 Conclusions

There have been reported c-Src clinical mutations, but these have not been characterized until our investigation. c-Src is the first proto-oncogene discovered, yet its role in cancer oncogenesis is poorly misunderstood. It is implicated in many cancers, usually due to overexpression, however its increased expression alone in

NIH 3T3 cells does not lead to cancer transformation. There has only been one reported case of an overactive mutation of c-Src that lead to cancer. If this is the case, then why are these clinical mutations present? If they are transformative, how do they disrupt c-Src's native function if these mutations do not increase catalytic activity?

Due to other literature studies, we wondered if these clinical mutations could be affecting conformational states, which in turn can influence phosphorylation state, localization, and protein-protein interactions. To answer the first fundamental question, we had to design a new high-throughput and robust assay, which uses the protease thermolysin. By cleaving the SH2-linker region that binds the SH3-domain, we found that the assay could give us a physical global conformational shape of c-Src similar to SAXS or hydrogen/deuterium exchange MS, albeit a rough version. Using the thermolysin protease assay, we tested 29 clinical and non-clinical mutations and found that mutations can affect conformational states.

Next, to probe SH2-domain accessibility we utilized a FITC-SH2-optimal peptide and measured the binding affinity to a few open/apo/closed mutations. We were interested to see FITC-SH2 peptide binding affinity could be equated to SH2-domain accessibility and then correlated to global conformations. Unfortunately, this was not the case as the FITC-SH2 peptide appeared to bind any open/apo/closed c-Src with similar binding affinity, leading us to believe that the SH2 domain is equally accessible in any global conformation.

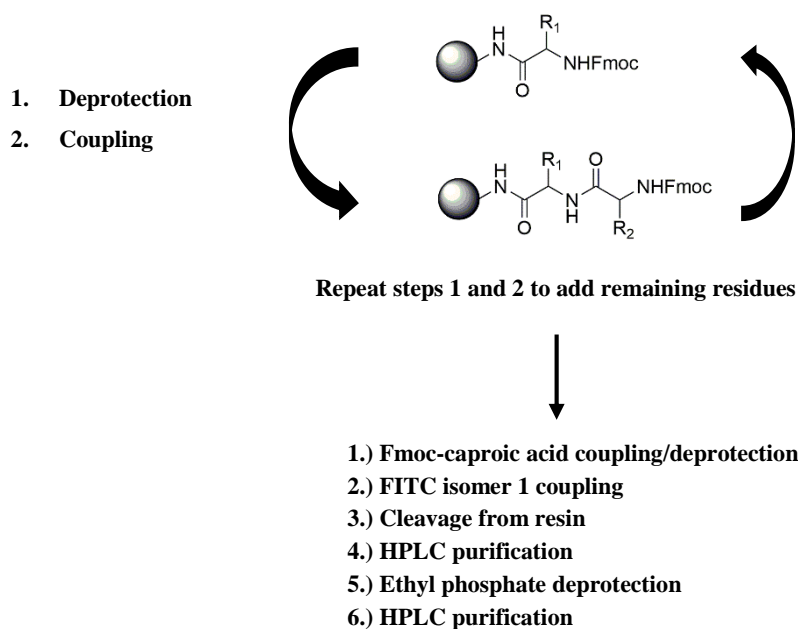
The activity of each active mutant was also characterized along with their binding affinity to ATP and peptide substrate. Most mutations were relatively similar in activity to wt-Src and as such, there does not appear to be any correlation between open conformations being more active than closed conformations. However, this result is most likely due to the individual point mutation affecting activity directly rather than affecting activity via altering conformations.

Since phosphorylation states can directly affect conformational states, we explored whether or not the opposite is true, can conformational states affect phosphorylation states at Y419 on the activation loop and Y530 on the C-terminus

tail. Using c-Src autophosphorylation, Y530F (apo), D120N-Y530F (open), R163W-Y5340F (open), and T341R-Y530F (closed) was tested to see if conformations can affect autophosphorylation rates at Y419, and it appears that there is a difference between closed conformation autophosphorylation rates (slower) compared to open conformation autophosphorylation rates (faster). This suggest that this is a mechanism in which mutations can cause c-Src dysfunction. By disrupting the native phosphorylation state balance, it can influence c-Src localization, thereby perturbing c-Src's proximity to its substrates and effecting when/how signal transduction pathways can get turned on/off.

Future studies will move this exploration of clinical mutations into the cells. Clinical mutations, thru CRISPR, can be natively transfected and assessed to see if there is any transformative potential. Overall phosphorylation status in the cells can be investigated to see possible signal transduction pathways these mutations affect, and further protein binding partners can be explored. To see if mutations, through conformational states, can affect localization, fluorescence microcopy experiments can be performed to track changes to its native location. Altogether, these future studies can build further understanding of c-Src's role in cancer progression. The thermolysin assay can also be applied to other kinases with 3 domains. Our lab is currently in the process of exploring c-Abl and c-Hck as the next kinases in which to explore conformational states.

2.10 Experimental Section



Scheme S2.1: Synthetic scheme for solid phase SH2-peptide (EPQpYEEIPIYL) synthesis

Peptide Synthesis: Standard solid phase Fmoc peptide synthesis using rink amide resin was performed. Briefly, to a 10 mL peptide synthesis vessel, rink amide resin (0.2 mmol) was added and swelled in deprotection solution (4 mL, 20% piperidine in NMP) for 30 min. The reaction solution was drained via vacuum filtration and the resin was rinsed with NMP (3x). In a separate vial, a solution of amino acid (0.3 mmol) and HBTU (0.3 mmol) in activator solution (5% DIPEA in NMP) was prepared and then added to the peptide synthesis vessel and agitated using a mechanical shaker for 1 hour. The reaction solution was removed via vacuum filtration and crude resin was rinsed with NMP (3x). Kaiser test was performed to ensure complete coupling before deprotection solution was added, vessel sealed and agitated for 30 min. Afterwards, the solution was drained and washed with NMP (3x) and Kaiser test was done to ensure Fmoc deprotection was complete. The coupling-deprotection sequence was repeated with the amino acids necessary to afford the final desired peptide. Fmoc-caproic acid (0.3 mmol) was added after the addition of the final amino acid and reacted overnight. After subsequent Fmoc deprotection, FITC isomer 1 (0.3 mmol) and coupling solution was added and

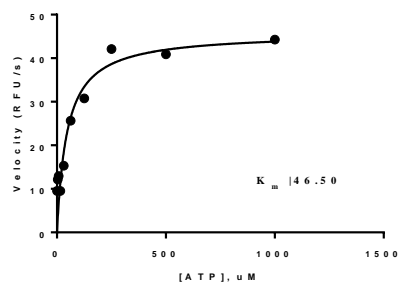
agitated overnight. Once coupled, the solution was drained and rinsed with NMP (3x) and dichlormethane (3x). The peptide was cleaved from resin using trifluoroacetic acid (TFA) solution (95% TFA, 2.5% water, 2.5% triisopropylsilane). TFA cleavage solution was drained and TFA was removed under pressure before ether precipitation. The resulting pellet was collected and dissolved in DMSO and purified using reverse phase HPLC (20%-60% acetonitrile in water). The ethyl protected phosphotyrosine was deprotected using 1 molar equivalent TMS-Br in acetonitrile at r.t. overnight. Afterwards, water was added to the reaction and acetonitrile removed under pressure. The peptide was then purified by reverse phase HPLC (20%-60% acetonitrile in water).

Biochemical Characterization

Determination of ATP K_M

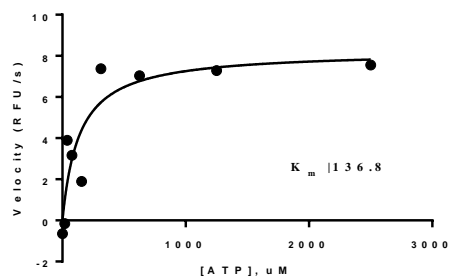
General procedure for ATP K_m determination. The previously described fluorescence assay²² was used to determine K_m values. Reaction volumes of 50 μ L were used in 96-well plates. 42.5 μ L of enzyme in buffer was added to each well. 1.25 μ L of DMSO was then added followed by 1.25 μ L of a substrate peptide (“compound 3” as described in Wang et al)²² solution (1.8 mM in DMSO). The reaction was initiated with 5 μ L of the appropriate ATP dilution (typically 1000, 500, 250, 125, 62.5, 31.3, 15.6, 7.8, 3.9, 2.0 μ M in H₂O) and reaction progress was immediately monitored at 405 nm (ex. 340 nm) for 10 minutes. Reactions had final concentrations of 60 nM enzyme, 45 μ M peptide substrate, 100 μ M Na₃VO₄, 100 mM Tris buffer (pH 8), 10 mM MgCl₂, 0.01% Triton X-100. The initial rate data collected was used for determination of K_m values. For K_m determination, the kinetic values were obtained directly from nonlinear regression of substrate-velocity curves in the presence of varying concentrations of ATP. The equation $Y = (V_{max} * X)/(K_m + X)$, X = substrate concentration (μ M) and Y = enzyme velocity (RFU/s); was used in the nonlinear regression. Each ATP K_m value was determined using at least three independent experiments; a representative K_m curve is shown.

ATP K_M Curves



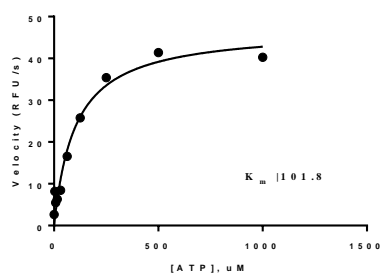
wt-Src

ATP $K_M = 43 \pm 5 \mu\text{M}$



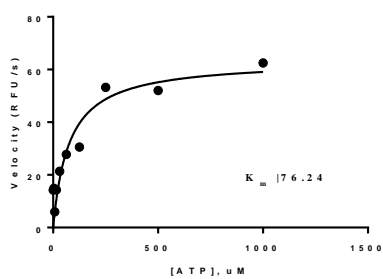
SH2-Eng

ATP $K_M = 148 \pm 11 \mu\text{M}$



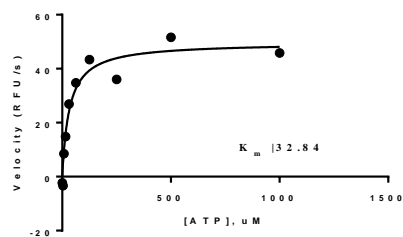
I113F

ATP $K_M = 111 \pm 12 \mu\text{M}$



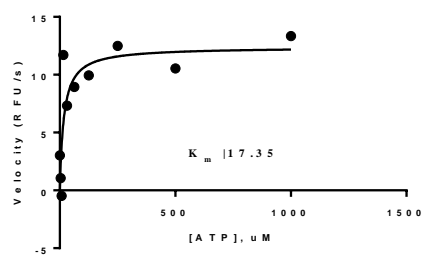
D521N

ATP $K_M = 81 \pm 9 \mu\text{M}$



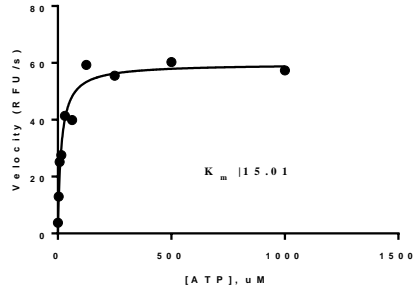
R163W

ATP $K_M = 31 \pm 4 \mu\text{M}$

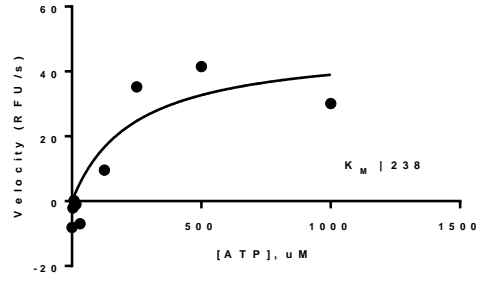


P307R

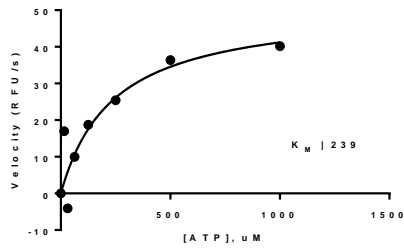
ATP $K_M = 17 \pm 5 \mu\text{M}$



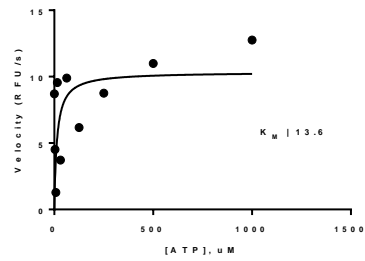
T341M
ATP $K_M = 17 \pm 3 \mu\text{M}$



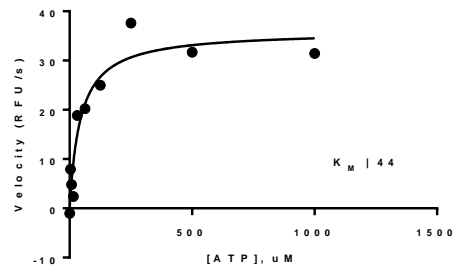
R483W
ATP $K_M = 215 \pm 34 \mu\text{M}$



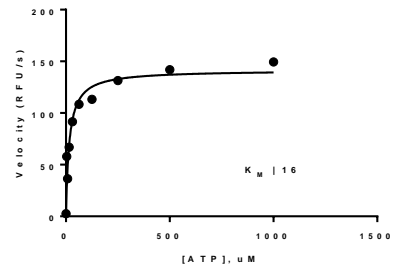
pY419-Y530F
ATP $K_M = 215 \pm 47 \mu\text{M}$



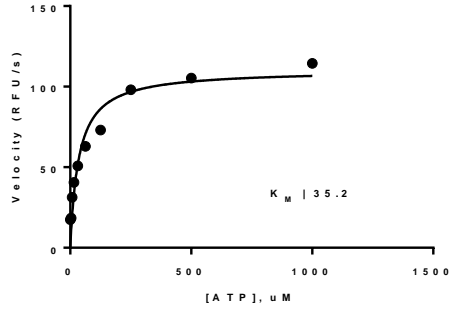
W263A
ATP $K_M = 7 \pm 3.5 \mu\text{M}$



T341R
ATP $K_M = 53 \pm 8 \mu\text{M}$

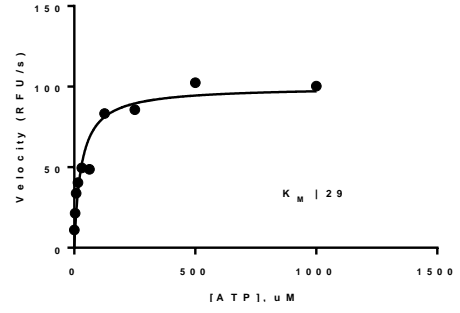


T341M-A406S
ATP $K_M = 13 \pm 3 \mu\text{M}$



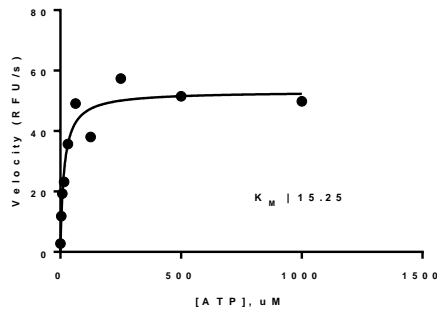
V140M

ATP $K_M = 35 \pm 7 \mu\text{M}$



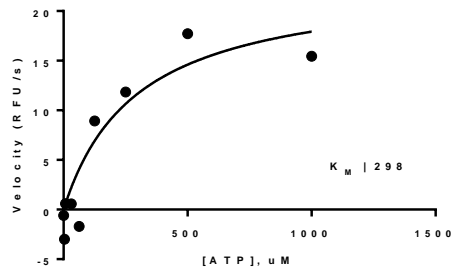
P171Q

ATP $K_M = 22 \pm 6 \mu\text{M}$



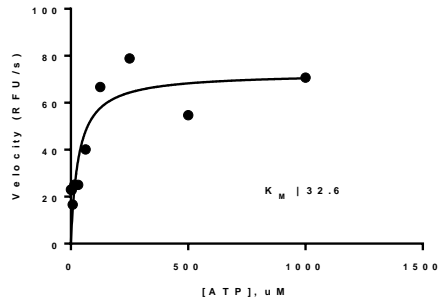
W121R

ATP $K_M = 20 \pm 4 \mu\text{M}$



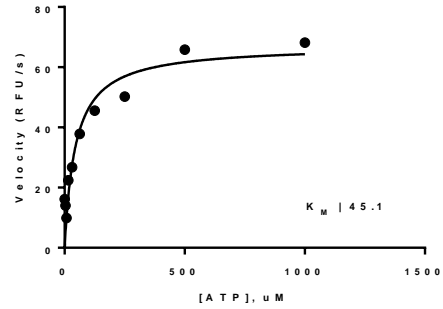
pY530-Y419F

ATP $K_M = 340 \pm 99 \mu\text{M}$



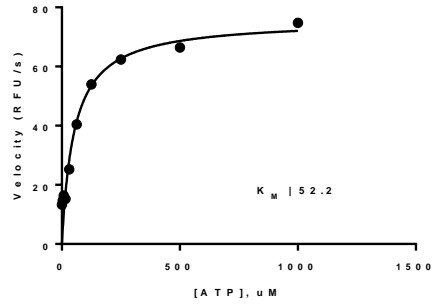
R98W

ATP $K_M = 34 \pm 5 \mu\text{M}$

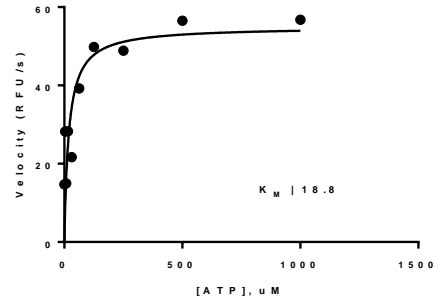


Y419F

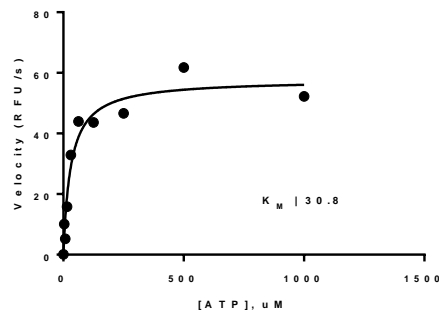
ATP $K_M = 46 \pm 1 \mu\text{M}$



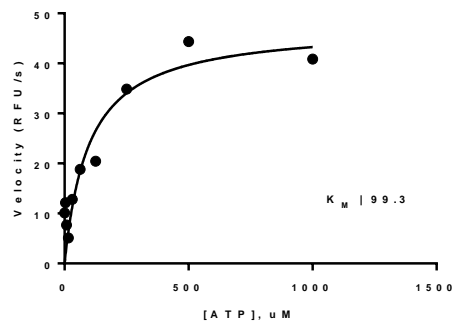
Y530F
ATP $K_M = 54 \pm 4 \mu\text{M}$



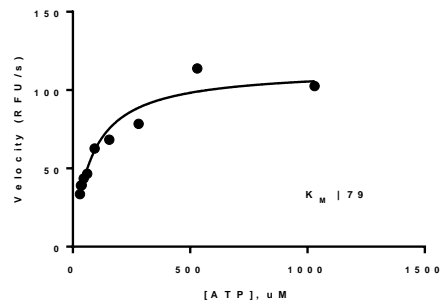
Q529H
ATP $K_M = 14 \pm 4 \mu\text{M}$



T341I
ATP $K_M = 33 \pm 4 \mu\text{M}$



E527K
ATP $K_M = 95 \pm 5 \mu\text{M}$

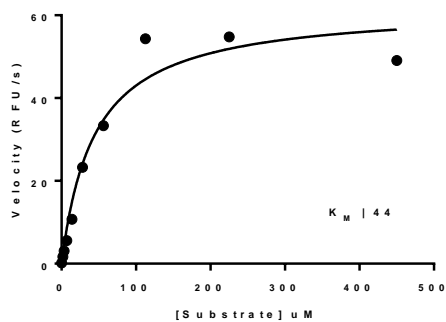


pY419-pY530
ATP $K_M = 79 \pm 17 \mu\text{M}$

Determination of substrate (compound 3) K_M

General procedure for substrate (pyrene) K_m determination. Similar to ATP K_M determination as written above except 1.25 μL of substrate peptide (“compound 3”) was added in the appropriate dilution (typically 450, 225, 112.5, 56, 28, 14, 7, 3.5, 1.7 μM in DMSO) and the reaction was initiated with 5 μL of 10mM ATP.

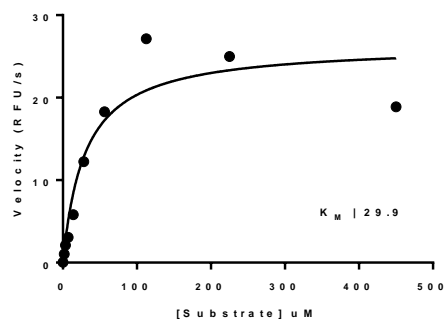
Substrate K_M Curves:



Wt-Src

Substrate $K_M = 43 \pm 2 \mu\text{M}$

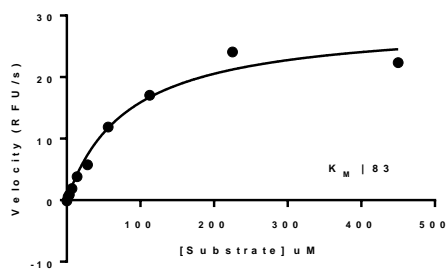
$V_{\max} = 56 \pm 6$



I113F

Substrate $K_M = 24 \pm 4 \mu\text{M}$

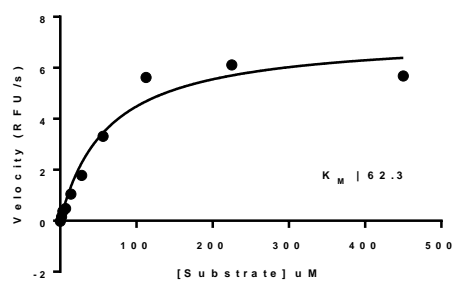
$V_{\max} = 30 \pm 5$



D521N

Substrate $K_M = 83 \pm 8 \mu\text{M}$

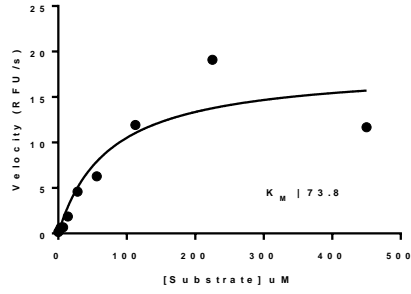
$V_{\max} = 29 \pm 1$



SH2-Eng

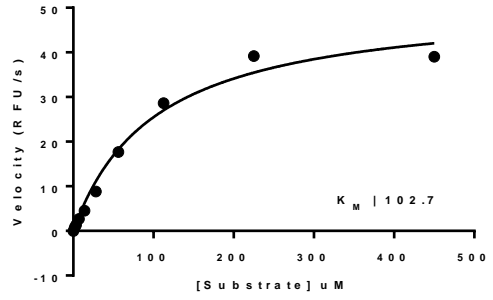
Substrate $K_M = 58 \pm 10 \mu\text{M}$

$V_{\max} = 6.5 \pm 0.5$



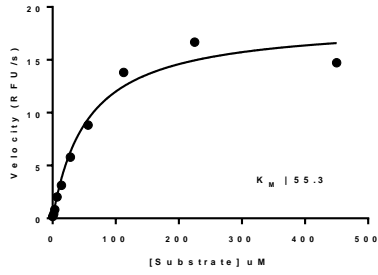
W263A

Substrate $K_M = 65 \pm 14 \mu\text{M}$
 $V_{\text{max}} = 16 \pm 0.2$



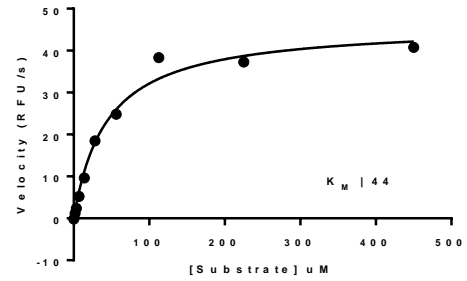
R163W

Substrate $K_M = 102 \pm 7 \mu\text{M}$
 $V_{\text{max}} = 50 \pm 5$



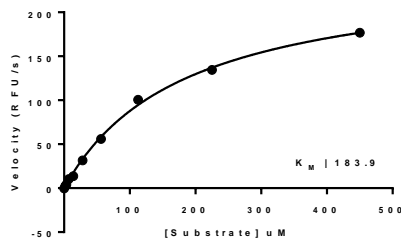
T341R

Substrate $K_M = 48 \pm 6 \mu\text{M}$
 $V_{\text{max}} = 17 \pm 1.4$



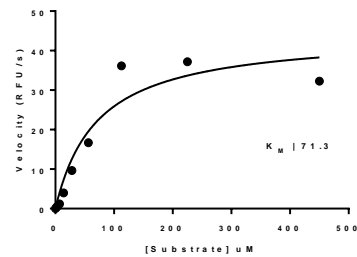
T341M

Substrate $K_M = 53 \pm 7 \mu\text{M}$
 $V_{\text{max}} = 54 \pm 5$



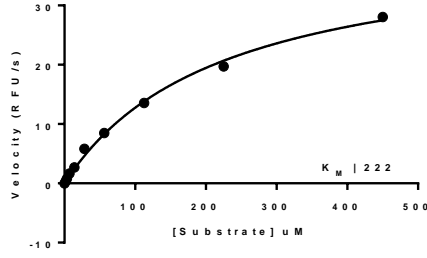
pY419-Y530F

Substrate $K_M = 169 \pm 18 \mu\text{M}$
 $V_{\text{max}} = 239 \pm 8$



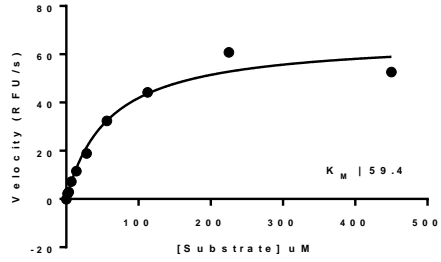
R483W

Substrate $K_M = 55 \pm 15 \mu\text{M}$
 $V_{\text{max}} = 35 \pm 6$



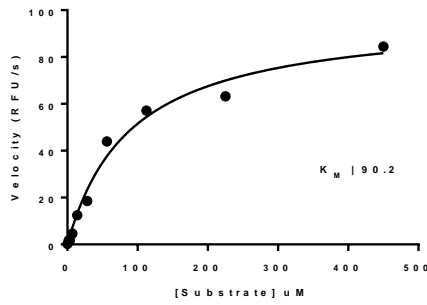
P307R

Substrate $K_M = 222 \pm 23 \mu\text{M}$
 $V_{\text{max}} = 23 \pm 2$



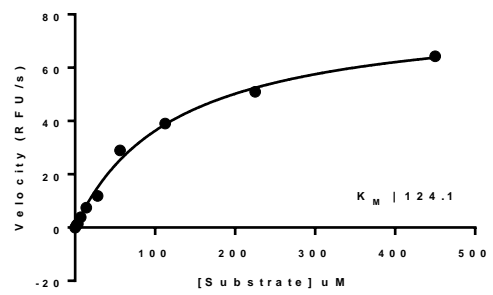
T341M-A406S

Substrate $K_M = 50 \pm 7 \mu\text{M}$
 $V_{\text{max}} = 74 \pm 6$



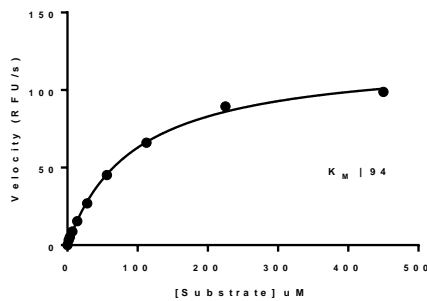
V140M

Substrate $K_M = 104 \pm 8 \mu\text{M}$
 $V_{\text{max}} = 152 \pm 1$



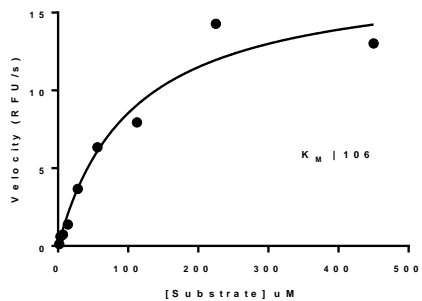
P171Q

Substrate $K_M = 142 \pm 29 \mu\text{M}$
 $V_{\text{max}} = 115 \pm 28$



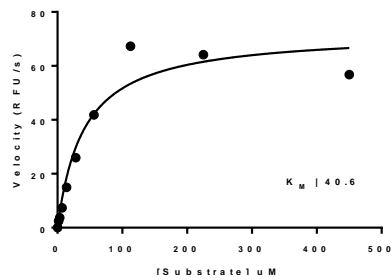
W121R

Substrate $K_M = 101 \pm 26 \mu\text{M}$
 $V_{\text{max}} = 128 \pm 21$



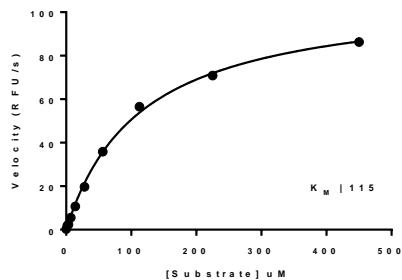
pY530-Y419

Substrate $K_M = 108 \pm 28 \mu\text{M}$
 $V_{\text{max}} = 25 \pm 6$



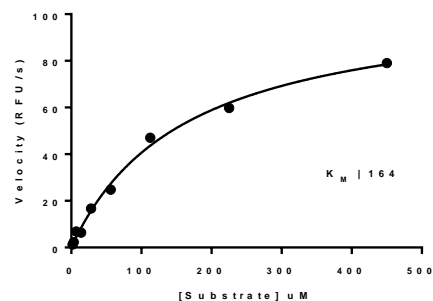
R98W

Substrate $K_M = 42 \pm 4 \mu\text{M}$
 $V_{\text{max}} = 74 \pm 7$



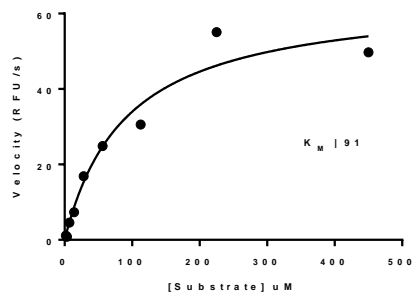
Y419F

Substrate $K_M = 127 \pm 14 \mu\text{M}$
 $V_{\text{max}} = 99 \pm 12$



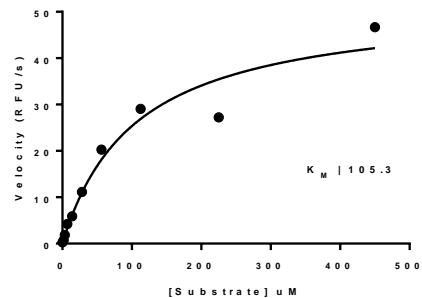
Y530F

Substrate $K_M = 155 \pm 14 \mu\text{M}$
 $V_{\text{max}} = 106 \pm 8$



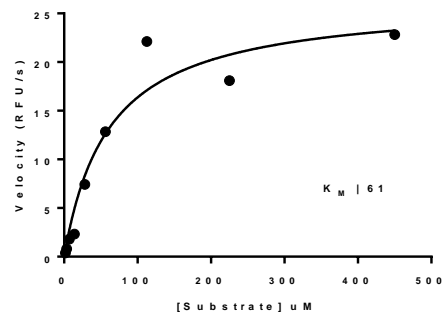
Q529H

Substrate $K_M = 89 \pm 9 \mu\text{M}$
 $V_{\text{max}} = 49 \pm 11$



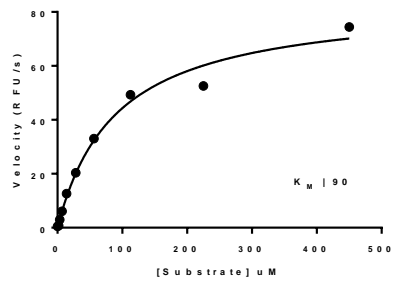
T341I

Substrate $K_M = 106 \pm 17 \mu\text{M}$
 $V_{\text{max}} = 58 \pm 7$



E527K

Substrate $K_M = 78 \pm 24 \mu\text{M}$
 $V_{\text{max}} = 28 \pm 10$



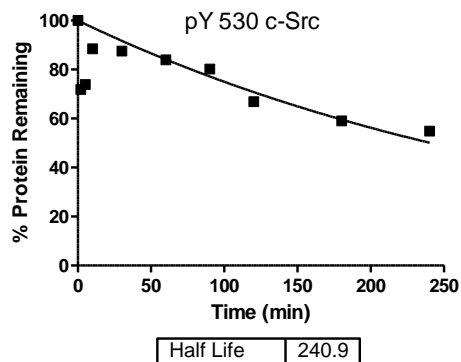
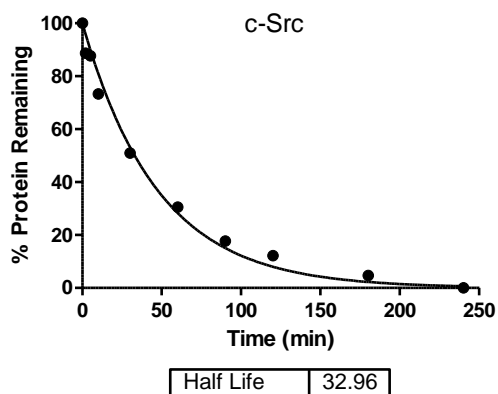
pY419-pY530

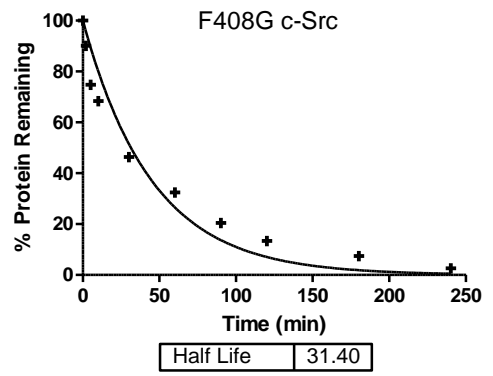
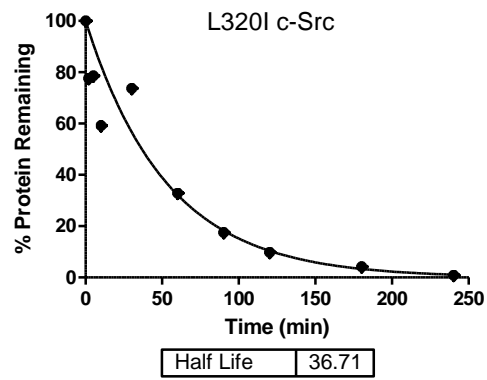
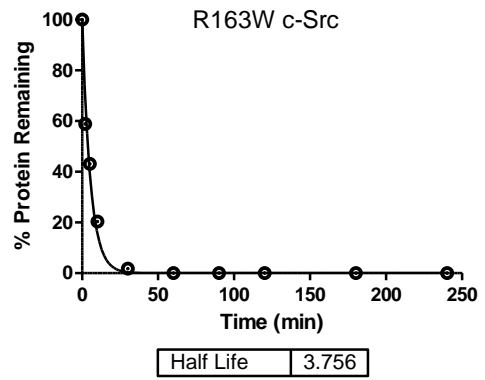
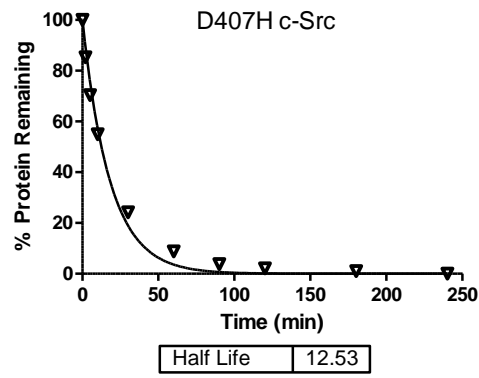
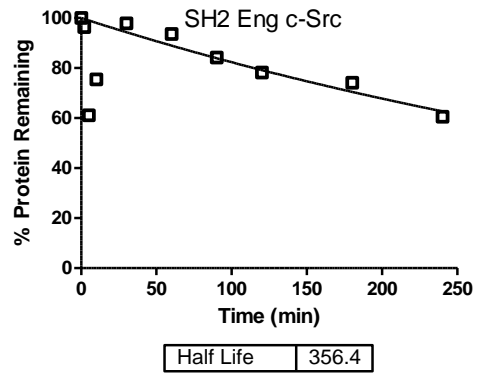
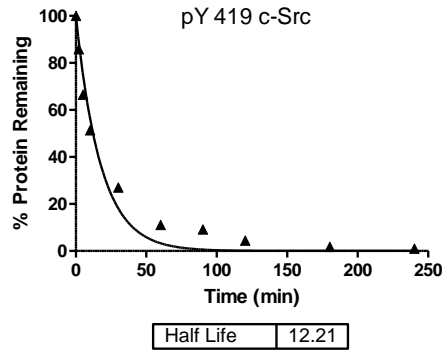
Substrate $K_M = 96 \pm 6 \mu\text{M}$

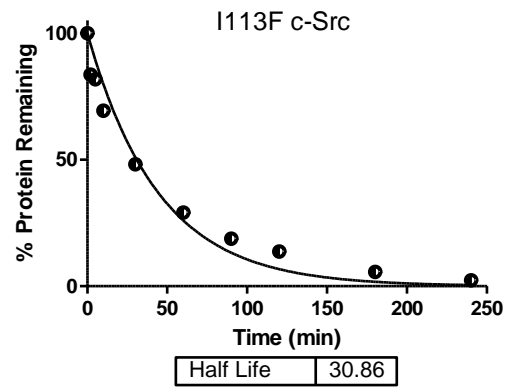
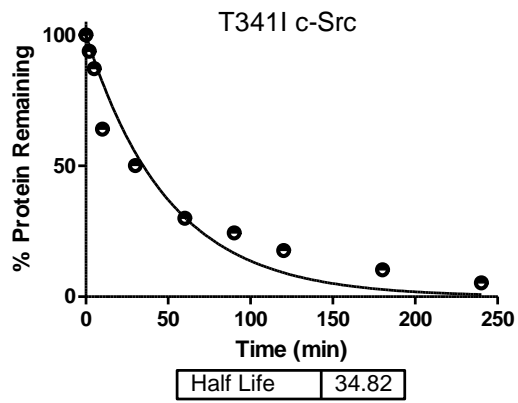
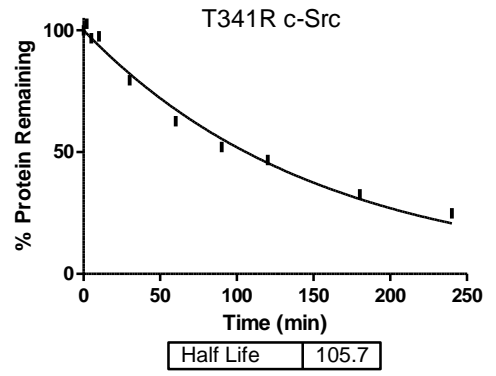
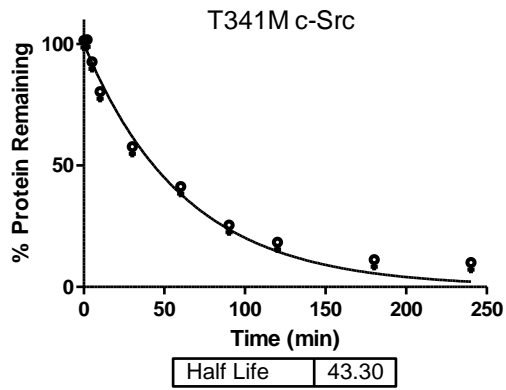
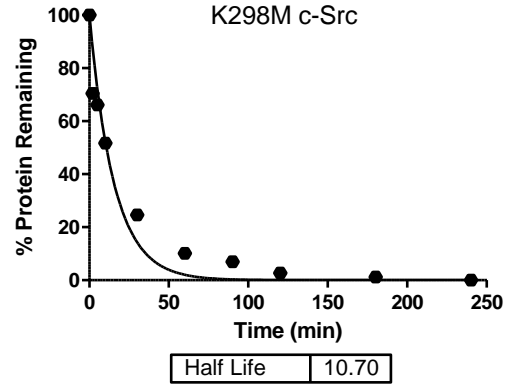
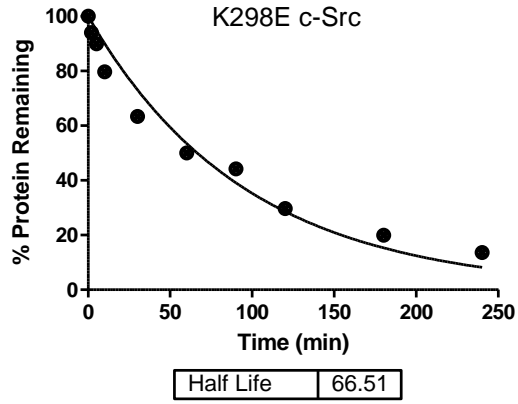
$V_{\text{max}} = 118 \pm 24$

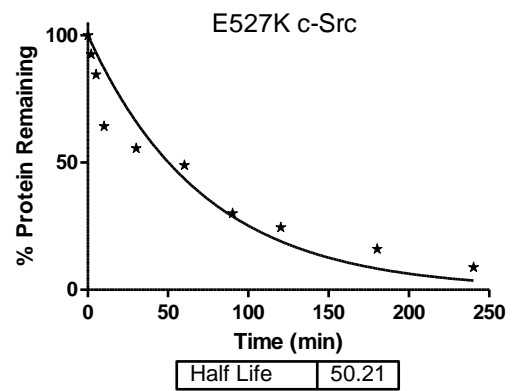
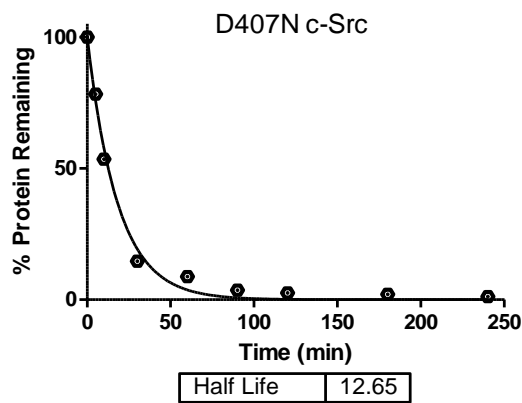
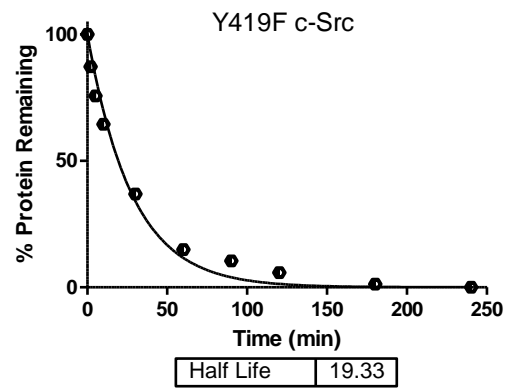
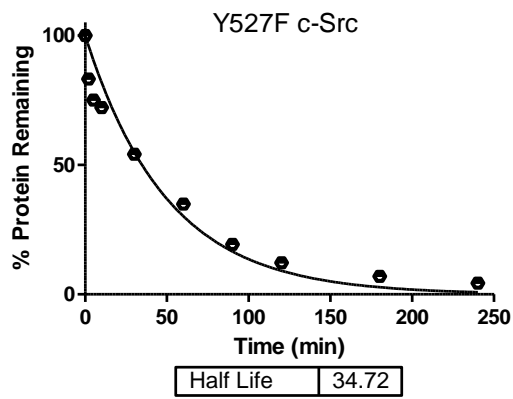
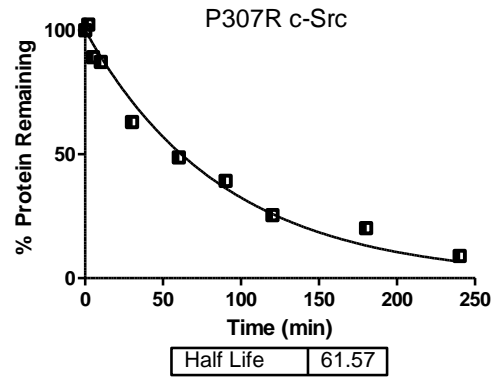
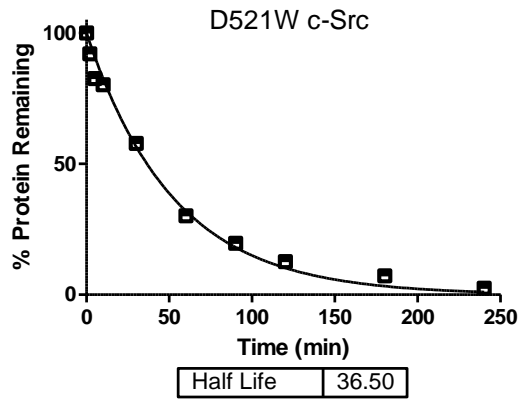
Thermolysin Half Life Assay

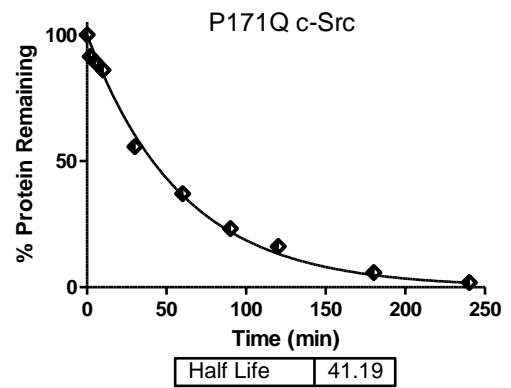
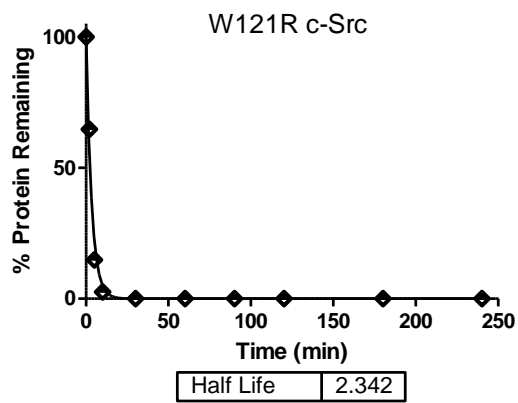
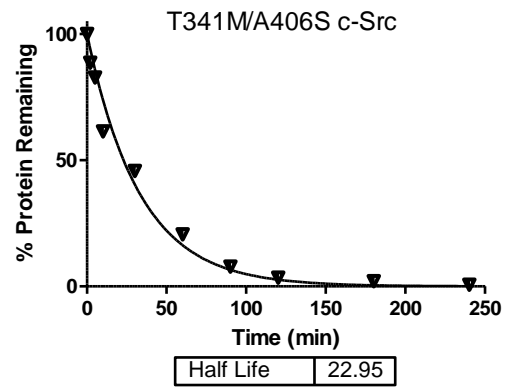
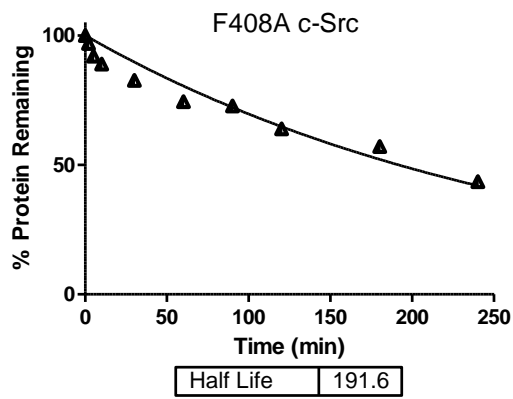
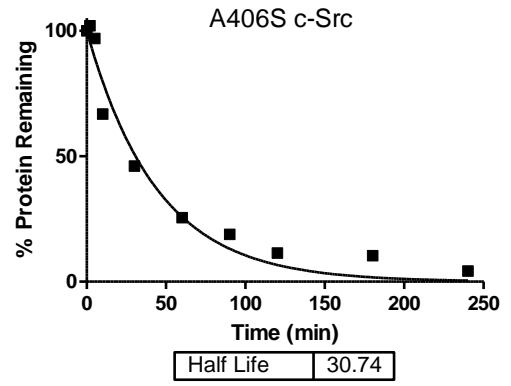
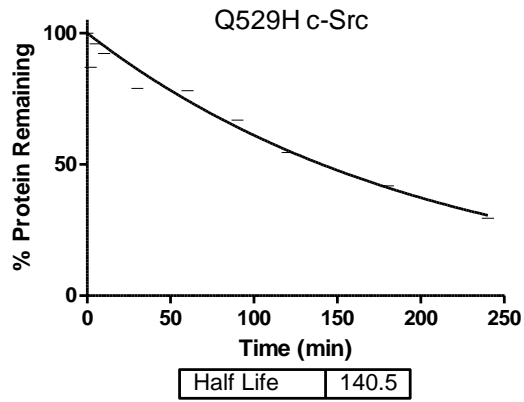
c-Src and c-Src mutants were diluted in proteolysis buffer (50 mM Tris-HCl pH 8.0, 100 mM NaCl, 0.5 mM CaCl₂) to yield a final protein concentration of 2 μM. Thermolysin from a 3.8 μM stock solution was added to the reaction mixture to a final concentration of 60 nM. 15 μL of the proteolysis reaction was added to 5 μL of 50 mM EDTA to quench proteolysis at various time points and stored at -20 °C. The quenched samples were analyzed by SDS-PAGE (12 % Bis-Tris gel in MES running buffer, staining with comassie blue). Band intensities were analyzed by ImageJ imaging software. Percent protein remaining was plotted against time and fit to an exponential decay equation to obtain the half-life of the protein using GraphPad Prizm software.

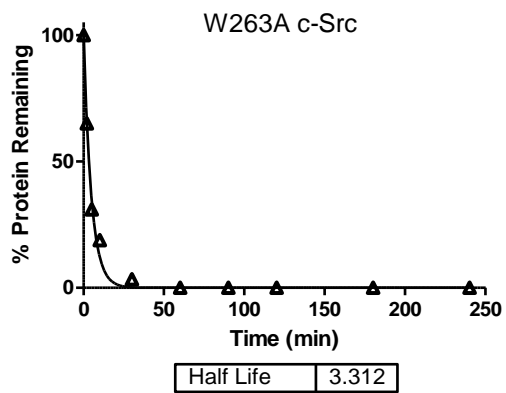
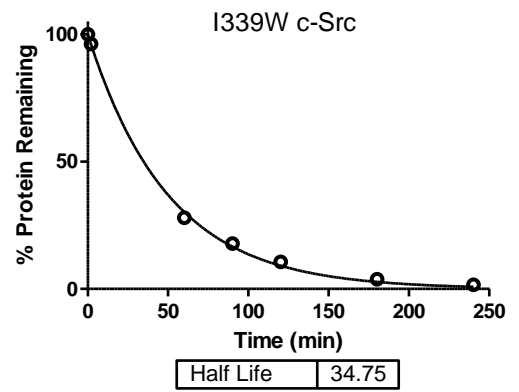
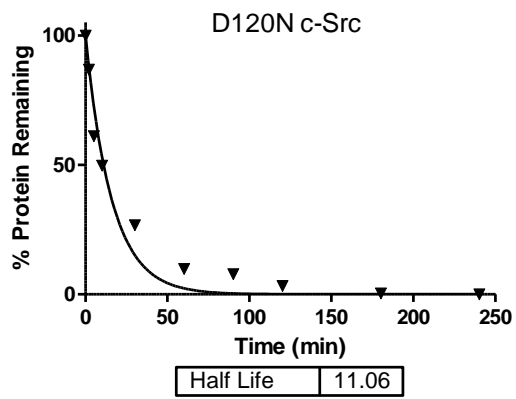
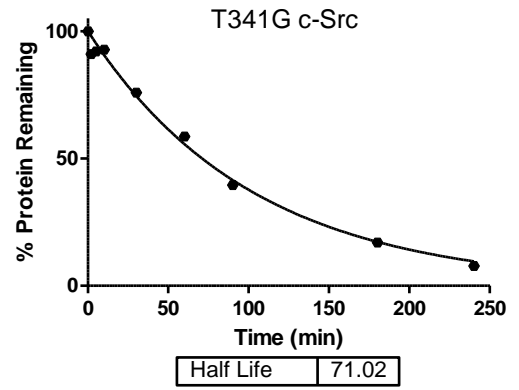
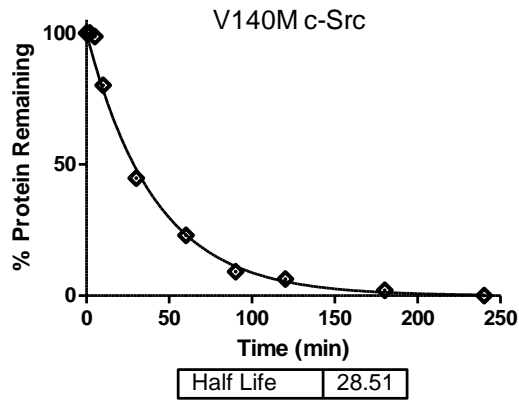






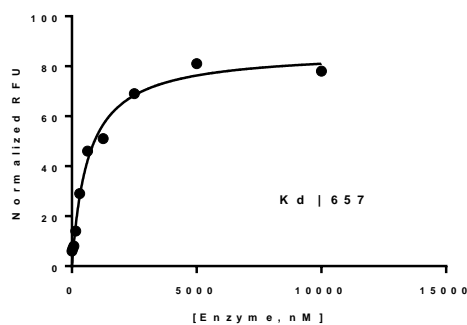






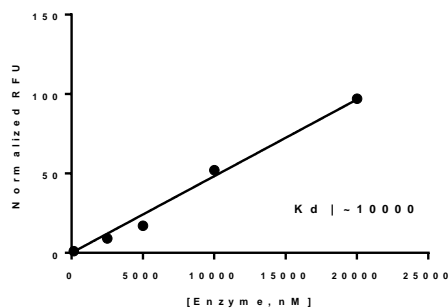
FITC SH2-peptide Fluorescence Polarization

General procedure for K_d determination using FITC- EPQpYEEIPIYL. Reactive volumes of 50 μL were used in 96-well plates. Enzyme in 50 mM Tris buffer (pH 8), 5% glycerol, and 100 mM NaCl, was diluted 2-fold (49 μL) over 10 wells. Final concentration of 200 nM FITC-SH2-peptide (10 μM stock in DMSO, 1 μL) was added to every well and allowed to incubate for 30 min. Blank well, which consisted of buffer and 200 nM FITC-SH2 peptide was included to subtract out the background signal. For K_d determination, the values were obtained directly from the nonlinear regression one-site binding curves (using data with background signal subtracted) in the presence of various concentrations of the enzyme. The equation $Y = (B_{\text{max}} * X)/(K_d + X)$; was used in the nonlinear regression. 3 runs were averaged together for each reported value. A represented K_d curve is shown



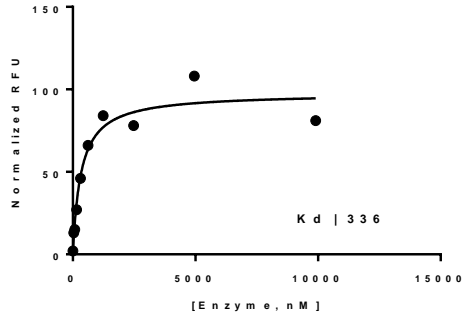
Wt-Src

FITC-SH2-peptide $K_d = 729 \pm 87$ nM

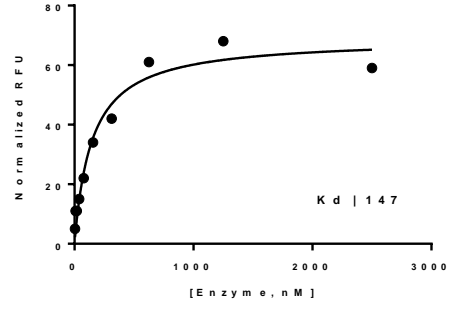


pY419

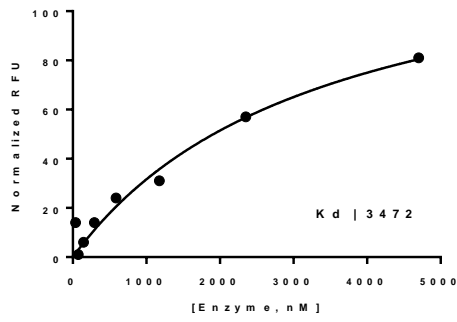
FITC-SH2-peptide $K_d = \sim 10,000$ nM



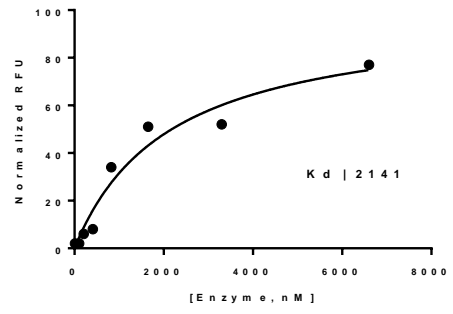
R163W
FITC-SH2-peptide $K_d = 397 \pm 89$ nM



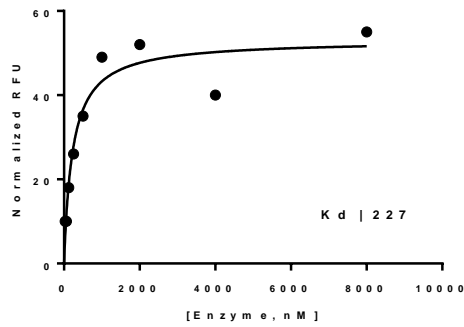
D407H
FITC-SH2-peptide $K_d = 146 \pm 12$ nM



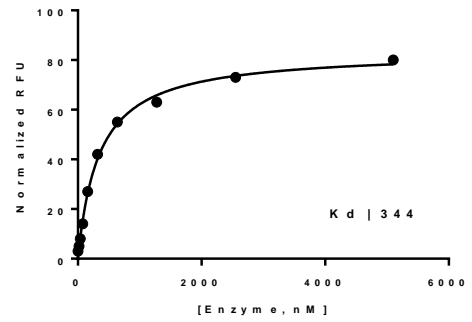
T341R
FITC-SH2-peptide $K_d = 3472$ nM



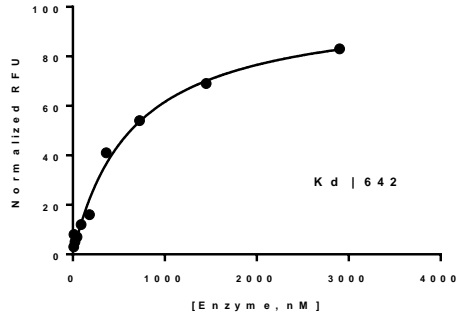
K298M
FITC-SH2-peptide $K_d = 2737 \pm 956$ nM



F408G
FITC-SH2-peptide $K_d = 297 \pm 51$ nM

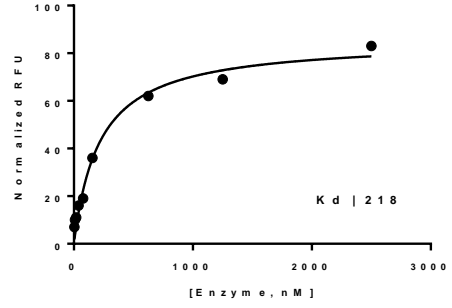


I113F
FITC-SH2-peptide $K_d = 332 \pm 18$ nM



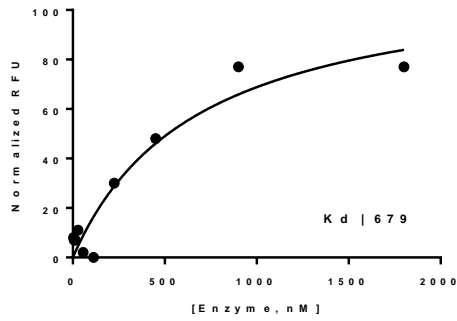
F408A

FITC-SH2-peptide $K_d = 699 \pm 32$ nM



K298E

FITC-SH2-peptide $K_d = 192 \pm 21$ nM

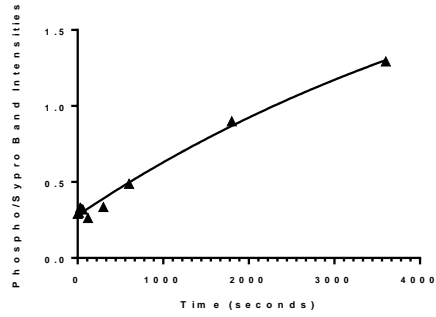


Y419F

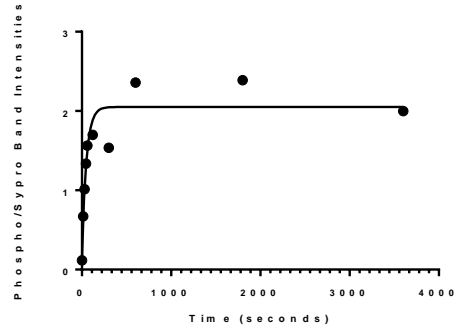
FITC-SH2-peptide $K_d = 682 \pm 47$ nM

Autophosphorylation Assay

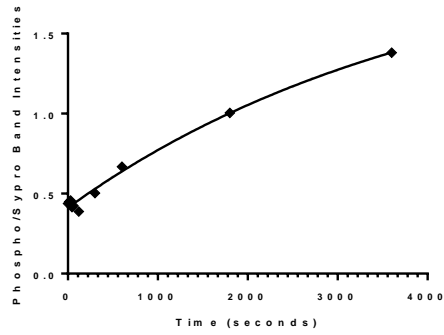
To determine the rate of autophosphorylation at Y419 on the activation loop of c-Src. Final concentration of c-Src (Y530F, D120N-Y530F, R163W-Y530F, T341R-Y530F) used is 2 μ M. The reaction mixture consist of $MgCl_2$ (10 mM), Na_3VO_4 (20mM), Triton X-100 (0.1%), and Buffer D (50 mM Tris (pH = 8), 100 mM NaCl, 5% glycerol). ATP (50mM) was added to initiate the reaction and incubated at 37 °C. At various time points (0, 15, 30, 45, 60, 180 sec and 5, 10, 30, 60 min) 15 μ L of the reaction mixture was taken out and quenched with 5 μ L of formic acid. Afterwards, 2 μ L of SDS-PAGE loading dye was added and analyzed by SDS-PAGE (12% Bis-Tris gel in MES running buffer. The gel was first stained with Invitrogen Pro-Q Diamond phosphoprotein gel stain as per instructions, and imaged on Typhoon 9410 using an excitation of 532 nm (green laser) and emission filter of 560 nm. Afterwards, the gel was post stained with Invitrogen Sypro Ruby protein gel stain as per instructions, and imaged on Typhoon 9410 using an excitation of 532 nm (green laser) and emission filter of 610 nm. Band intensities from both the Sypro ruby stain and phosphoprotein gel stain were analyzed by ImageJ software. The phosphoprotein gel stain showed amount of protein phosphorylated and Sypro ruby shows the total amount of protein loaded in each well. Taken together, both band intensities would show percent protein phosphorylated and was plotted against time and fit to non-linear regression curve to obtain the amount of time needed for half the amount of c-Src to be phosphorylated at Y419. Sample gels are shown as well as plot data.



T341R-Y530F
 Half Life = 4077 sec
 Plateau = 2.5

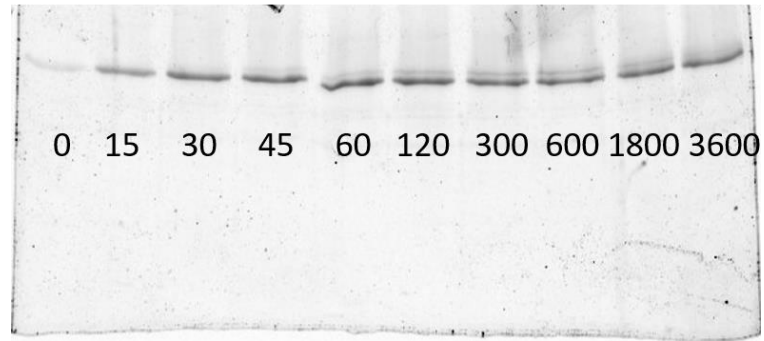


Y530F
 Half Life = 34 sec.
 Plateau = 2

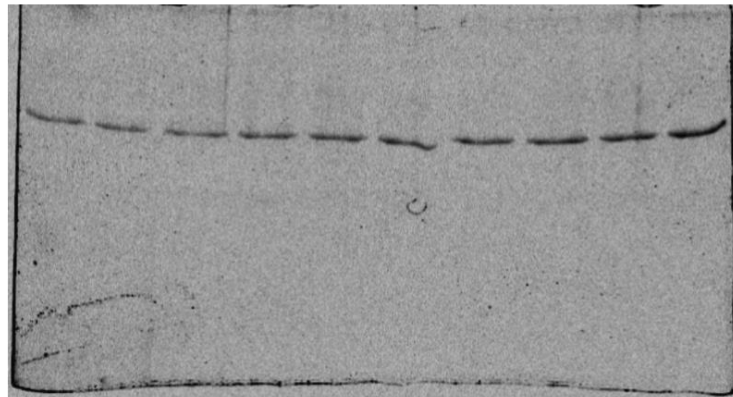


Y419F-Y530F
 Half Life = 2812 sec
 Plateau = 2

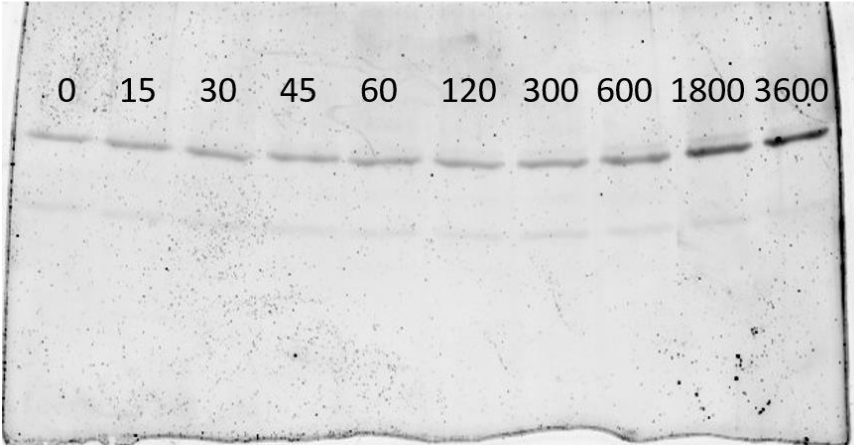
2 μ M Y530F, Phospho Stain



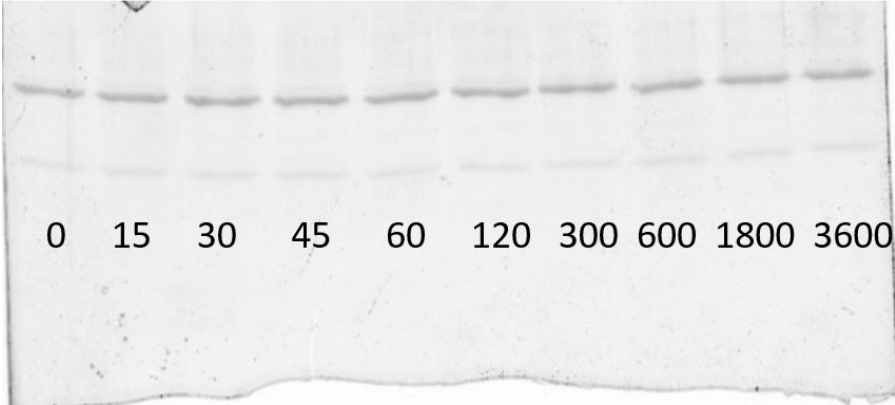
2 μ M Y530F, Sypro Ruby Stain



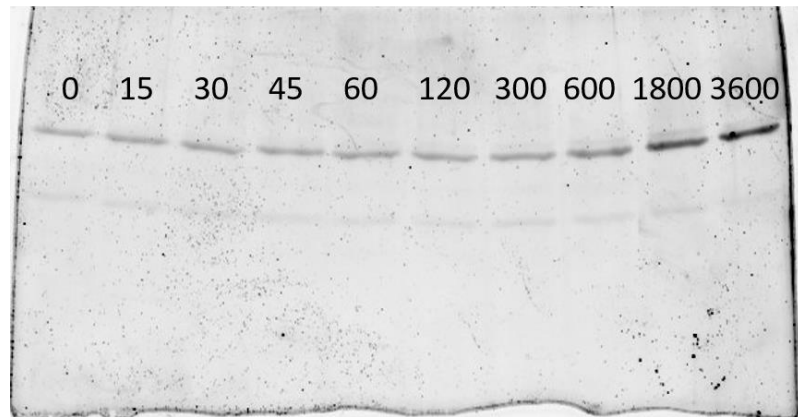
2 μ M T341R-Y530F, Phosphostain



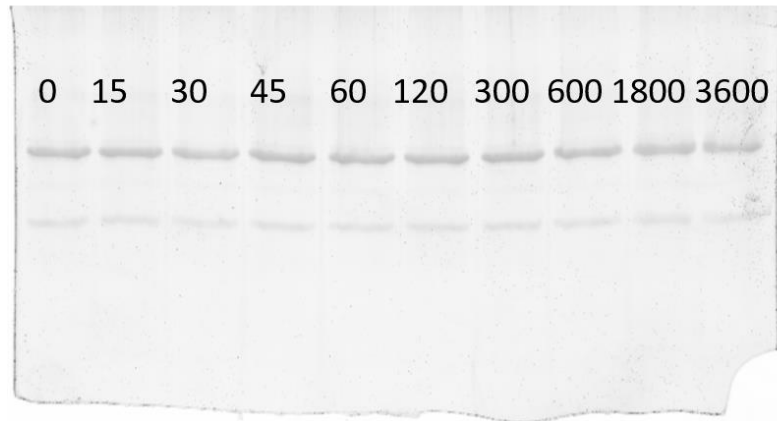
2 μ M T341R-Y530F, Sypro Ruby



2 μ M T341R-Y530F, Phosphostain



2 μ M Y530F-Y419F, Sypro Ruby Stain



2.11 References

- (1) Brown, M. T.; Cooper, J. A. *Biochim. Biophys. Acta - Rev. Cancer* **1996**, *1287* (2–3), 121.
- (2) Roskoski Jr., R. *Biochem. Biophys. Res. Commun.* **2005**, *331* (1), 1.
- (3) Biscardi, J. S.; Tice, D. A.; Parsons, S. J. In *Advances in Cancer Research*; 1999; Vol. 76, pp 61–119.
- (4) Yeatman, T. J. *Nat Rev Cancer* **2004**, *4* (6), 470.
- (5) Wheeler, D. L.; Iida, M.; Dunn, E. F. *Oncol.* **2009**, *14* (7), 667.
- (6) Irby, R. B.; Yeatman, T. J. *Oncogene* **2000**, *19* (49), 5636.
- (7) Mao, W.; Irby, R.; Coppola, D.; Fu, L.; Wloch, M.; Turner, J.; Yu, H.; Garcia, R.; Jove, R.; Yeatman, T. J. *Oncogene* **1997**, *15* (25), 3083.
- (8) Biscardi, J. S.; Ishizawar, R. C.; Silva, C. M.; Parsons, S. J. *Breast Cancer Res.* **2000**, *2* (3), 203.
- (9) Irby, R. B.; Mao, W.; Coppola, D.; Kang, J.; Loubeau, J. M.; Trudeau, W.; Karl, R.; Fujita, D. J.; Jove, R.; Yeatman, T. J. *Nat Genet* **1999**, *21* (2), 187.
- (10) Sugimura, M.; Kobayashi, K.; Sagae, S.; Nishioka, Y.; Ishioka, S.; Terasawa, K.; Tokino, T.; Kudo, R. *Jpn. J. Cancer Res.* **2000**, *91* (4), 395.
- (11) Wang, N. M.; Yeh, K.-T.; Tsai, C.-H.; Chen, S.-J.; Chang, J.-G. *Cancer Lett.* **2000**, *150* (2), 201.
- (12) Nilbert, M.; Fernebro, E. *Cancer Genet. Cytogenet.* **2000**, *121* (1), 94.
- (13) Laghi, L.; Bianchi, P.; Orbetegli, O.; Gennari, L.; Roncalli, M.; Malesci, A. *Br. J. Cancer* **2001**, *84* (2), 196.
- (14) Ishizawar, R.; Parsons, S. J. *Cancer Cell* **2004**, *6* (3), 209.
- (15) Barretina, J.; Caponigro, G.; Stransky, N.; Venkatesan, K.; Margolin, A. A.; Kim, S.; Wilson, C. J.; Lehar, J.; Kryukov, G. V.; Sonkin, D.; Reddy, A.; Liu, M.; Murray, L.; Berger, M. F.; Monahan, J. E.; Morais, P.; Meltzer, J.; Korejwa, A.; Jane-Valbuena, J.; Mapa, F. A.; Thibault, J.; Bric-Furlong, E.; Raman, P.; Shipway, A.; Engels, I. H.; Cheng, J.; Yu, G. K.; Yu, J.; Aspesi, P.; de Silva, M.; Jagtap, K.; Jones, M. D.; Wang, L.; Hatton, C.; Palesscandolo, E.; Gupta, S.; Mahan, S.; Sougnez, C.; Onofrio, R. C.; Liefeld, T.; MacConaill, L.; Winckler, W.; Reich, M.; Li, N.; Mesirov, J. P.; Gabriel, S. B.; Getz, G.; Ardlie, K.; Chan, V.; Myer, V. E.; Weber, B. L.; Porter, J.; Warmuth, M.; Finan, P.; Harris, J. L.; Meyerson, M.; Golub, T. R.; Morrissey, M. P.; Sellers, W. R.; Schlegel, R.; Garraway, L. A. *Nature* **2012**, *483* (7391), 307.
- (16) Forbes, S. A.; Bhamra, G.; Bamford, S.; Dawson, E.; Kok, C.; Clements, J.; Menzies, A.; Teague, J. W.; Futreal, P. A.; Stratton, M. R. *Curr. Protoc. Hum. Genet.* **2008**, *Chapter 10*, Unit 10.11.
- (17) Cowan-Jacob, S. W.; Fendrich, G.; Manley, P. W.; Jahnke, W.; Fabbro, D.; Liebetanz, J.; Meyer, T. *Structure* **2005**, *13* (6), 861.
- (18) Irtegun, S.; Wood, R. J.; Ormsby, A. R.; Mulhern, T. D.; Hatters, D. M. *PLoS One* **2013**, *8* (7), e71035.
- (19) Chong, Y.-P.; Ia, K. K.; Mulhern, T. D.; Cheng, H.-C. *Biochim. Biophys. Acta - Proteins Proteomics* **2005**, *1754* (1–2), 210.

- (20) Xu, W.; Doshi, A.; Lei, M.; Eck, M. J.; Harrison, S. C. *Mol. Cell* **1999**, *3* (5), 629.
- (21) Hunter, T. *Cell* **1987**, *49* (1), 1.
- (22) Superti-Furga, G.; Courtneidge, S. A. *BioEssays* **1995**, *17* (4), 321.
- (23) Matsuda, M.; Mayer, B. J.; Fukui, Y.; Hanafusa, H. *Science* **1990**, *248* (4962), 1537.
- (24) Masaki, T.; Okada, M.; Tokuda, M.; Shiratori, Y.; Hatase, O.; Shirai, M.; Nishioka, M.; Omata, M. *Hepatology* **1999**, *29* (2), 379.
- (25) Zheng, X. M.; Wang, Y.; Pallen, C. J. *Nature* **1992**, *359* (6393), 336.
- (26) den Hertog, J.; Pals, C. E.; Peppelenbosch, M. P.; Tertoolen, L. G.; de Laat, S. W.; Kruijer, W. *EMBO J.* **1993**, *12* (10), 3789.
- (27) Sefton, B. M.; Hunter, T. *Cancer Surv.* **1986**, *5* (2), 159.
- (28) Chang, B. Y.; Conroy, K. B.; Machleder, E. M.; Cartwright, C. A. *Mol. Cell. Biol.* **1998**, *18* (6), 3245.
- (29) Mamidipudi, V.; Zhang, J.; Lee, K. C.; Cartwright, C. A. *Mol. Cell. Biol.* **2004**, *24* (15), 6788.
- (30) Li, S.; Couet, J.; Lisanti, M. P. *J. Biol. Chem.* **1996**, *271* (46), 29182.
- (31) Takeuchi, S.; Takayama, Y.; Ogawa, A.; Tamura, K.; Okada, M. *J. Biol. Chem.* **2000**, *275* (38), 29183.
- (32) Thomas, J. W.; Ellis, B.; Boerner, R. J.; Knight, W. B.; White, G. C.; Schaller, M. D. *J. Biol. Chem.* **1998**, *273* (1), 577.
- (33) Gonfloni, S.; Weijland, A.; Kretzschmar, J.; Superti-Furga, G. *Nat Struct Mol Biol* **2000**, *7* (4), 281.
- (34) Frame, M. C. *Biochim. Biophys. Acta - Rev. Cancer* **2002**, *1602* (2), 114.
- (35) MacAuley, A.; Cooper, J. A. *Mol. Cell. Biol.* **1989**, *9* (6), 2648.
- (36) Hubbard, S. R. *Nature structural biology*. UNITED STATES August 1999, pp 711–714.
- (37) Nada, S.; Okada, M.; MacAuley, A.; Cooper, J. A.; Nakagawa, H. *Nature* **1991**, *351* (6321), 69.
- (38) Lerner, E. C.; Smithgall, T. E. *Nat Struct Mol Biol* **2002**, *9* (5), 365.
- (39) Lerner, E. C.; Tribble, R. P.; Schiavone, A. P.; Hochrein, J. M.; Engen, J. R.; Smithgall, T. E. *J. Biol. Chem.* **2005**, *280* (49), 40832.
- (40) Foda, Z. H.; Shan, Y.; Kim, E. T.; Shaw, D. E.; Seeliger, M. A. *Nat Commun* **2015**, *6*.
- (41) LaFevre-Bernt, M.; Sicheri, F.; Pico, A.; Porter, M.; Kuriyan, J.; Miller, W. T. *J. Biol. Chem.* **1998**, *273* (48), 32129.
- (42) Gonfloni, S.; Williams, J. C.; Hattula, K.; Weijland, A.; Wierenga, R. K.; Superti-Furga, G. *EMBO J.* **1997**, *16* (24), 7261.
- (43) Young, M. A.; Gonfloni, S.; Superti-Furga, G.; Roux, B.; Kuriyan, J. *Cell* **2001**, *105* (1), 115.
- (44) Lamontanara, A. J.; Georgeon, S.; Tria, G.; Svergun, D. I.; Hantschel, O. *Nat. Commun.* **2014**, *5*, 5470.
- (45) Krishnamurty, R.; Brigham, J. L.; Leonard, S. E.; Ranjitkar, P.; Larson, E. T.; Dale, E. J.; Merritt, E. A.; Maly, D. J. *Nat Chem Biol* **2013**, *9* (1), 43.

Chapter 3

Development of a chimeric c-Src kinase and HDAC inhibitor

Reprinted with permission from Ko, K. S.; Steffey, M. E.; Brandvold, K. R.; Soellner, M. B. ACS Med. Chem. Lett. **2013**, 4 (8), 779. Copyright 2013. ACS Med. Chem. Lett.

3.1 Abstract

On the basis of synergism observed between a selective c-Src kinase inhibitor with an HDAC inhibitor, the development of the first chimeric c-Src kinase and HDAC inhibitor is described. The optimized chimeric inhibitor is shown to be a potent c-Src and HDAC inhibitor. Chimeric inhibitor 4 is further shown to be highly efficacious in cancer cell lines and significantly more efficacious than a dual-targeting strategy using discrete c-Src and HDAC inhibitors.

3.2 Introduction

The non-receptor tyrosine kinase c-Src plays an important role in many aspects of cell physiology, regulating diverse cellular processes including division, motility, adhesion, angiogenesis, and survival.^{1,2} c-Src was the first proto-oncogene identified, is frequently over-expressed in cancer, and the extent of over-expression of c-Src correlates with malignant potential.^{1,2} Furthermore, c-Src expression levels inversely correlate with patient survival.^{1,2} Recently, c-Src activity was shown to be a main mode of resistance to Herceptin, a first line therapy for Her2+ breast cancer.³ Therefore, c-Src kinase is an attractive therapeutic target in cancer.

We recently reported the first highly selective inhibitor of c-Src (**3.1**).⁴ Despite potent biochemical activity against c-Src, our selective c-Src inhibitor (**3.1**) is only modestly potent in cellular proliferation assays using breast cancer cell lines.⁴

Following the success of combinatorial drug therapies in the treatment of HIV,⁵ tuberculosis, and other microbial infections,⁶ the use of multiple targeted drugs for cancer chemotherapy is increasingly being pursued.⁷ We reasoned that multi-target inhibition using our selective c-Src inhibitor might lead to improved cellular efficacy.

To identify drug combinations that would be synergistic with c-Src inhibition, we examined a small library of targeted inhibitors in combination with our selective c-Src inhibitor **3.1**. These studies were performed in SK-BR-3 cells, a Her2+ breast cancer cell line previously shown to be growth dependent upon c-Src kinase activity.^{4,8} From these experiments, we identified that panobinostat, a histone

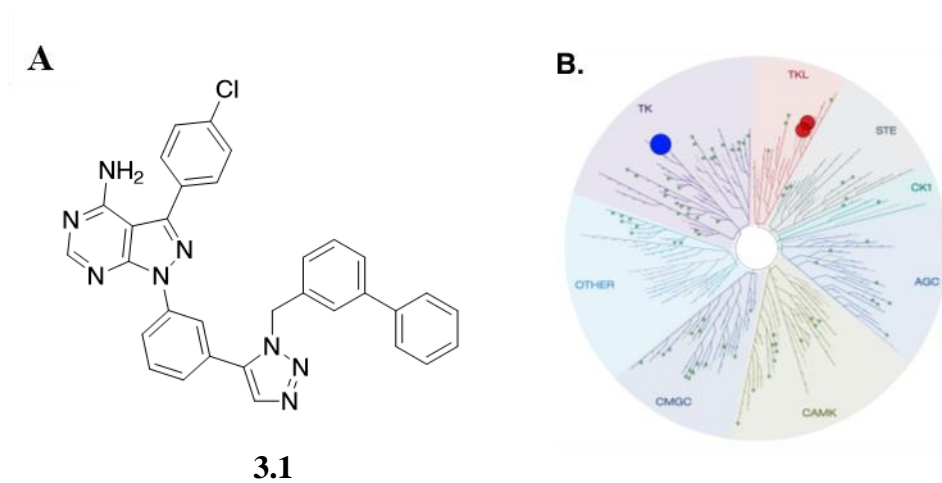


Figure 3.1: (A) Structure of highly selective c-Src inhibitor **3.1** (B) Kinome dendrogram for selectivity profiling of **3.1** at 10 μ M. c-Src is colored blue, and off-target kinases of **3.1** are colored red. Dendrogram was generated using TREEspot software tool with 10% cutoff. Green circles denote kinases included in panel that show no binding below cutoff.

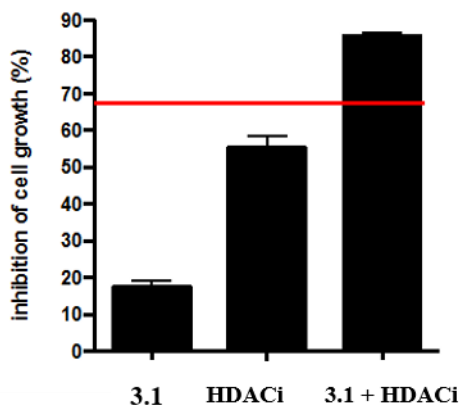


Figure 3.2: Synergy studies of selective c-Src inhibitor **3.1** (2 μ M), panobinostat (HDACi, 10 nM), and combination (**3.1** + HDACi, 2 μ M **3.1**, 10 nM panobinostat) in SK-BR-3 cell line. Red line denotes predicted additivity of **3.1**+ panobinostat. The higher level of inhibition than the predicted additivity indicated synergism between **3.1** and panobinostat. Work done by Mike Steffey.

deacetylase (HDAC) inhibitor in clinical trials,⁹ was highly synergistic with c-Src inhibitor **3.1** (Figure 3.2). HDAC inhibitors have been shown to promote the growth arrest and apoptosis of cancer cells with minimal toxicity.¹⁰ We believe that the observed synergy is due to previously reported mechanisms whereby HDAC inhibitors can down-regulate c-Src levels through repression of SRC transcription.¹¹

3.3 Results and Discussion

To determine whether the synergy observed with c-Src inhibition and panobinostat was general for any HDAC inhibitor, we performed combination experiments with vorinostat,¹² an FDA approved HDAC inhibitor, and c-Src inhibitor **3.1** (Figure 3.2). c-Src inhibitor **3.1** and vorinostat have a GI₅₀ of 4.8 μ M and 1.2 μ M, respectively, for SK-BR-3 proliferation. In combination, c-Src inhibitor **3.1** + vorinostat (1:1) has a GI₅₀ for SK-BR-3 proliferation of 0.8 μ M, which is an improvement over either inhibitor dosed alone.¹³ Next, as a measure of cellular toxicity, we examined each compound's ability to inhibit proliferation of primary human mammary epithelial cells (HMEC). c-Src inhibitor **3.1** and vorinostat have a GI₅₀ of 4.3 μ M and 5.8 μ M, respectively, for HMEC proliferation.

The combination of **3.1** + vorinostat (1:1) has a GI₅₀ of 5.4 μM against primary mammary epithelial cells. Using the SK-BR-3 and HMEC data, we calculated a therapeutic index (GI₅₀ HMEC / GI₅₀ SK-BR-3) for c-Src inhibitor **3.1**, vorinostat, and the combination of **3.1** + vorinostat (Table 3.1).¹⁴ c-Src inhibitor **3.1** has a poor therapeutic index of 0.9 while vorinostat's therapeutic index is 4.8. Disappointingly, the combination of **3.1** + vorinostat has an insignificant improvement in therapeutic index (6.8) relative to vorinostat alone (4.8). We wondered whether there would be any advantage for a chimeric inhibitor, where a single molecule could serve as both a c-Src kinase and HDAC inhibitor, rather than using two separate agents in combination. For example, we thought that we might obtain improved cellular efficacy. In addition, using a single agent to inhibit both c-Src and HDAC does not lead to the additive toxicity that is often observed with combination therapy.¹³ Chimeric kinase-HDAC inhibitors have previously been developed, however, no Src-HDAC chimeric compounds have been reported.¹⁵⁻¹⁷ In addition, previously

	GI ₅₀ (μM), SK-BR-3	GI ₅₀ (μM), HMEC	Therapeutic Index
Compound 3.1	4.8	4.3	0.9
Vorinostat	1.2	5.8	4.8
3.1 + Vorinostat	0.8	5.4	6.8
Chimera 3.4	0.2	4.7	23.5

Table 3.1: Cellular efficacy of selective c-Src inhibitor **3.1**, vorinostat, **3.1**:vorinostat (1:1), and chimera **3.4**. Work done by Mike Steffey.

reported studies of kinase-HDAC chimeras lack a comparison of therapeutic indices between combination therapy and chimeric inhibition.¹⁵⁻¹⁷

We previously reported PP2~alkyne (**3.2**), a modular and selective c-Src inhibitor scaffold.⁴ We envisioned using this kinase inhibitor scaffold to append HDAC pharmacophores. The classic pharmacophore for HDAC inhibitors consists of a zinc-binding motif, a hydrophobic linker, and a recognition cap.¹⁸ Using PP2~alkyne, HDAC elements can readily be appended using “click” chemistry.¹⁹

Importantly, the use of a triazole ring as the recognition cap in HDAC inhibitors has previously been reported and shown to be highly efficacious both *in vitro* and *in cellulo*. Previous reports with triazole-based HDAC inhibitors have demonstrated that a 6-carbon hydrophobic linker will provide potent HDAC inhibition.²⁰ While only 1,4-[1,2,3]-triazoles have been reported as HDAC inhibitors,²⁰ we reasoned that because our selective c-Src inhibitor **3.1** contains a 1,5-[1,2,3]-triazole,⁴ we would synthesize and evaluate both regioisomers.

We synthesized compounds **3.3** and **3.4** as chimeric Src/HDAC inhibitors. Compound **3.3** has a 1,4-triazole and was synthesized using a copper-mediated cycloaddition reaction,¹⁹ while compound **3.4** has a 1,5-triazole synthesized using a ruthenium-mediated cycloaddition reaction (Figure 3.3, see experimental for synthetic details).²¹ Using a previously reported fluorescence assay for c-Src kinase activity,²² we found that **3.3** and **3.4** were competent c-Src kinase inhibitors

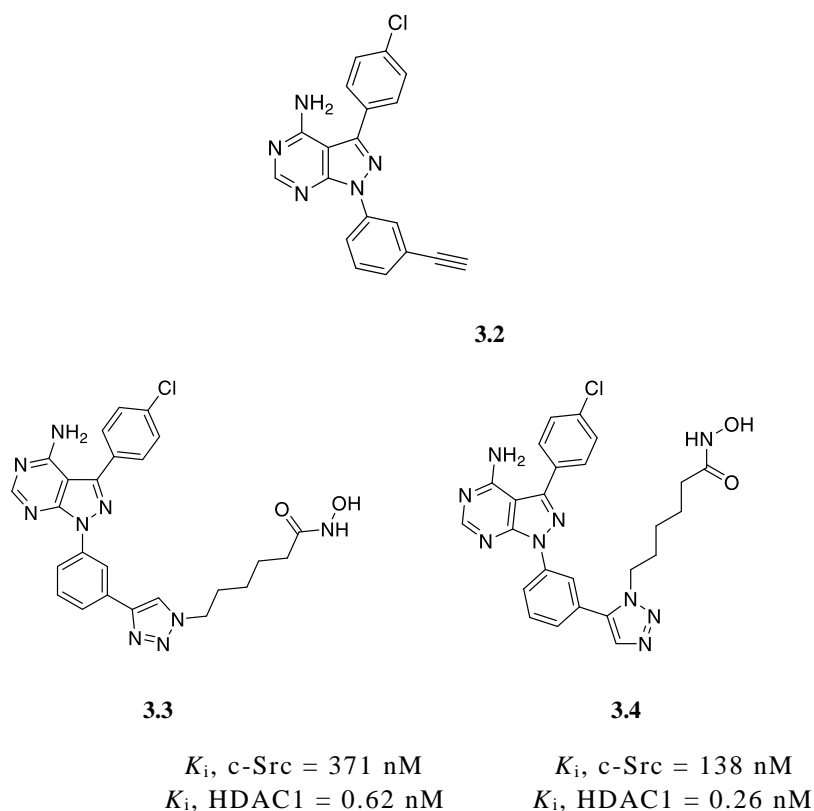
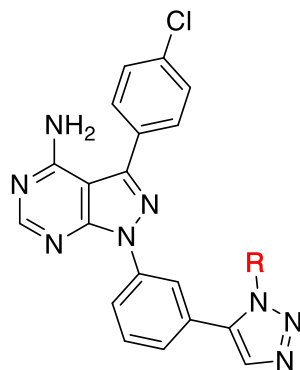


Figure 3.3: Structure of PP2~Alkyne (**3.2**) and chimeric inhibitors **3.3** and **3.4**

($K_i = 371$ and 138 nM, respectively). We next examined the ability of **3.3** and **3.4** to inhibit HDAC1 using a Fluor de Lys based-assay²³ and found both compounds were potent inhibitors of HDAC-1 ($K_i = 0.62$ and 0.26 nM, respectively, Figure 3.3). In our assays, compound **3.4** was a better inhibitor of both c-Src and HDAC-1. Thus, the 1, 5-triazole regiochemistry was used exclusively for subsequent linker optimization.

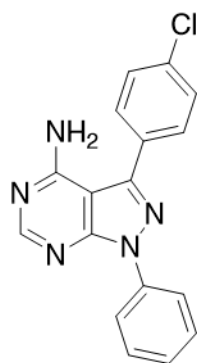
In an effort to optimize potency for both c-Src and HDAC-1, we synthesized a series of chimeric HDAC-Src inhibitors containing varied hydrophobic linkers (Table 3.2). This series included alkyl linkers of varied length as well as styrene-containing linkers that are found in panobinostat.⁹ The six-carbon alkyl linker (compound **3.4**) was found to be optimal for inhibition of both c-Src kinase and HDAC-1. Of note, we found the styrene linkers (compounds **3.6** and **3.5**) were ineffective as c-Src inhibitors and only modest inhibitors of HDAC-1 compared to the *n*-alkyl linkers. Chimeric inhibitor **3.4** is one of the most potent HDAC-1 inhibitors reported to date ($K_i = 260$ pM) and is also a potent c-Src inhibitor ($K_i = 138$ nM). To decipher the binding contributions for each half of the chimera, two fragments of inhibitor **3.4** were synthesized (Figure 3.4). Compound **3.9** contains only the HDAC inhibitor pharmacophore, while compound **3.10** includes the c-Src kinase binding elements. Interestingly, we observe a marked decrease in affinity for both c-Src and HDAC-1 when both elements are not present. Specifically, compound **3.9**, which retains all of the HDAC inhibitor pharmacophore elements, has a K_i for HDAC-1 that is >170-times higher than found with chimeric inhibitor **3.4**. These data imply that the c-Src binding elements enhance HDAC-1 inhibition observed with compound **3.4**. Likewise, the c-Src inhibitor fragment **3.10** has nearly 10x less affinity for c-Src than chimera **3.4**, suggesting that the addition of the HDAC fragment is important for c-Src inhibition. Together, these data demonstrate that chimera **3.4** is not simply two inhibitors linked together, but rather represents a merged inhibitor where both elements are required for affinity against each target.

Our chimeric inhibitor was initially optimized for HDAC inhibition using HDAC-1, however, we assumed it could be a promiscuous inhibitor of HDACs. Profiling of compound **3.4** against a panel of 11 HDACs was performed by Reaction



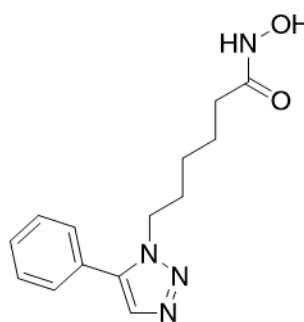
Compound	R =	K_i , c-Src (nM)	K_i , HDAC1 (nM)
3.4		138	0.26
3.8		190	0.22
3.7		407	9.8
3.6		4300	35
3.5		2140	23

Table 3.2: SAR of Linker



3.10

K_i , c-Src = 605 nM
 K_i , HDAC1 = >12,500 μ M



3.9

K_i , c-Src = > 12,500 μ M
 K_i , HDAC1 = 45 nM

Figure 3.4: c-Src inhibitor **3.10** and HDAC inhibitor **3.9**

Biology (Malvern, PA). The HDAC profiling revealed that our chimera is a potent and non-selective inhibitor against class I, IIa, and IV HDACs (Table 3.3). Consistent with Vorinostat's selectivity, chimera 4 is not an effective inhibitor of class IIb HDACs (Table 3.3). Relative to vorinostat, chimera **3.4** has improved affinity to all HDACs except HDAC-8 and HDAC-11.

In previously published work, we found that c-Src inhibitors that are selective for c-Src over c-Abl are more efficacious in cell culture with non-hematopoietic cancers.⁴ Thus, we wanted to determine whether chimera **3.4** has selectivity for c-Src over c-Abl. Gratifyingly, in our biochemical assay, chimera **3.4** was selective for c-Src over c-Abl (K_i for c-Src = 138 nM, K_i for c-Abl = 2,350 nM). We next tested the ability of **3.4** to inhibit Hck, a SRC-family kinase with 85% similarity across the kinase domain to c-Src, and found it is a modest inhibitor (K_i for Hck = 504 nM). Together, these data demonstrate that chimera **3.4** is selective for c-Src over homologous kinases. Given that our compound shares many features with our highly selective c-Src inhibitor **3.1**,⁴ the results demonstrating that chimera **3.4** is a selective kinase inhibitor are not surprising.

	HDAC Class	IC ₅₀ (nM), Chimera 4	IC ₅₀ (nM), Vorinostat
HDAC1	I	86	306
HDAC2	I	231	232
HDAC3	I	19	132
HDAC4	IIb	3,982	76,000
HDAC5	IIb	3,891	27,200
HDAC6	IIa	2.7	20
HDAC7	IIb	13,220	105,000
HDAC8	I	2,311	306
HDAC9	IIb	28,020	141,000
HDAC10	IIa	51	432
HDAC11	IV	224	200

Table 3.3: HDAC Profiling of Chimera 4 and Vorinostat

We next probed the efficacy of chimera **3.4** *in cellulo* to determine whether there was any advantage with a chimeric compound over the dual-targeting of c-Src and HDAC with two compounds. Combination dosing of selective c-Src inhibitor **3.1** + vorinostat (1:1) was found to have a GI₅₀ = 0.78 μM for SK-BR-3 cells and a GI₅₀ = 5.4 μM for non-cancer HME cells. This resulted in a therapeutic index of 6.8 (*vide supra*). In comparison, chimeric inhibitor **3.4** was more efficacious at inhibiting the growth of SK-BR-3 cells (GI₅₀ = 0.2 μM) and has similar non-cancer cellular toxicity (GI₅₀ = 4.7 μM for HME cells), resulting in a cellular therapeutic index of 23.5 (Table 3.1). This corresponds to chimeric inhibitor **3.4** having an improvement in therapeutic index significantly higher than dual targeting c-Src and HDACs with two distinct compounds (23.5 versus 6.8, respectively). These results highlight an important advantage for chimeric inhibition over dual-agent targeting:

Cell line	GI ₅₀ (μM),		
	chimera 3.4	vorinostat	dasatinib
a) KM12	0.47	1.88	7.44
MCF7	0.35	2.19	8.32
U251	0.28	1.53	2.81
b) DU-145	0.39	1.36	0.16
HS 578T	0.17	4.83	0.03
MDA-MB-231	0.39	2.32	0.02
c) HCT-116	0.22	0.37	3.70
MALME-3M	0.07	0.37	6.61
SW-620	0.25	0.54	8.43

Table 3.4: NCI-60 Panel Data for Chimera 3.4, Vorinostat, and Dasatinib against Select Cell Lines

we observe synergistic activity against cancer cells while not increasing the cellular toxicity relative to the single agent counterparts.

To better characterize the cellular efficacy of our chimeric c-Src/HDAC inhibitor, compound 3.4 was submitted to the National Cancer Institute for screening in the NCI-60 panel (see Supporting Information for full NCI-60 data).²⁴ From this panel, chimera 3.4 has an average GI₅₀ = 0.26 μM. Significantly, the efficacy of chimera 3.4 across the NCI-60 is better than vorinostat (NCI-60 average GI₅₀ = 0.53 μM) and a FDA-approved c-Src inhibitor (dasatinib, NCI-60 average GI₅₀ = 5.7 μM). In addition to the improved efficacy across the NCI-60 panel, chimera 3.4 does not have increased toxicity relative to primary human mammary cells (chimera 3.4, HMEC GI₅₀ = 4.7 μM; vorinostat, HMEC GI₅₀ = 5.8 μM; dasatinib, HMEC GI₅₀ = 1.8 μM). Analysis of the NCI-60 data demonstrates that chimera 3.4 is a highly efficacious agent in cell lines where vorinostat and dasatinib are ineffective alone (Table 3.4a). Furthermore, chimera 3.4 is more efficacious than vorinostat when c-Src inhibition is shown to be efficacious (Table 3.4b). For example, chimera 3.4 is an efficacious inhibitor of Hs 578T, a triple negative breast cancer cell line, cell growth (GI₅₀ = 0.17 μM) while vorinostat is not (GI₅₀ = 4.83 μM), due to c-Src

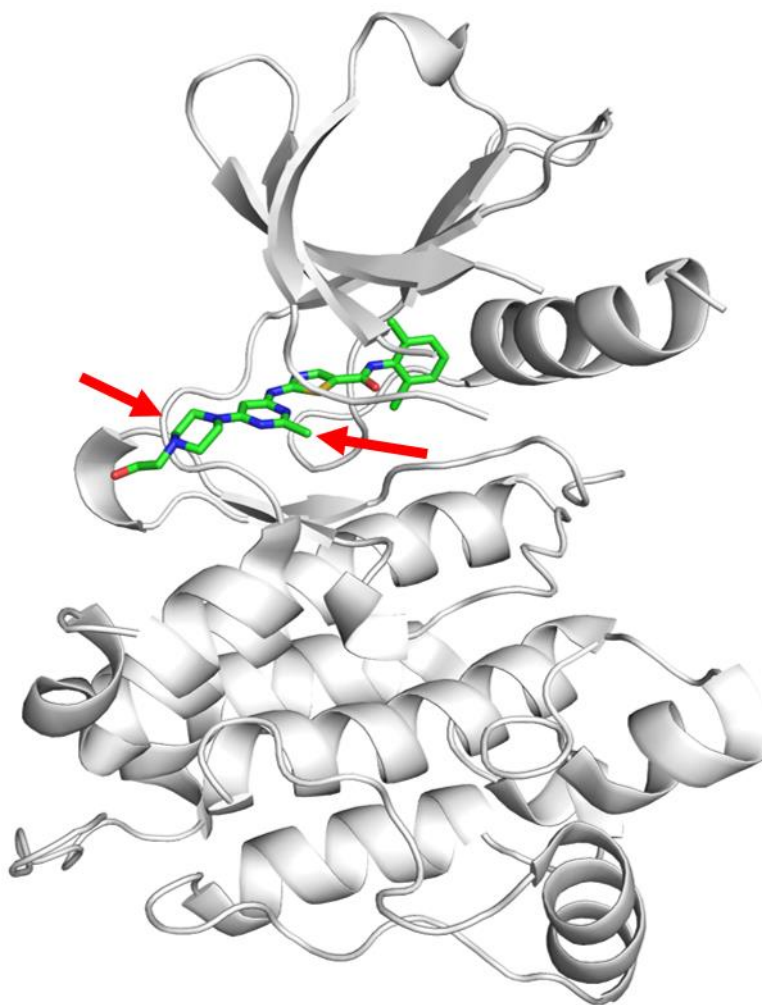


Figure 3.5: PDB 3G5D of c-Src bound dasatinib (green). The arrows indicate the ideal groups that can be substituted with the HDAC pharmacophore without disrupting binding to c-Src.

inhibition having an important role in Hs 578T cell proliferation (dasatinib $GI_{50} = 0.03 \mu\text{M}$). Finally, chimera **3.4** is observed to be more effective than dasatinib in cell lines where cellular proliferation is dependent upon HDAC-1 activity (Table 3.4c). Together, these data demonstrate that compound **3.4**'s impressive cellular efficacy in the NCI-60 panel is inherent in its chimeric nature and the ability to inhibit both c-Src kinase and HDAC1 is required for the cellular potency observed.

To explore avenues to further increase **3.4** cellular efficacy we decided to deploy the same dual inhibitor HDAC/c-Src strategy using a more drug-like scaffold. The pyrazolo-pyrimidine scaffold of **3.4**, while effective *in cellulo*, is not ideal because of its inherent structure, which consist of four hydrophobic aromatic

rings which are greasy and most likely not druggable. We decided to utilize the dasatinib scaffold to append with the HDAC pharmacophore, phenyl 1, 5 triazole hydroxamic acid, Figure 3.6.

From the crystal structure of dasatinib bound c-Src, shown in Figure 3.6, it appears that there are two places where substitution and thereby the addition of the HDAC pharmacophore could work without interfering with c-Src binding. The hydroxyethyl piperazine and 4-methyl group off of the pyrimidine stick out into the solvent and could be used to append the HDAC pharmacophore. For compound **3.12**, the hydroxyethyl piperazine was replaced with morpholine to help decrease the molecular weight and ease of synthesis. Past experience with hydroxyethyl piperazine usually makes the compounds more difficult to purify without using a reverse phase column. The addition of the HDAC pharmacophore was at the 4-methyl group on the pyrimidine. **3.11** directly swapped the piperazine group with the 1, 5 triazole hydroxamic acid. The usual phenyl group was left out to help reduce the molecular weight as well as simplifying the chemistry. Adding into the 6' position of the pyrimidine ring is difficult as that position is quite deactivate. A Suzuki coupling, which would have been require to append the phenyl group, has not worked. Instead, an alkyne can be more easily attached thru Sonogashira reaction.

Compound **3.12** and **3.11** were tested biochemically against HDAC1 and c-Src and the results are shown in Table 3.5. Changing the scaffold from pyrazolo- pyrimidine to dasatinib greatly increased its affinity to c-Src and mostly maintains dasatinib level potency (pM). However, we could not ascertain the exact value in our assay due to titration of the enzyme despite increasing the ATP concentration to 5mM. Unfortunately, potency against HDAC1 was lost. Both **3.12** and **3.11** decreased binding about 16-fold and 50-fold respectively compared to 3.3 3.4, however K_i values remain in the low single digit/low double digit nM range.

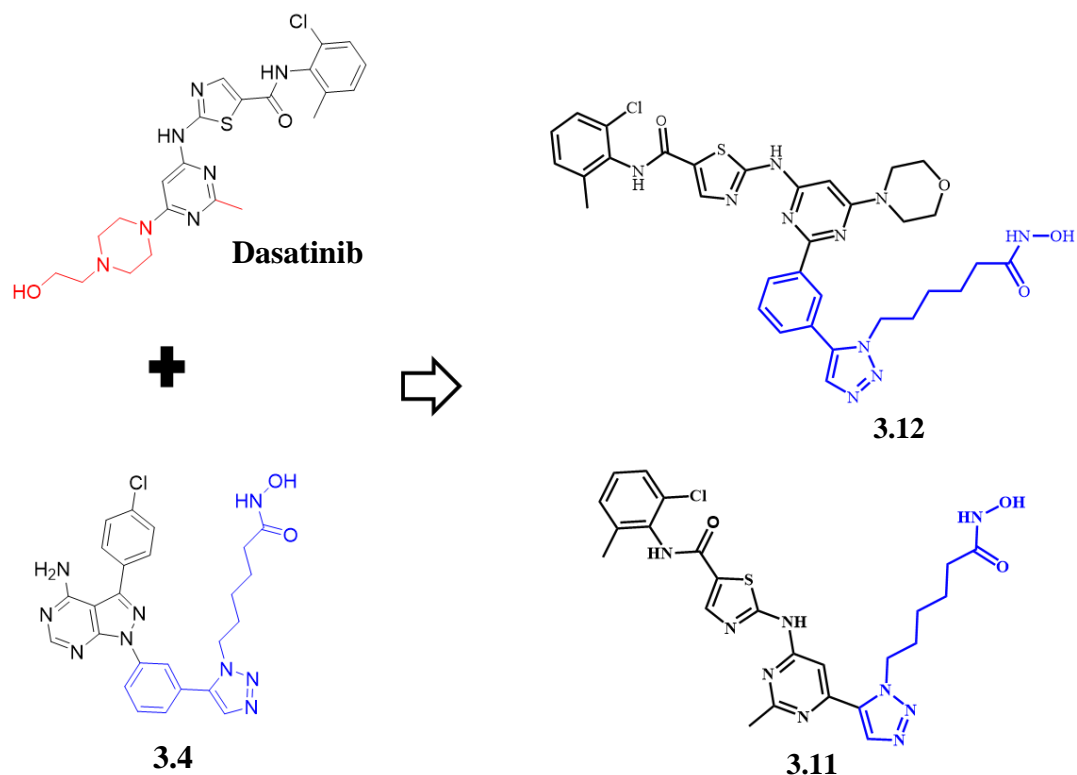


Figure 3.6: Structure of the new dual c-Src/HDAC inhibitor that utilizes the dasatinib scaffold as the c-Src pharmacophore, replacing the pyrazolo-pyrimidine core while maintaining the same phenyl triazole hydroxamic acid as the HDAC warhead. Replacement of the 4-methyl group off of the pyrimidine results in compound **3.12** using a morpholine instead of the hydroxyethyl piperazine to help decrease MW. Replacing the hydroxyethyl piperazine results in compound **3.11**.

Compound (K_i)	GI_{50}	
	c-Src (nM)	HDAC1 (nM)
3.4	138 ± 15	0.26 ± 0.02
3.12	< 30	4.2 ± 0.3
3.11	< 30	13 ± 1

Table 3.5: Biochemical evaluation of compound **3.12** and **3.11** against c-Src and HDAC1

3.4 Conclusion

In summary, we have reported the first chimeric c-Src kinase and HDAC inhibitor. Furthermore, we have performed detailed studies that demonstrate that chimera **3.4** is a potent and selective c-Src kinase inhibitor as well as a potent and

non-selective HDAC inhibitor. We demonstrated that our chimeric inhibitor has improved efficacy in cellular experiments compared to dosing two individual inhibitors targeting c-Src and HDACs. Chimera **3.4** has significant efficacy in the NCI-60 panel, while not possessing significant toxicity to primary human cells, and represents a novel small molecule probe that can provide simultaneous inhibition of c-Src and HDACs. Our approach to constructing kinase-HDAC inhibitor hybrids should be general and readily adapted to any kinase and/or HDAC pair of interest.

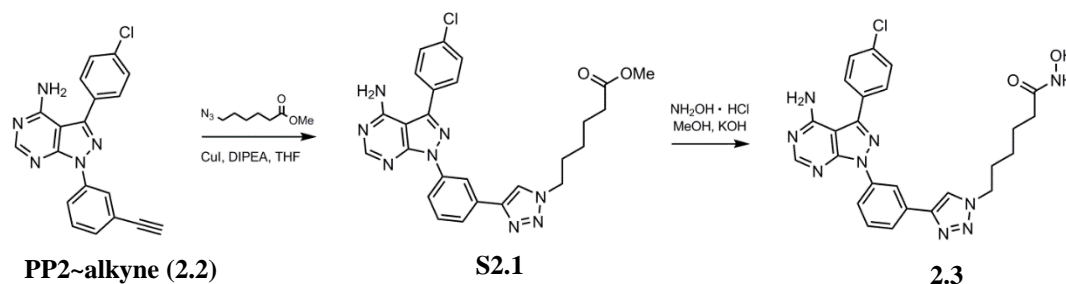
Compounds **3.12** and **3.11** will need to be tested in the future against SK-BR-3 and HMEC cells to evaluate if there is any benefits using the more druggable dasatinib scaffold. Despite the decrease to HDAC1 potency, these compounds could enable us to study the opposite effects of having a dual c-Src/HDAC inhibitor that has greater potency against c-Src as oppose to **3.4**, which had better affinity for HDAC1 than c-Src. Fragment study of the separate pharmacophores could be done to assess whether or not these “improved” chimeric inhibitors act like a true dual-acting compound in cells such as those studies used for **3.4** in Figure 3.4.

3.5 Experimental Section

General Synthetic Methods

Unless otherwise noted, all reagents were obtained from commercial suppliers and used without further purification. Recombinant, human histone deacetylase 1 was obtained from Cayman Chemicals. Trypsin was purchased from Sigma-Aldrich. Black, opaque-bottom 96 well plates were purchased from Nunc. All ^1H and ^{13}C NMR spectra were measured with a Varian MR400 and Inova 500 spectrometer. Mass spectrometry (HRMS) was carried out by the University of Michigan Ann Arbor Mass Spectrometry Facility (J. Windak, Director). Azido alkyl esters of 5-7 methylene length were synthesized from adapting literature procedure.²⁰ 3-(4-chlorophenyl)-1-(4-ethynylphenyl)-1H-pyrazolo [3,4-d]pyrimidin-4-amine (PP2~alkyne) was prepared as described before.⁴ (E)-ethyl 3-(4-(azidomethyl)phenyl)acrylate was synthesized by adapting literature protocol.^{4,25} Flash column chromatography was performed using a Biotage Isolera 1 Flash Purification System using KP-Sil SNAP cartridges. In all cases, ethyl acetate was used to transfer the crude reaction material onto the silica gel samplet. A gradient elution using hexane and ethyl acetate was performed, based on the recommendation from the Biotage TLC Wizard.

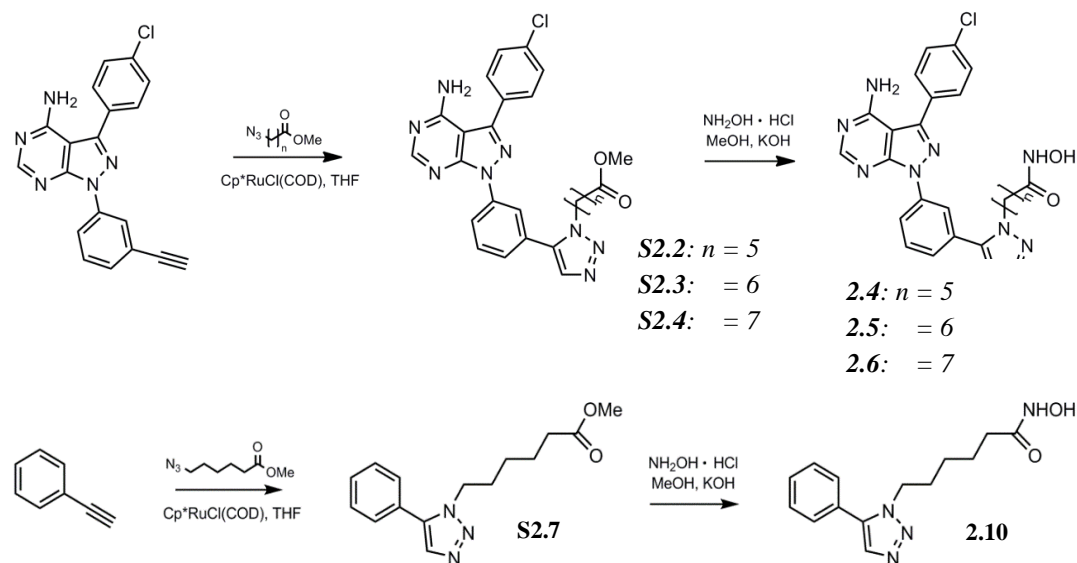
Synthesis of Compounds 2.3-2.10



Scheme S 2: Synthesis of Compound 3.3

Synthesis of S2.1: PP2~alkyne (0.14 mmol) and methyl 6-azidohexanoate (0.318 mmol) were dissolved in THF (1 mL) and stirred under nitrogen at room temperature. Copper (I) iodide (0.011 mmol) and Hunig's base (0.038 mL) were added to the reaction mixture which was stirred under nitrogen overnight. The reaction mixture was diluted with dichloromethane (8 mL) and washed with 1:4 NH_4OH /saturated NH_4Cl (3x 12 mL) and saturated NH_4Cl (12 mL). The organic layer was dried over MgSO_4 , filtered, and concentrated *in vacuo*. The crude product was purified by Biotage Isolera 1 Flash Purification System to give 20 mg (27% yield) of **S2.1** as a white solid. **Spectral Data.** ^1H NMR (500 MHz, CDCl_3): δ 8.65 (s, 1 H), 8.52 (s, 1 H), 8.26-8.24 (m, 1H), 7.89 (s, 2 H), 7.77 (d, $J = 10.0$ Hz, 2 H), 7.62-7.56 (m, 3 H), 5.59 (s, 2H), 4.44 (t, $J = 8.0$ Hz, 2 H), 3.67 (s, 3 H), 2.34 (t, $J = 8$ Hz, 2 H), 2.02-1.97 (m, 2 H), 1.72-1.68 (m, 2 H), 1.43-1.39 (m, 2H); ^{13}C NMR (100 MHz, CDCl_3): δ 173.77, 157.97, 156.53, 154.68, 147.14, 144.41, 139.23,

135.59, 131.73, 131.15, 129.90, 129.62, 123.79, 121.12, 120.0, 118.76, 99.69, 51.56, 50.12, 33.62, 29.99, 25.91, 24.17; HRMS-ESI (m/z): $[M + H]^+$ calcd for $C_{26}H_{25}ClN_8O_2$, 517.1862; found, 517.1863.



Scheme S 3: Synthesis of Compound 2.4-2.6 and 2.10

Procedure of $Cp^*RuCl(COD)$ catalyzed cycloaddition reaction.

Synthesis of S2.2: PP2~alkyne (50 mg, 0.14 mmol) and $Cp^*RuCl(COD)$ (5.3 mg, 0.014 mmol) were added into a flame-dried round bottom flask and subsequently purged with nitrogen gas for 5 min. THF (1mL) and methyl 6-azidohexanoate (50 μ L, 0.43 mmol) were then added. The reaction was allowed to stir under nitrogen at room temperature overnight. The reaction mixture was diluted with ethyl acetate (10mL) and washed with water and brine, dried over $MgSO_4$, filtered, and concentrated in vacuo. The crude product was purified by Biotage Isolera 1 Flash Purification System to give a 28 mg (37% yield) of compound **S2.2** as a yellow solid. **Spectral Data.** 1H NMR (400 MHz, $CDCl_3$): δ 8.47 (s, 1 H), 8.42 (s, 2 H), 7.77 (s, 1 H), 7.72 (s, $J = 7.2$ Hz, 2 H), 7.63 (t, $J = 8.0$ Hz, 1 H), 7.56 (d, $J = 8.4$ Hz, 2 H), 7.33 (d, $J = 8.0$ Hz, 1 H), 5.67 (s, 1H), 4.44 (t, $J = 8$ Hz, 2 H), 3.59 (s, 3 H), 2.21 (t, $J = 8.0$ Hz, 2 H), 1.94-1.86 (m, 2 H), 1.61-1.53 (m, 2 H), 1.35-1.27 (m, 2 H); ^{13}C NMR (100 MHz, $CDCl_3$): δ 173.71, 157.94, 156.72, 154.98, 144.89, 139.52, 137.09, 135.92, 133.26, 130.96, 129.99, 129.61, 128.11, 126.49, 121.90, 121.19, 99.93, 51.49, 48.27, 33.64, 29.82, 25.99, 24.23; HRMS-ESI (m/z): $[M + H]^+$ calcd for $C_{26}H_{25}ClN_8O_2$, 517.1862; found, 517.1861.

Synthesis of S2.3: Reaction of PP2~alkyne (50 mg, 0.14 mmol) and methyl 7-azidohexanoate (40 μ L, 0.28 mmol) was prepared as described for the synthesis of **S2.2**. The crude product was purified by Biotage Isolera 1 Flash Purification System to give a 36 mg (47% yield) of compound **S2.3** as a yellow solid. **Spectral Data.** 1H

NMR (500 MHz, CDCl₃): 8.48 (s, 1H), 8.43 (s, 2H), 7.77 (s, 1H), 7.72 (d, *J* = 6.8, 2H), 7.64 (t, *J* = 8 Hz, 1H), 7.58-7.53 (m, 2H), 7.34 (d, *J* = 8.0 Hz, 1H), 4.44 (t, *J* = 7.2 Hz, 2H), 3.61 (s, 3H), 2.19 (t, *J* = 7.6 Hz, 2H), 1.92-1.85 (m, 2H), 1.56-1.48 (m, 2H), 1.28-1.23 (m, 4H); ¹³C NMR (100 MHz, CDCl₃): 173.93, 158.07, 156.63, 154.94, 144.92, 139.50, 137.07, 135.86, 133.20, 130.95, 129.83, 128.12, 126.46, 121.86, 121.17, 99.88, 51.43, 48.37, 33.76, 29.96, 28.42, 26.14, 24.57 HRMS-ESI (*m/z*): [M + H]⁺ calcd for C₂₇H₂₇ClN₈O₂, 531.2018; found, 531.2022.

Synthesis of S2.4: Reaction of PP2~alkyne (50 mg, 0.14 mmol) and methyl 8-azidohexanoate (40 μL, 0.28 mmol) was prepared as described for the synthesis of S2.2. The crude product was purified by Biotage Isolera 1 Flash Purification System to give a 36 mg (45% yield) of compound S2.4 as a yellow solid. **Spectral Data.** ¹H NMR (500 MHz, CDCl₃): δ 8.52 (s, 1 H), 8.46 (s, 2 H), 7.81 (s, 1 H), 7.77-7.73 (m, 2 H), 7.70-7.64 (m, 1 H), 7.61-7.58 (m, 2 H), 7.37 (d, *J* = 7.5 Hz, 1 H), 5.52 (s, 2H), 4.46 (t, *J* = 10 Hz, 2 H), 3.65 (s, 3 H), 2.24 (t, *J* = 7.5 Hz, 2 H), 1.94-1.88 (m, 2 H), 1.57-1.51 (m, 2 H), 1.32-1.23 (m, 6 H); ¹³C NMR (100 MHz, CDCl₃): 174.08, 158.03, 156.65, 154.94, 144.91, 139.49, 137.06, 135.87, 133.22, 130.95, 129.84, 128.17, 126.49, 121.86, 121.21, 99.89, 51.44, 48.44, 33.88, 30.08, 28.8, 28.58, 26.27, 24.69; HRMS-ESI (*m/z*): [M + H]⁺ calcd for C₂₈H₂₉ClN₈O₂, 545.2180; found, 545.2180. **Synthesis of S2.7:** Reaction of phenylacetylene (54 μL, 0.49 mmol) and methyl 6-azidohexanoate (69 μL, 0.59 mmol) was prepared as described for the synthesis of S2.2. The crude product was purified by Biotage Isolera 1 Flash Purification System to give 70 mg (52% yield) of compound S2.7 as light brown oil. **Spectral Data.** ¹H NMR (500 MHz, CDCl₃): δ 7.69 (s, 1 H), 7.51-7.49 (m, 3 H), 7.39-7.38 (m, 2 H), 4.36 (t, *J* = 10 Hz, 2 H), 3.65 (s, 3 H), 2.29-2.22 (m, 2 H), 1.85 (m, 2 H), 1.59-1.55 (m, 2 H), 1.32-1.26 (m, 2 H); ¹³C NMR (100 MHz, CDCl₃): δ 173.68, 137.64, 132.98, 129.41, 129.07, 128.66, 127.14, 51.45, 47.96, 33.57, 29.64, 25.84, 24.12; HRMS-ESI (*m/z*): [M + H]⁺ calcd for C₁₅H₁₉N₃O₂, 274.2550; found, 274.1553.

Procedure for conversion of methyl esters to hydroxamic acid

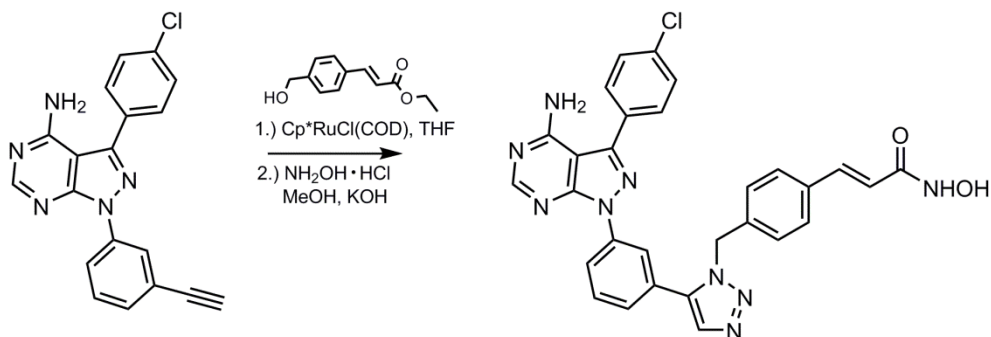
Synthesis of 2.3: A solution of hydroxylamine hydrochloride (271 mg, 3.9 mmol) in 10 mL of MeOH, KOH (219 mg, 3.9 mmol) was added and stirred at 40 °C for 10 min. The reaction mixture was cooled to 0 °C and filtered. Compound **S2.1** (10 mg, 0.02 mmol) was added to the filtrate followed by KOH (0.04 mmol) at room temperature for 3 hours. The reaction mixture was extracted with EtOAc. The organic layer was washed with saturated NH₄Cl solution and brine, and dried over MgSO₄, filtered and concentrated. The residue was purified by reverse-phase preparative HPLC (linear gradient of 5 to 95% acetonitrile and water) to give 7.3 mg of compound **2.3** (73%) as a white powder. **Spectral Data.** ¹H NMR (500 MHz, CD₃OD): δ 8.64 (s, 1H), 8.47 (s, 2H), 8.16 (d, J = 5 Hz, 1H), 7.92-7.86 (m, 1H), 7.86-7.79 (m, 2H), 7.67-7.63 (m, 3H), 4.49 (t, J = 7 Hz, 2H), 2.12 (t, J = 7.5 Hz, 2H), 2.03-1.99 (m, 2H), 1.74-1.68 (m, 2H), 1.44-1.34 (m, 2H); ¹³C NMR (100 MHz, DMSO-d₆): 169.32, 157.08, 155.06, 146.32, 145.06, 139.62, 134.36, 132.31, 131.47, 130.75, 130.20, 129.64, 123.52, 122.22, 120.81, 117.85, 99.19, 49.89, 32.47, 29.77, 25.89, 24.93; HRMS-ESI (m/z): [M + H]⁺ calcd for C₂₅H₂₄ClN₉O₂, 518.1814; found, 518.1822.

Synthesis of 2.4: Compound **S2.1** (8.9 mg, 0.02 mmol) was added to the hydroxylamine hydrochloride solution as described for the synthesis of **3** to give 7.2 mg of compound **2.4** (82%) as a white powder. **Spectral Data.** ¹H NMR (500 MHz, CD₃OD): δ 8.49 – 8.43 (m, 2H), 8.34 (d, J = 10 Hz, 1 H), 7.92 (s, 1 H), 7.83-7.80 (m, 2 H), 7.77 (t, J = 8.0 Hz, 1 H), 7.65-7.63 (m, 2 H), 7.59 (d, J = 8.0 Hz, 1 H), 4.57 (t, J = 7.0 Hz, 2 H), 2.01 (t, J = 7.0 Hz, 2 H), 1.93-1.87 (m, 2 H), 1.60-1.54 (m, 2 H), 1.35-1.28 (m, 2 H); ¹³C NMR (100 MHz, DMSO-d₆): δ 169.26, 157.77, 155.76, 154.74, 145.69, 139.26, 137.05, 134.58, 133.46, 131.07, 130.74, 129.69, 128.16, 127.04, 122.16, 121.26, 99.27, 48.35, 32.44, 29.62, 25.96, 24.94; HRMS-ESI (m/z): [M + H]⁺ calcd for C₂₅H₂₄ClN₉O₂, 518.1814; found, 518.1811.

Synthesis of 2.5: Compound **S2.3** (36 mg, 0.07 mmol) was added to the hydroxylamine hydrochloride solution as described for the synthesis of **2.3** to give 19 mg of compound **2.5** (53%) as a white powder. **Spectral Data.** ¹H NMR (500 MHz, DMSO-d₆): δ 8.42 (s, 2 H), 8.34 (d, J = 7.4 Hz, 1 H), 7.98 (d, J = 0.9 Hz, 1 H), 7.81 – 7.77 (m, 2 H), 7.74 (t, J = 8.0 Hz, 1 H), 7.65 (d, J = 8.5 Hz, 2 H), 7.56 (d, J = 7.8 Hz, 1 H), 4.46 (t, J = 7.2 Hz, 2 H), 1.85 (t, J = 7.4 Hz, 2 H), 1.79-1.75 (m, 2 H), 1.41-1.37 (m, 2 H), 1.20-1.16 (m, 4 H); ¹³C NMR (100 MHz, DMSO-d₆): δ 169.59, 158.63, 156.05, 154.86, 145.39, 139.33, 137.06, 134.52, 133.44, 131.13, 130.71, 129.67, 128.16, 126.92, 122.05, 121.11, 99.31, 48.43, 32.51, 29.77, 28.34, 26.00, 25.29; HRMS-ESI (m/z): [M + H]⁺ calcd for C₂₆H₂₆ClN₉O₂, 532.1971; found, 532.1978.

Synthesis of 2.6: Compound **S2.4** (35 mg, 0.06 mmol) was added to the hydroxylamine hydrochloride solution as described for the synthesis of **2.3** to give 5.4 mg of compound **2.6** (15%) as a white powder. **Spectral Data.** ^1H NMR (500 MHz, CD_3OD): δ 8.49 (s, 1 H), 8.43 (s, 1 H), 8.36 (d, $J = 7.5$ Hz, 1 H), 7.92 (s, 1 H), 7.84-7.80 (m, 2 H), 7.78 (t, $J = 8.0$ Hz, 1 H), 7.67-7.63 (m, 2 H), 7.60 (d, $J = 7.7$ Hz, 1 H), 4.56 (t, $J = 7.5$ Hz, 2 H), 1.99 (t, $J = 7.3$ Hz, 2 H), 1.89-1.84 (m, 2H), 1.51-1.46 (m, 2H), 1.29-1.20 (m, 6H); ^{13}C NMR (100 MHz, DMSO-d_6): δ 169.43, 158.21, 156.29, 154.90, 145.56, 139.36, 137.06, 134.52, 133.41, 131.16, 130.72, 129.67, 128.19, 126.92, 122.03, 121.08, 99.30, 48.34, 32.57, 29.83, 28.76, 28.43, 26.14, 25.37; HRMS-ESI (m/z): $[\text{M} + \text{H}]^+$ calcd for $\text{C}_{27}\text{H}_{28}\text{ClN}_9\text{O}_2$, 546.2127; found, 546.2129.

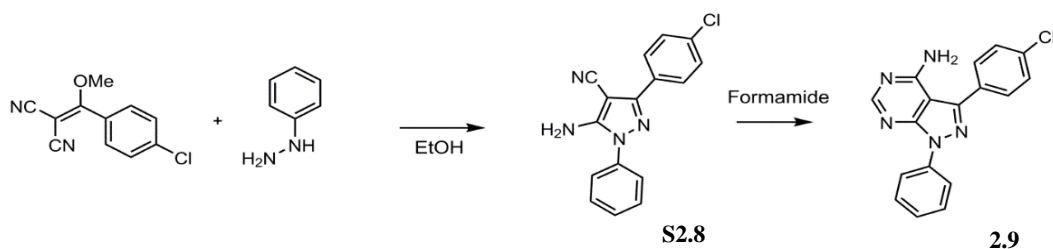
Synthesis of 2.10: Compound **S2.7** (30 mg, 0.11 mmol) was added to the hydroxylamine hydrochloride solution as described for the synthesis of **2.3** to give 15 mg of compound **2.10** (50%) as an oil. **Spectral Data.** ^1H NMR (500 MHz, CD_3OD): δ 7.79 (s, 1 H), 7.58-7.50 (m, 5 H), 4.49 (t, $J = 7.0$ Hz, 2 H), 2.01 (t, $J = 7.4$ Hz, 2 H), 1.84-1.78 (m, 2 H), 1.57-1.51 (m, 2 H), 1.27-1.20 (m, 2 H); ^{13}C NMR (100 MHz, DMSO-d_6): δ 169.28, 137.69, 133.70, 129.75, 129.55, 128.97, 127.30, 48.13, 32.39, 29.40, 25.85, 24.85; HRMS-ESI (m/z): $[\text{M} + \text{H}]^+$ calcd for $\text{C}_{14}\text{H}_{18}\text{N}_4\text{O}_2$, 275.1503; found, 275.1508.



Scheme S 4: Synthesis of Compound **2.7** and **2.8**

Synthesis of 2.7: Reaction of PP2~alkyne (20 mg, 0.06 mmol) and (E)-ethyl 3-(4-(azidomethyl)phenyl)acrylate (16 mg, 0.07 mmol) was prepared as described for the synthesis of **S2.2**. The crude product was carried on without further purification and was added to the hydroxylamine hydrochloride solution as described for the synthesis of **2.3** to give 1.3 mg of compound **2.7** (20%) as a white powder. **Spectral Data.** $^1\text{H NMR}$ (500 MHz, DMSO-d_6): δ 8.35 (s, 3 H), 8.10 (s, 1 H), 7.75-7.63 (m, 5 H), 7.47 (t, $J = 8.1$ Hz, 3 H), 7.37 (d, $J = 15.72$ Hz, 1 H), 7.09 (d, $J = 7.5$ Hz, 2 H), 6.40 (d, $J = 15.84$ Hz, 1 H), 5.79 (s, 2 H); $^{13}\text{C NMR}$ (100 MHz, DMSO-d_6): 158.79, 157.05, 155.12, 145.33, 139.43, 138.16, 137.69, 137.15, 135.64, 134.44, 133.83, 131.30, 130.71, 130.54, 129.79, 129.65, 128.39, 127.76, 126.84, 126.02, 122.08, 121, 120.02, 99.23, 51.51; HRMS-ESI (m/z): $[\text{M} - \text{H}]^-$ calcd for $\text{C}_{29}\text{H}_{22}\text{ClN}_9\text{O}_2$, 562.1512; found, 562.1502.

Synthesis of 2.8: Reaction of PP2~alkyne (10 mg, 0.03 mmol) and (E)-ethyl 3-(4-(azidomethyl)phenyl)acrylate (8 mg, 0.04 mmol) was prepared as described for the synthesis of **S2.2**. The crude product was carried on without further purification and was added to the hydroxylamine hydrochloride solution as described for the synthesis of **2.3** to give 1.4 mg of compound **2.8** (74%) as a white powder. **Spectral Data.** $^1\text{H NMR}$ (500 MHz, DMSO-d_6): δ 8.38 – 8.28 (m, 2 H), 8.09 (s, 1 H), 7.74 - 7.64 (m, 6 H), 7.49 (d, $J = 7.75$ Hz, 1 H), 7.42 (d, $J = 7.9$ Hz, 1 H), 7.37 – 7.24 (m, 3 H), 7.05 (d, $J = 7.8$ Hz, 1 H), 6.35 (d, $J = 15.8$ Hz, 1 H), 5.78 (s, 2 H); $^{13}\text{C NMR}$ (100 MHz, DMSO-d_6): δ 158.80, 157.06, 145.34, 139.44, 138.18, 137.69, 137.16, 134.45, 133.84, 131.31, 130.71, 130.55, 129.79, 129.66, 128.40, 127.77, 126.85, 126.04, 122.09, 120.03, 99.23, 51.51; HRMS-ESI (m/z): $[\text{M} - \text{H}]^-$ calcd for $\text{C}_{29}\text{H}_{22}\text{ClN}_9\text{O}_2$, 562.1512; found, 562.1496.

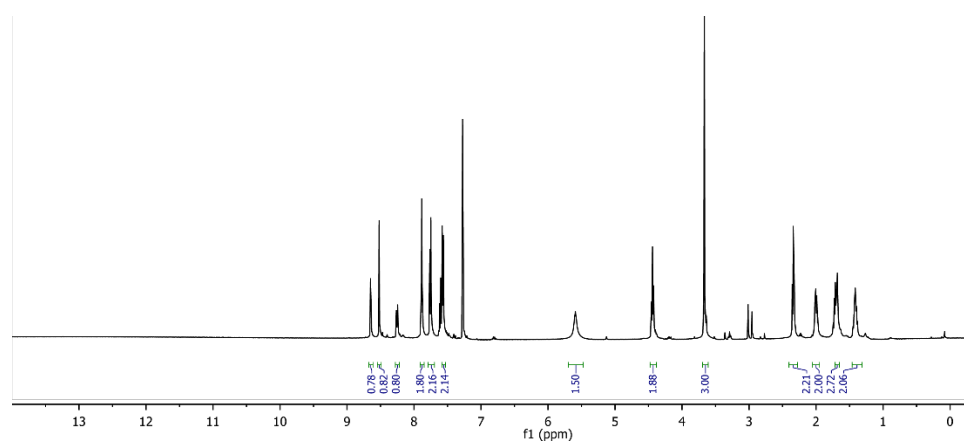
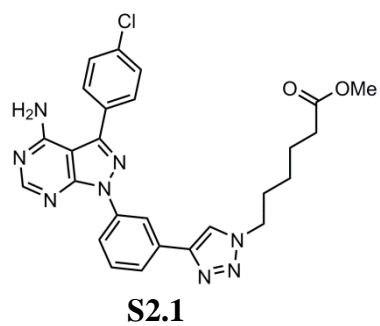


Scheme S 5: Synthesis of Compound **2.9**

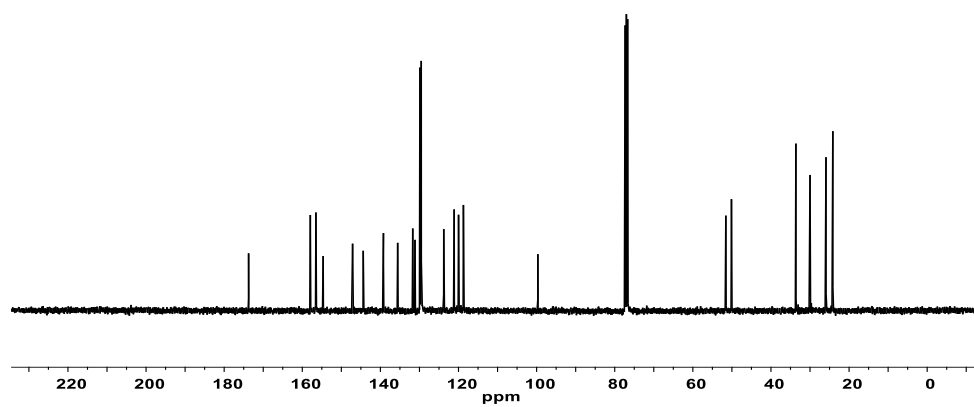
Synthesis of S2.8: To an oven-dried round bottom flask was added 2-((4-chlorophenyl)(methoxy)methylene)malononitrile² (500 mg, 2.29 mmol). Ethanol (11.4 mL) was added, followed by phenylhydrazine (247 mg, 2.29 mmol). The reaction mixture was then heated to 85 °C for 1 hour. The reaction was then allowed to cool to room temperature. During the cooling process visible precipitation began to occur. After sufficient cooling the reaction mixture was filtered to provide the product **S2.8** as a fluffy light pink solid (290 mg, 43% yield). **Spectral data.** ¹H NMR (500 MHz, DMSO-d₆): δ 7.89-7.85 (m, 2 H), 7.60-7.53 (m, 2 H), 7.49-7.44 (m, 1 H), 6.88 (s, 2 H); ¹³C NMR (100 MHz, DMSO-d₆): δ 153.44, 149.50, 137.70, 134.18, 130.49, 129.95, 129.36, 128.56, 128.05, 124.79, 115.83; HRMS-APCI (m/z): [M + H]⁺ calcd for C₇₉H₉₅ClN₂₀O₂₂, 295.0746; found 295.0746.

Synthesis of 2.9: To an oven-dried round bottom flask was added **S2.8** (205 mg, 0.7 mmol). Formamide (2 mL) was then added. The reaction mixture was heated to 220 °C for 5 hours. The reaction was then allowed to cool to room temperature. After sufficient cooling, water (6 mL) was added to precipitate the reaction. The reaction was then filtered, and the resulting solid was rinsed with water (2 mL x 3). After drying the product **2.9** was obtained as a light brown solid (190 mg, 85% yield). **Spectral data.** ¹H NMR (500 MHz, DMSO-d₆): δ 8.38 (s, 1 H), 8.23-8.20 (m, 2 H), 7.79-7.76 (m, 2 H), 7.66-7.62 (m, 2 H), 7.59-7.54 (m, 2 H), 7.39-7.34 (m, 1 H); ¹³C NMR (100 MHz, DMSO-d₆): δ 158.84, 157.02, 154.91, 144.88, 139.03, 134.31, 131.53, 130.70, 129.64, 129.59, 129.83, 121.55, 99.13; HRMS-APCI (m/z): [M + H]⁺ calcd for C₇₉H₉₅ClN₂₀O₂₂, 322.0854; found 322.0864.

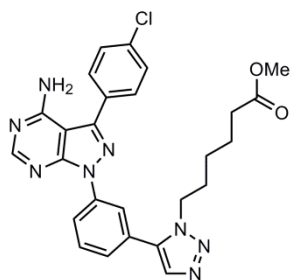
Spectral Data for Compounds 2.3-2.10



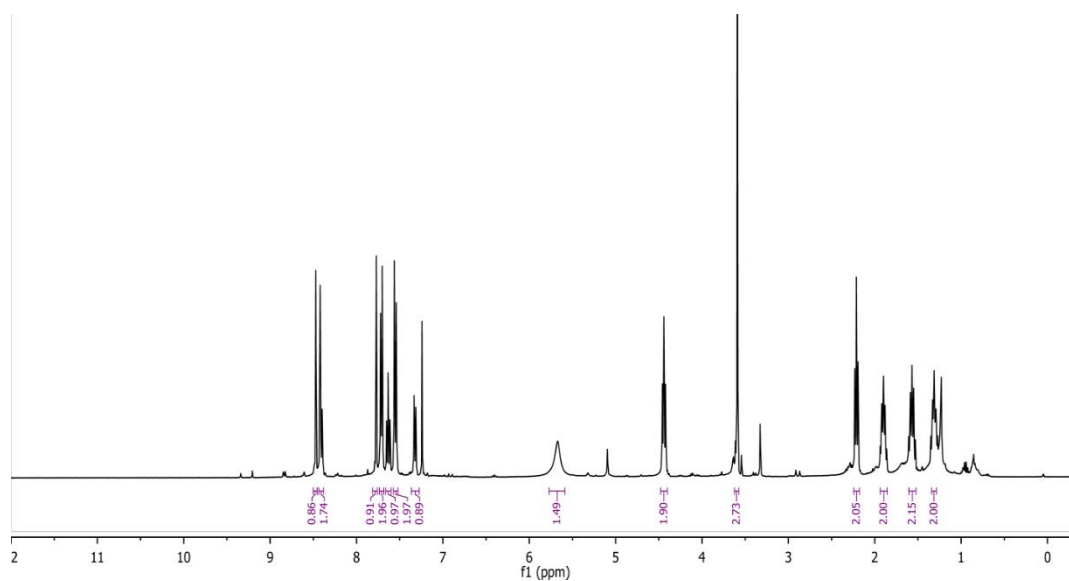
Compound S2.1 ¹H



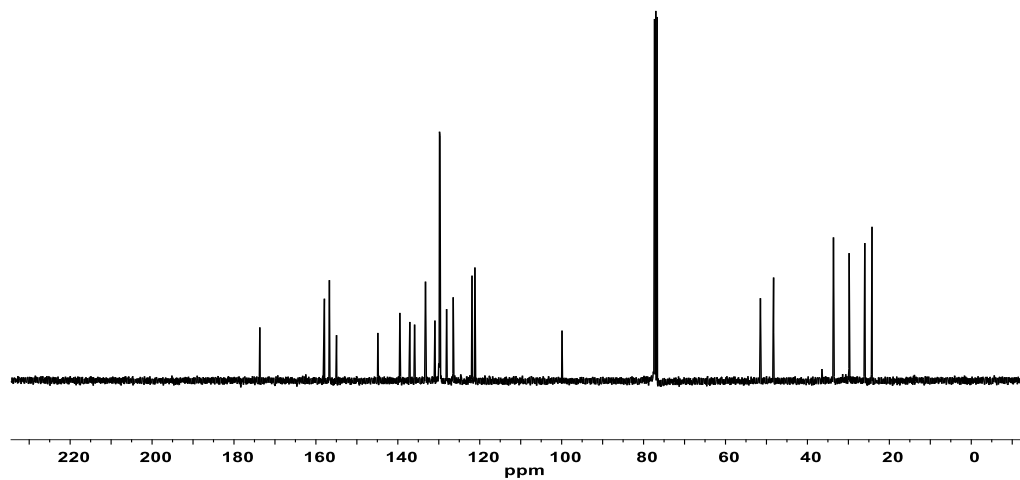
Compound S2.1 ¹³C



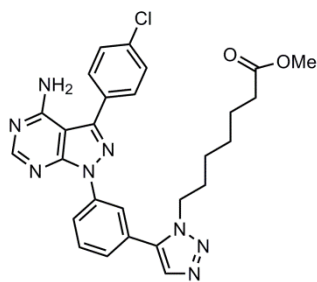
S2.2



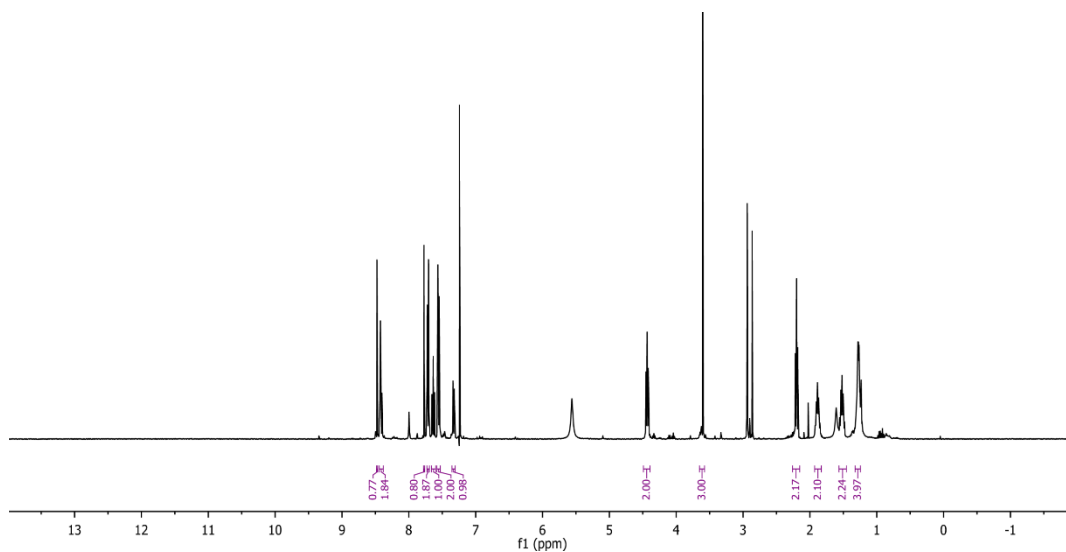
Compound S2.2 ¹H



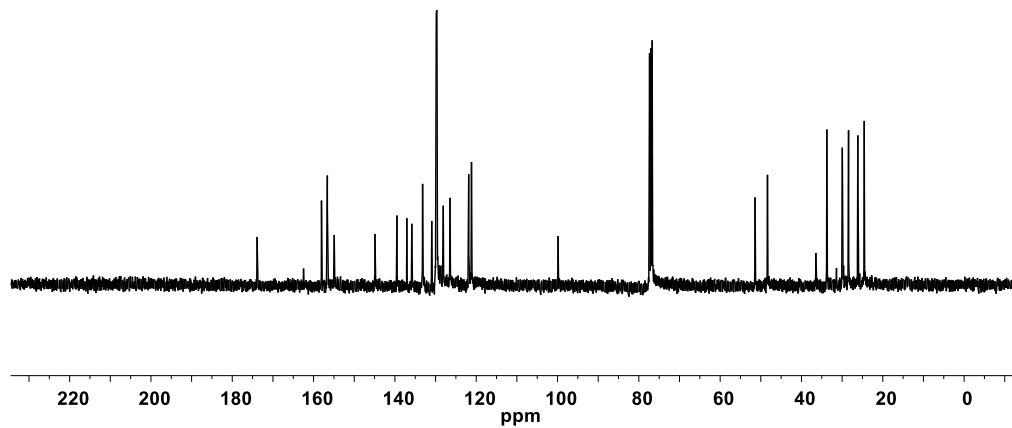
Compound S2.2 ¹³C



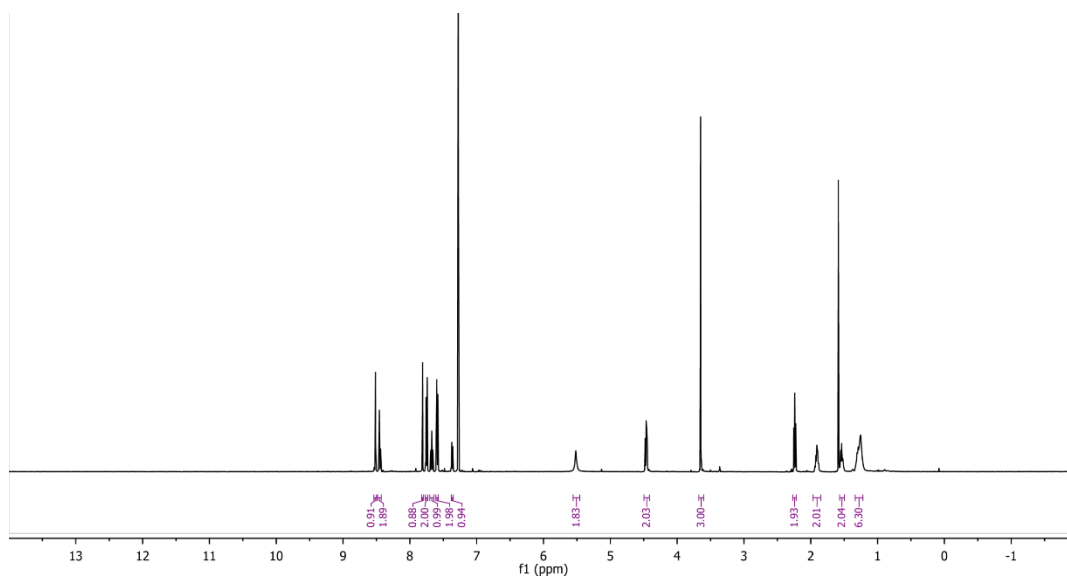
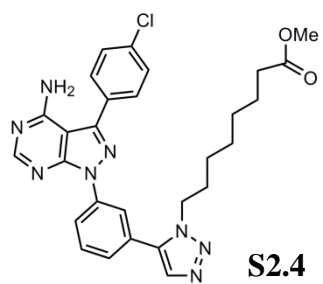
S2.3



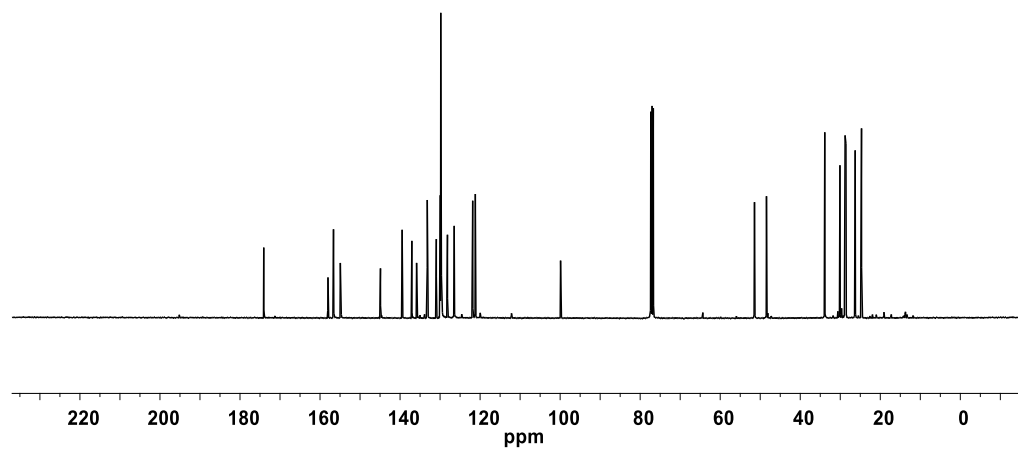
Compound S2.3 ¹H



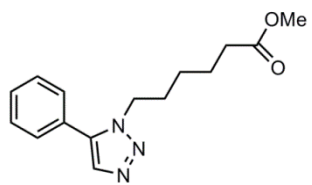
Compound S2.3 ¹³C



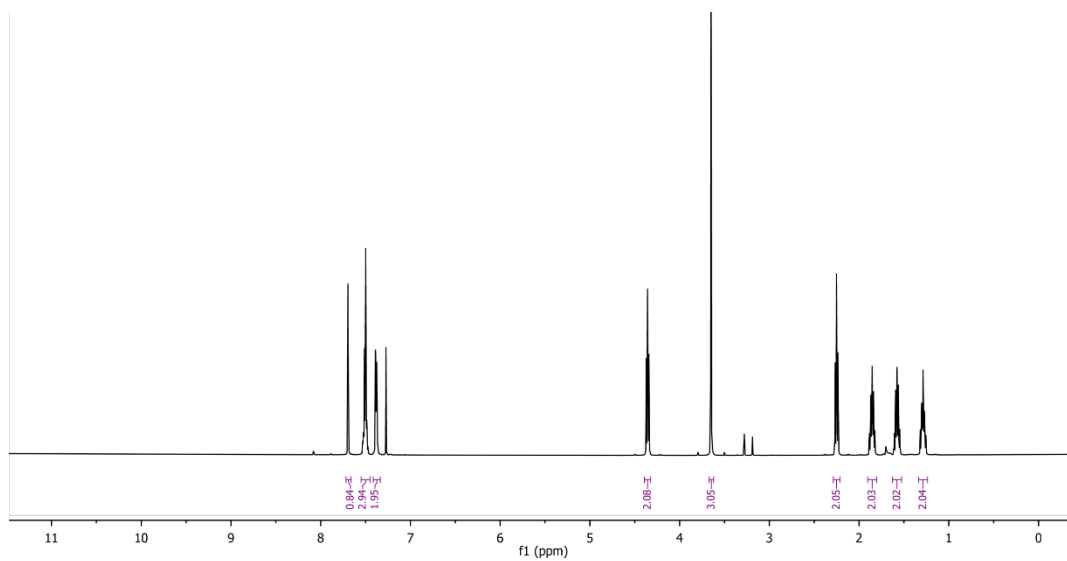
Compound **S2.4** ^1H



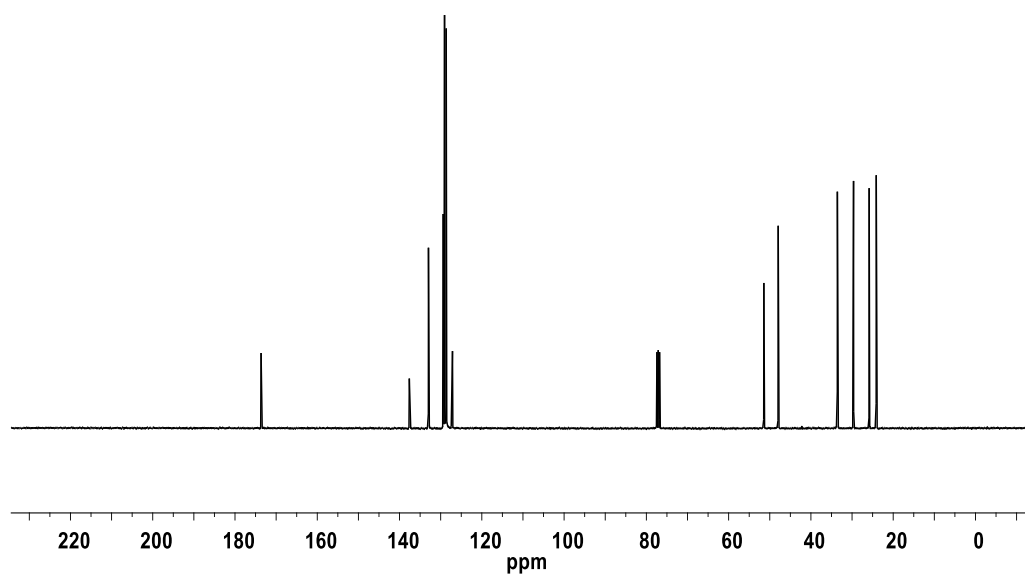
Compound **S2.4** ^{13}C



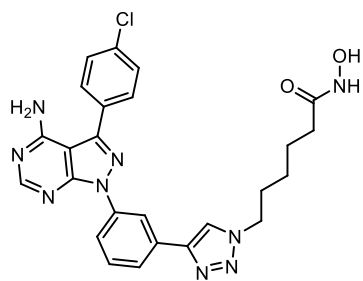
S2.7



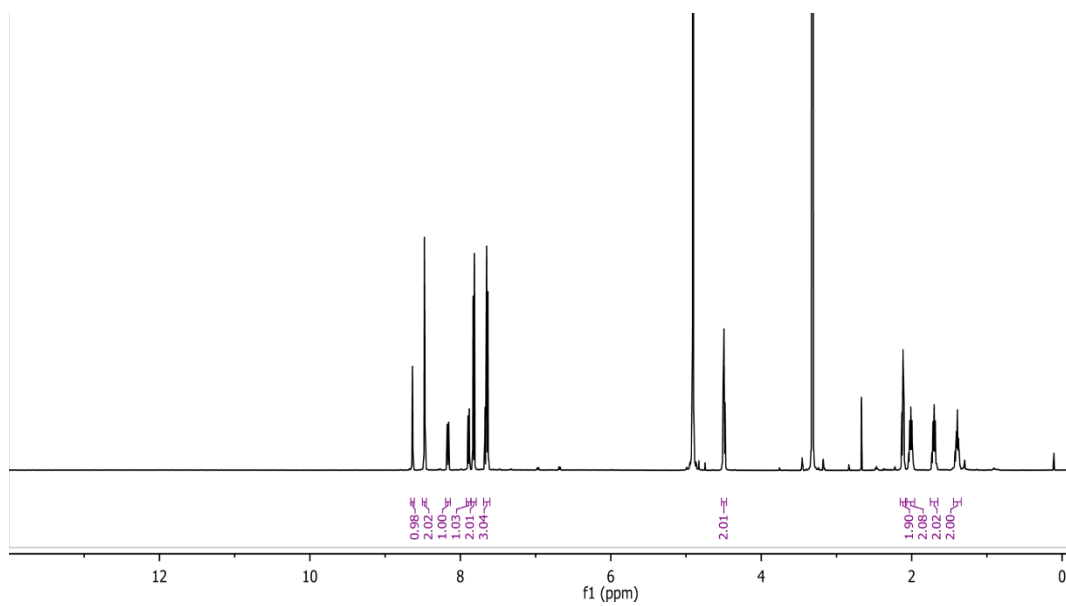
Compound **S2.7** ^1H



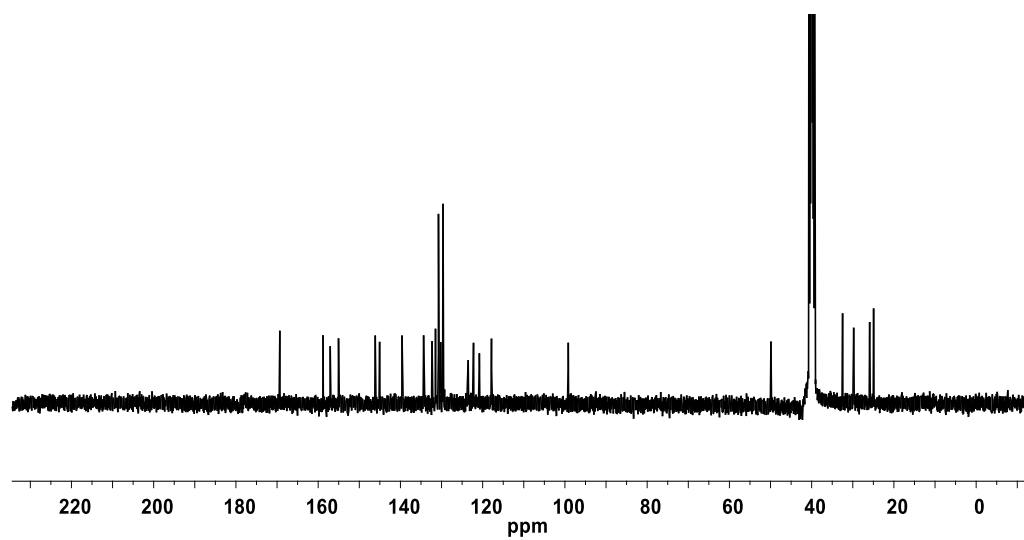
Compound **S2.7** ^{13}C



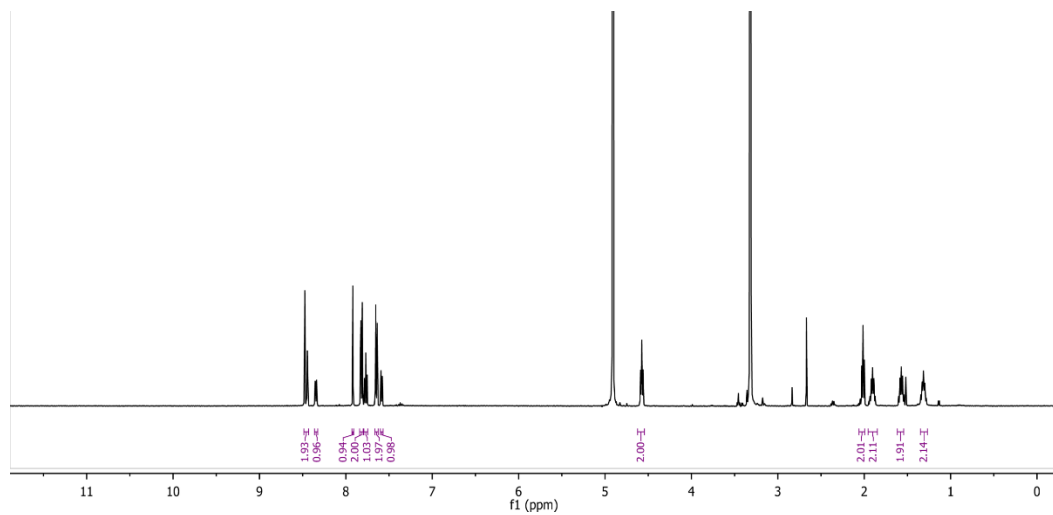
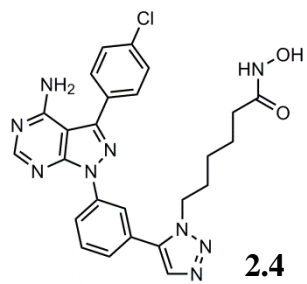
2.3



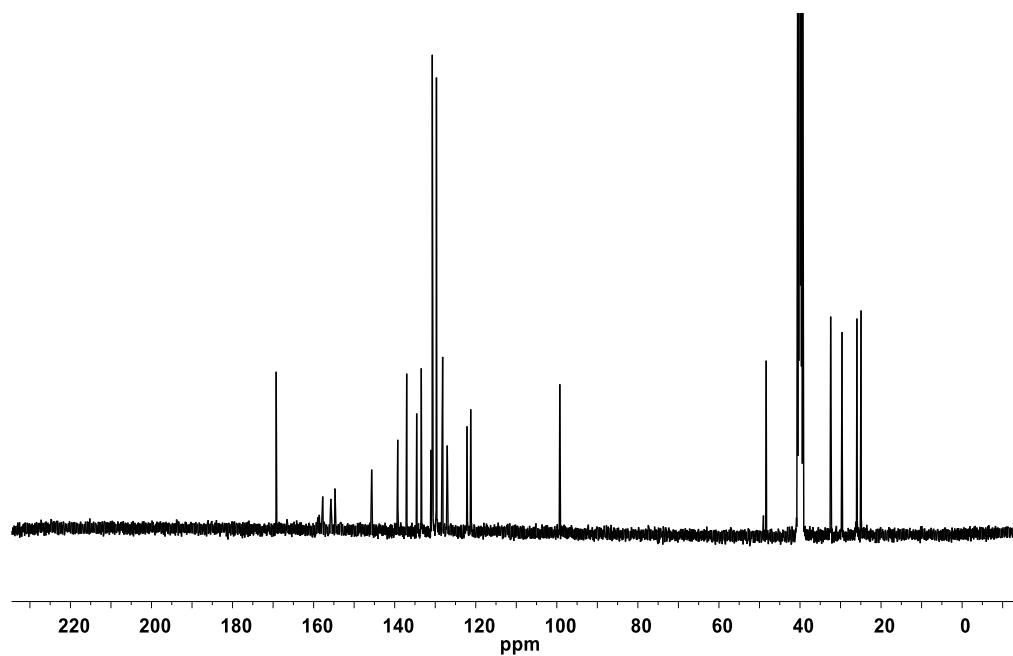
Compound **2.3** ^1H



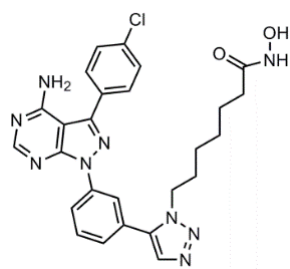
Compound **2.3** ^{13}C



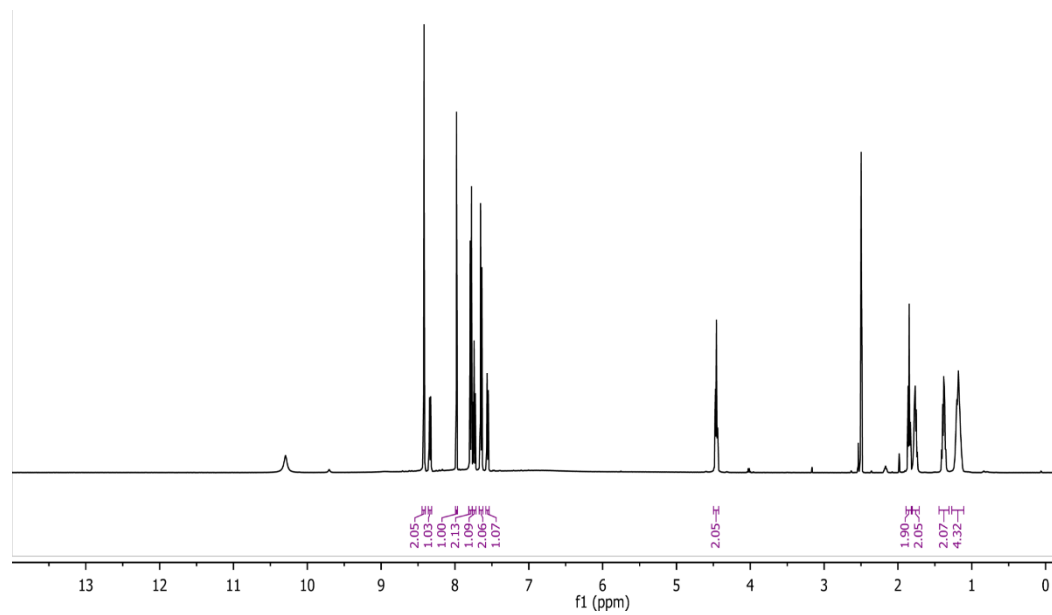
Compound **2.4** ^1H



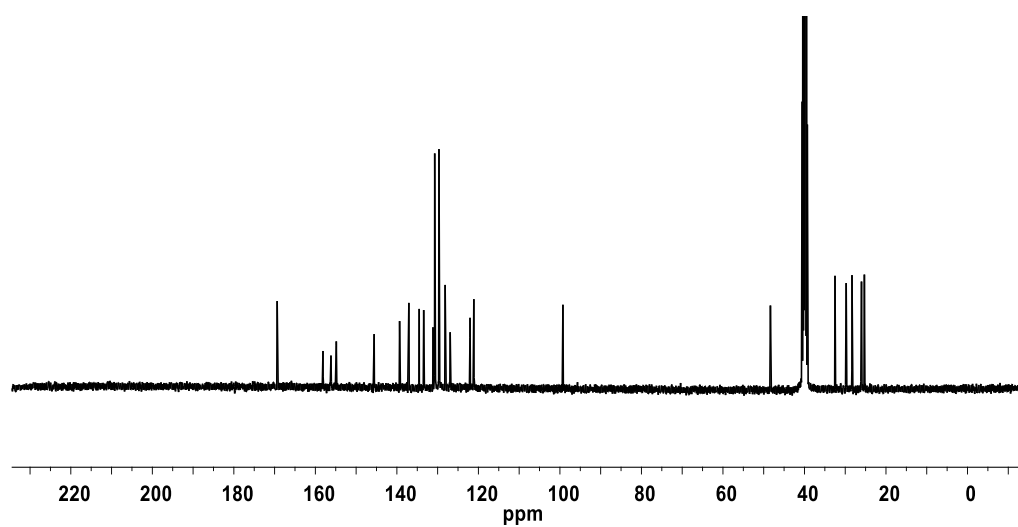
Compound **2.4** ^{13}C



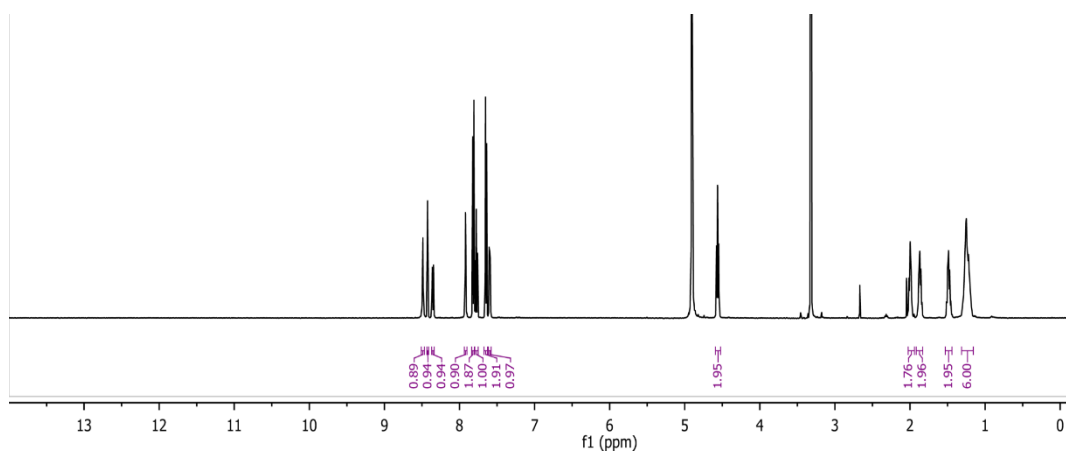
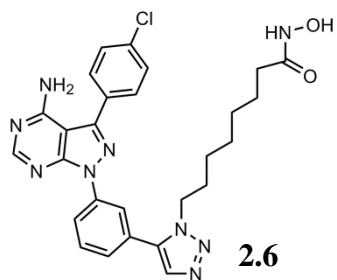
2.5



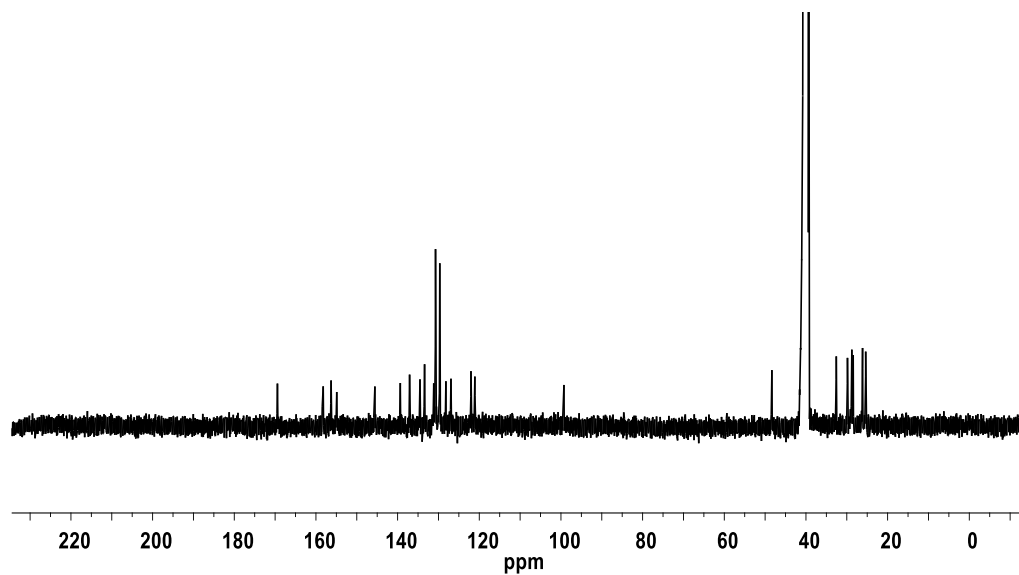
Compound **2.5** ¹H



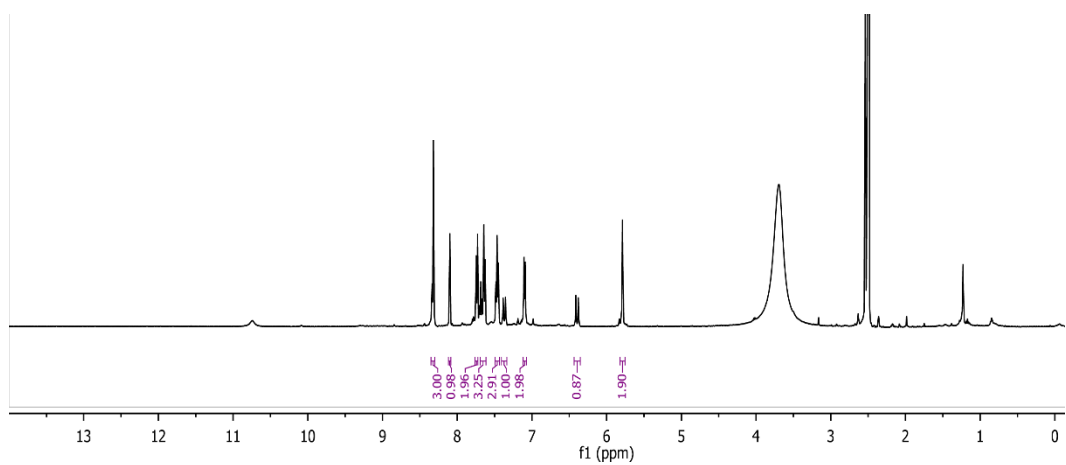
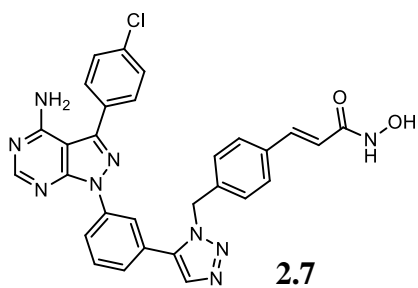
Compound **2.5** ¹³C



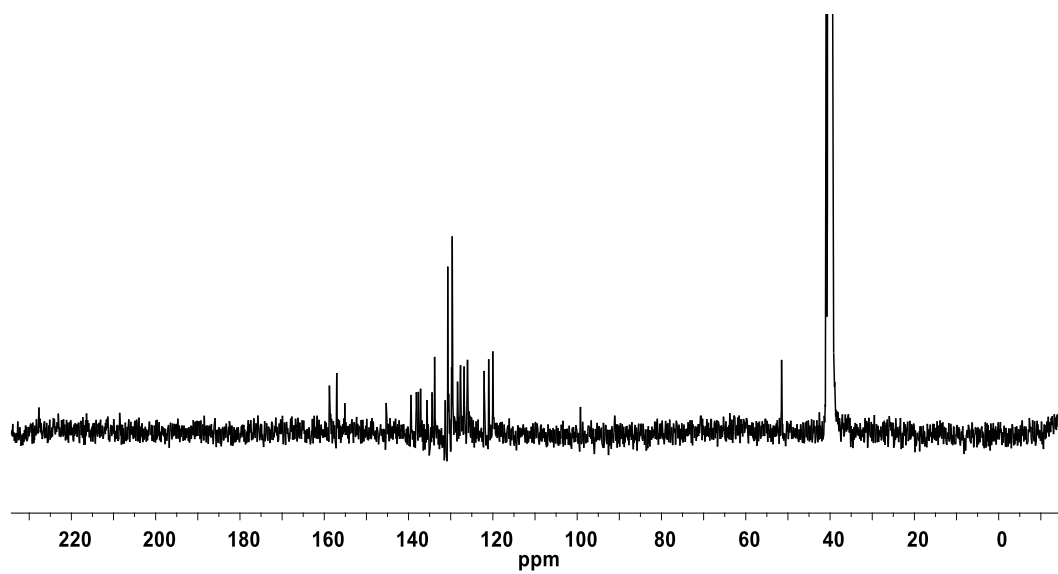
Compound **2.6** ^1H



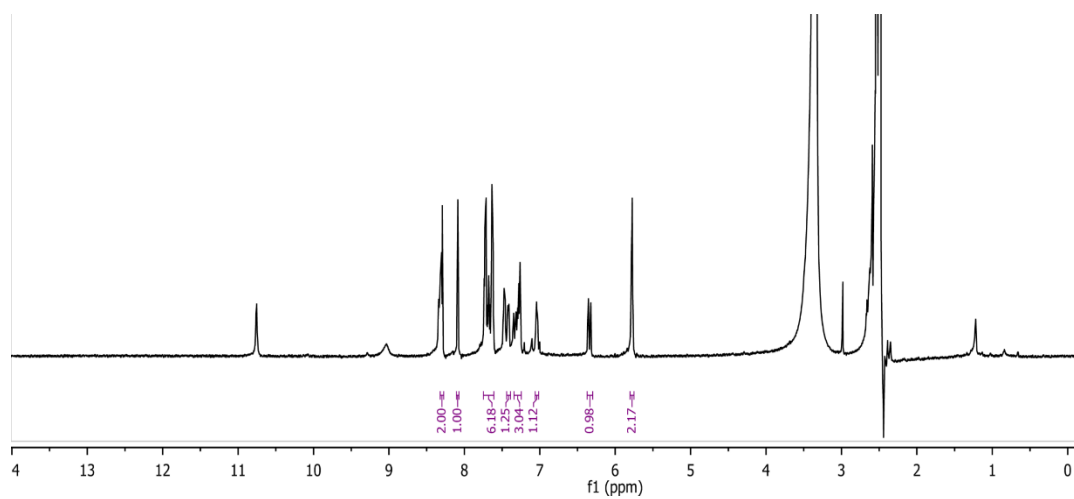
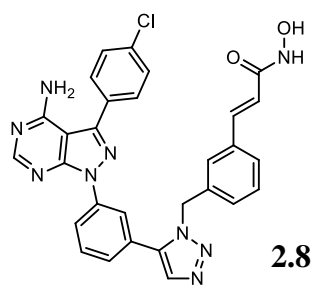
Compound **2.6** ^{13}C



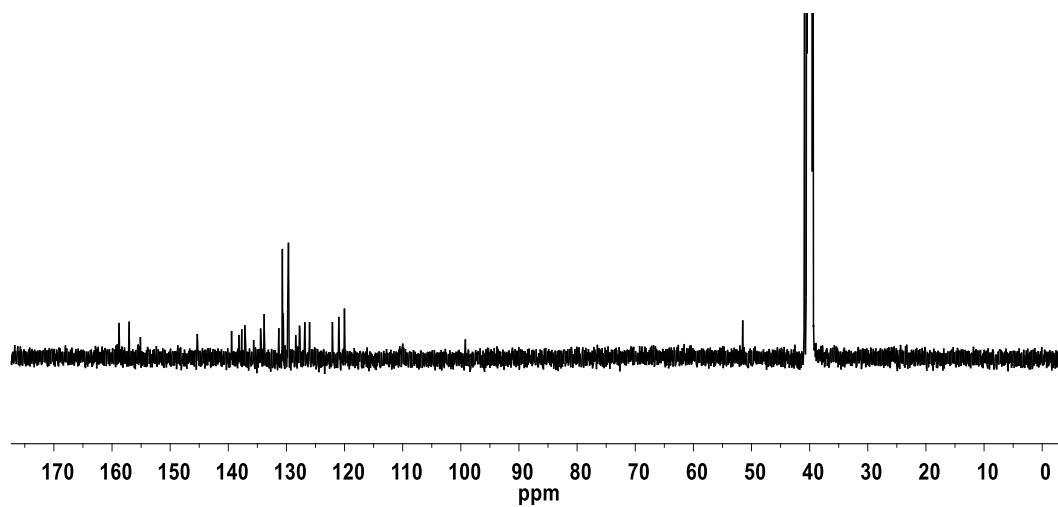
Compound **2.7** ¹H



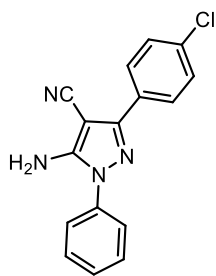
Compound **2.7** ¹³C



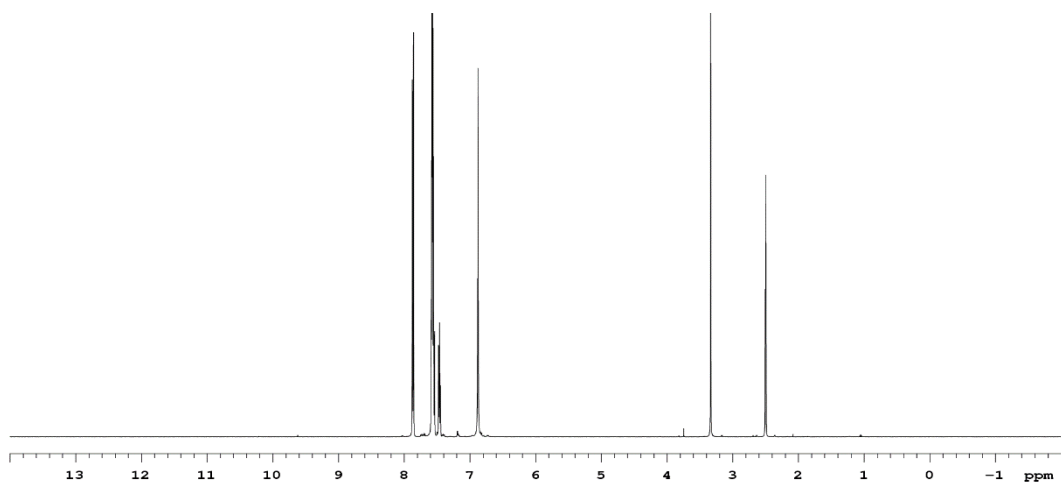
Compound **2.8** ^1H



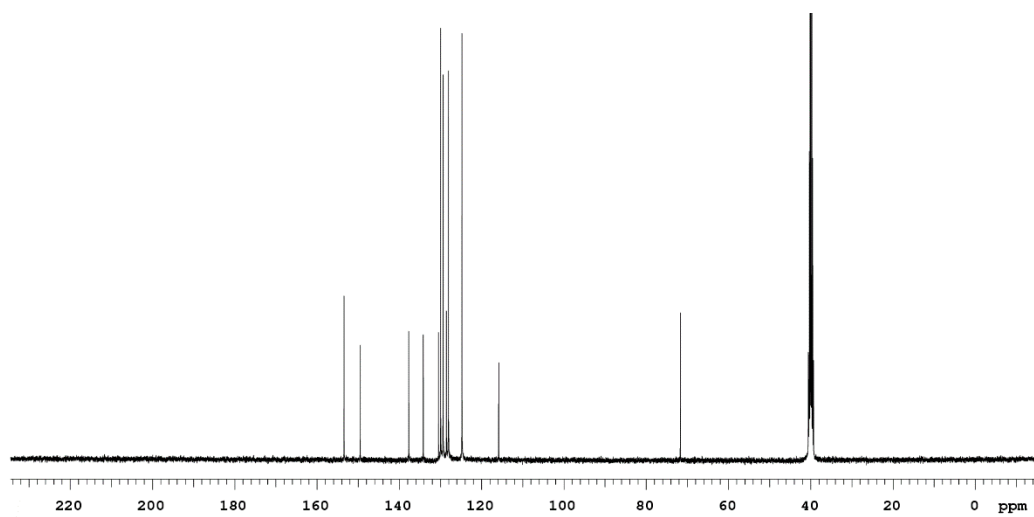
Compound **2.8** ^{13}C



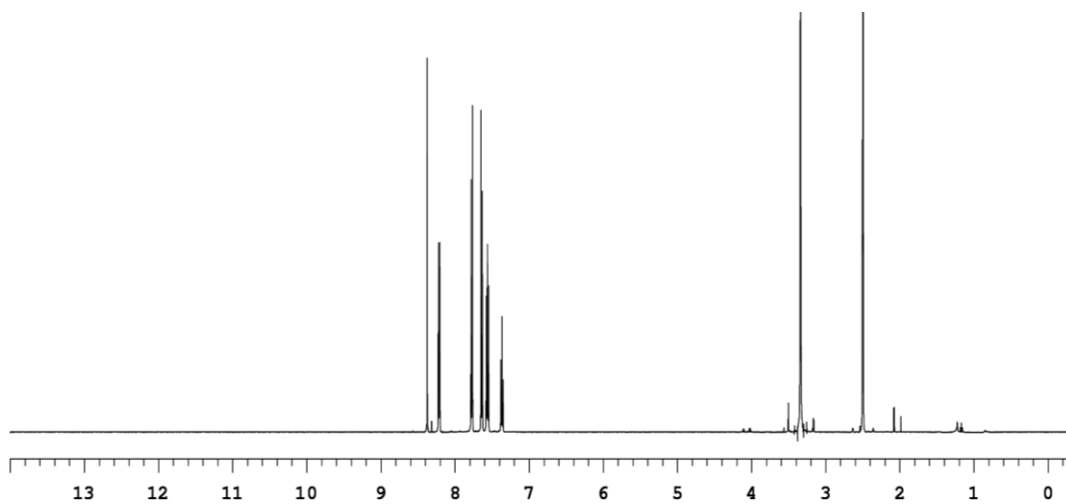
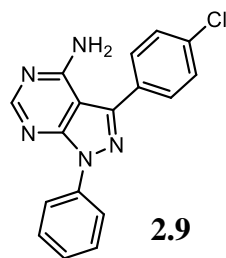
S2.8



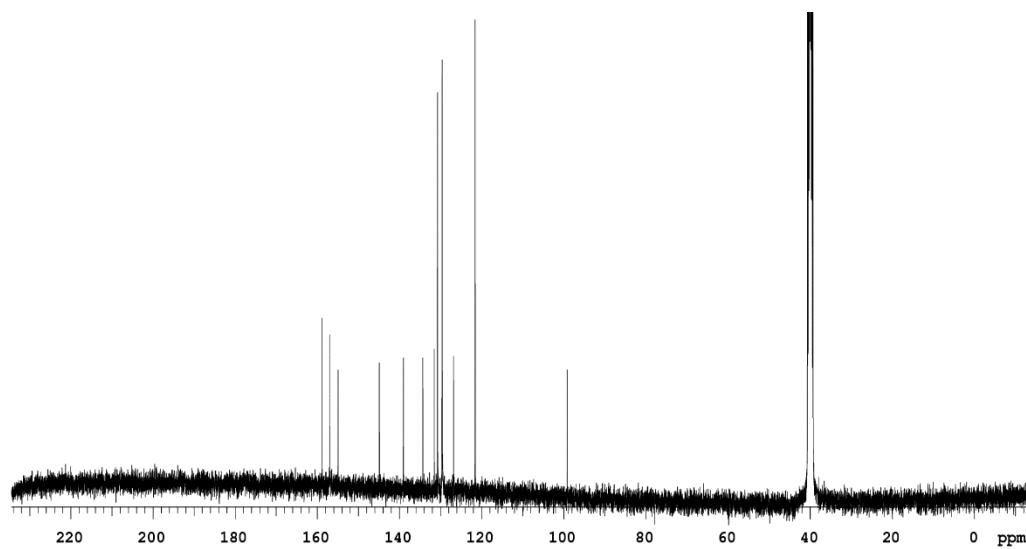
Compound **S2.8** ¹H



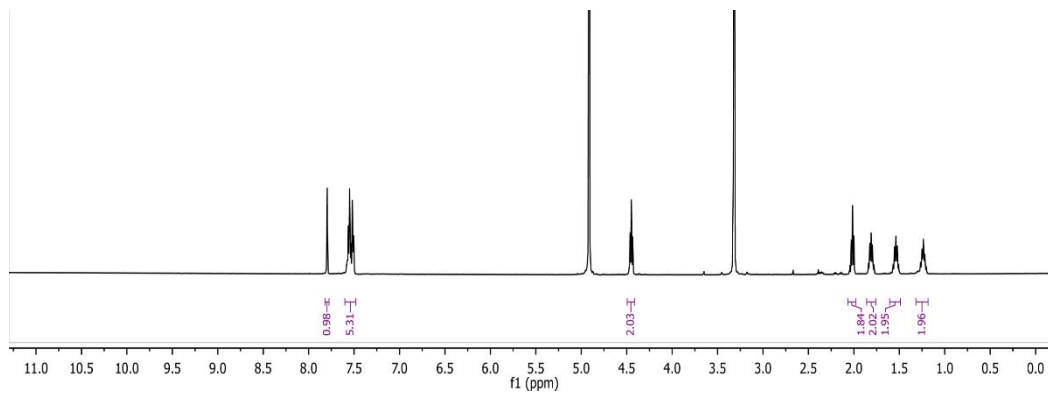
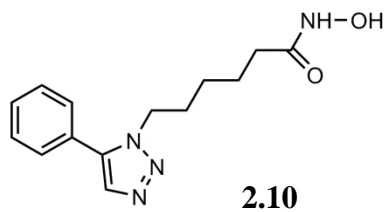
Compound **S2.8** ¹³C



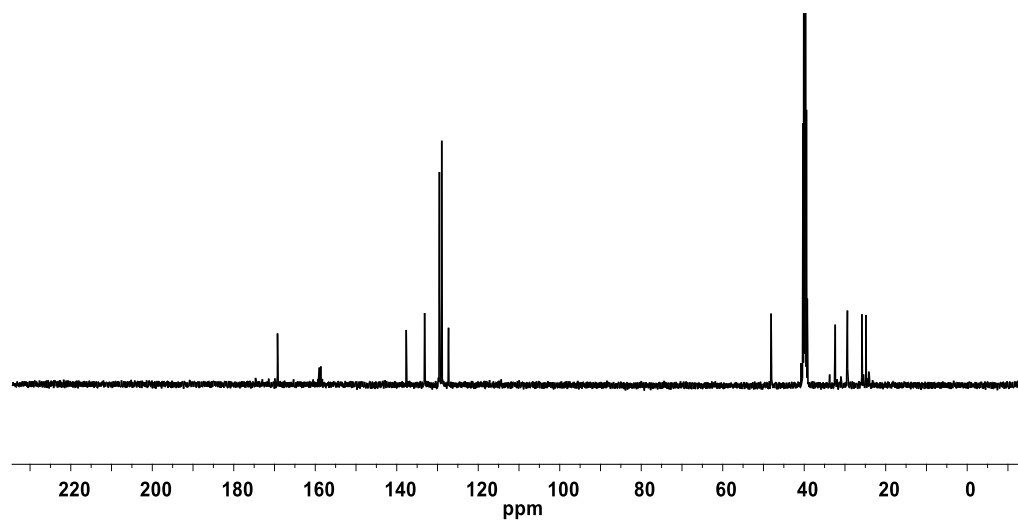
Compound **2.9** ¹H



Compound **2.9** ¹³C



Compound **2.10** ¹H



Compound **2.10** ¹³C

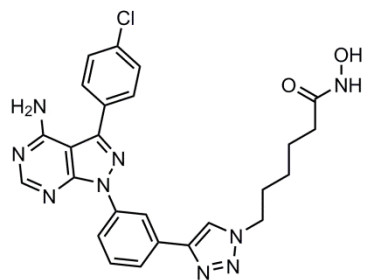
Biochemical Characterization

General procedure for determination of inhibitor K_i for c-Src: c-Src inhibition assay was performed using a continuous, fluorimetric assay as previously described.²² Reaction volumes of 100 μ L were used in 96-well plates. To each well was added 85 μ L of buffer + enzyme. 2.5 μ L of varying concentrations of inhibitor was then added (typically 10000, 2500, 625, 156, 39, 10, 2.4, 0.61, 0.15, 0 μ M in DMSO). 2.5 μ L of peptide substrate (“compound 3” as described in Wang et. al.)²² solution (1.8 mM in DMSO) was added. 10 μ L of ATP (1 mM in water) was added to initiate the reaction and was immediately monitored at 405 nm (ex. 340 nm) for 10 minutes. Final concentrations in the reaction are 30 nM enzyme, 45 μ M peptide substrate, 100 μ M ATP, 100 μ M Na_3VO_4 , 100 mM Tris buffer (pH 8), 10 mM MgCl_2 , 0.01% Triton X-100. The initial rate of the reaction was used to determine K_i values. For K_i determination, the kinetic values were obtained directly from nonlinear regression of substrate-velocity curves in the presence of various concentrations of the inhibitor. The equation $Y = \text{Bottom} + (\text{Top} - \text{Bottom}) / (1 + 10^X - \text{LogEC}_{50})$, $X = \log(\text{concentration})$ and $Y = \text{binding}$; was used in the nonlinear regression.

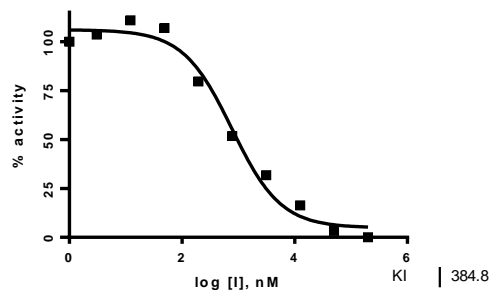
General procedure for determination of inhibitor K_i for HDAC 1: HDAC 1 assay was performed in a fluorescence assay in 96-well plates with a reaction volume of 100 μ L as was previously described.²³ To each well was added buffer (75 μ L), trypsin (10 μ L), and HDAC 1 enzyme (10 μ L). 2.5 μ L of varying concentrations of inhibitor was then added (typically 781, 195, 49, 12, 3, 0.76, 0.19, 0.05, 0.01, 0.003, 0 nM in DMSO). 2.5 μ L of peptide substrate (Ac-Leu-Gly-Lys(Ac)AMCA) solution (2 mM in DMSO) was added to initiate the reaction and was monitored at 370 nm (ex. 455 nm) for 30 min. after a 30 min. lag phase. Final concentrations in the reaction are 400 pM HDAC 1, 1 μ M trypsin, 50 μ M peptide substrate ($K_M = 39.5$ μ M), 15 mM Tris buffer (pH 8.1), 250 μ M EDTA, 250 mM NaCl, 10% glycerol, and 0.01% Triton X-100. The initial rate of the reaction was used to determine K_i values. Note: For those compounds where it is titrating with enzyme (**2.3-2.5**), the compound was reassess at a higher peptide substrate concentration of 500 μ M and the K_i remained unchanged (data not shown). For K_i determination, the kinetic values were obtained directly from nonlinear regression of substrate-velocity curves in the presence of various concentrations of the inhibitor. The equation $Y = \text{Bottom} + (\text{Top} - \text{Bottom}) / (1 + 10^X - \text{LogEC}_{50})$, $X = \log(\text{concentration})$ and $Y = \text{binding}$; was used in the nonlinear regression.

Analytical data for K_i determination. Each inhibitor K_i value was determined using at least 3 independent measurements. An example curve is provided for each inhibitor.

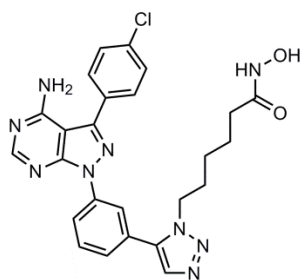
c-Src Assay Data: Representative Curves



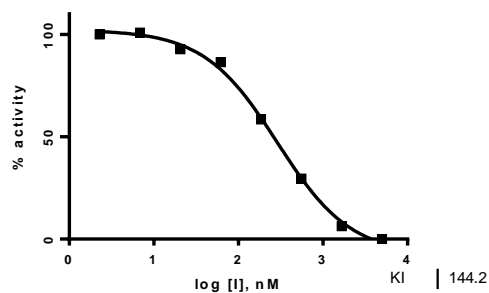
2.3



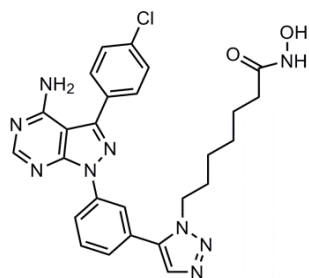
Avg $K_i = 371 \pm 12.0$ nM



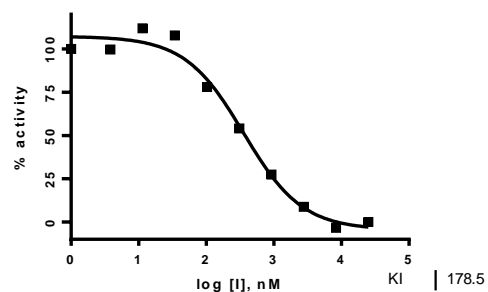
2.4



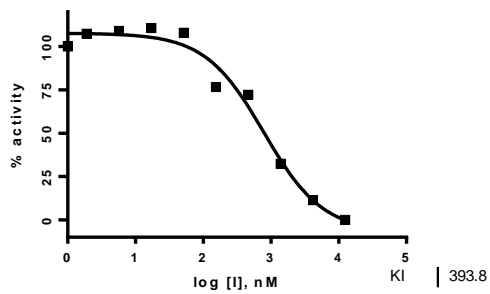
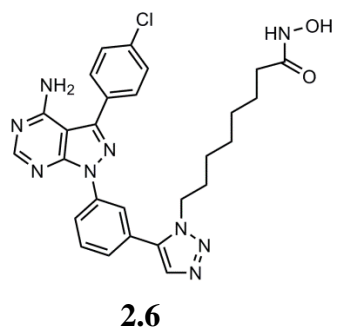
Avg $K_i = 371 \pm 12.0$ nM



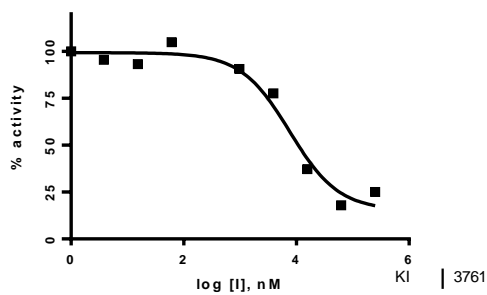
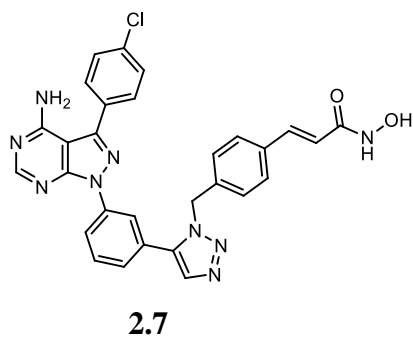
2.5



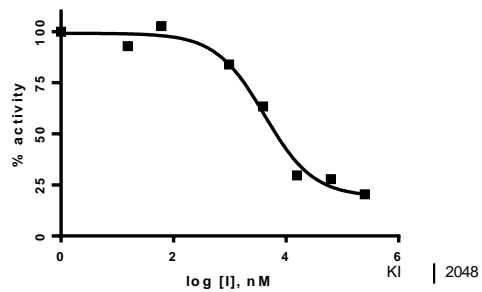
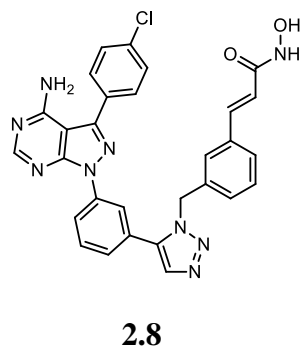
Avg $K_i = 371 \pm 12.0$ nM



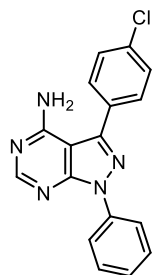
Avg $K_i = 371 \pm 12.0$ nM



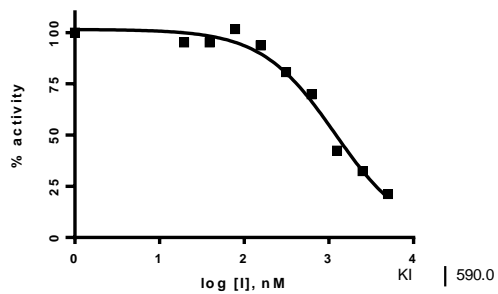
Avg $K_i = 4305$ nM



Avg $K_i = 2136 \pm 393$ nM

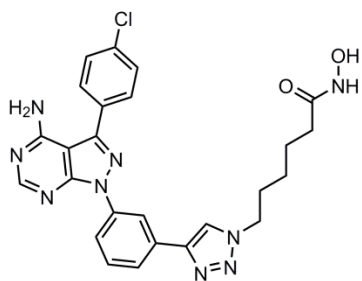


2.9

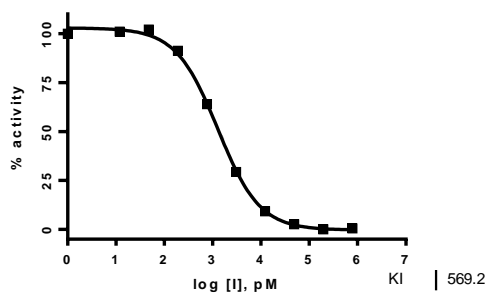


Avg $K_i = 2136 \pm 393$ nM

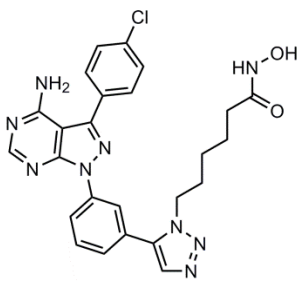
HDAC 1 Assay Data: Representative Curve



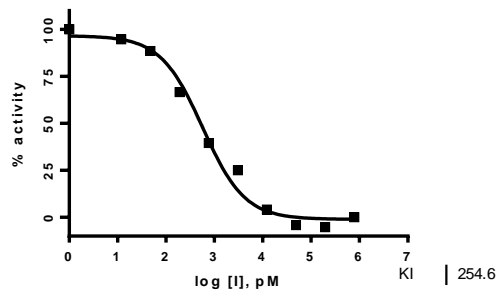
2.3



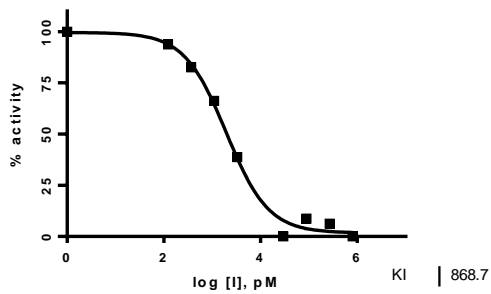
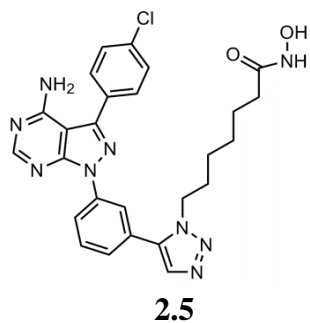
Avg $K_i = 621 \pm 46$ pM



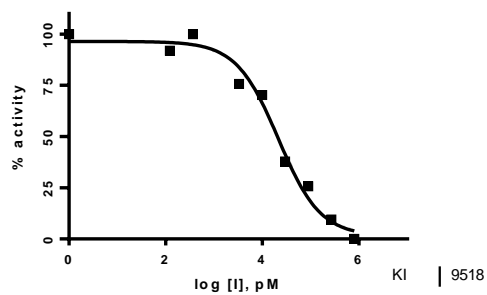
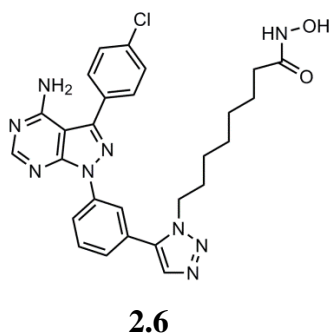
2.4



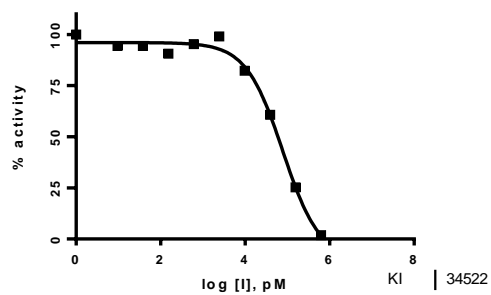
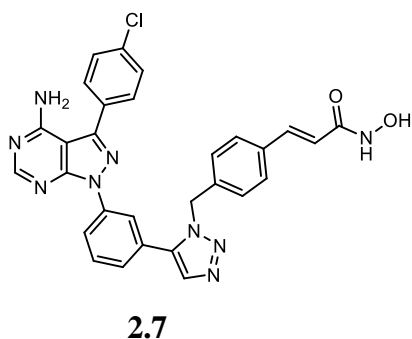
Avg $K_i = 256 \pm 22$ pM



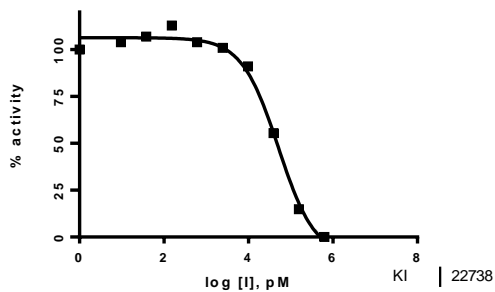
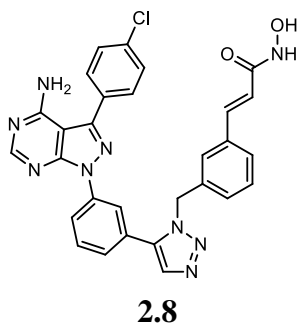
Avg $K_i = 820 \pm 285$ pM



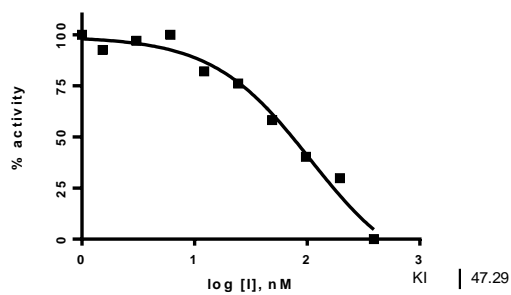
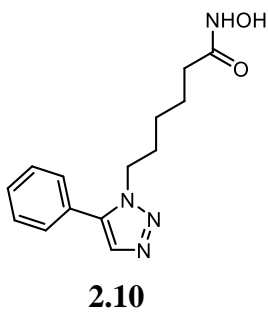
Avg $K_i = 9800 \pm 804$ pM



Avg $K_i = 35 \pm 0.6$ nM

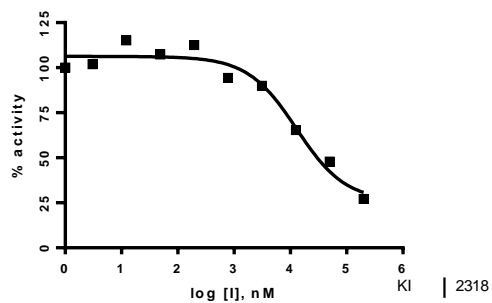
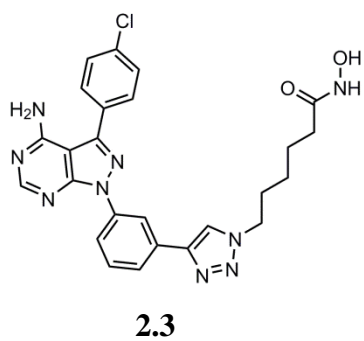


Avg $K_i = 23 \pm 1.5$ nM

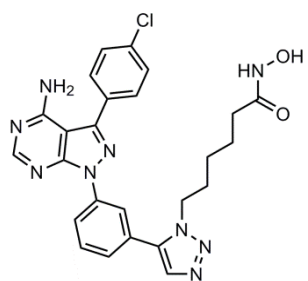


Avg $K_i = 45.5 \pm 1.6$ nM

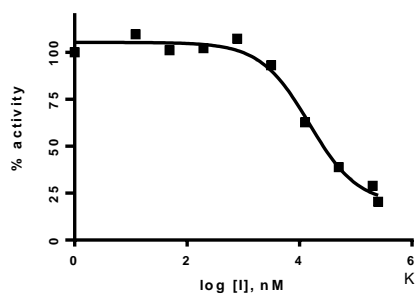
c-Abl Assay Data: Representative Curve



Avg $K_i = 2929 \pm 1190$ nM

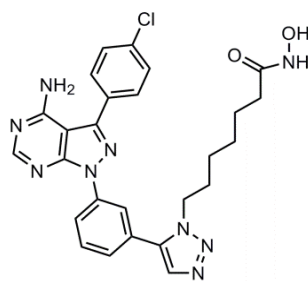


2.4

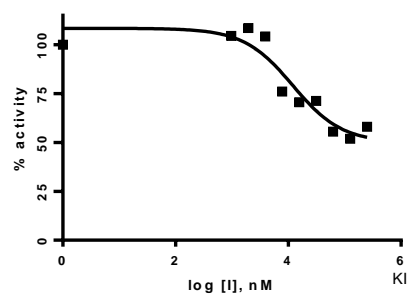


| 2674

Avg $K_i = 2347 \pm 249$ nM

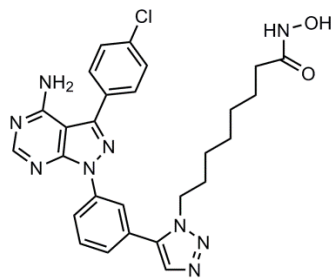


2.5

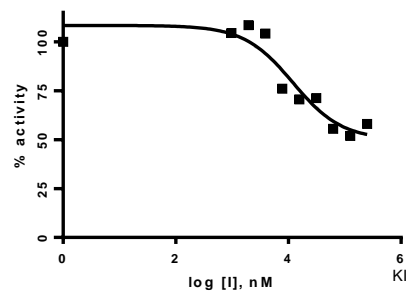


| 2163

Avg $K_i = 1866 \pm 147$ nM



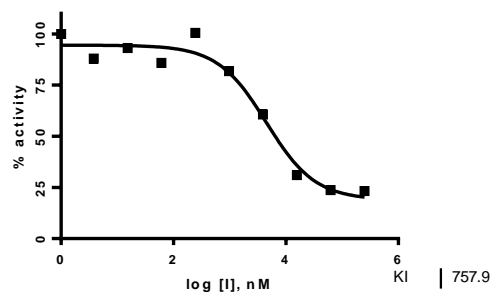
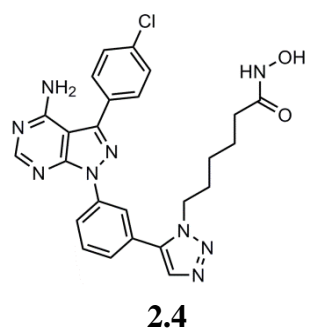
2.6



| 2163

Avg $K_i = 1659 \pm 336$ nM

c-Hck Assay Data:

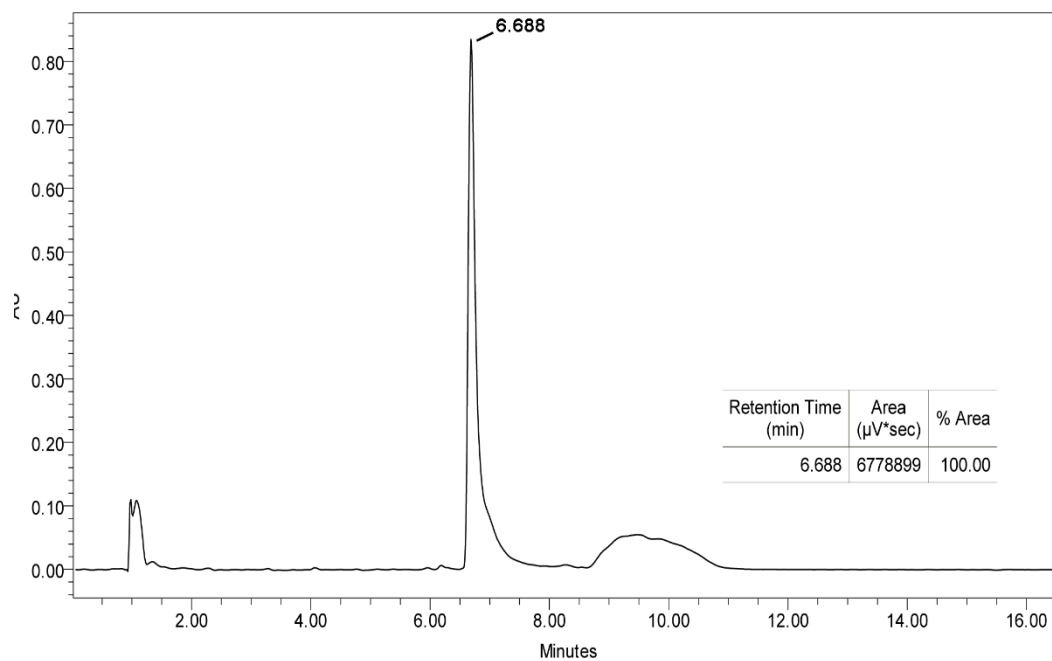


Avg $K_i = 504 \pm 172$ nM

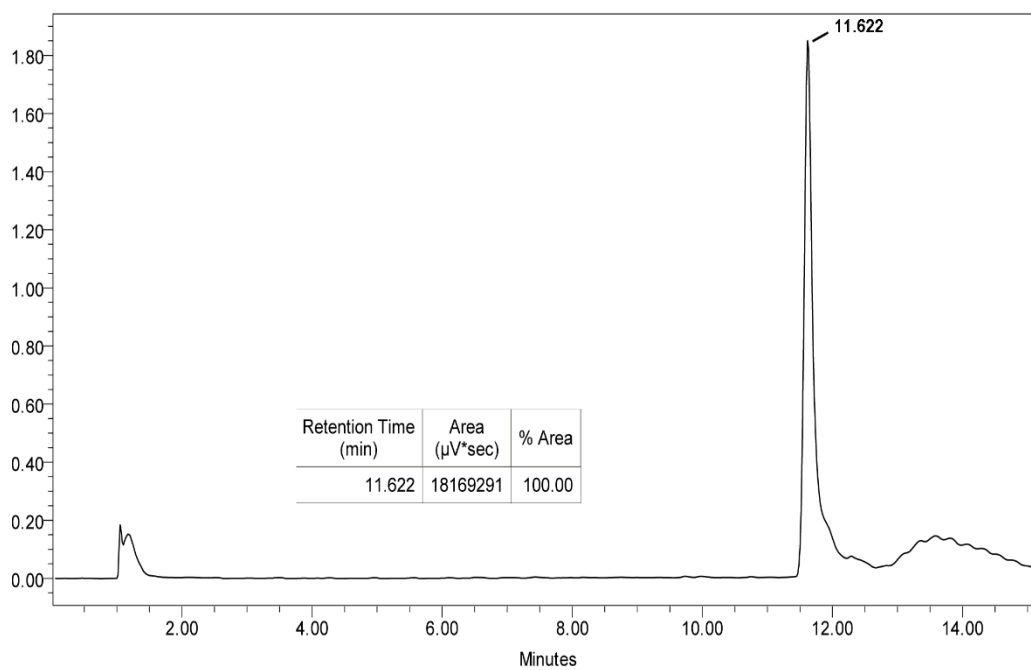
Analytical HPLC trace for Compounds 2.3-2.10

Compound 2.3:

5-95% CH₃CN/H₂O gradient

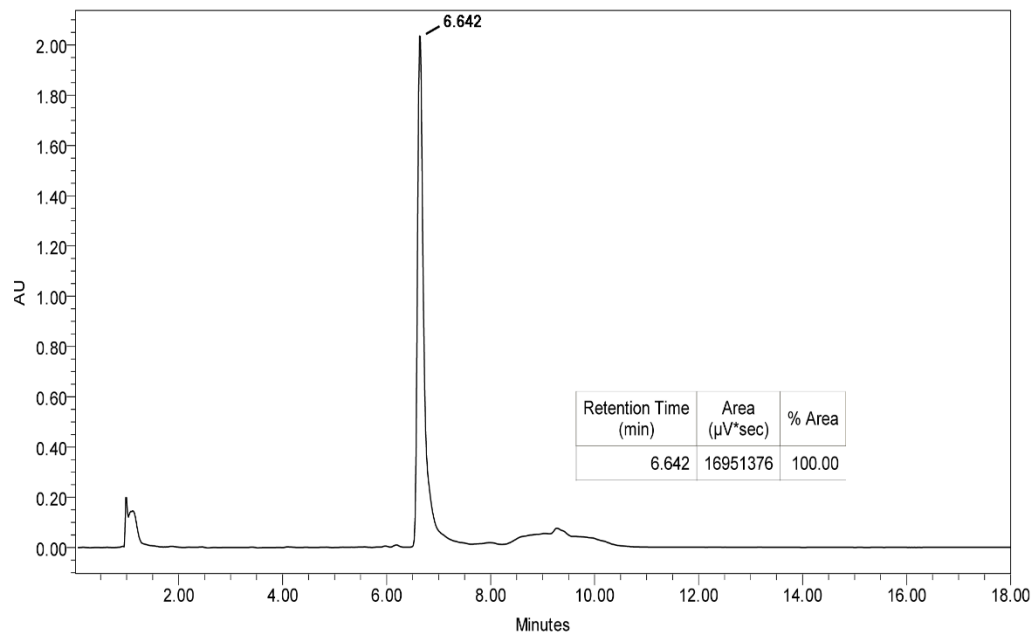


95% CH₃OH/H₂O gradient

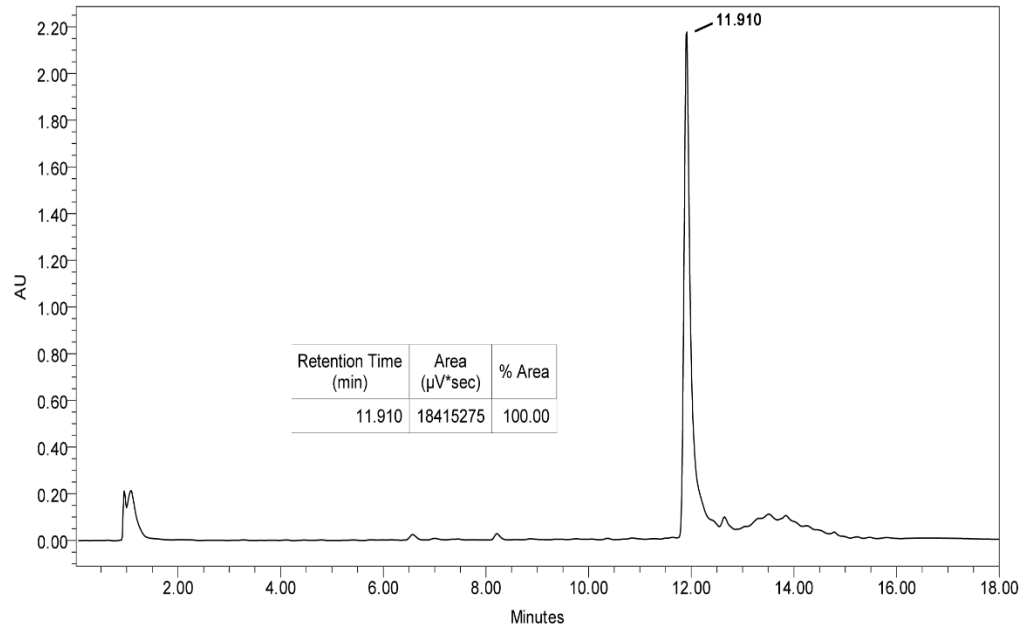


Compound 2.4:

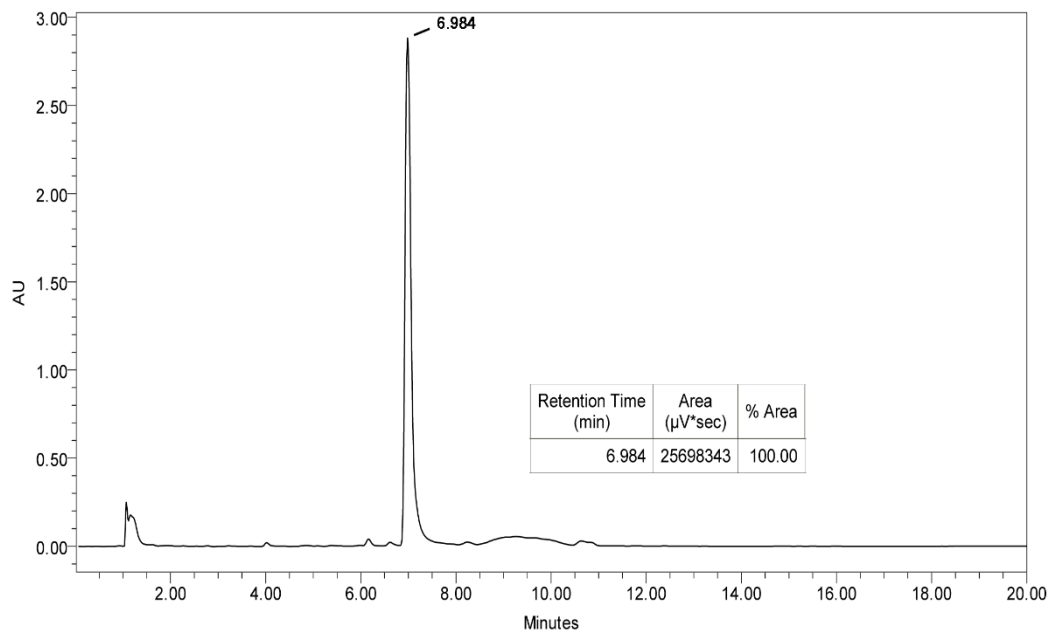
5-95% CH₃CN/H₂O gradient



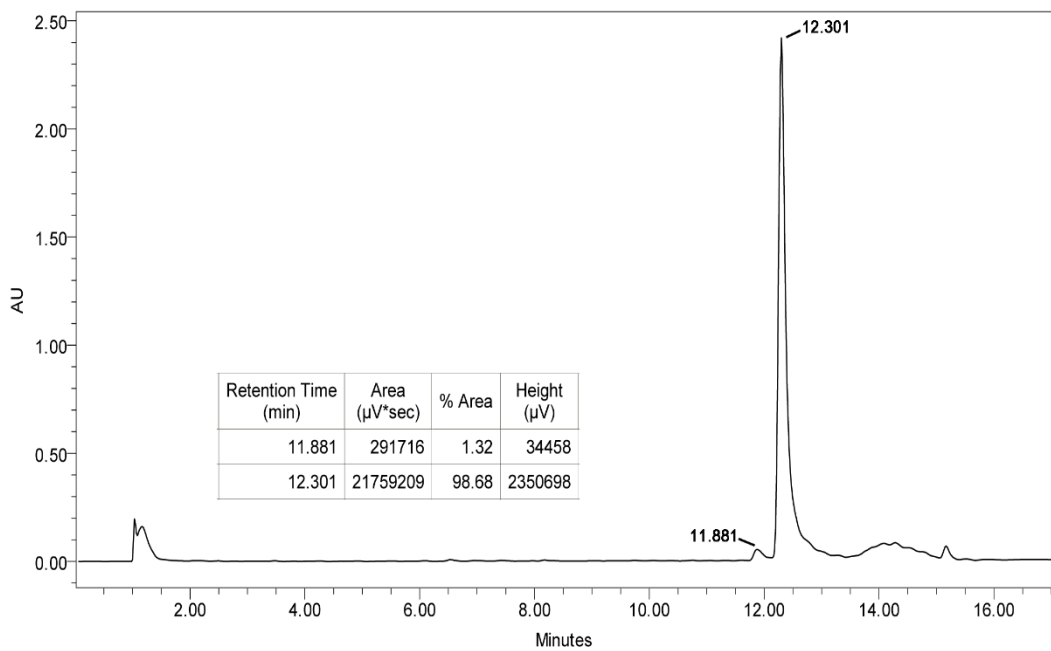
5-95% CH₃OH/H₂O gradient



Compound 2.5
5-95% CH₃CN/H₂O gradient



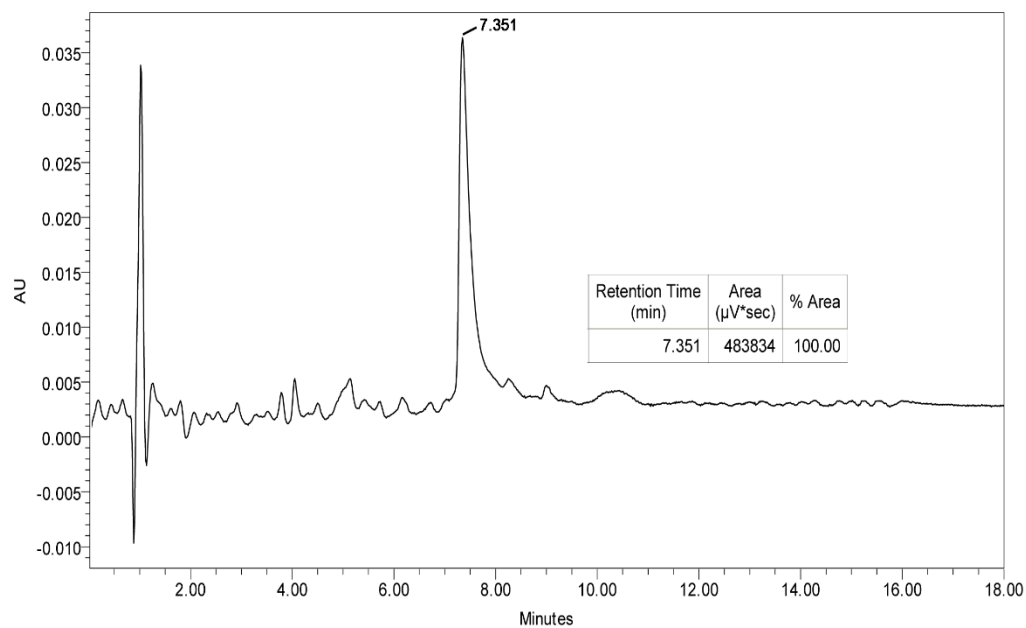
5-95% CH₃OH/H₂O gradient



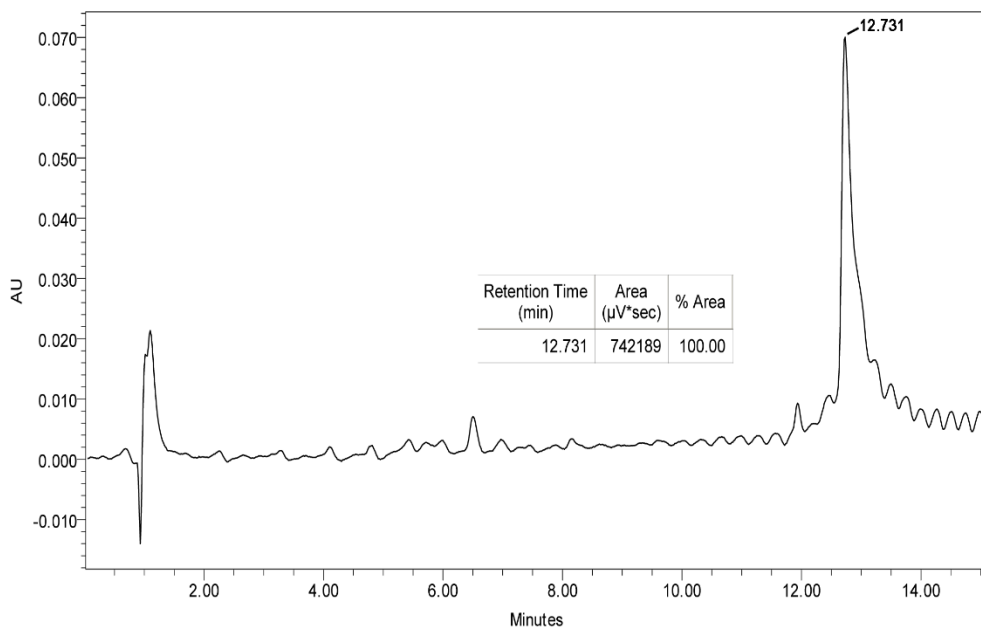
Compound 2.6

Concentration of compound 6 is less than 100 μM

5-95% $\text{CH}_3\text{CN}/\text{H}_2\text{O}$ gradient



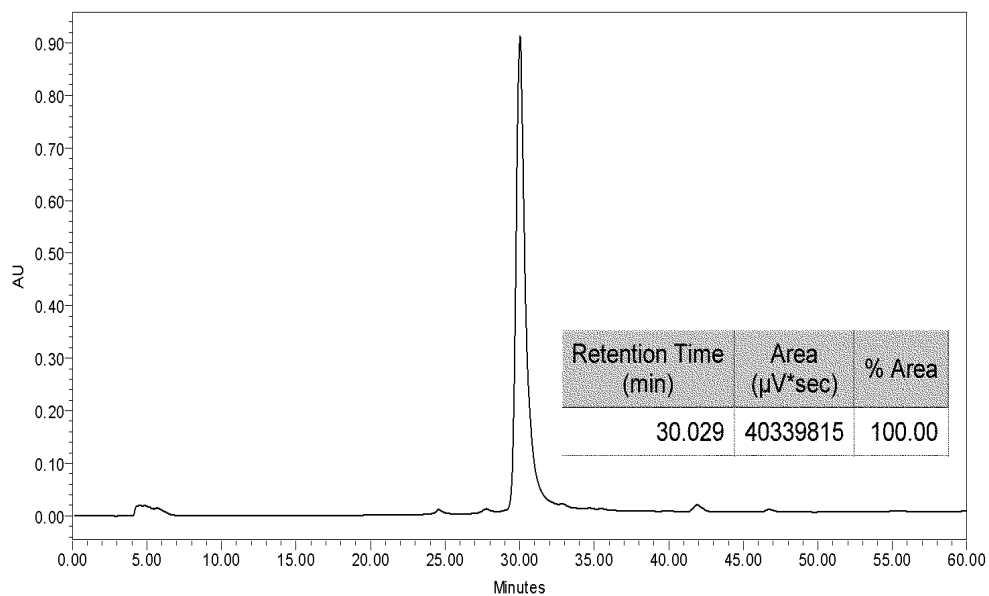
5-95% $\text{CH}_3\text{OH}/\text{H}_2\text{O}$ gradient



Compound 2.7

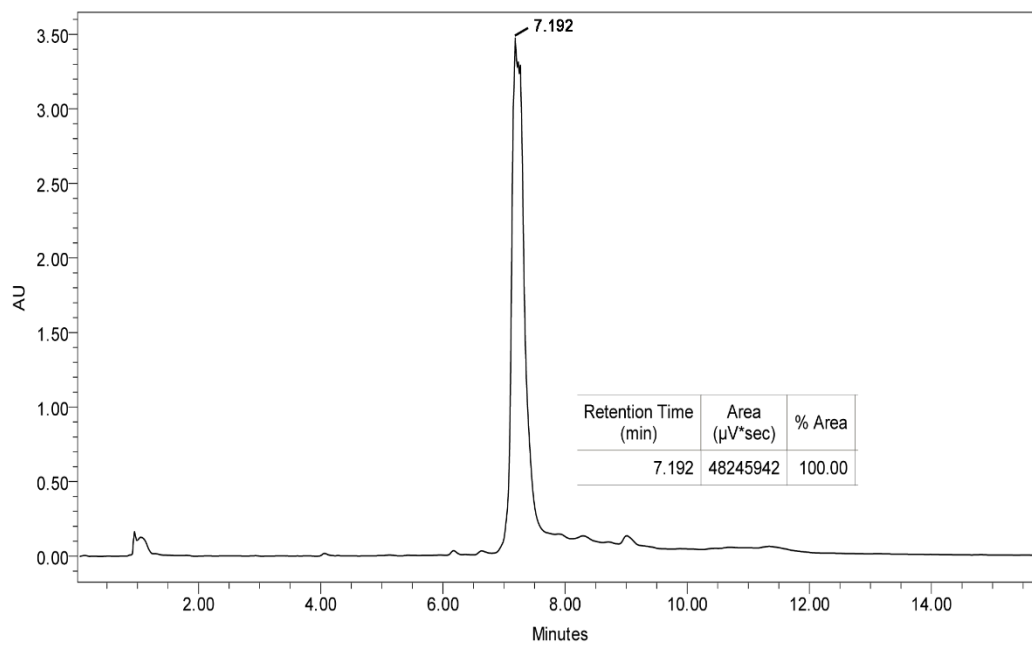
Compound 7 was dissolved in 100% DMSO to 1 mg/mL and injected into Waters and eluted using a linear gradient of CH₃CN (5-95%) in H₂O over 60 min. at a flow rate of 10 mL/min.

5-95% CH₃OH/H₂O gradient

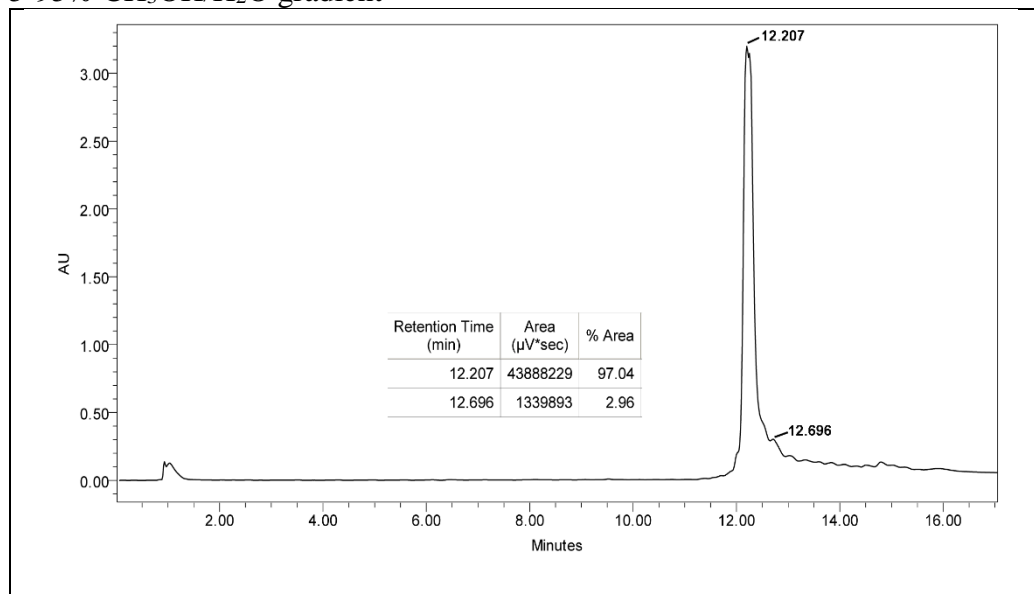


Compound 2.8

5-95% CH₃CN/H₂O gradient

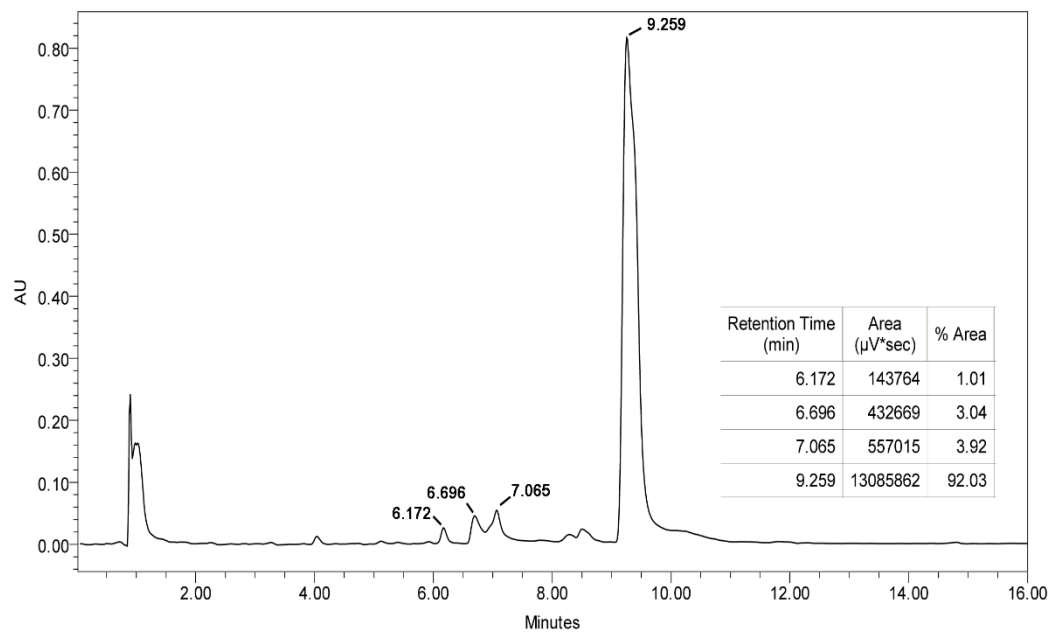


5-95% CH₃OH/H₂O gradient

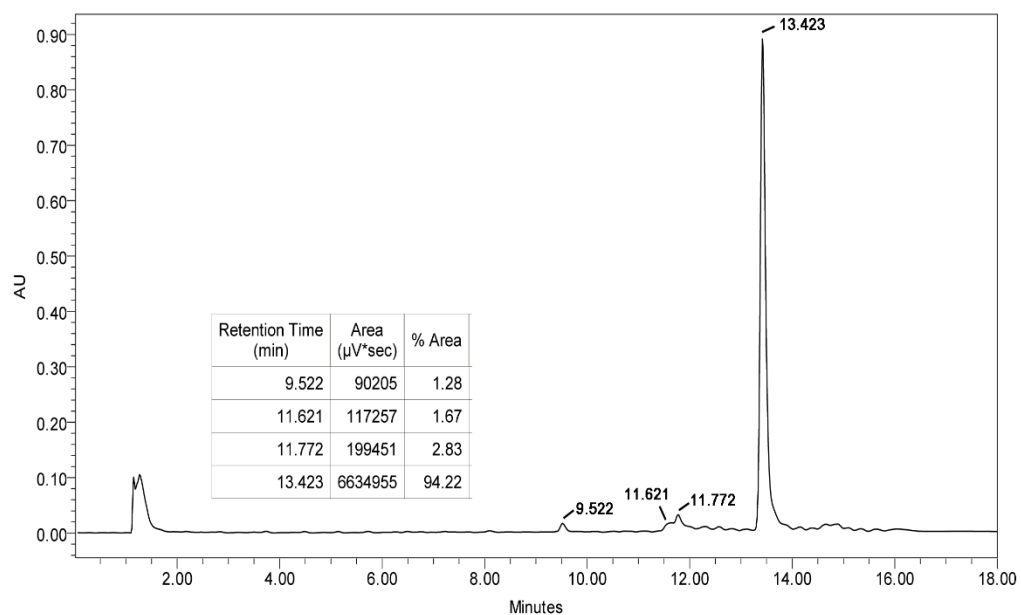


Compound 2.9

5-95% CH₃CN/H₂O gradient

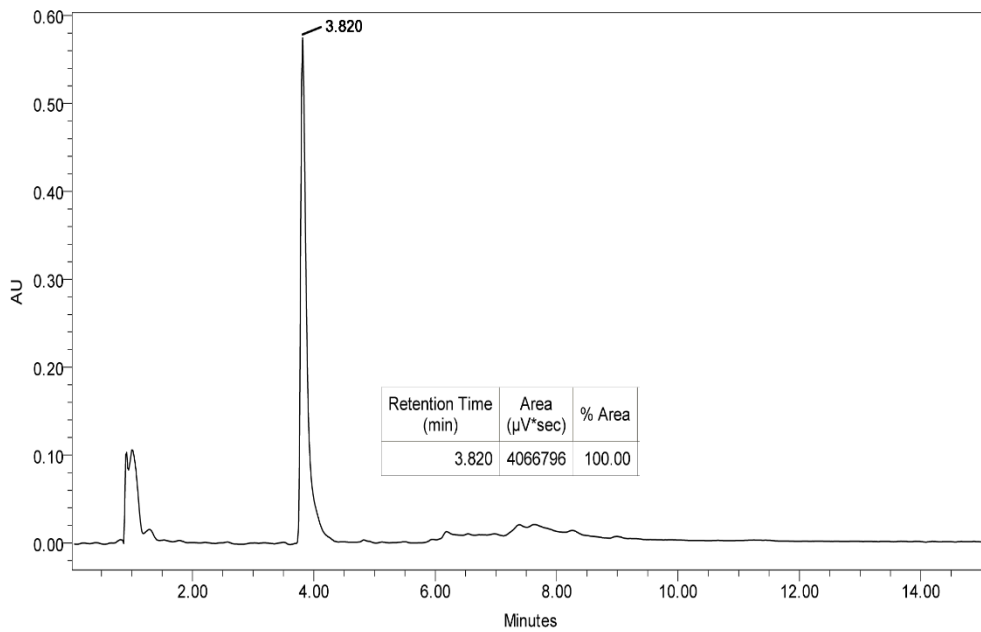


5-95% CH₃OH/H₂O gradient

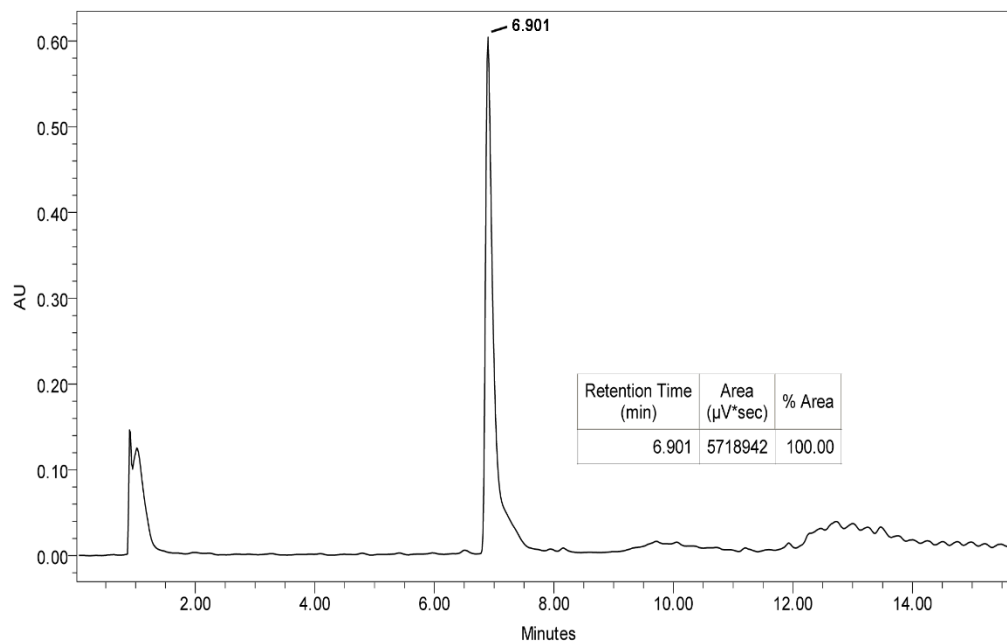


Compound 2.10

5-95% CH₃CN/H₂O gradient



5-95% CH₃OH/H₂O gradient

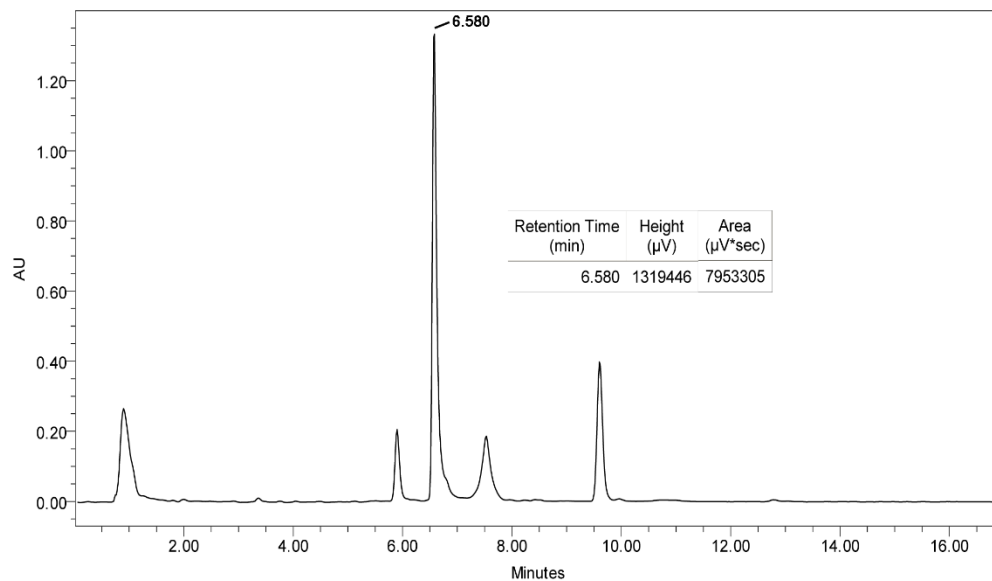


Analytical HPLC trace of Compound 2.4 stability in cell lysate

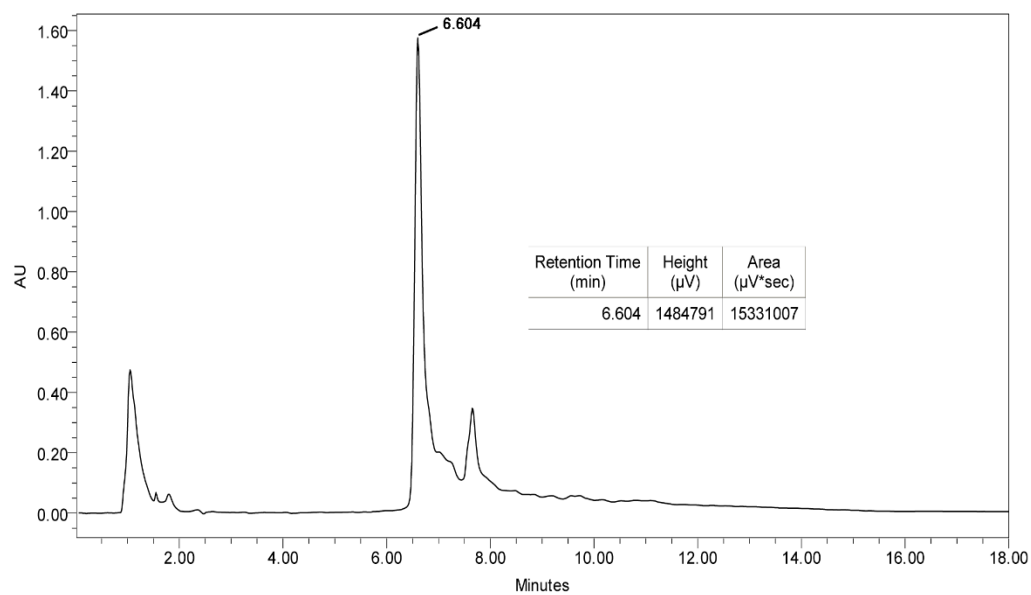
Compound 2.4 was incubated with SK-BR-3 cell lysate at 500 μ M for 24 hours at 37°C. Afterwards, an aliquot (10 μ L) was injected into a Waters© Xbridge C18 column (2.1 x 100 mm) and eluted using a linear gradient of CH₃CN (5-95%) in H₂O over 15 min. at a flow rate of 0.5 mL/min.

Time = 0 min.

Retention time of Compound 4 was determined from previous HPLC trace previously shown.



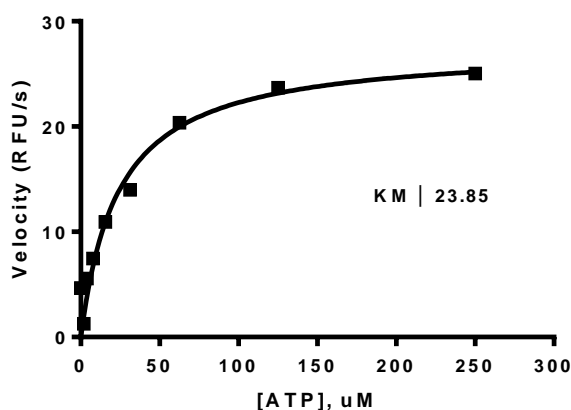
Time = 24 hours



ATP K_M CURVES

General procedure for ATP K_m determination. The previously described fluorescence assay²² was used to determine K_m values. Reaction volumes of 100 μL were used in 96-well plates. 85 μL of enzyme in buffer was added to each well. 2.5 μL of DMSO was then added followed by 2.5 μL of a substrate peptide (“compound 3” as described in Wang et al)²² solution (1.8 mM in DMSO). The reaction was initiated with 10 μL of the appropriate ATP dilution (typically 1000, 500, 250, 125, 62.5, 31.3, 15.6, 7.8, 3.9, 2.0 μM in H_2O) and reaction progress was immediately monitored at 405 nm (ex. 340 nm) for 10 minutes. Reactions had final concentrations of 30 nM enzyme, 45 μM peptide substrate, 100 μM Na_3VO_4 , 100 mM Tris buffer (pH 8), 10 mM MgCl_2 , 0.01% Triton X-100. The initial rate data collected was used for determination of K_m values. For K_m determination, the kinetic values were obtained directly from nonlinear regression of substrate-velocity curves in the presence of varying concentrations of ATP. The equation $Y = (V_{\text{max}} * X)/(K_m + X)$, X = substrate concentration (μM) and Y = enzyme velocity (RFU/s); was used in the nonlinear regression. Each ATP K_m value was determined using at least three independent experiments; a representative K_m curve is shown. The K_m for c-Src that was used here is 98 μM and was previously determined by our group.²⁶

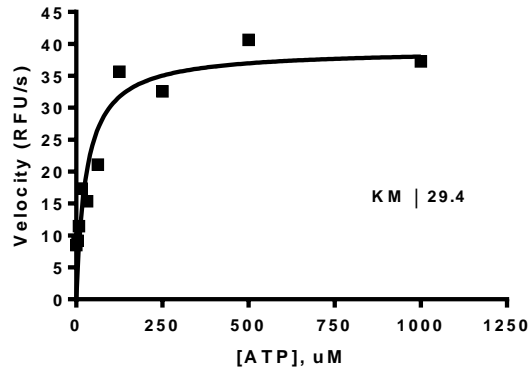
ATP K_m Curve with KD c-Hck enzyme:



$$K_m = 20 \pm 1.6 \mu\text{M}$$

$$V_{\text{max}} = 23 \pm 2.9 \mu\text{M (RFU/s)}$$

ATP K_m Curve with KD c-Abl enzyme:



$$K_m = 22 \pm 7.0 \mu\text{M}$$

$$V_{\text{max}} = 45 \pm 4.2 \mu\text{M (RFU/s)}$$

CELLULAR CHARACTERIZATION

Cell growth inhibition assays.

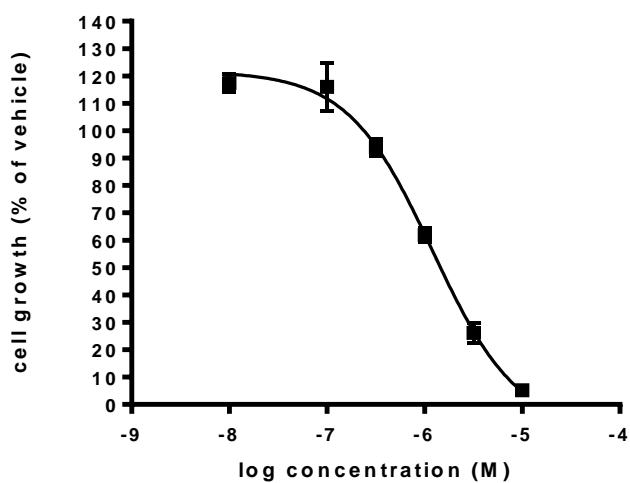
WST-1 reagent was obtained from Roche. The cell proliferation colorimetric assay using WST-1 was performed following the protocol provided by Roche.

Cell Culture and Seeding Procedure: Cells were dispersed from flasks and collected by centrifugation (200xg for 5 minutes at room temperature). An aliquot of the resuspended cells was mixed with trypan blue solution and the cell number was quantified using a hemacytometer. In general, depending on the growth rate of the untreated cells, the cells were plated at $5.0 - 7.5 \times 10^3$ cells per well. The cells were plated into sterile, clear bottom 96 well plates and cultured under normal growth conditions overnight prior to dosing with compound.

Dosing: 100% DMSO compound stocks were prepared to 100X the final concentration desired in the assay. 3 μ L of the DMSO stock solution was then added to 297 μ L of the cell growth media to give a DMSO concentration of 1%. The cell media was removed by aspiration for adherent cells and replaced with 100 μ L per well of the cell growth media containing the compound. In general, each compound concentration was dosed in triplicate wells. **Assay:** After the dosing period (24 hours) was complete, the plates were removed from the incubator and 10 μ L per well of WST-1 reagent was added. The plates were returned to the incubator and incubated for 1 hr, followed by shaking on a plate shaker for 60 seconds prior to the absorbance read (450 nm) on a BioTek Synergy 4 multimode plate reader.

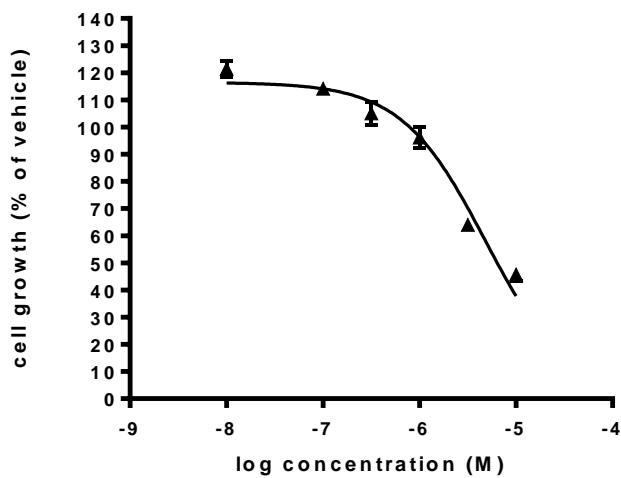
Data Analysis: The reference absorbance reading was subtracted from the formazan absorbance (background control well no compound added, 1% DMSO) and the data was plotted as a percentage of the vehicle (1% DMSO alone). Data analysis and curve fitting was performed using Graphpad Prism. For each cell line, there were $n = 3$ data points for each concentration. Each dose response curve was performed at least twice, providing $n \geq 6$ for each data point.

A. SK-BR-3 with Vorinostat:



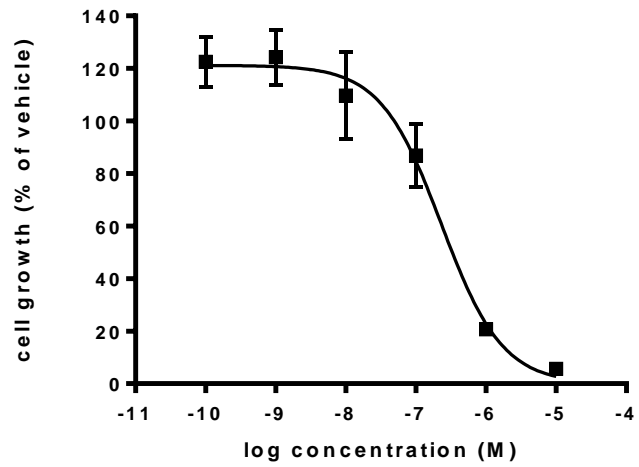
	vorinostat
EC50	1.205e-006

B. SK-BR-3 with Compound 2.1:



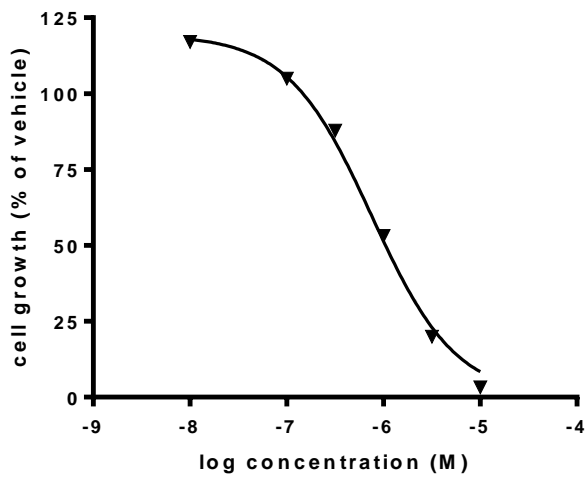
	Compound 1
EC50	4.801e-006

C. SK-BR-3 with Compound 2.4:



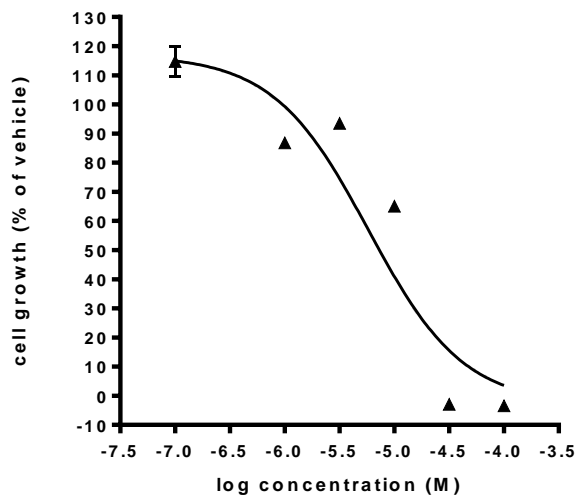
	Compound 4
EC50	2.308e-007

D. SK-BR-3 with 1:1 combination of Vorinostat + Compound 2.1:



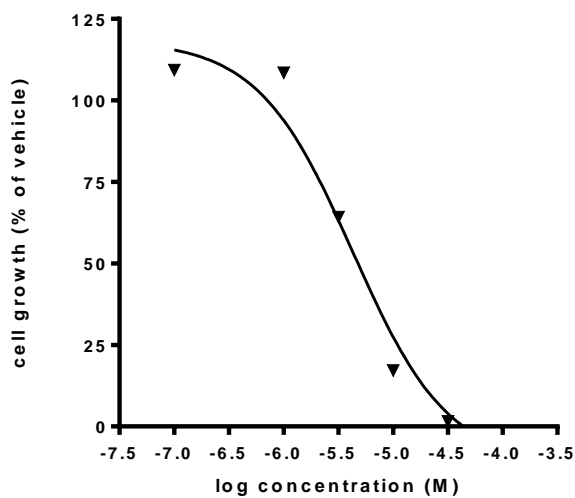
	Vorinostat + Compound 1
EC50	7.558e-007

E. HMEC with Vorinostat:



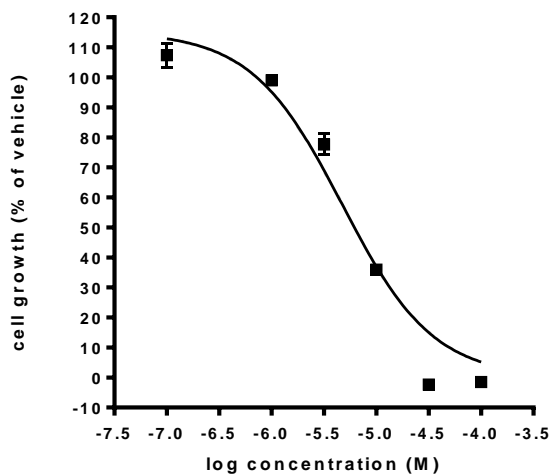
	Vorinostat
EC50	5.791e-006

F. HMEC with Compound 2.1:



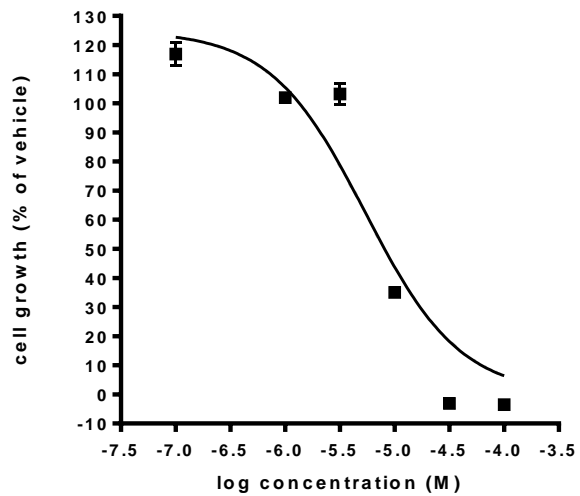
	Compound 1
EC50	4.294e-006

G. HMEC with Compound 4:



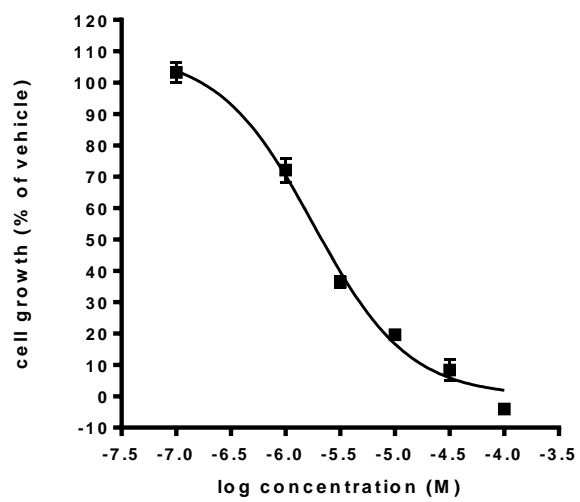
EC50	Compound 4
	4.734e-006

H. HMEC with 1:1 combination of Vorinostat + Compound 2.1:



EC50	Vorinostat + Compound 1
	5.397e-006

I. HMEC with Dasatinib



	dasatinib
EC50	1.804e-006

NCI Cancer Cell Profiling for Compound 2.4

For the most up to date, detailed protocol for the NCI-60 screen is provided by the Developmental Therapeutics Program National Cancer Institute/National Institute of Health (DTP NCI/NCI) website.²⁷

National Cancer Institute Developmental Therapeutics Program In-Vitro Testing Results															
NSC : D - 763846 / 1				Experiment ID : 1203NS37				Test Type : 08			Units : Molar				
Report Date : May 14, 2012				Test Date : March 26, 2012				QNS :			MC :				
COMI : KK-137 (115692)				Stain Reagent : SRB Dual-Pass Related				SSPL : 0XSK							
Panel/Cell Line	Time	Log10 Concentration						Percent Growth				GI50	TGI	LC50	
		Zero	Ctrl	-8.0	-7.0	-6.0	-5.0	-4.0	-8.0	-7.0	-6.0				-5.0
Leukemia															
CCRF-CEM	0.709	2.464	2.480	2.098	0.729	0.423	0.621	101	79	1	-40	-12	2.36E-7	1.06E-6	> 1.00E-4
HL-60(TB)	0.902	2.582	2.672	2.669	1.104	0.484	0.637	105	105	12	-46	-29	3.91E-7	1.81E-6	> 1.00E-4
K-562	0.273	1.696	1.680	1.466	0.408	0.316	0.389	99	84	9	3	8	2.85E-7	> 1.00E-4	> 1.00E-4
MOLT-4	0.728	2.328	2.261	1.912	0.551	0.396	0.639	96	74	-24	-46	-12	1.75E-7	5.66E-7	> 1.00E-4
RFMI-8226	0.911	2.351	2.418	2.452	1.045	0.613	0.755	105	107	9	-33	-17	3.83E-7	1.66E-6	> 1.00E-4
SR	0.453	1.459	1.421	0.999	0.543	0.336	0.524	96	54	9	-26	7	1.24E-7	.	> 1.00E-4
Non-Small Cell Lung Cancer															
A549(ATCC)	0.256	1.124	1.115	1.119	0.722	0.161	0.159	99	99	54	-37	-38	1.10E-6	3.90E-6	> 1.00E-4
HOP-62	0.332	0.975	0.983	0.926	0.596	0.319	0.144	101	92	41	-4	-57	6.68E-7	8.12E-6	7.44E-5
HOP-92	1.339	1.669	1.635	1.553	1.027	0.369	0.438	89	65	-23	-72	-67	1.47E-7	5.43E-7	3.49E-6
NCI-H226	0.563	1.107	1.097	1.078	1.031	0.530	0.253	98	95	96	-6	-55	2.46E-6	8.62E-6	7.89E-6
NCI-H23	0.598	1.786	1.755	1.680	1.080	0.305	0.252	97	91	41	-49	-58	6.51E-7	2.84E-6	1.30E-6
NCI-H322M	0.849	1.539	1.502	1.471	1.054	0.572	0.399	95	90	30	-33	-54	4.61E-7	2.99E-6	6.39E-6
NCI-H460	0.255	1.993	2.053	2.007	0.802	0.232	0.101	103	101	31	-9	-60	5.40E-7	5.93E-6	6.27E-6
Colon Cancer															
COLO 205	0.321	1.125	1.197	1.101	0.509	0.085	0.124	109	97	23	-74	-62	4.35E-7	1.74E-6	5.70E-6
HCC-2998	0.364	1.120	1.121	0.994	0.588	0.047	0.098	100	83	30	-87	-73	4.17E-7	1.79E-6	4.81E-6
HCT-116	0.227	1.625	1.594	1.283	0.241	0.039	0.043	98	76	1	-83	-81	2.20E-7	1.03E-6	4.06E-6
HCT-15	0.311	1.825	1.717	1.704	1.445	0.604	0.538	93	92	75	19	15	2.80E-6	> 1.00E-4	> 1.00E-4
HT29	0.223	1.183	1.106	1.000	0.323	0.128	0.095	92	81	10	-43	-58	2.74E-7	1.57E-6	3.05E-6
RM12	0.443	1.959	1.934	1.793	0.914	0.080	0.087	98	89	31	-82	-80	4.71E-7	1.88E-6	5.21E-6
SW-620	0.288	1.659	1.684	1.425	0.295	0.223	0.214	102	83	1	-23	-26	2.51E-7	1.05E-6	> 1.00E-4
CNS Cancer															
SF-268	0.605	1.761	1.693	1.552	0.827	0.184	0.102	94	82	19	-70	-83	3.22E-7	1.64E-6	6.01E-6
SF-295	0.963	2.290	2.230	2.252	1.598	0.642	0.633	96	97	48	-33	-34	9.04E-7	3.88E-6	> 1.00E-4
SF-539	0.954	2.372	2.289	2.135	1.362	0.797	0.633	94	83	29	-17	-34	4.08E-7	4.32E-6	> 1.00E-4
SNB-75	0.687	1.396	1.276	1.094	0.834	0.616	0.502	83	57	21	-10	-27	1.58E-7	4.62E-6	> 1.00E-4
U251	0.326	1.385	1.326	1.195	0.417	0.106	0.140	94	82	9	-67	-57	2.73E-7	1.30E-6	5.89E-6
Melanoma															
LOX IMVI	0.300	1.906	1.838	1.578	0.381	0.029	0.096	96	80	5	-91	-68	2.49E-7	1.13E-6	3.77E-6
MALME-3M	0.686	1.167	1.094	0.894	0.632	0.565	0.351	85	43	-8	-18	-49	6.84E-8	7.01E-7	> 1.00E-4
M14	0.454	1.436	1.422	1.229	0.617	0.200	0.072	99	79	17	-66	-84	2.91E-7	1.69E-6	8.25E-6
MDA-MB-435	0.461	1.788	1.716	1.516	0.467	0.242	0.244	95	79	-	-48	-47	2.36E-7	1.02E-6	> 1.00E-4
SK-MEL-28	0.371	0.950	0.991	0.845	0.507	0.374	0.241	107	82	23	1	-35	3.51E-7	1.03E-5	> 1.00E-4
SK-MEL-5	0.681	2.262	2.202	2.040	0.852	0.050	0.044	96	86	11	-93	-94	3.01E-7	1.27E-6	3.87E-6
UACC-257	0.558	1.205	1.167	0.967	0.618	0.313	0.306	94	63	9	-44	-45	1.76E-7	1.49E-6	> 1.00E-4
UACC-62	0.917	2.102	2.114	1.788	0.939	0.262	0.422	101	73	2	-71	-54	2.13E-7	1.06E-6	5.10E-6
Ovarian Cancer															
IGROV1	0.652	1.692	1.669	1.697	0.901	0.262	0.274	98	100	24	-60	-58	4.56E-7	1.93E-6	7.62E-6
OV-CAR-3	0.521	1.470	1.451	1.289	0.659	0.142	0.130	98	81	14	-73	-75	2.92E-7	1.47E-6	5.49E-6
OV-CAR-4	0.418	0.816	0.790	0.782	0.612	0.442	0.207	93	91	49	6	-51	9.28E-7	1.28E-5	9.76E-5
OV-CAR-5	0.453	1.278	1.213	1.191	0.703	0.368	0.358	92	89	30	-19	-21	4.64E-7	1.14E-6	> 1.00E-4
OV-CAR-8	0.282	1.144	1.124	0.947	0.359	0.214	0.206	98	77	9	-24	-27	2.50E-7	1.88E-6	> 1.00E-4
NCI-ADR-RES	0.393	1.428	1.428	1.369	1.105	0.610	0.544	100	94	69	21	15	2.47E-6	> 1.00E-4	> 1.00E-4
SK-OV-3	0.531	1.096	1.125	1.028	0.770	0.177	0.118	105	88	42	-67	-78	6.77E-7	2.44E-6	7.03E-6
Renal Cancer															
786-O	0.774	2.313	2.285	2.138	1.547	0.144	0.090	98	89	50	-81	-88	1.00E-6	2.41E-6	5.77E-6
A498	1.111	1.671	1.589	1.524	1.158	0.090	0.105	85	74	8	-92	-91	2.30E-7	1.21E-6	3.82E-6
ACHN	0.344	1.448	1.381	1.340	0.833	0.255	0.216	94	90	44	-26	-37	7.50E-7	4.28E-6	> 1.00E-4
CAK1-1	0.809	2.162	2.130	2.121	1.731	0.411	0.432	98	97	68	-49	-47	1.43E-6	3.81E-6	> 1.00E-4
RXF 393	0.682	1.085	1.037	0.979	0.667	0.099	0.051	88	74	-2	-85	-93	2.06E-7	9.36E-7	3.75E-6
SN 12C	0.545	1.762	1.707	1.545	0.984	0.489	0.473	95	82	36	-10	-13	4.98E-7	5.98E-6	> 1.00E-4
UO-31	0.897	1.955	1.822	1.757	1.330	0.479	0.501	87	81	41	-47	-44	5.96E-7	2.93E-6	> 1.00E-4
Prostate Cancer															
PC-3	0.466	1.720	1.689	1.500	0.781	0.522	0.389	97	82	25	4	-17	3.68E-7	1.62E-5	> 1.00E-4
DU-145	0.365	1.324	1.309	1.229	0.579	0.251	0.232	98	90	22	-31	-37	3.90E-7	2.60E-6	> 1.00E-4
Breast Cancer															
MCF7	0.330	1.665	1.535	1.501	0.592	0.205	0.204	90	88	20	-38	-38	3.57E-7	2.19E-6	> 1.00E-4
MDA-MB-231(ATCC)	0.599	1.147	1.173	1.098	0.720	0.290	0.320	105	91	22	-52	-47	3.92E-7	1.99E-6	.
HS 578T	0.853	1.499	1.453	1.292	0.805	0.649	0.704	93	68	-6	-24	-17	1.75E-7	8.37E-7	> 1.00E-4
BT-549	0.908	1.722	1.703	1.671	1.302	0.444	0.405	98	94	48	-51	-55	9.18E-7	3.06E-6	9.75E-6
T-47D	0.558	1.262	1.230	1.064	0.639	0.596	0.494	95	72	11	5	-11	2.30E-7	2.09E-5	> 1.00E-4
MDA-MB-468	0.551	1.211	1.125	1.016	0.665	0.190	0.106	87	70	17	-66	-81	2.42E-7	1.62E-6	6.49E-6

National Cancer Institute Developmental Therapeutics Program		NSC : D - 763846/1		Units :Molar		SSPL :0XSK		EXP.ID :1203NS37	
Mean Graphs		Report Date :May 14, 2012				Test Date :March 26, 2012			
Panel/Cell Line	Log ₁₀ GI50	GI50	Log ₁₀ TGI	TGI	Log ₁₀ LC50	LC50			
Leukemia									
CCRF-CEM	-6.63		-5.97		> 4.00				
HL-60(TB)	-6.41		-6.79		> 4.00				
K-562	-6.54		> 4.00		> 4.00				
MOLT-4	-6.78		-6.25		> 4.00				
RPMI-8226	-6.42		-6.78		> 4.00				
SR	-6.91				> 4.00				
Non-Small Cell Lung Cancer									
A549ATCC	-6.96		-6.41		> 4.00				
HOP-62	-6.18		-6.09		-4.13				
HOP-92	-6.83		-6.27		-5.46				
NCI-H226	-5.61		-6.06		-4.10				
NCI-H23	-6.19		-5.55		-4.89				
NCI-H322M	-6.34		-5.52		-4.19				
NCI-H460	-6.27		-5.23		-4.20				
Colon Cancer									
COLO 205	-6.36		-6.76		-5.34				
HCC-2998	-6.38		-6.75		-5.32				
HCT-116	-6.66		-5.99		-5.39				
HCT-15	-5.55		> 4.00		> 4.00				
HT29	-6.56		-5.61		-4.52				
KM12	-6.33		-6.73		-5.28				
SW620	-6.60		-5.98		> 4.00				
ONS Cancer									
SF-268	-6.49		-6.78		-5.22				
SF-295	-6.04		-6.41		> 4.00				
SF-539	-6.39		-5.36		> 4.00				
SNB-75	-6.80		-5.33		> 4.00				
U251	-6.56		-5.89		-5.23				
Melanoma									
LOX IMVI	-6.60		-5.95		-5.42				
MALME-3M	-7.17		-6.15		> 4.00				
MH	-6.54		-5.77		-5.08				
MDAMB-435	-6.63		-5.99		> 4.00				
SK-MEL-28	-6.45		-4.99		> 4.00				
SK-MEL-5	-6.52		-5.90		-5.41				
UACC-257	-6.76		-5.83		> 4.00				
UACC-62	-6.67		-5.98		-5.23				
Ovarian Cancer									
IGROV1	-6.34		-6.71		-5.12				
OVCAR-3	-6.53		-6.83		-5.26				
OVCAR-4	-6.03		-4.89		-4.01				
OVCAR-5	-6.33		-5.38		> 4.00				
OVCAR-8	-6.60		-5.73		> 4.00				
NCIADR-RES	-5.61		> 4.00		> 4.00				
SK-OV3	-6.17		-5.61		-5.15				
Renal Cancer									
786-O	-6.00		-5.62		-5.24				
A498	-6.64		-5.92		-5.42				
ACHN	-6.12		-5.37		> 4.00				
CHL1	-5.65		-5.42		> 4.00				
RFP_303	-6.69		-6.03		-5.43				
SNZC	-6.30		-5.22		> 4.00				
UD-31	-6.22		-5.53		> 4.00				
Prostate Cancer									
PC-3	-6.43		-4.79		> 4.00				
DU-145	-6.41		-5.58		> 4.00				
Breast Cancer									
MCF7	-6.45		-6.66		> 4.00				
MDAMB-231ATCC	-6.41		-5.70		> 4.00				
HS 578T	-6.76		-6.08		> 4.00				
BT-549	-6.04		-6.51		-5.01				
T47D	-6.64		-4.88		> 4.00				
MDAMB-468	-6.62		-5.79		-5.19				
MD Delta Range									
MD	-6.4		-5.54		-4.49				
Delta	0.77		0.73		0.97				
Range	1.62		2.27		1.46				

NCI Cancer Cell Profiling for Vorinostat (Zolinza), NSC 701852

Data provided by the DTP NCI/NIH website, NCI 60 cell line screen dose response data from 08/2012.⁷

Concentration	Unit	CellPanelName	CellLineName	logValue, GI50	logValue, TGI50	logValue, LC50
log10(M)		Leukemia	CCRF-CEM	-6.133	-5.082	-4
log10(M)		Leukemia	HL-60(TB)	-5.901	-4.855	-4
log10(M)		Leukemia	K-562	-6.318	-4.926	-4.17
log10(M)		Leukemia	MOLT-4	-6.433	-4.957	-4
log10(M)		Leukemia	RPMI-8226	-6.515	-5.427	-4.151
log10(M)		Leukemia	SR	-6.403	-4.471	-4
log10(M)		Non-Small Cell Lung	A549/ATCC	-5.766	-4.655	-4.081
log10(M)		Non-Small Cell Lung	EKVX	-5.848	-4.277	-4
log10(M)		Non-Small Cell Lung	HOP-62	-5.805	-4.112	-4
log10(M)		Non-Small Cell Lung	HOP-92	-5.534	-4.488	-4
log10(M)		Non-Small Cell Lung	NCI-H226	-5.375	-4.192	-4
log10(M)		Non-Small Cell Lung	NCI-H23	-5.953	-5.009	-4.233
log10(M)		Non-Small Cell Lung	NCI-H322M	-6.072	-4.886	-4.159
log10(M)		Non-Small Cell Lung	NCI-H460	-6.111	-4.146	-4
log10(M)		Non-Small Cell Lung	NCI-H522	-6.331	-5.161	-4.051
log10(M)		Colon	COLO 205	-6.051	-5.581	-5.084
log10(M)		Colon	HCC-2998	-5.733	-4.819	-4.154
log10(M)		Colon	HCT-116	-6.411	-5.231	-4.633
log10(M)		Colon	HCT-15	-5.562	-4.071	-4
log10(M)		Colon	HT29	-6.127	-4.807	-4.054
log10(M)		Colon	KM12	-5.732	-4.64	-4.058
log10(M)		Colon	SW-620	-6.205	-5.051	-4.165
log10(M)		Central Nervous System	SF-268	-5.775	-4.477	-4.044

log10(M)	Central Nervous System	SF-295	-5.88	-5.046	-4.166
log10(M)	Central Nervous System	SF-539	-5.723	-4.316	-4
log10(M)	Central Nervous System	SNB-19	-5.681	-4.748	-4.037
log10(M)	Central Nervous System	SNB-75	-6.1	-4.258	-4
log10(M)	Central Nervous System	U251	-5.805	-4.766	-4.328
log10(M)	Melanoma	LOX IMVI	-5.939	-4.99	-4.474
log10(M)	Melanoma	MALME-3M	-6.576	-5.417	-4
log10(M)	Melanoma	M14	-5.886	-4.695	-4.067
log10(M)	Melanoma	MDA-MB-435	-6.294	-5.228	-4.043
log10(M)	Melanoma	MDA-N	-6.271	-5.495	-4.458
log10(M)	Melanoma	SK-MEL-2	-5.889	-4.767	-4.033
log10(M)	Melanoma	SK-MEL-28	-5.926	-5.07	-4.227
log10(M)	Melanoma	SK-MEL-5	-6.183	-5.574	-5.056
log10(M)	Melanoma	UACC-257	-6.308	-5.028	-4.049
log10(M)	Melanoma	UACC-62	-6.351	-5.561	-4.826
log10(M)	Ovarian	IGROV1	-5.963	-5.089	-4.372
log10(M)	Ovarian	OVCAR-3	-5.867	-5.01	-4.226
log10(M)	Ovarian	OVCAR-4	-5.38	-4.011	-4
log10(M)	Ovarian	OVCAR-5	-6.091	-4.944	-4.111
log10(M)	Ovarian	OVCAR-8	-6.286	-4.649	-4
log10(M)	Ovarian	NCI/ADR-RES	-6.806	-5.568	-4.375
log10(M)	Ovarian	SK-OV-3	-5.955	-4.881	-4.134
log10(M)	Renal	786-0	-5.52	-4.258	-4.03
log10(M)	Renal	A498	-5.865	-5.174	-4.628
log10(M)	Renal	ACHN	-5.855	-5.124	-4.305
log10(M)	Renal	CAKI-1	-5.921	-5.403	-4.721
log10(M)	Renal	RXF 393	-5.9	-5.266	-4.334

log10(M)	Renal	SN12C	-5.645	-4.515	-4.238
log10(M)	Renal	TK-10	-6.194	-5.095	-4.188
log10(M)	Renal	UO-31	-6.262	-5.199	-4.159
log10(M)	Prostate	PC-3	-5.683	-4.174	-4
log10(M)	Prostate	DU-145	-5.89	-4.747	-4
log10(M)	Breast	MCF7	-5.644	-4.385	-4
log10(M)	Breast	MDA-MB-231/ATCC	-5.607	-4	-4
log10(M)	Breast	HS 578T	-5.449	-4.155	-4
log10(M)	Breast	BT-549	-5.77	-4.629	-4.016
log10(M)	Breast	T-47D	-6.278	-5.36	-4
log10(M)	Breast	MDA-MB-468	-6.046	-4.965	-4.067

NCI Cancer Cell Profiling for Dasatinib (Sprycel), NSC 723517

Data provided by the DTP NCI/NIH website, NCI 60 cell line screen dose response data from 08/2012.⁷

Concentration Unit	Cell Panel Name	Cell Line Name	logValue, GI50	logValue, TGI	logValue, LC50
log10(M)	Leukemia	CCRF-CEM	-5.135	-4.699	-4.699
log10(M)	Leukemia	HL-60(TB)	-5.111	-4.699	-4.699
log10(M)	Leukemia	K-562	-8.699	-4.699	-4.699
log10(M)	Leukemia	MOLT-4	-5.271	-4.699	-4.699
log10(M)	Leukemia	RPMI-8226	-5.132	-4.699	-4.699
log10(M)	Leukemia	SR	-5.199	-4.699	-4.699
log10(M)	Non-Small Cell Lung	A549/ATCC	-7.378	-5.484	-4.699
log10(M)	Non-Small Cell Lung	EKVX	-5.374	-4.699	-4.699
log10(M)	Non-Small Cell Lung	HOP-62	-7.439	-4.699	-4.699
log10(M)	Non-Small Cell Lung	NCI-H226	-7.334	-4.699	-4.699
log10(M)	Non-Small Cell Lung	NCI-H23	-5.282	-4.699	-4.699
log10(M)	Non-Small Cell Lung	NCI-H322M	-6.757	-4.699	-4.699
log10(M)	Non-Small Cell Lung	NCI-H460	-5.054	-4.699	-4.699
log10(M)	Non-Small Cell Lung	NCI-H522	-6.939	-4.825	-4.699
log10(M)	Colon	COLO 205	-7.431	-4.699	-4.699
log10(M)	Colon	HCC-2998	-4.887	-4.699	-4.699
log10(M)	Colon	HCT-116	-5.431	-4.699	-4.699
log10(M)	Colon	HCT-15	-6.101	-4.699	-4.699
log10(M)	Colon	HT29	-7.883	-4.699	-4.699
log10(M)	Colon	KM12	-5.128	-4.699	-4.699
log10(M)	Colon	SW-620	-5.074	-4.699	-4.699
log10(M)	Central Nervous System	SF-268	-6.95	-4.782	-4.699
log10(M)	Central Nervous System	SF-295	-5.479	-4.865	-4.699
log10(M)	Central Nervous System	SF-539	-7.273	-4.699	-4.699

log10(M)	Central Nervous System	SNB-19	-5.264	-7.25	-4.699
log10(M)	Central Nervous System	SNB-75	-8.329	-4.699	-4.699
log10(M)	Central Nervous System	U251	-5.551	-6.435	-4.699
log10(M)	Melanoma	LOX IMVI	-8.017	-4.699	-5.226
log10(M)	Melanoma	MALME-3M	-5.18	-4.699	-4.699
log10(M)	Melanoma	M14	-5.309	-4.699	-4.699
log10(M)	Melanoma	MDA-MB-435	-5.221	-4.699	-4.699

log10(M)	Melanoma	SK-MEL-2	-5.11	-4.699	-4.699
log10(M)	Melanoma	SK-MEL-28	-5.038	-4.699	-4.699
log10(M)	Melanoma	SK-MEL-5	-5.171	-4.76	-4.699
log10(M)	Melanoma	UACC-257	-5.571	-4.699	-4.699
log10(M)	Melanoma	UACC-62	-5.245	-4.699	-4.699
log10(M)	Ovarian	IGROV1	-7.599	-4.699	-4.699
log10(M)	Ovarian	OVCAR-3	-6.761	-4.699	-4.699
log10(M)	Ovarian	OVCAR-4	-5.151	-4.699	-4.699
log10(M)	Ovarian	OVCAR-5	-7.302	-6.294	-4.699
log10(M)	Ovarian	OVCAR-8	-7.307	-4.699	-4.699
log10(M)	Ovarian	NCI/ADR-RES	-5.363	-5.476	-4.699
log10(M)	Ovarian	SK-OV-3	-6.649	-4.699	-4.699
log10(M)	Renal	786-0	-6.909	-6.728	-4.699
log10(M)	Renal	A498	-7.65	-4.699	-4.983
log10(M)	Renal	ACHN	-7.736	-6.059	-4.699
log10(M)	Renal	CAKI-1	-7.725	-7.014	-4.699
log10(M)	Renal	RXF 393	-8.045	-4.699	-5.003
log10(M)	Renal	SN12C	-7.545	-7.14	-4.699
log10(M)	Renal	TK-10	-8.074	-4.769	-4.699
log10(M)	Renal	UO-31	-7.705	-4.699	-4.699
log10(M)	Prostate	PC-3	-5.646	-4.699	-4.699
log10(M)	Prostate	DU-145	-6.801	-4.699	-4.699
log10(M)	Breast	MCF7	-5.08	-5.42	-4.699
log10(M)	Breast	MDA-MB-231/ATCC	-7.809	-4.699	-4.729
log10(M)	Breast	HS 578T	-7.601	-4.699	-4.699
log10(M)	Breast	BT-549	-5.117	-4.699	-4.699
log10(M)	Breast	T-47D	-6.387	-5.902	-4.699
log10(M)	Breast	MDA-MB-468	-7.065		-4.699

3.6 References

- (1) Thomas, S. M.; Brugge, J. S. *Annu. Rev. Cell Dev. Biol.* **1997**, *13*, 513.
- (2) Martin, G. S. *Nat. Rev. Mol. Cell Biol.* **2001**, *2* (6), 467.
- (3) Zhang, S.; Huang, W.-C.; Li, P.; Guo, H.; Poh, S.-B.; Brady, S. W.; Xiong, Y.; Tseng, L.-M.; Li, S.-H.; Ding, Z.; Sahin, A. a; Esteva, F. J.; Hortobagyi, G. N.; Yu, D. *Nat. Med.* **2011**, *17* (4), 461.
- (4) Brandvold, R.; Ste, M. E.; Fox, C. C.; Soellner, M. B. *ACS Chem. Biol.* **2012**, *7*, 1393.
- (5) Pirrone, V.; Thakkar, N.; Jacobson, J. M.; Wigdahl, B.; Krebs, F. C. *Antimicrob. Agents Chemother.* **2011**, *55* (5), 1831.
- (6) Bouza, E.; Muñoz, P. *Med. Clin. North Am.* **2000**, *84* (6), 1357.
- (7) Dancey, J. E.; Chen, H. X. *Nat. Rev. Drug Discov.* **2006**, *5* (8), 649.
- (8) Zheng, X.; Resnick, R. J.; Shalloway, D. *Int. J. Cancer* **2008**, *122* (9), 1999.
- (9) Atadja, P. *Cancer Lett.* **2009**, *280* (2), 233.
- (10) Bolden, J. E.; Peart, M. J.; Johnstone, R. W. *Nat. Rev. Drug Discov.* **2006**, *5* (9), 769.
- (11) Kostyniuk, C. L.; Dehm, S. M.; Batten, D.; Bonham, K. *Oncogene* **2002**, *21* (41), 6340.
- (12) Marks, P. a; Breslow, R. *Nat. Biotechnol.* **2007**, *25* (1), 84.
- (13) Zimmermann, G. R.; Lehár, J.; Keith, C. T. *Drug Discov. Today* **2007**, *12* (1-2), 34.
- (14) Muller, P. Y.; Milton, M. N. *Nat. Rev. Drug Discov.* **2012**, *11* (10), 751.
- (15) Cai, X.; Zhai, H. X.; Wang, J.; Forrester, J.; Qu, H.; Yin, L.; Lai, C. J.; Bao, R.; Qian, C. *J. Med. Chem.* **2010**, *53* (5), 2000.
- (16) Mahboobi, S.; Sellmer, a; Winkler, M.; Eichhorn, E.; Pongratz, H.; Ciossek, T.; Baer, T.; Maier, T.; Beckers, T. *J. Med. Chem.* **2010**, *53* (24), 8546.
- (17) Mahboobi, S.; Dove, S.; Sellmer, A.; Winkler, M.; Eichhorn, E.; Pongratz, H.; Ciossek, T.; Baer, T.; Maier, T.; Beckers, T. *J. Med. Chem.* **2009**, *52* (8), 2265.
- (18) Paris, M.; Porcelloni, M.; Binaschi, M.; Fattori, D. *J. Med. Chem.* **2008**, *51* (6), 1505.
- (19) Kolb, H. C.; Finn, M. G.; Sharpless, K. B. *Angew. Chemie - Int. Ed.* **2001**, *40* (11), 2004.
- (20) Chen, P. C.; Patil, V.; Guerrant, W.; Green, P.; Oyelere, A. K. *Bioorganic Med. Chem.* **2008**, *16* (9), 4839.
- (21) Zhang, L.; Chen, X.; Xue, P.; Sun, H. H. Y.; Williams, I. D.; Sharpless, K. B.; Fokin, V. V.; Jia, G. *J. Am. Chem. Soc.* **2005**, *127* (46), 15998.
- (22) Wang, Q.; Cahill, S. M.; Blumenstein, M.; Lawrence, D. S. *J. Am. Chem. Soc.* **2006**, *128* (6), 1808.
- (23) Schultz, B. E.; Misialek, S.; Wu, J.; Tang, J.; Conn, M. T.; Tahilramani, R.; Wong, L. *Biochemistry* **2004**, *43* (34), 11083.
- (24) Shoemaker, R. H. *Nat. Rev. Cancer* **2006**, *6* (10), 813.
- (25) Fretz, H. *Tetrahedron Lett.* **1996**, *37* (47), 8475.
- (26) Kwarcinski, F. E.; Fox, C. C.; Steffey, M. E.; Soellner, M. B. *ACS Chem. Biol.* **2012**, *7* (11), 1910.

- (27) Developmental Therapeutics Program National Cancer Institute/National Institute of Health. <http://dtp.nci.nih.gov/index.html>.

Chapter 4

Development of a dual p38 β /c-Src Inhibitor for Triple Negative Breast Cancer

4.1 Introduction

Metastasis is not a term a patient wants to hear in regards to their cancer. It is an extremely aggressive stage of cancer with nearly a 90% fatality rate.¹ One of the most commonly known cancers associated with metastasis is breast cancer mainly due to its consistent repeat as the second leading cause of death of women in the United States.²⁻⁵ The three most prevalent types of breast cancers are ER+/PR+, HER2+, and ER+/PR+/HER2+. ER+ stands for estrogen receptor, PR+ as progesterone receptor, and HER2+ refers to EGFR kinase. In these types of cancers, those particular hormone receptors are overexpressed and as such, are the driving force for those breast cancers. Hence the specific targeting of these overabundant species have proven to be an effective treatment. However, a fourth category of breast cancer, triple negative breast cancer (TNBC), aptly named because of the lack of ER/PR/HER2 hormone receptor expression, has no known driving force and thus, no known target. This is particularly disconcerting as TNBCs are notoriously lethal due to their high risk of metastasis and proclivity to rapidly reoccur.⁶⁻¹⁰ Unfortunately, 10-15% of breast cancers fall into this subcategory and the lack of treatment target for these patients often results in a poor prognosis. There are no FDA-approved targeted therapies.¹¹ Treatment is entirely dependent upon cytotoxic agents, but even such methods are not effective as non-metastatic TNBC reoccurs in about 40% of the patients, a much higher rate than in HER2+ breast cancer, which is less than 25% reoccurrence. There is evident need for a specific therapeutic

against TNBCs. Chapter 4 addresses this issue and proposes c-Src as a target of choice.

A previous *in vitro* study involving gene expression profiling had identified dasatinib, a c-Src tyrosine kinase inhibitor, to be sensitized to TNBC tumors and was demonstrated to reduce cell proliferation. As such, the results from the study validated c-Src as a viable target for TNBC. As mentioned (*vide supra*), c-Src is a ubiquitously expressed membrane-associated non-receptor kinase. c-Src participates in signaling pathways for adhesion, migration, and invasion, which are all characteristic functions hacked by TNBC. Thus, c-Src, with high expression levels found in TNBCs, has been implicated in a role in cancer progression of TNBC cancer cell lines, making it an attractive therapeutic target.¹²⁻¹⁵

Unfortunately, targeting of c-Src using existing FDA approved inhibitors for c-Src have not translated successfully to the clinical setting. Patients with advanced or metastatic TNBC showed little improvement while on dasatinib or bosutinib in a recent phase II trial.¹⁶⁻¹⁸ These results are puzzling as *in vitro* studies have proven targeted c-Src inhibition to be effective against TNBCs. In an effort to understand this perplexing issue, our lab has decided to design our own c-Src ligand.

Many TNBC cancer cell lines have an overexpression of c-Src which is usually in its fully activated form, pY419 and thus open conformation. Type II (DFG-out) ligands prefer binding to the open conformation of c-Src and therefore we reasoned that designing a Type II ligand for c-Src might be more efficacious.^{19,20} As previously described in Chapter 2, different ligands can have varying non-catalytic effects and so using a Type II vs. Type I (DFG-in) could also provide additional efficacy. There are currently no FDA-approved Type II inhibitors for c-Src. Both dasatinib and bosutinib are Type I inhibitors. Perhaps our designed Type II ligand would prove more successful for TNBC and show better results in a clinical setting, helping to provide evidence that c-Src can be used as a target.

4.2 Rational Design in Improving Dasatinib Efficacy in TNBC

To evaluate if any variable differences are due to the ligand type, we previously designed a Type II inhibitor based off of the dasatinib scaffold (

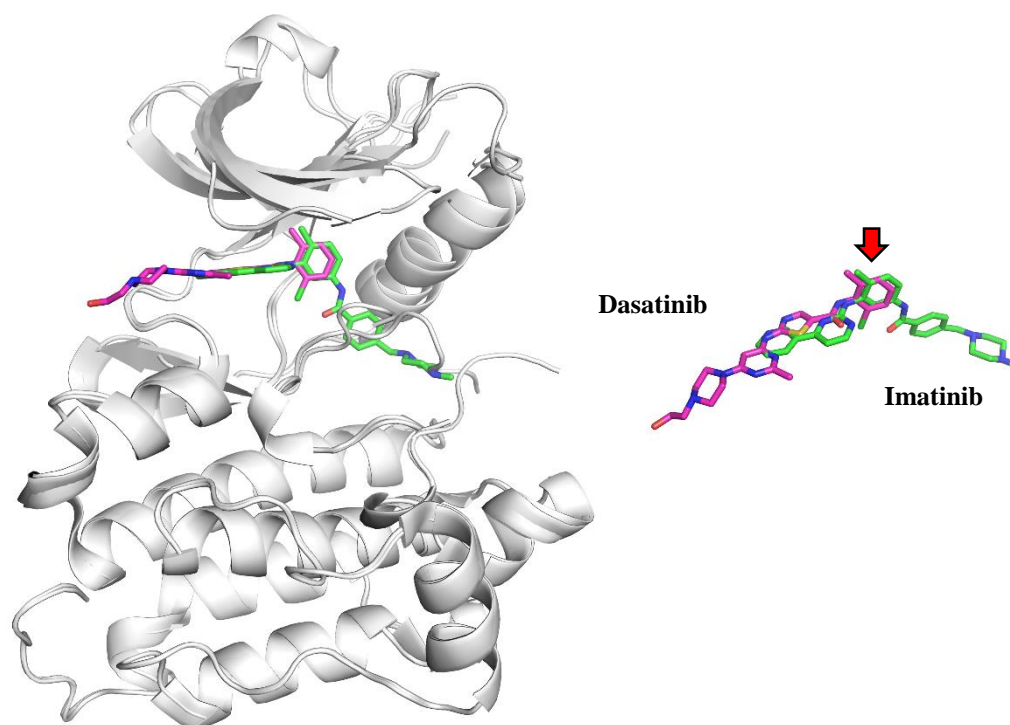
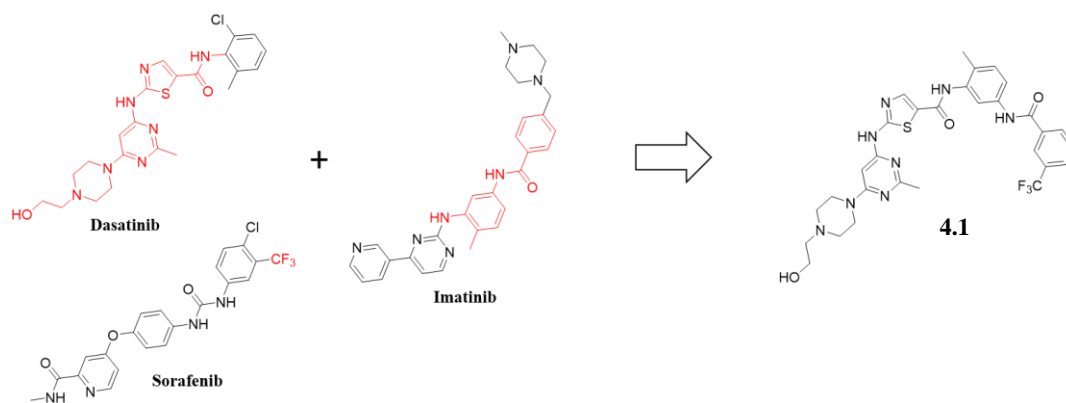


Figure 4.1: From PDB 3G5D (c-Src and dasatinib) and 2HYY (c-Abl and imatinib). Picture on the left depicts an overlay of both c-Src and c-Abl crystal structures, shown in white, and both dasatinib (magenta) and imatinib (green) ligands. The picture on the right shows the ligands alone. From the ligand overlay, the methyl phenyl ring (red arrow) are almost perfectly aligned, giving the rationale that using the dasatinib scaffold and adding the phenyl methyl piperazine of imatinib (the DFG-out portion) would create a DFG-out ligand that would bind c-Src.

Figure 4.1). Using crystal structures, dasatinib was overlaid with imatinib, a c-Abl Type II inhibitor. The dasatinib portion that bound in the ATP pocket was utilized and the Type II piece of imatinib was appended. This rationale design gives us a more definite chance of designing a ligand that binds c-Src in a DFG-out conformation. For the ease of synthesis, the para methyl piperazine was replaced with a meta CF₃ group which was borrowed from the type II sorafenib scaffold. Previous literature SAR studies of imatinib has found the methyl piperazine group was added as a solubilizing group and thus, not as necessary for potency. Instead, a CF₃ group was substituted, as previous compounds synthesized in our lab using a pyrazolopyrimidine scaffold had suggested this group was necessary for more potent binding to c-Src. Altogether, this would help us to explore Type I vs Type II effect in TNBC without varying effects from differing scaffolds.

4.3 Biochemical Evaluation of 4.1 using BODIPY

As a result, Compound **4.1**, was synthesized. Since dasatinib is extremely potent against c-Src with pM affinity, it was not surprising that **4.1** titrates enzyme (less than 30 nM) in our biochemical assay. To properly evaluate binding affinities of **4.1**, a BODIPY version was developed, which can be used in a binding assay to ascertain K_d values. A BODIPY version of dasatinib was made as well for comparison. Along with K_d values, k_{off} rates can be obtained, which would allow us to assess residency times of inhibitors. It has been previously described that one advantage of Type II inhibitors over Type I is a longer k_{off} rate which would prove beneficial in a clinical setting. The results are shown in Table 4.2. Dasatinib-BODIPY (0.74 nM) is 3.6 fold more potent than **4.1-BODIPY** (2.7 nM). However, as expected, **4.1-BODIPY** has a longer k_{off} value ($1.8E-04 \text{ sec}^{-1}$) than dasatinib ($7.9E-04 \text{ sec}^{-1}$) which is a 4.4 fold longer residency time. Since c-Src is oftentimes phosphorylated in cancer cell lines, its phosphorylated (pY419) version was assessed as well. Gratifyingly, compound **4.1** remains similarly effective against pY419 c-Src as in wt-Src.

4.4 Cellular Evaluation of 4.1

With similar biochemical data, we wanted to assess cellular proliferation in TNBC cancer cell lines. First, using MDA-MB-231 cell lines, we were surprised to see that compound **4.1** (GI50 = 6nM) is 138-fold more potent than dasatinib (GI50 = 830nM),

Table 4.1. To ensure the potency is not the result of toxicity, both **4.1** and dasatinib was dosed in HMECs, a healthy human mammary epithelial cell line. Satisfyingly, **4.1** is only 1800 nM vs. 700 nM for dasatinib and thus relatively resistant to the anti-proliferation effects of either compound. Overall these results, could explain dasatinib's poor effect in clinical trials of TNBC patients. While the large increase of potency between compound **4.1** and dasatinib could be attributed to a longer k_{off} rate, it is more plausible that there are a number of other factors at play. One easily explored factor is kinase selectivity. It is known that dasatinib is a promiscuous inhibitor of other kinases besides c-Src, which could lead to possible negation of its inhibition of c-Src, as inhibition of other pathways through other kinases could be detrimental to killing TNBC cell line. Another more easily considered explanation is compound **4.1** could be inhibiting another kinase important in TNBC proliferation that dasatinib does not target. As such, a proteomic profiling in MDA-MB-231 lysate was performed with both compounds. In a proteomic profiling, an active-site directed covalent probe, ATP-biotin, is used to label any ATP binding enzyme, which in our case is kinases. Inhibitors, such as **4.1** and dasatinib, can block ATP-biotin from labeling kinases which is how kinase selectivity can be assessed in a cell line. From the profiling, **4.1** and dasatinib have similar targets except p38 kinases. Specifically, compound **4.1** potently inhibits p38 α and p38 β . Biochemical K_d values were found against p38 β to be 7.8 nM (data from DiscoverX). p38 phosphorylation in MDA-MB-231 was stopped upon treatment with compound **4.1** in 15 min, lending further credence to the profiling results, Figure 4.2.

To see if this dual inhibition effect of **4.1** is consistent and necessary, dasatinib and BIRB-796, a potent and selective p38 kinase family inhibitor, was dosed together in 3D cell culture. Dasatinib + BIRB-796 was found to have similar

effect as **4.1**, suggesting inhibition of both p38 and c-Src is synergistic and important for anti-TNBC activity (data not shown).

From this preliminary data, we hoped to improve on compound **4.1** and further explore this dual p38/c-Src inhibition which will be addressed in this chapter.

<i>Compound</i>	GI ₅₀	
	MDA-MB-231 (nM)	HMEC (nM)
Dasatinib	830	700
4.1	6	1800

Table 4.1: GI₅₀ (nM) of dasatinib and **2.1** in MDA-MB-231 and HMEC cells.

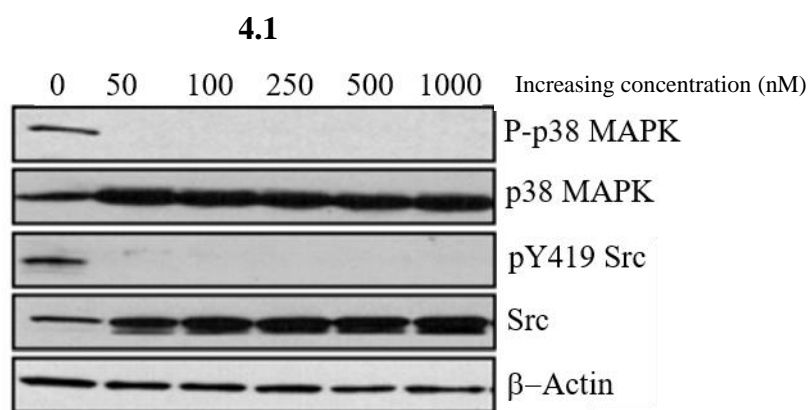


Figure 4.2: Western Blot data in MDA-MB-231 cells of increasing concentration (0, 50, 100, 250, 500, 1000 nM) of compound **4.1**. From selectivity data, p38 MAPK kinases were potently inhibited and thus it was of interest to see if it had any cellular activity. At 50 nM, both phosphorylated p38 MAPK (P-p38 MAPK) and phosphorylated Src (pY419) were completely absent suggesting both Src and p38 MAPK are inhibited.

4.5 Metabolic Stability of **4.1**

One area of improvement to address is metabolic stability of compound **4.1**. In collaboration with the Sun Lab, preliminary metabolic stability of **4.1** and dasatinib was found. Compounds (1 μ M final) are incubated in mouse liver microsomes and initiated with the addition of NADPH. At various time points, samples were taken and analyzed by LC/MS/MS. The results are shown in

Table 4.3. The half-life of compound **4.1** (3 min.) was 6.5 fold worse than dasatinib (22 min.). As such, modifications to **4.1** is needed to improve its metabolic stability. Half-life results were compared to dasatinib as it is an FDA approved drug and thus gave us a standard half-life to achieve in creating a more metabolically stable c-Src drug inhibitor.

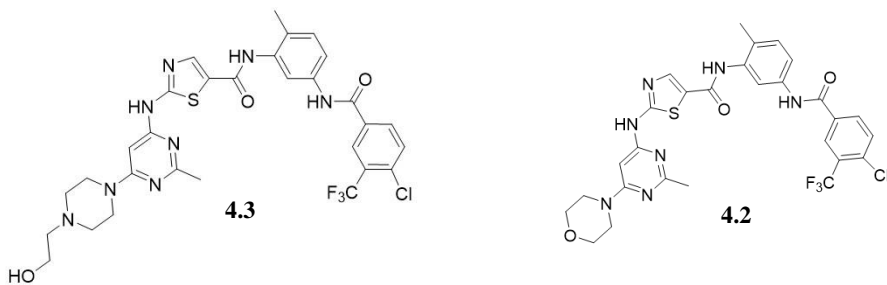


Figure 4.3: Compound **4.3** and **4.2**. Similar to **4.1**, however there is an additional chlorine on the CF₃ phenyl ring which was installed in hopes of increasing metabolic stability due to increased residency times as well as substituting the hydroxyethyl piperazine, as the major metabolite of **4.1** was oxidation of the piperazine.

4.6 Analogs of 4.1

A derivative of compound **4.1**, **4.3** (Figure 4.3) was synthesized and includes an additional chlorine to the CF₃-phenyl ring, thereby replicating sorafenib's type II fragment. Reports have suggested that this added chlorine improves residency times and hopefully this addition would translate into a prolonged half-life in metabolic stability test.

Preliminary metabolic study was performed on **4.3** and unfortunately, the added chlorine only increased the half-life to 9.3 min, which is still 2.2-fold worse than dasatinib. Further analysis of the results revealed a major metabolite from the oxidation at the hydroxyethyl piperazine which would also explain the abysmal metabolic stability of its parent compound, Figure 4.4. Of note, dasatinib was previously found to have similar metabolites as well as additional modifications on its phenyl ring. Another derivative, **4.2** was synthesized, in which the hydroxyethyl piperazine was substituted for a morpholine, Figure 4.3, and a metabolic stability test was performed. Half-life of **4.2** was greatly improved, >60min demonstrating

that the major metabolite was indeed happening at the piperazine ring and could be improved by removing the oxidation site.

While swapping the hydroxyethyl piperazine for other substituents is a logical next step, the piperazine group serves as a favorable solubility factor and one in which dasatinib was able to retain while maintaining an increased half-life. In a compound consisting of greasy hydrophobic rings, its beneficial effects should be retained. Therefore, we decided to take a second approach towards improving the metabolic stability of **4.1**.

From previous experience of developing c-Src kinase inhibitors, we have gathered that compounds derive most of its potency from the fragment residing in the ATP-pocket as they make key hydrogen bonding interactions with the hinge region. Therefore, in designing a new derivative of either compound **4.1** or **4.3**, the core pyrimidine and thiazole rings should remain unchanged. This leaves us with

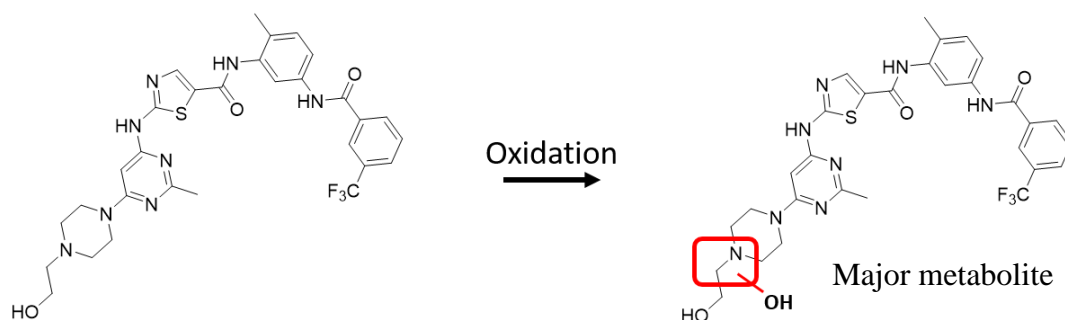


Figure 4.4: Major metabolite of **4.1**, which is oxidation of the N off of the hydroxyethyl end of piperazine.

modifying the type II fragment. Since the dual inhibition of p38 and c-Src kinases and DFG-out binding mode needs to be preserved, we reasoned a type II fragment from a p38 ligand could be utilized. Crystal structures of BIRB-796 and dasatinib were overlaid and a hybrid molecule was proposed (Figure 4.5). Also, previous literature and compounds synthesized in our lab has utilized the phenyl pyrazole type II fragment on a pyrazolopyrimidine scaffold and found to be an excellent substitute/potent inhibitor of c-Src. We hypothesize that the added large phenyl

pyrazole ring could sterically block its binding to cytochrome p450s, making it a poorer substrate and thus less prone to metabolic modifications.

4.7 Evaluation of 4.4 Analog

Compound **4.4** was biochemically evaluated in our activity assay and was found to titrate enzyme. Therefore, a BODIPY version of compound **4.4** was synthesized and the binding affinity was assessed. The K_d of **4.4** was 2 nM and had a $k_{off} = 3.3E 10^{-4} sec^{-1}$. As expected, the phenyl pyrazole had a longer residency time than the type I dasatinib due to the binding mode. However, there was a 2-fold decrease in k_{off} rate than **4.1** suggesting that a larger Type II fragment hinders the ability of the compound to stay bound to c-Src.

Compound (wt-Src)	K_d (nM)		$k_{off}(sec^{-1})$	
	wt-Src		pY419 wt-Src	
Dasatinib-BODIPY	0.74	7.9E-04	0.7	5.15E-04
4.1 -BODIPY	2.7	1.8E-04	3.0	1.48E-04
4.4 -BODIPY	2	3.3 E-04	-	-

Table 4.2: Fluorescence assay, K_d values from BODIPY version of compounds dasatinib, **4.1**, and **4.4**

Compound	Half-Life (min)
Dasatinib	22
4.1	3
4.2	9.3
4.3	> 60
4.4	41.2

Table 4.3: Microsomal half-life in minutes of dasatinib, **4.1**, **4.2**, **4.3**, and **4.4**.

Next, a preliminary metabolic study was performed on **4.4**. The theory was that the additional bulky phenyl pyrazole could help decrease binding to cytochrome P450 and hence increase its metabolic stability. Gratifyingly, the half-life was improved 2-fold compared to dasatinib to 41 min.

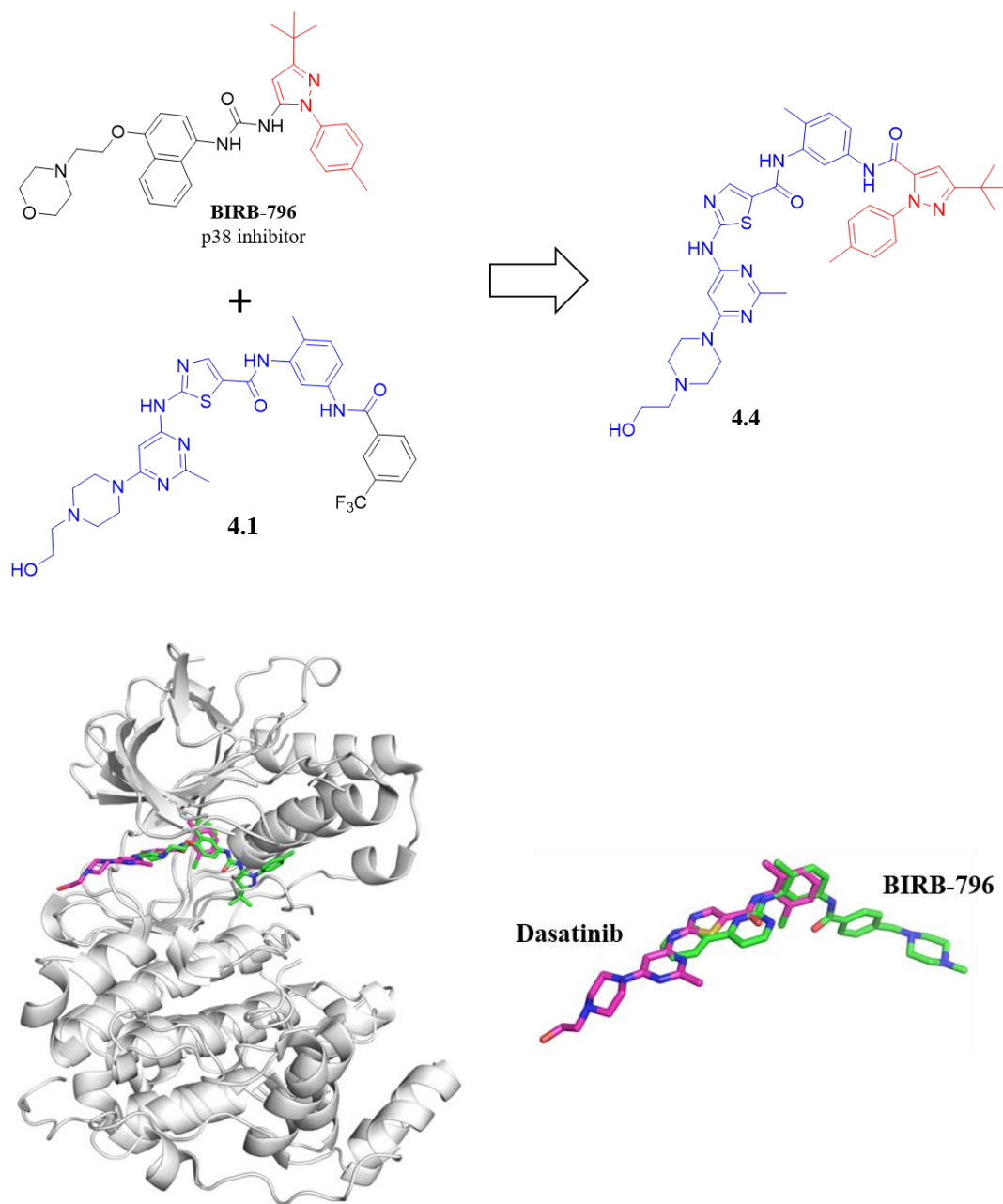


Figure 4.5: Top picture depicts how compound **4.4** is derived from **4.1** and BIRB-796. Bottom picture: PDB 3G5D (c-Src + dasatinib) and 1KV2 (p38 + BIRB 796) with dasatinib shown in magenta and BIRB-796 in green overlaid within the kinase (left) and ligand only overlay on the right.

Kinase	% Activity Remaining		
	4.2	4.4	4.1
FGFR2	15.8	88.1	30.1
FLT1	4.1	80.7	6.7
LOK	45.1	-0.6	DNT
PKN3	21.9	100	67
RIPK2	2.4	80.6	51.8
TESK1	45.4	98.8	78.3
TESK2	33.5	83.9	50.4
TRKB	23.2	76.8	54.8
VEGFR2	8.3	77.7	49.3

Table 4.4: The nine kinases that differed in the Luceome selectivity panel between **4.2** and **4.4**. Compound **4.1** is shown as well but was done in a separate Luceome panel which is why LOK was not tested.

Both 4.2 and 4.4 were sent to Luceome to be profiled against 131 kinases at a concentration of 500 nM. The full selectivity data is shown in the experimental section. Besides a handful of kinases, their selectivity looks relatively similar. Unfortunately, Luceome did not carry p38 β which will have to be tested at a later date by DiscoverX. The nine kinases, FGFR2, FLT1, LOK, PKN3, RIPK2, TSK1, TSK2, TRKB, and VEGFR2 they differ in selectivity is shown in

Table 4.4. When **4.4** was compared to both **4.2** and **4.1**, all nine kinases were generally less inhibited by **4.4** than either **4.2** or **4.1**. Highlighted in red are kinases that still have at least 50% activity remaining. This leaves FGFR2 and FLT1 that are

better inhibited by **4.1** and **4.2** and only LOK where **4.4** is a better inhibitor, though **4.1** was not tested in this panel.

The selectivity data shown above is interesting with respect to the compounds response in MDA-MB-231 cells. Compound **4.2**, **4.3**, and **4.4** were dosed and the results are shown in Table 4.5. Both compounds **4.3** and **4.4** demonstrated a

GI ₅₀ (nM)	4.1	4.2	4.3	4.4
MDA-MB-231	6	49	539	546

Table 4.5: MDA-MB-231 GI₅₀ values for compounds **4.1, **4.2**, **4.3**, and **4.4**.**

substantial decrease in potency (539 nM and 546 nM respectively) whereas **4.2** decrease in potency by 8-fold to 49 nM. From this data, the substitution of hydroxyethyl piperazine to morpholine is responsible for the decrease in potency between **4.2** and **4.3** demonstrating that the piperazine group is an essential pharmacophore, despite the morpholine possessing better metabolic stability. Interestingly, swapping of the DFG-out fragment of **4.1** for BIRB-796 phenyl pyrazole also devastates its cellular activity. This brings into question whether or not p38 β inhibition is necessary in these TNBC cell line, however **4.3** inhibition of p38 β biochemically remains to be seen. It does inhibit p38 α and since it takes on BIRB-796's DFG-out head group, one would assume that p38 β would be maintained. From the selectivity data, it could also be that FLT1 and FGFR2 would be necessary to inhibit and could explain the loss of potency. However, a previous KiNativ assay done with dasatinib and **4.1** in MDA-MB-231 cells does not show FLT1 and FGFR2 to be expressed in the cell line.

4.8 Conclusions

In an effort to improve upon dasatinib c-Src inhibition in triple negative breast cancer, we designed a DFG-out inhibitor. Utilizing dasatinib as the core ATP-pocket scaffold, we installed the imatinib DFG-out fragment to make a Type II

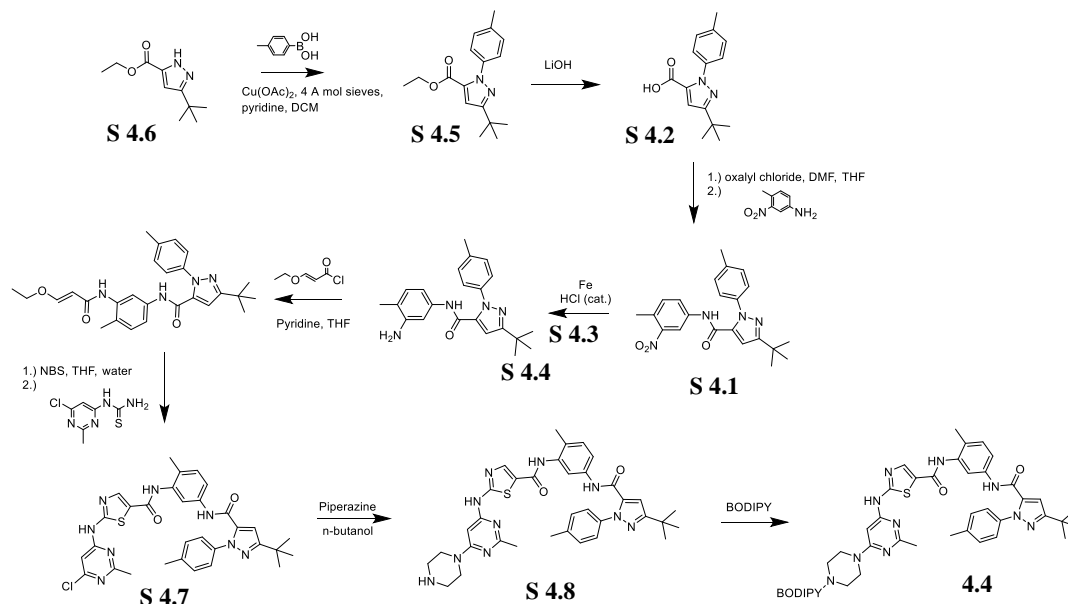
inhibitor, **4.1**. Compound **4.1** was tested against MDA-MB-231 and showed surprisingly potent activity of 6 nM, nearly a 140-fold improvement over dasatinib (830 nM). We were curious if the increased in potency was related to a kinase that **4.1** inhibited but dasatinib did not, thus providing a synergy combination that could be used against triple negative breast cancer cells alongside c-Src inhibition. Kinome selectivity scan from Luceome pinpointed the inhibition of p38 β as a possible reason for **4.1** efficacy over dasatinib. In a separate assay, it was confirmed that inhibition of p38 β and c-Src from two separate inhibitors lead to synergy. Unfortunately, the metabolic stability of **4.1** is poor (3min) compared to dasatinib (22min) and to improve upon the pharmacophore kinetics, we decided to rationally design a dasatinib/BIRB-796 (Das-BIRB) hybrid molecule, **4.4**. Due to the BIRB-796 piece, inhibition against p38 should be maintained if not improved while hopefully decreasing binding to cytochrome P450 in an attempt to bolster metabolic stability.

This strategy worked and metabolic stability was increased, as found in mouse liver microsome LC/MS/MS assay (**4.4** half-life = 42min from **4.1** half-life = 3min), which prompted us to send **4.4** to Luceome to assess kinase selectivity against 137 kinases to compare against the original p38 β /c-Src inhibitor, **4.1** as well as **4.2**. Selectivity was relatively similar. Luceome, however, did not carry p38 β which will need to be tested later at DiscoverX, but due to the **4.4** being able to inhibit p38 α , one would assume that p38 β is also inhibited. Unfortunately, the Das-BIRB inhibitor as poor against MDA-MB-231 cell lines (546 nM) compared to the original **4.1** (6 nM) so despite the improved metabolic stability, the decrease in *in cellulo* potency was not acceptable. This result might throw into doubt whether or not p38 β and c-Src dual inhibition is responsible for the parent p38 β /c-Src inhibitor's success, compared to dasatinib, against MDA-MB-231 cell, and if it is actually another unknown kinase or non-kinase target that is needed for efficacy. A full kinome scan against all 518 kinases is warranted to further explore all possible kinase targets as the previous kinome scan was only a panel of 137 kinases.

4.9 Experimental Section

General Synthetic Methods. Unless otherwise noted, all reagents were obtained from commercial suppliers and used without further purification. Black, opaque-bottom 96 well plates were purchased from Nunc. BODIPY FL NHS ester was purchased from Lumiprobe. All ^1H and ^{13}C NMR spectra were measured with a Varian MR400 and Inova 500 spectrometer. Mass spectrometry (HRMS) was carried out by the University of Michigan Ann Arbor Mass Spectrometry Facility (J. Windak, Director). Flash column chromatography was performed using a Biotage Isolera 1 Flash Purification System using KP-Sil SNAP cartridges. In all cases, ethyl acetate was used to transfer the crude reaction material onto the silica gel samplet. A gradient elution using hexane and ethyl acetate was performed, based on the recommendation from the Biotage TLC Wizard.

Synthesis of Compound 4.4



Scheme S 4.4: Synthesis of **4.4** and **4.4**-BODIPY

Synthesis of S4.2: Ethyl 3-(tert-butyl)-1H-pyrazole-5-carboxylate (0.87 g, 4.4 mmol) was added to a flamed dried rbf containing 4Å molecular sieves in 50 mL dichloromethane. p-tolylboronic acid (1.2 g, 8.8 mmol), copper II acetate (1.2 g, 6.6 mmol), and pyridine (0.7 mL, 8.8 mmol) was added and the reaction was stirred over night at r.t. Afterwards, the reaction was filtered over celite and the crude product was purified by Biotage Isolera 1 Flash Purification System to give 0.54 mg (43% yield) of compound **S4.2** as a clear oil. **Spectral Data.** $^1\text{H NMR}$ (500 MHz, CD_3Cl_2-d) δ 7.31 (d, $J = 8.2$ Hz, 2H), 7.24 (d, $J = 8.0$ Hz, 2H), 6.87 (s, 1H), 4.24 (q, $J = 7.1$ Hz, 2H), 2.41 (s, 4H), 1.59 (s, 1H), 1.37 (s, 11H), 1.27 (t, $J = 7.1$ Hz, 4H).

Synthesis of S4.3: (.54 mg, 1.9 mmol) was added to THF (40 mL) and water (10mL). Lithium hydroxide (0.9 mg, 37.5 mmol) was then added and the reaction was refluxed overnight. Afterwards, the reaction mixture was acidified (pH = 2.0) and extracted with EtOAc. The organic layer was washed with water and brine, dried over MgSO_4 , filtered, and concentrated in vacuo. The crude solid was carried forward without further purification.

Synthesis of S4.4: Compound **S4.3** (0.58 mg, 2.2 mmol) was dissolved in THF (10 mL) and was cooled to 10 °C. Oxalyl chloride (589 μ L, 6.7 mmol) was added along with DMF (few drops). The reaction mixture was allowed to warm to r.t. and stirred for 3 hours. Afterwards, the reaction mixture was concentrated. DIPEA (779 μ L, 4.4 mmol), THF (10 mL), and 4-methyl-3-nitroaniline (0.68 mg, 4.5 mmol) was added and stirred at r.t. overnight. Afterwards, THF was removed in vacuo, diluted with EtOAc and washed with water, brine, dried over $MgSO_4$, filtered, and concentrated in vacuo. The crude product was purified by Biotage Isolera 1 Flash Purification System to give compound **S4.4** as a yellow solid (224 mg, 39% yield). **Spectral Data.** 1H NMR (500 MHz, $DMSO-d_6$) δ 10.15 (s, 1H), 7.28 (s, 3H), 7.24 (s, 3H), 7.05 (s, 1H), 6.87 – 6.79 (m, 2H), 6.68 (s, 1H), 2.33 (s, 4H), 1.99 (s, 3H), 1.32 (s, 9H).

Synthesis of S4.5: Compound **S4.4** (0.22 mg, 0.56 mmol), iron (0.16 mg, 2.9mmol), and HCl (few drops) were dissolved in 80% EtOH and refluxed for 3 hours. Afterwards, the reaction mixture was filtered thru celite, concentrated in vacuo and precipitated with water. The crude product was carried forward without further purification.

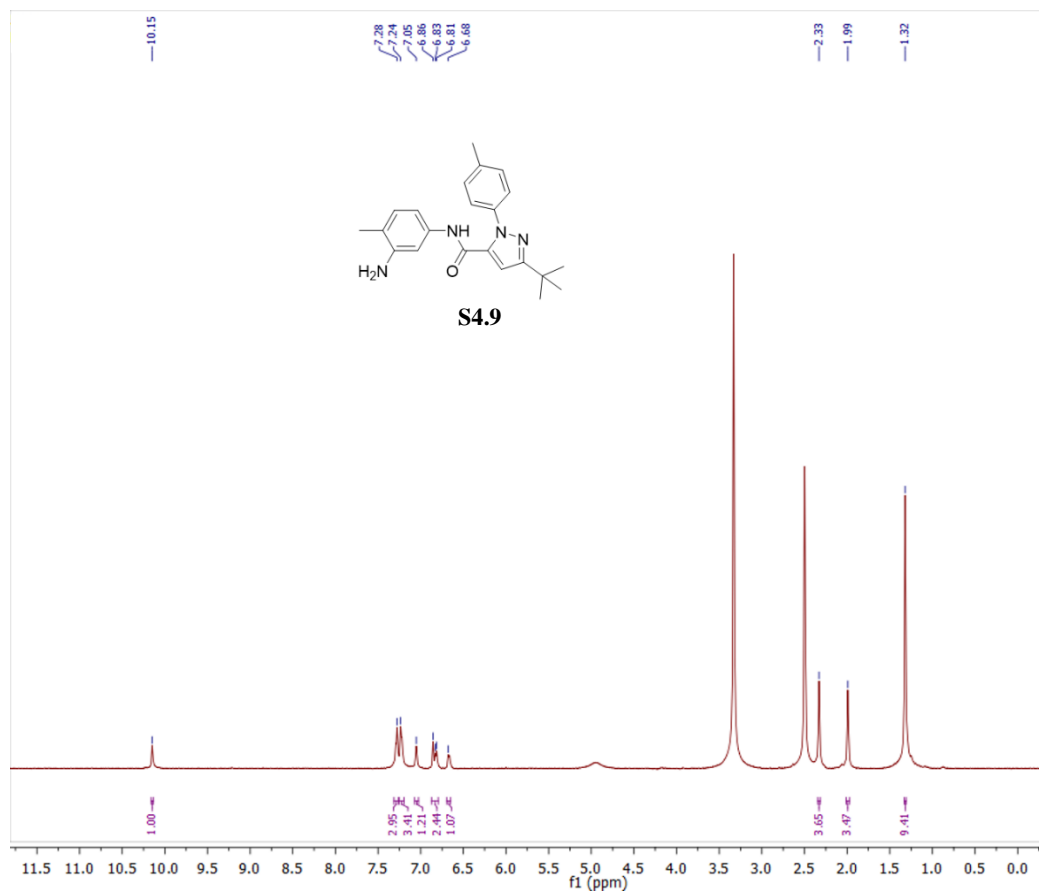
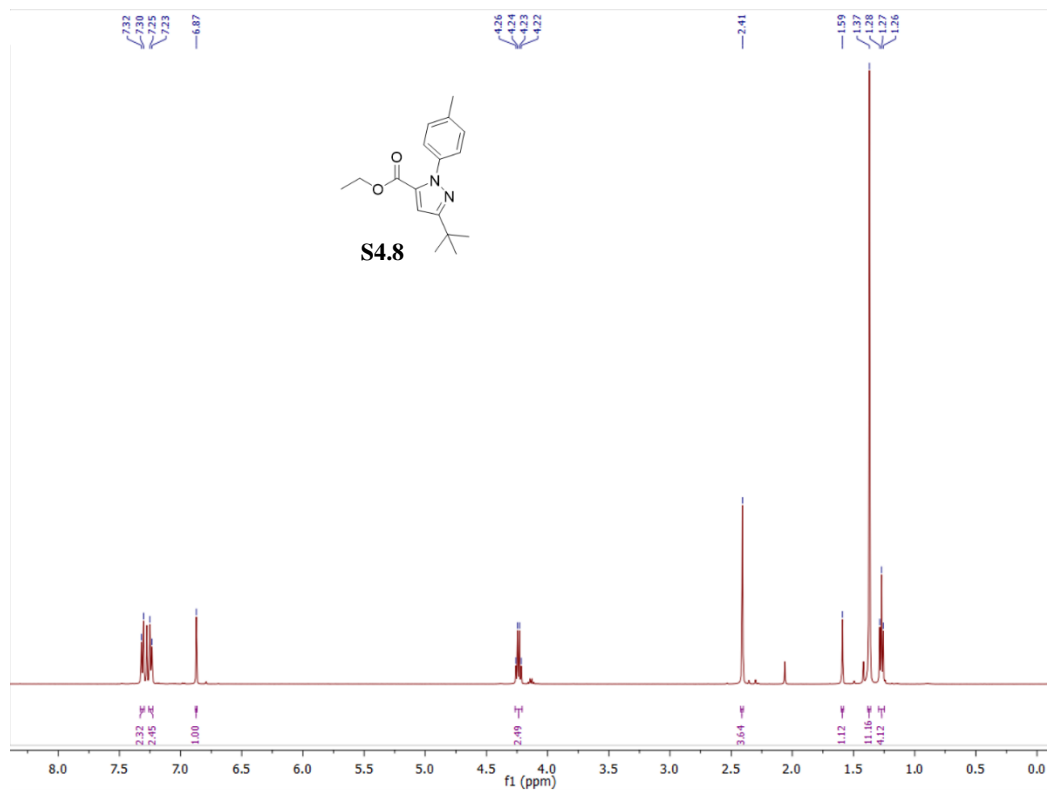
Synthesis of S4.6: Compound **S4.5** (0.2 mg, 0.55 mmol), pyridine (53 μ L, 0.67 mmol), and THF was added and cooled on ice before (E)-3-ethoxyacryloyl chloride (0.97 mg, 0.72 mmol) was added. The reaction mixture was allowed to warm to r.t. and stirred for 2 hours. Afterwards, the reaction was cooled on ice, 1N HCl (3 mL) was added and then diluted with water (9 mL), concentrated in vacuo to give a slurry, and filtered. The crude product was carried forward without further purification.

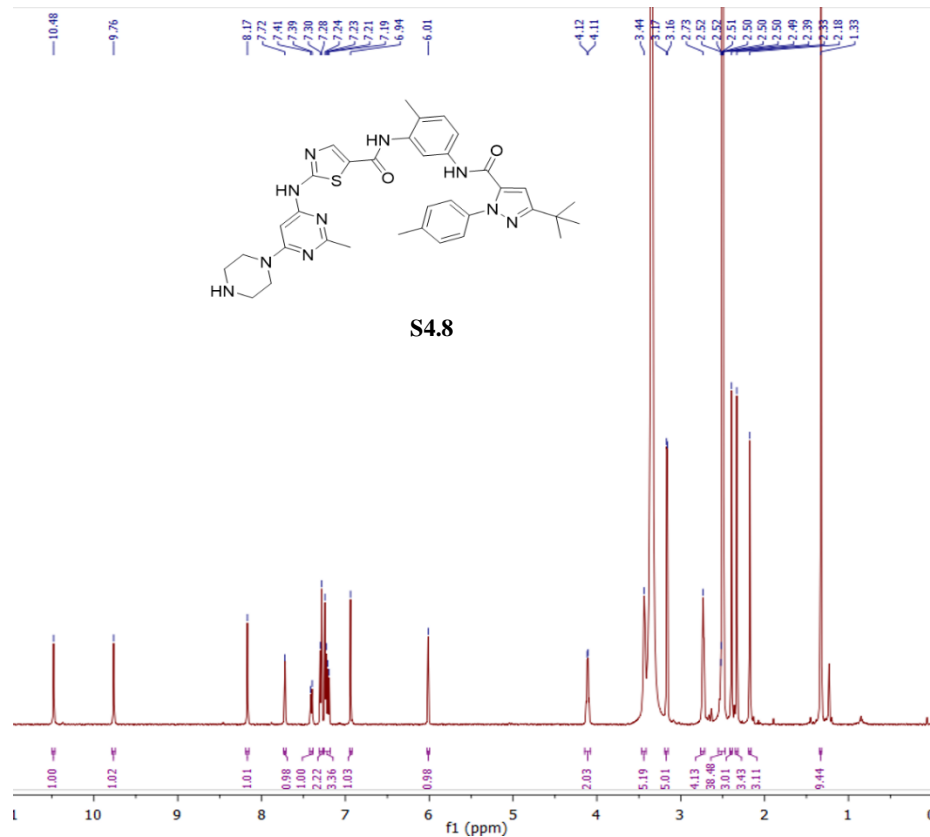
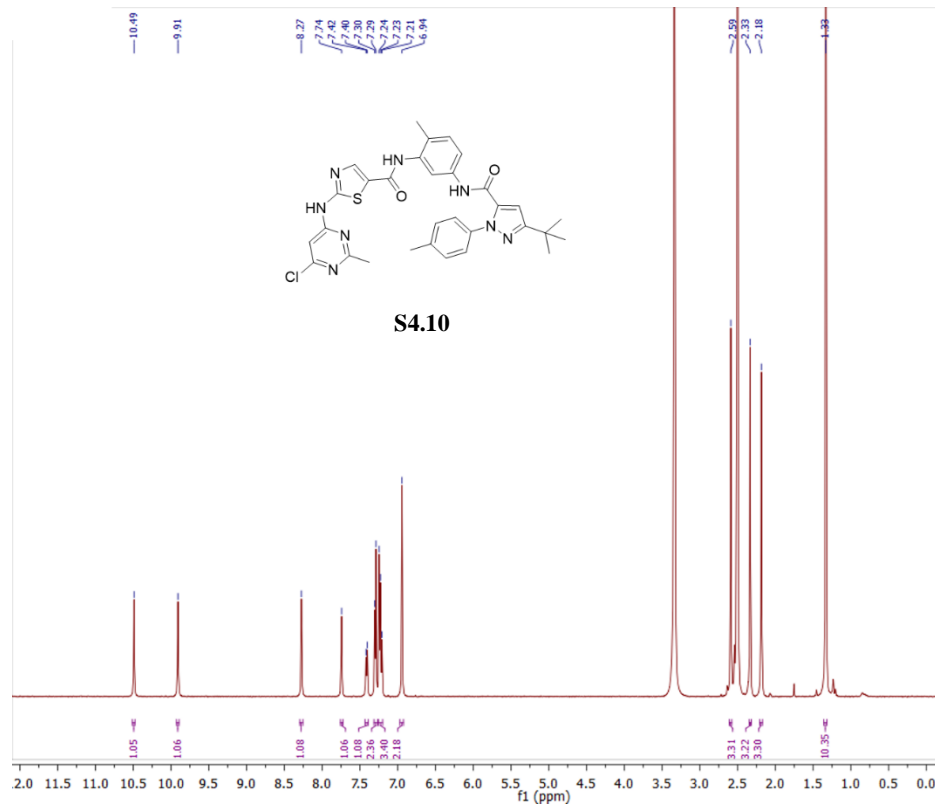
Synthesis of S4.7: Compound **S4.6** (0.23 mg, 0.49 mmol) was added to THF/water and cooled to 0 °C. N-bromosuccinimide (0.09 mg, 0.51 mmol) was added and the reaction mixture was allowed to warm to r.t. and stirred for 3 hours. Afterwards, 1-(6-chloro-2-methylpyrimidin-4-yl)thiourea (0.1 mg, 0.49 mmol) was added and the reaction mixture was refluxed for 2 hours. The reaction was then cooled and filtered. The resulting solid was purified by reverse phase preparative HPLC (linear gradient of 5 to 95% acetonitrile in water) to give compound **S4.7** (38%) as a white powder. **Spectral Data.** 1H NMR (500 MHz, $DMSO-d_6$) δ 10.49 (s, 1H), 9.91 (s, 1H), 8.27 (s, 1H), 7.74 (s, 1H), 7.41 (d, J = 8.2 Hz, 1H), 7.29 (d, J = 8.2 Hz, 2H), 7.25 – 7.20 (m, 3H), 6.94 (s, 2H), 2.59 (s, 3H), 2.33 (s, 3H), 2.18 (s, 3H), 1.33 (s, 9H).

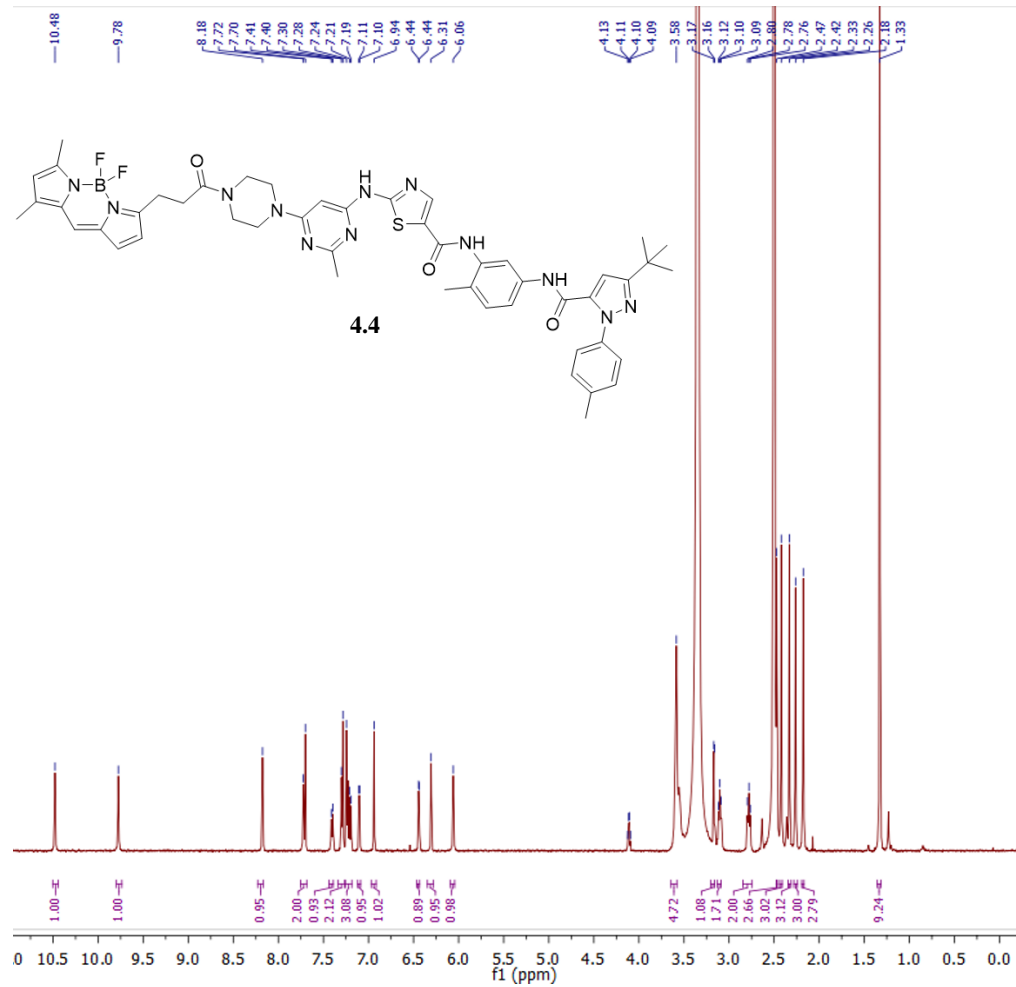
Synthesis of S4.8: Compound **S4.7** (5 mg, 0.008 mmol) was added to n-butanol (1 mL), DIPEA (7 μ L, 0.04 mmol), and piperazine () and refluxed overnight. The reaction mixture was purified by reverse-phase preparative HPLC (linear gradient 20-95% acetonitrile in water) to give compound **S4.7** (37%) as a white powder. **Spectral Data.** 1H NMR (500 MHz, $DMSO-d_6$) δ 10.48 (s, 1H), 9.76 (s, 1H), 8.17 (s, 1H), 7.72 (s, 1H), 7.40 (d, J = 9.8 Hz, 1H), 7.29 (d, J = 8.3 Hz, 2H), 7.22 (dd,

$J = 17.4, 8.4$ Hz, 3H), 6.94 (s, 1H), 6.01 (s, 1H), 4.11 (d, $J = 5.2$ Hz, 2H), 3.44 (s, 5H), 3.16 (d, $J = 4.9$ Hz, 5H), 2.73 (s, 4H), 2.50 (p, $J = 1.9$ Hz, 38H), 2.39 (s, 3H), 2.33 (s, 3H), 2.18 (s, 3H), 1.33 (s, 9H).

Synthesis of 4.4-BODIPY: BDP FL NHS ester (2 mg, 0.005 mmol) was added to **S4.8** (2 mg, 0.003 mmol) and DIPEA (14 μ L, 0.010 mmol) in DMF (1 mL) and stirred at r.t. overnight. The crude mixture was purified by reverse-phase preparative HPLC (linear gradient of 30-95% acetonitrile in water) to give compound **4.4-BODIPY** (1.8 mg, 36%) as powder. **Spectra Data.** ^1H NMR (500 MHz, DMSO- d_6) δ 10.48 (s, 1H), 9.78 (s, 1H), 8.18 (s, 1H), 7.71 (d, $J = 11.4$ Hz, 2H), 7.40 (d, $J = 8.2$ Hz, 1H), 7.29 (d, $J = 8.3$ Hz, 2H), 7.26 – 7.19 (m, 3H), 7.10 (d, $J = 4.0$ Hz, 1H), 6.94 (s, 1H), 6.44 (d, $J = 3.9$ Hz, 1H), 6.31 (s, 1H), 6.06 (s, 1H), 3.58 (s, 5H), 3.17 (s, 1H), 3.11 (d, $J = 7.3$ Hz, 2H), 2.85 – 2.75 (m, 2H), 2.47 (s, 3H), 2.42 (s, 3H), 2.33 (s, 3H), 2.26 (s, 3H), 2.18 (s, 3H), 1.33 (s, 9H).







Biochemical Characterization

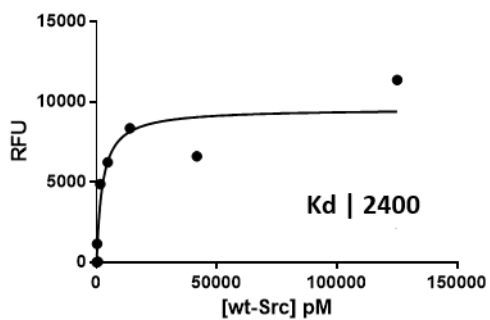
Affinity Measurements:

General Procedure for BODIPY probe K_d for c-Src: c-Src binding affinity was done as previously described.¹ Briefly, reaction volumes of 50 μ L were used in 96-well plates. 49 μ L of c-Src kinase (125 nM, 3-fold serial dilution down to 0.006 nM) in 100 mM Tris buffer (pH 8) and 10 mM $MgCl_2$ was incubated with 1 μ L of compound. Reference source not found. (10 nM in DMSO) for 30 min. Fluorescence was read at room temperature (excitation = 485 nm; emission = 535 nm). The K_d was determined by fitting the data to non-linear regression analysis (one site total binding) with Prism GraphPad software.

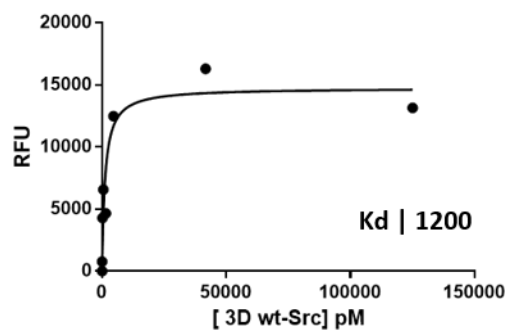
General procedure for inhibitor off-rate determination.

A multiple time point read fluorescence assay was used to determine dasatinib analog BODIPY off-rates, similar to past published reports.¹ Briefly, 60 μ L of total volume with 700 nM c-Src kinase and 500 nM probe (**4.4-BODIPY**) in buffer A 1X (Master Mix) was incubated at rt for 4 h along with 60 μ L of 500 nM probe (**4.4-BODIPY**) alone in buffer A 1X (Blank Mix). Following this incubation period, 4 μ L of the master mix was added into 5 wells and 4 μ L of the blank mix was added into 2 wells via multichannel pipette into 116 μ L of buffer A 1X containing 5 μ M (final concentration) unlabeled dasatinib (120 μ L total, 30-fold dilution). Additionally, 4 μ L of master mix was added into a single well of 116 μ L of buffer A 1X containing 100 nM (final concentration) probe to maintain consistent plate reader gain values over the course of the fluorescent reads. Master mix dilutions with competitor had final concentrations of 23 nM enzyme, 17 nM BODIPY-probe, 5 μ M unlabeled dasatinib, 100 mM Tris buffer pH 8 and 10 mM $MgCl_2$. Reads (ex/em 485/535 nm) were taken every 10 minutes for the first 2 h, then every 20 min for next two hours and finally every 30 min for the remainder of the assay (12 h total). The values for k_{off} determination were obtained directly from the nonlinear regression fits for one-phase decay curves (using blanked data). The equation $Y = (Y_0 - \text{Plateau}) * \exp(-K * X) + \text{Plateau}$; was used in the nonlinear regression. An average of 5 wells at each time point was utilized for the final fit values produced.

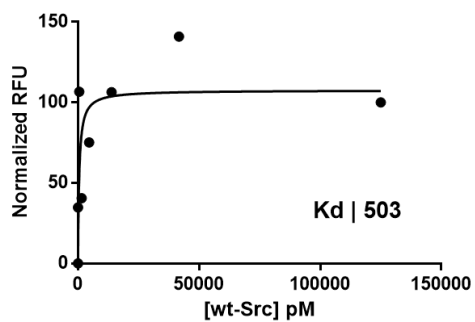
K_d Determination



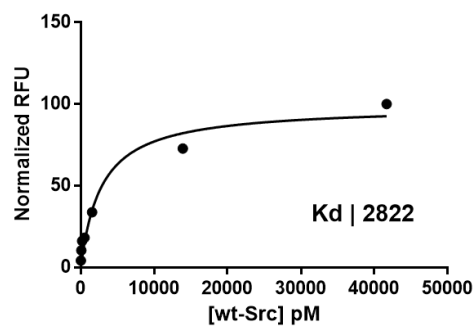
KD wt-Src
4.4-BODIPY K_d = 2 nM



3D wt-Src
4.4-BODIPY K_d = 4.2 ± 3 nM

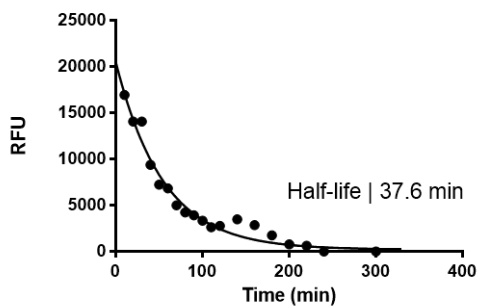


KD wt-Src
Dasatinib-BODIPY K_d = 0.74 nM



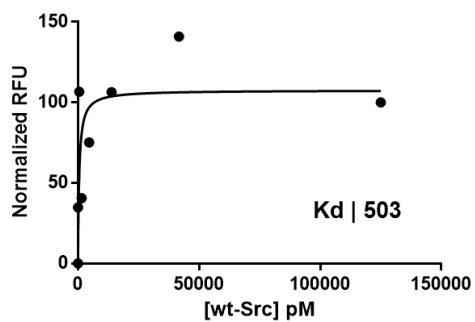
KD wt-Src
4.1-BODIPY K_d = 2.7 nM

K_{off} Curves

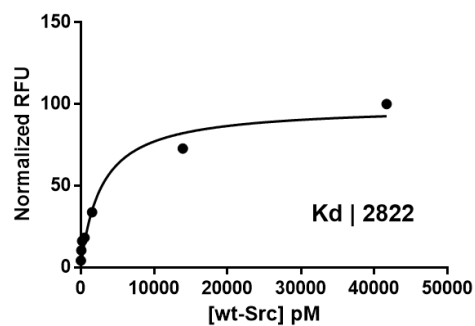


KD wt-Src
4.4-BODIPY $k_{\text{off}} = 3.3\text{E } 10^{-4} \text{ sec}^{-1}$
Half-Life = 34.5 min

KD wt-Src
Dasatinib-BODIPY $k_{\text{off}} = 7.88\text{E } 10^{-4} \text{ sec}^{-1}$
Half-Life = 14.67 min



KD wt-Src
Dasatinib-BODIPY $K_d = 0.74 \text{ nM}$



KD wt-Src
4.1-BODIPY $K_d = 2.7 \text{ nM}$

Cellular Characterization

Cell growth inhibition assays.

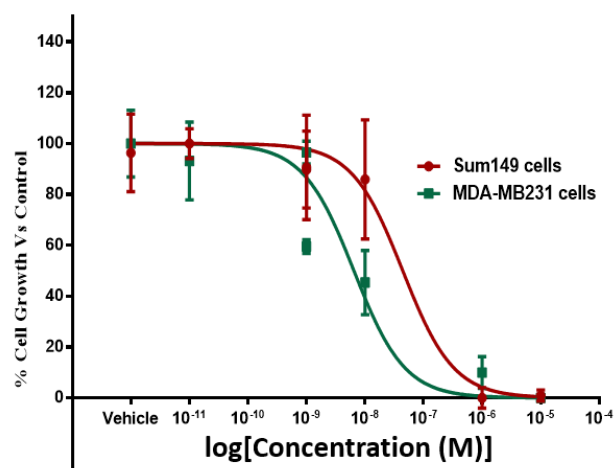
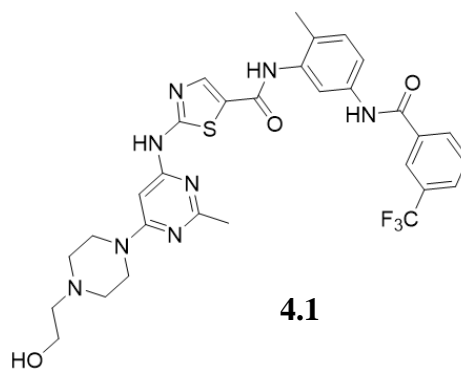
WST-1 reagent was obtained from Roche. The cell proliferation colorimetric assay using WST-1 was performed following the protocol provided by Roche.

Cell Culture and Seeding Procedure: Cells were dispersed from flasks and collected by centrifugation (200xg for 5 minutes at room temperature). An aliquot of the resuspended cells was mixed with trypan blue solution and the cell number was quantified using a hemacytometer. In general, depending on the growth rate of the untreated cells, the cells were plated at $5.0 - 7.5 \times 10^3$ cells per well. The cells were plated into sterile, clear bottom 96 well plates and cultured under normal growth conditions overnight prior to dosing with compound.

Dosing: 100% DMSO compound stocks were prepared to 100X the final concentration desired in the assay. 3 μ L of the DMSO stock solution was then added to 297 μ L of the cell growth media to give a DMSO concentration of 1%. The cell media was removed by aspiration for adherent cells and replaced with 100 μ L per well of the cell growth media containing the compound. In general, each compound concentration was dosed in triplicate wells. **Assay:** After the dosing period (24 hours) was complete, the plates were removed from the incubator and 10 μ L per well of WST-1 reagent was added. The plates were returned to the incubator and incubated for 1 hr, followed by shaking on a plate shaker for 60 seconds prior to the absorbance read (450 nm) on a BioTek Synergy 4 multimode plate reader.

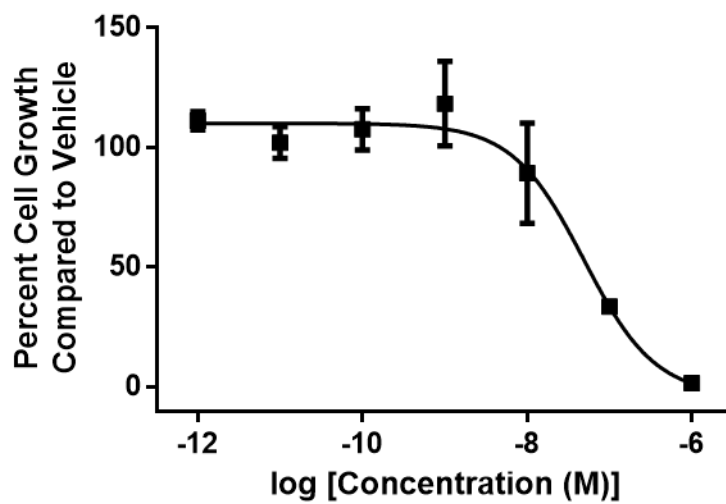
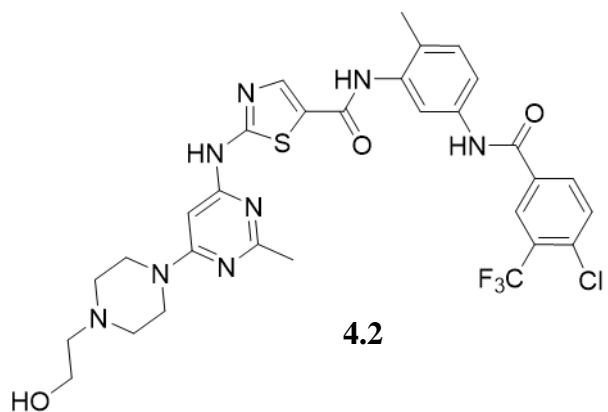
Data Analysis: The reference absorbance reading was subtracted from the formazan absorbance (background control well no compound added, 1% DMSO) and the data was plotted as a percentage of the vehicle (1% DMSO alone). Data analysis and curve fitting was performed using Graphpad Prism. For each cell line, there were $n = 3$ data points for each concentration. Each dose response curve was performed at least twice, providing $n \geq 6$ for each data point.

MDA-MB-231 with Compound 4.1



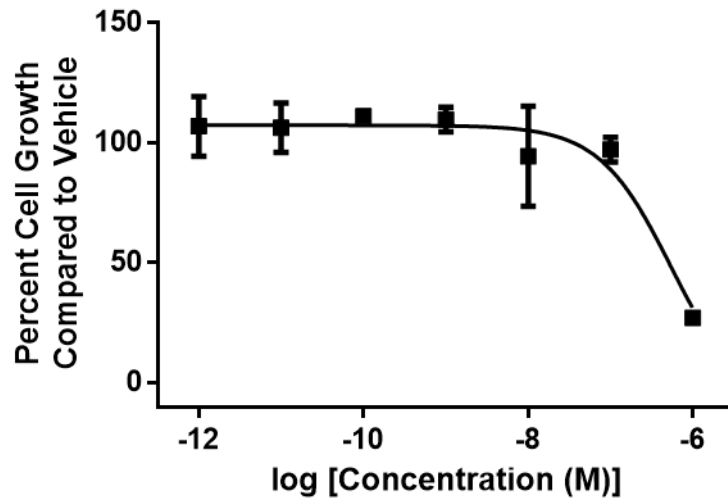
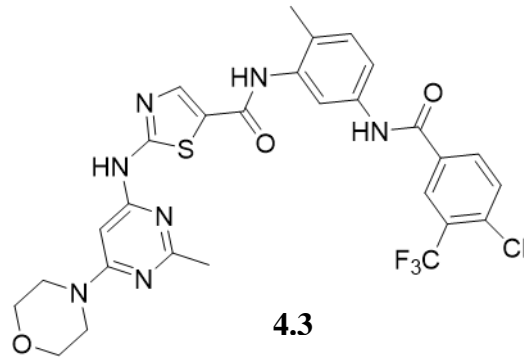
GI₅₀ | 6 nM

MDA-MB-231 with Compound 4.2



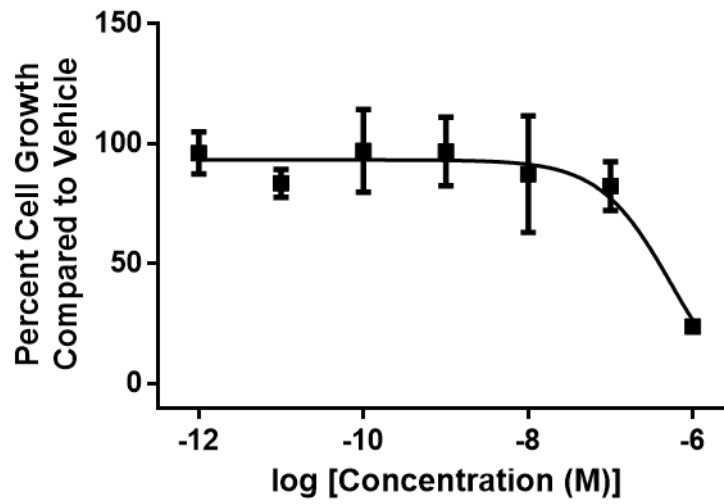
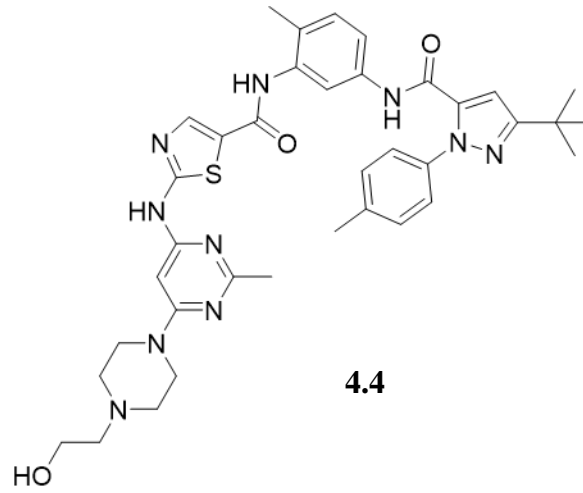
GI₅₀ | 49 nM

MDA-MB-231 with Compound **4.3**



GI₅₀ | 539 nM

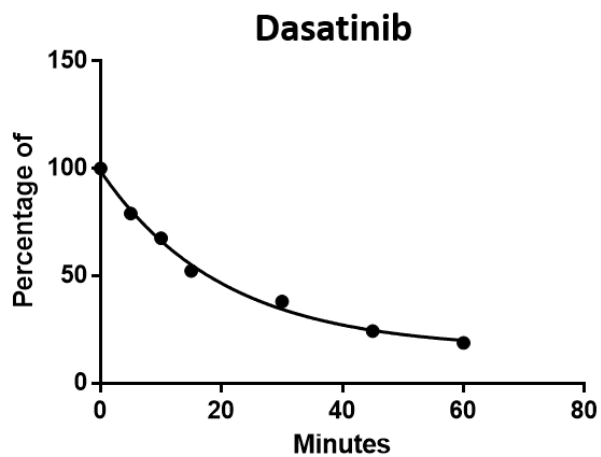
MDA-MB-231 with Compound 4.4



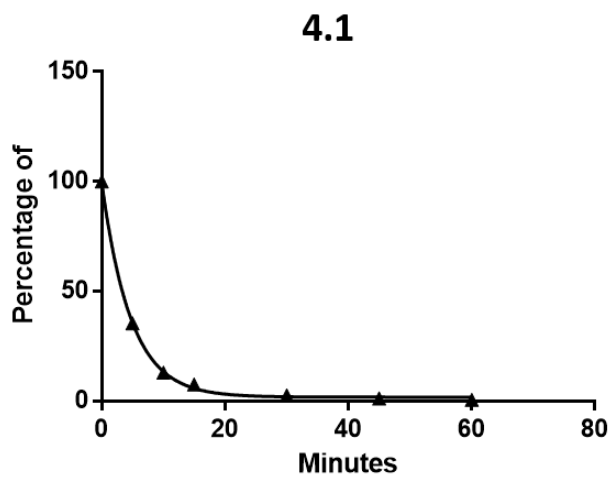
GI₅₀ | 546 nM

Microsomal Stability Studies

Compounds were sent to Duxin Sun Laboratory, University of Michigan Pharmacokinetics Core for metabolic stability test using mouse microsomes.

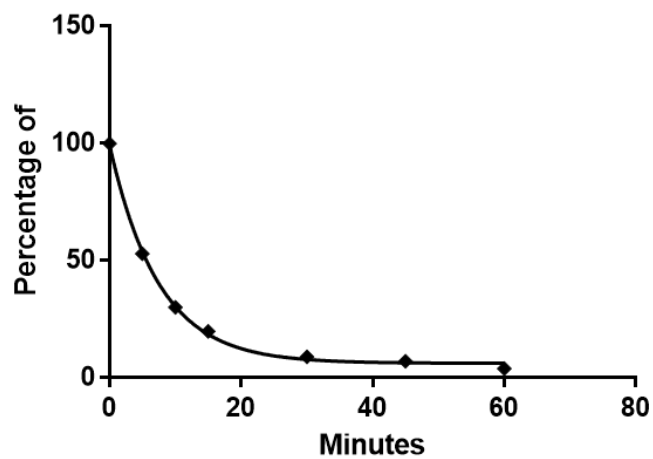


Half-Life | 22 min



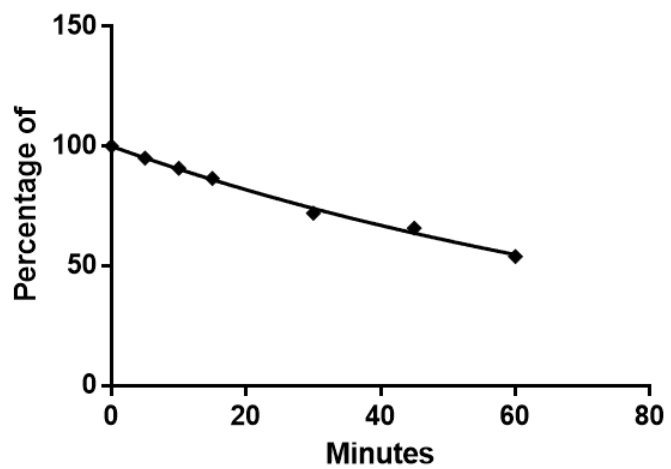
Half-Life | 3 min

4.2

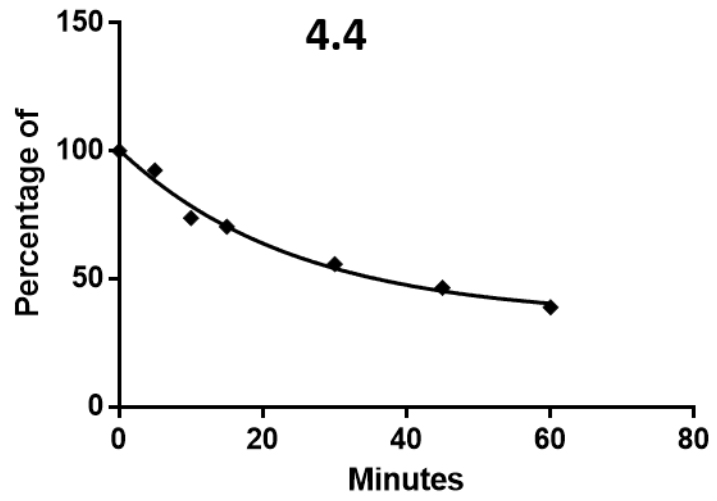


Half-Life | 9.3 min

4.3



Half-Life | >60 min



Half-Life | 41.2 min

Kinome Selectivity

Compounds dasatinib, **4.1**, **4.2**, and **4.4** were sent to Luceome Biotechnologies (Tucson, Arizona) to be profiled against 131 kinases in their KinaseSeeker platform. The compounds were profiled at 500 nM.

Dasatinib

Kinases	Family	% Activity Remaining
ABL1	TK	1.9
ABL2	TK	50.7
AKT1	AGC	95.1
AKT1(FL)	AGC	100
AKT2	AGC	100
AKT2(S474A)	AGC	100
AKT2(S474D)	AGC	66.2
AKT2(T309A,S474A)	AGC	90.2
AKT2(T309D,S474D)	AGC	81
AKT3	AGC	73.3
AMPK- α 1	CAMK	93
AMPK- α 2	CAMK	67.8
AURKA	Other	100
AURKB	Other	100
AURKC	Other	80.7
AXL	TK	27.4
BIKE	Other	100
BLK	TK	0
BTK	TK	35.5
CAMK1	CAMK	100
CAMK1D	CAMK	99.3
CAMK1G	CAMK	100
CAMK2A	CAMK	85.8
CAMK2B	CAMK	68.4
CAMK2D	CAMK	79.8
CAMKK1	Other	75
CAMKK2	Other	78.9
CHEK1	CAMK	90.9
CK1D	CK1	100
CLK1	CMGC	100
CLK2	CMGC	100
CSK	TK	31.3
DAPK1	CAMK	100
DAPK2	CAMK	100
DAPK3	CAMK	100

DDR1	TK	84.8
DDR2	TK	51.8
DMPK	AGC	100
EPHA1	TK	1.1
EPHA2	TK	1.3
EPHA3	TK	5.8
EPHA4	TK	0
EPHB2	TK	0
EPHB3	TK	35.2
EPHB4	TK	1.8
FGFR2	TK	100
FLT1	TK	100
FLT2	TK	57.2
FLT3	TK	36.8
FYN	TK	3.8
GSK3a	CMGC	100
HCK	TK	16.6
IGF1R	TK	75.7
IKK-e	Other	100
INSR	TK	100
ITK	TK	42.3
LIMK1	TKL	50
LYN	TK	5.9
MARK1	CAMK	100
MARK2	CAMK	100
MARK3	CAMK	100
MARK4	CAMK	100
MELK	CAMK	92
MET	TK	100
MLK1	TKL	38.4
MLK3	TKL	18.3
MST2	STE	83.3
MUSK	TK	86.4
MYLK	CAMK	75.4
MYLK2	CAMK	100
MYT1	Other	46.9
p38-g	CMGC	100
PAK1	STE	100
PAK1(T423A)	STE	100
PAK1(T423E)	STE	95.2
PDGFRA	TK	21.3
PDGFRB	TK	38.4
PDK1	AGC	100

PHKG1	CAMK	95.7
PIM1	CAMK	96.1
PIM2	CAMK	97.4
PKAC-a	AGC	78.1
PKAC-b	AGC	95.1
PKC-d	AGC	100
PKC-e	AGC	100
PKC-g	AGC	100
PKC-h	AGC	92.4
PKC-t	AGC	100
PRKD2	CAMK	100
PRKD3	CAMK	100
PKG1	AGC	100
PKN3	AGC	92
PLK4	Other	12.4
PKX	AGC	72.8
PTK2	TK	100
PTK2B	TK	100
PTK6	TK	33.8
RET	TK	92.2
RIPK2	TK	0.1
RPS6KA1/RSK1	AGC	92.5
RPS6KA2/RSK3	AGC	100
RPS6KA3/RSK2	AGC	100
RPS6KA4/MSK2	AGC	100
RPS6KA5/MSK1	AGC	88.3
RPS6KA6/RSK4	AGC	100
SGK2	AGC	74.3
SGK3	AGC	100
SNF1LK	CAMK	12.9
SNF1LK2	CAMK	41.3
SIK3	CAMK	57
SLK	STE	100
SNARK	CAMK	81.3
SRC	TK	8.8
STK16	Other	79.4
STK33	CAMK	100
SYK	TK	73.3
TBK1	Other	39.5
TEC	TK	41.6
TESK1	TKL	49.1
TESK2	TKL	45.1
TIE1	TK	100

TIE2	TK	100
TNK2	TK	24.8
TNNI3K	TKL	25.9
TRKB	TK	100
TRKC	TK	100
TXK	TK	16.2
VEGFR2	TK	100
YANK2	AGC	100
YES1	TK	8
YSK1	STE	100

Compound 4.1

Kinases	Family	% Activity Remaining
ABL1	TK	10.9
ABL2	TK	12.2
AKT1	AGC	100
AKT1(FL)	AGC	100
AKT2	AGC	100
AKT2(S474A)	AGC	100
AKT2(S474D)	AGC	100
AKT2(T309A,S474A)	AGC	100
AKT2(T309D,S474D)	AGC	100
AKT3	AGC	100
AMPK- α 1	CAMK	100
AMPK- α 2	CAMK	100
AURKA	Other	93.9
AURKB	Other	100
AURKC	Other	94.1
AXL	TK	100
BIKE	Other	100
BLK	TK	6.2
BTK	TK	26.4
CAMK1	CAMK	100
CAMK1D	CAMK	100
CAMK1G	CAMK	97.2
CAMK2A	CAMK	100
CAMK2B	CAMK	100
CAMK2D	CAMK	100
CAMKK1	Other	100
CAMKK2	Other	100
CHEK1	CAMK	100
CK1D	CK1	100
CLK1	CMGC	100
CLK2	CMGC	100
CSK	TK	11.5
DAPK1	CAMK	97.4
Kinases	Family	% Activity Remaining
DAPK2	CAMK	100
DAPK3	CAMK	100
DDR1	TK	1.1
DDR2	TK	9.1
DMPK	AGC	100
EPHA1	TK	7.9
EPHA2	TK	68.9

EPHA3	TK	11.7
EPHA4	TK	2.7
EPHB2	TK	4.4
EPHB3	TK	47.6
EPHB4	TK	4
FGFR2	TK	30.1
FLT1	TK	6.7
FLT2	TK	56.7
FLT3	TK	91.5
FYN	TK	53.7
GSK3a	CMGC	100
HCK	TK	10
IGF1R	TK	94.5
IKK-e	Other	100
INSR	TK	64.2
ITK	TK	100
LIMK1	TKL	63.9
LYN	TK	54.1
MARK1	CAMK	100
MARK2	CAMK	100
MARK3	CAMK	100
MARK4	CAMK	100
MELK	CAMK	95.9
MET	TK	97
MLK1	TKL	100
MLK3	TKL	96.6
MST2	STE	97.6
MUSK	TK	60.6
MYLK	CAMK	100
MYLK2	CAMK	100
MYT1	WEE	100
p38-g	CMGC	100
PAK1	STE	100
PAK1(T423A)	STE	100
PAK1(T423E)	STE	100
Kinases	Family	% Activity Remaining
PDGFRA	TK	79.1
PDGFRB	TK	57.8
PDK1	AGC	100
PHKG1	CAMK	98.2
PIM1	CAMK	97.5
PIM2	CAMK	100
PKAC-a	AGC	97.7

PKAC-b	AGC	100
PKC-d	AGC	92.3
PKC-e	AGC	100
PKC-g	AGC	100
PKC-h	AGC	100
PKC-t	AGC	100
PRKD2	CAMK	97.9
PRKD3	CAMK	100
PKG1	AGC	97.4
PKN3	AGC	67
PLK4	Other	100
PKX	AGC	100
PTK2	TK	100
PTK2B	TK	100
PTK6	TK	27
RET	TK	11.9
RIPK2	TK	51.8
RPS6KA1/RSK1	AGC	100
RPS6KA2/RSK3	AGC	100
RPS6KA3/RSK2	AGC	99.1
RPS6KA4/MSK2	AGC	100
RPS6KA5/MSK1	AGC	100
RPS6KA6/RSK4	AGC	100
SGK2	AGC	96.4
SGK3	AGC	100
SNF1LK	CAMK	10
SNF1LK2	CAMK	47.9
SIK3	CAMK	95
SLK	STE	95.3
SNARK	CAMK	100
SRC	TK	16
STK16	Other	100
STK33	CAMK	100
SYK	TK	100
TBK1	Other	100
Kinases	Family	% Activity Remaining
TEC	TK	28.8
TESK1	TKL	78.3
TESK2	TKL	50.4
TIE1	TK	64.9
TIE2	TK	15.2
TNK2	TK	39.6

TNNI3K	TKL	20.1
TRKB	TK	54.8
TRKC	TK	48.3
TXK	TK	18
VEGFR2	TK	49.3
YANK2	AGC	88.2
YES1	TK	12.7
YSK1	STE	98.6

Compound 4.2

Kinases	Family	% Activity Remaining
ABL1	TK	0.6
ABL2	TK	1.1
AKT1	AGC	100
AKT1-FL	AGC	100
AKT2	AGC	96.3
AKT3	AGC	100
AMPKa1	CAMK	100
AMPKa2	CAMK	89.8
AURKA	Other	100
AURKB	Other	69.2
AURKC	Other	95.6
AXL	TK	83.3
BIKE	Other	92.2
BLK	TK	0.8
BTK	TK	2.1
CAMK1	CAMK	100
CAMK1D	CAMK	100
CAMK1G	CAMK	99.5
CAMK2A	CAMK	93.1
CAMK2B	CAMK	94.4
CAMK2D	CAMK	100
CAMKK1	Other	95.1
CAMKK2	Other	64.5
CHK1	CAMK	100
CK1d	CK1	98.4
CLK1	CMGC	100
CLK2	CMGC	97
CSK	TK	6
DAPK1	CAMK	99.3
DAPK2	CAMK	97.5
DAPK3	CAMK	100
DDR1	TK	0
DDR2	TK	0.3
DMPK	AGC	100
EGFR	TK	68.4
EPHA1	TK	3.4
EPHA2	TK	1.2
EPHA3	TK	7.3
EPHA4	TK	4
EPHB2	TK	2.7
EPHB3	TK	2.8

EPHB4	TK	8.7
FAK	TK	64.3
FGFR2	TK	15.8
FGR	TK	2.7
FLT1	TK	4.1
FLT2	TK	31.4
FLT3	TK	90.3
FYN	TK	1.5
GSK3A	CMGC	100
HCK	TK	3.4
IGF1R	TK	90.9
IKKe	Other	77.3
INSR	TK	63.5
ITK	TK	95.9
LCK	TK	-0.2
LIMK1	TKL	36.1
LOK	STE	45.1
LYN	TK	1.4
MARK1	CAMK	100
MARK2	CAMK	100
MARK3	CAMK	84.1
MARK4	CAMK	78.1
MELK	CAMK	100
MET	TK	90.1
MLK1	TKL	88.5
MLK3	TKL	92
MSK1	AGC	88.8
MSK2	AGC	77.5
MST2	STE	85.2
MUSK	TK	26.6
MYLK	CAMK	89.2
MYLK2	CAMK	97.5
MYT1	Other	100
p38a	CMGC	5.4
p38d	CMGC	100
p38g	CMGC	100
PAK1	STE	83.8
PDGFRA	TK	35.7
PDGFRB	TK	6.9
PDPK1	AGC	100
PHKG1	CAMK	75.4
PIM1	CAMK	84.1
PIM2	CAMK	92.9

PKA	AGC	90
PKAb	AGC	97.6
PKCd	AGC	99.4
PKCe	AGC	68.1
PKCg	AGC	88.4
PKCh	AGC	100
PKCt	AGC	96.9
PKG1	AGC	87.7
PKN3	AGC	21.9
PLK4	Other	100
PRKD2	CAMK	100
PRKD3	CAMK	100
PRKX	AGC	85.6
PTK6	TK	2.4
PYK2	TK	86.3
QSK	CAMK	99.6
RET	TK	1.9
RIPK2	TKL	2.4
RSK1	AGC	88.8
RSK2	AGC	100
RSK3	AGC	100
RSK4	AGC	100
SGK2	AGC	100
SGK3	AGC	100
SLK	STE	80.7
SNARK	CAMK	96.2
SNF1LK	CAMK	0.4
SNF1LK2	CAMK	2.8
SRC	TK	0.4
STK16	Other	100
STK33	CAMK	100
SYK	TK	92.2
TBK1	Other	79
TEC	TK	1.2
TESK1	TKL	45.4
TESK2	TKL	33.5

Compound 4.4

Kinases	Family	% Activity Remaining
ABL1	TK	1.9
ABL2	TK	3.8
AKT1	AGC	98.2
AKT1-FL	AGC	95.4
AKT2	AGC	98.1
AKT3	AGC	99.6
AMPKa1	CAMK	98.8
AMPKa2	CAMK	81.4
AURKA	Other	100
AURKB	Other	90.7
AURKC	Other	97.6
AXL	TK	95
BIKE	Other	94.4
BLK	TK	0.3
BTK	TK	10.8
CAMK1	CAMK	95.8
CAMK1D	CAMK	94.1
CAMK1G	CAMK	87.9
CAMK2A	CAMK	79.3
CAMK2B	CAMK	92.6
CAMK2D	CAMK	100
CAMKK1	Other	88.6
CAMKK2	Other	66.9
CHK1	CAMK	100
CK1d	CK1	100
CLK1	CMGC	100
CLK2	CMGC	93.7
CSK	TK	3.7
DAPK1	CAMK	100
DAPK2	CAMK	95.6
DAPK3	CAMK	100
DDR1	TK	2.8
DDR2	TK	0
DMPK	AGC	98.4
EGFR	TK	72.2
EPHA1	TK	5.6
EPHA2	TK	1.2
EPHA3	TK	2.1
EPHA4	TK	2.6
EPHB2	TK	3.5
EPHB3	TK	15.1

EPHB4	TK	5.6
FAK	TK	66.8
FGFR2	TK	88.1
FGR	TK	6
FLT1	TK	80.7
FLT2	TK	100
FLT3	TK	88.5
FYN	TK	1.1
GSK3A	CMGC	100
HCK	TK	6
IGF1R	TK	89.6
IKKe	Other	100
INSR	TK	77.1
ITK	TK	96.3
LCK	TK	1.2
LIMK1	TKL	41
LOK	STE	-0.6
LYN	TK	3.3
MARK1	CAMK	92
MARK2	CAMK	85.4
MARK3	CAMK	88.6
MARK4	CAMK	94.3
MELK	CAMK	98.4
MET	TK	95.9
MLK1	TKL	56
MLK3	TKL	87.6
MSK1	AGC	84.1
MSK2	AGC	74.6
MST2	STE	94.3
MUSK	TK	89.3
MYLK	CAMK	85.2
MYLK2	CAMK	97.3
MYT1	Other	69.4
p38a	CMGC	6.9
p38d	CMGC	100
p38g	CMGC	100
PAK1	STE	95.5
PDGFRA	TK	42
PDGFRB	TK	17.9
PDPK1	AGC	89.1
PHKG1	CAMK	65.7
PIM1	CAMK	81.7
PIM2	CAMK	91.9

PKA	AGC	87.4
PKAb	AGC	98.6
PKCd	AGC	93.9
PKCe	AGC	66
PKCg	AGC	95.5
PKCh	AGC	85.6
PKCt	AGC	99.5
PKG1	AGC	78.8
PKN3	AGC	100
PLK4	Other	100
PRKD2	CAMK	93.8
PRKD3	CAMK	91.2
PRKX	AGC	80.1
PTK6	TK	25.9
PYK2	TK	76.7
QSK	CAMK	100
RET	TK	5.7
RIPK2	TKL	80.6
RSK1	AGC	70.7
RSK2	AGC	97.4
RSK3	AGC	100
RSK4	AGC	96.1
SGK2	AGC	100
SGK3	AGC	100
SLK	STE	56.5
SNARK	CAMK	86.2
SNF1LK	CAMK	1.4
SNF1LK2	CAMK	4.2
SRC	TK	0.8
STK16	Other	96.7
STK33	CAMK	100
SYK	TK	99.3
TBK1	Other	93
TEC	TK	11.4
TESK1	TKL	98.8
TESK2	TKL	83.9

4.10 References

- (1) Weigelt, B.; Peterse, J. L.; van 't Veer, L. J. *Nat. Rev. Cancer* **2005**, *5* (8), 591.
- (2) Perou, C. M.; Sorlie, T.; Eisen, M. B.; van de Rijn, M.; Jeffrey, S. S.; Rees, C. A.; Pollack, J. R.; Ross, D. T.; Johnsen, H.; Akslen, L. A.; Fluge, O.; Pergamenschikov, A.; Williams, C.; Zhu, S. X.; Lonning, P. E.; Borresen-Dale, A.-L.; Brown, P. O.; Botstein, D. *Nature* **2000**, *406* (6797), 747.
- (3) Sorlie, T.; Tibshirani, R.; Parker, J.; Hastie, T.; Marron, J. S.; Nobel, A.; Deng, S.; Johnsen, H.; Pesich, R.; Geisler, S.; Demeter, J.; Perou, C. M.; Lonning, P. E.; Brown, P. O.; Borresen-Dale, A.-L.; Botstein, D. *Proc. Natl. Acad. Sci. U. S. A.* **2003**, *100* (14), 8418.
- (4) Sørli, T.; Perou, C. M.; Tibshirani, R.; Aas, T.; Geisler, S.; Johnsen, H.; Hastie, T.; Eisen, M. B.; van de Rijn, M.; Jeffrey, S. S.; Thorsen, T.; Quist, H.; Matese, J. C.; Brown, P. O.; Botstein, D.; Lønning, P. E.; Børresen-Dale, A.-L. *Proc. Natl. Acad. Sci.* **2001**, *98* (19), 10869.
- (5) Jemal, A.; Siegel, R.; Xu, J.; Ward, E. *CA. Cancer J. Clin.* **2010**, *60* (5), 277.
- (6) Finnegan, T. J.; Carey, L. A. *Future Oncol.* **2007**, *3* (1), 55.
- (7) Schneider, B. P.; Winer, E. P.; Foulkes, W. D.; Garber, J.; Perou, C. M.; Richardson, A.; Sledge, G. W.; Carey, L. A. *Clin. Cancer Res.* **2008**, *14* (24), 8010.
- (8) Anders, C. K.; Carey, L. A. *Clin. Breast Cancer* **2009**, *9* (Suppl 2), S73.
- (9) Carey, L.; Winer, E.; Viale, G.; Cameron, D.; Gianni, L. *Nat. Rev. Clin. Oncol.* **2010**, *7* (12), 683.
- (10) Foulkes, W. D.; Smith, I. E.; Reis-Filho, J. S. *N. Engl. J. Med.* **2010**, *363* (20), 1938.
- (11) Bayraktar, S.; Gluck, S. *Breast Cancer Res. Treat.* **2013**, *138* (1), 21.
- (12) Aleshin, A.; Finn, R. S. *Neoplasia* **2010**, *12* (8), 599.
- (13) Mayer, E. L.; Krop, I. E. *Clin. Cancer Res.* **2010**, *16* (14), 3526.
- (14) Tryfonopoulos, D.; Walsh, S.; Collins, D. M.; Flanagan, L.; Quinn, C.; Corkery, B.; McDermott, E. W.; Evoy, D.; Pierce, A.; O'Donovan, N.; Crown, J.; Duffy, M. J. *Ann. Oncol.* **2011**, *22* (10), 2234.
- (15) Sánchez-Bailón, M. P.; Calcabrini, A.; Gómez-Domínguez, D.; Morte, B.; Martín-Forero, E.; Gómez-López, G.; Molinari, A.; Wagner, K.-U.; Martín-Pérez, J. *Cell. Signal.* **2012**, *24* (6), 1276.
- (16) Finn, R. S.; Bengala, C.; Ibrahim, N.; Roche, H.; Sparano, J.; Strauss, L. C.; Fairchild, J.; Sy, O.; Goldstein, L. J. *Clin. Cancer Res.* **2011**, *17* (21), 6905.
- (17) Gucalp, A.; Sparano, J. A.; Caravelli, J.; Santamauro, J.; Patil, S.; Abbruzzi, A.; Pellegrino, C.; Bromberg, J.; Dang, C.; Theodoulou, M.; Massague, J.; Norton, L.; Hudis, C.; Traina, T. A. *Clin. Breast Cancer* **2011**, *11* (5), 306.
- (18) Campone, M.; Bondarenko, I.; Brincat, S.; Hotko, Y.; Munster, P. N.; Chmielowska, E.; Fumoleau, P.; Ward, R.; Bardy-Bouxin, N.; Leip, E.; Turnbull, K.; Zacharchuk, C.; Epstein, R. J. *Ann. Oncol.* **2012**, *23* (3), 610.

- (19) Moroco, J. A.; Baumgartner, M. P.; Rust, H. L.; Choi, H. G.; Hur, W.; Gray, N. S.; Camacho, C. J.; Smithgall, T. E. *Chem. Biol. Drug Des.* **2015**, *86* (2), 144.
- (20) Krishnamurty, R.; Brigham, J. L.; Leonard, S. E.; Ranjitkar, P.; Larson, E. T.; Dale, E. J.; Merritt, E. A.; Maly, D. J. *Nat Chem Biol* **2013**, *9* (1), 43.

Chapter 5

Conclusions and Future Outlook

Despite being the first proto-oncogene discovered, c-Src's role in cancer remains poorly understood. The usual implication of kinase involvement in oncogenesis is generally due to mutations leading to over-activity and thus dysregulation of those signal transduction pathways. However, c-Src is unusual in that it is frequently observed to be overexpressed and implicated in cancer, and yet there are very rare cases of overactive c-Src mutation. Somatic mutations of c-Src have been found but, with regards to their role in c-Src dysregulation, if not to cause increase in activity, how might these mutations disrupt c-Src's regulation? This work is explored in Chapter 2, which is a project that is more mechanistic based, and attempts to study the structure-function of c-Src.

Chapter 3 and 4 takes on more of an application approach. Since there are studies throughout literature that implicates c-Src in cancer progression, we aimed to explore methods to make targeting c-Src more efficacious. The approach in Chapter 3 takes a selective c-Src inhibitor, designed in our lab, to look for inhibiting other protein targets which would work in synergy with c-Src inhibition. We found HDAC inhibitors to work in synergy, and with that information, we explored the design process for the first dual acting HDAC/c-Src inhibitor. The goals of Chapter 4 are along the same lines except the approach was to improve the efficacy of dasatinib in triple negative breast cancer. The resulting inhibitor was a DFG-out dasatinib/imatinib hybrid which had unprecedented activity in MDA-MB-231 cell lines. This led us to find the increased in potency over dasatinib was the result of the new inhibitor acting as a dual p38 β /c-Src inhibitor and we describe the process of further improving this new dual acting inhibitor.

The work in Chapter 2 attempts to elucidate the possible role of c-Src mutations. Because c-Src is regulated thru localization, phosphorylation, and conformational states, we were curious whether or not mutations participate in disrupting any of these native regulation mechanism. Because there are previous studies that have found ligand binding to the kinase domain to influence the global conformational state of c-Src, we reasoned that clinical mutations could affect the same changes. Therefore, if clinical mutations were to destabilize the native conformational states of c-Src, it would be affecting its regulation thereby causing dysfunction to c-Src's native function. Whether or not this dysfunction can lead to c-Src's role in oncogenesis remains to be seen but first, to explore this possibility, we had to design an assay that would allow us to detect changes imparted by clinical mutations on the conformational state of c-Src.

The assay designed had to be high-thru put, robust, and consistent. We decided to look at a total of 29 mutations (clinical and non-clinical), of which 16 were clinical mutations and 13 were non-clinical mutations. Non-clinical mutations were of interest as they have been utilized in various structure-function studies of c-Src kinase domain. Other techniques such as NMR, H/D exchange MS, and SAXS could be utilized to investigate conformational changes, however they had disadvantages that we would not be able to overcome. NMR would require high concentrations of protein (100-200 μ M) which would be difficult given poor c-Src yields and 29 mutations that needed to be expressed. SAXS and H/D exchange MS would require special equipment and be more expensive as a result.

We eventually settled on developing a protease assay, visualized by SDS-PAGE. After optimization, we determined that thermolysin would be the best protease to use, as it cleaves between G257 and L258 which is located on the SH2-linker. We later discovered that cleavage at this site was opportune as this was where the SH3 domain binds. The affinity of the SH3 domain to the SH2-linker happens to determine the global conformation of c-Src and surprisingly gives us an actual crude physical assessment of c-Src's conformational state, similar to the information obtained by SAXS and H/D exchange MS but more high-thru put and cheaper to conduct.

Mutations that stabilized a more open conformation would display a faster rate of cleavage as the SH2-linker cleavage site is more accessible and vice versa. The rate was shown in half-life of total c-Src concentration. To validate the thermolysin assay, we tested three c-Src control constructs, pY419, apo-wt-Src, and pY530 (open, apo, and closed respectively). Gratifyingly, the thermolysin assay was able to relate half-life to different conformational states, with a lower half-life corresponding to open conformation and slower half-life to a close conformation. 29 mutations were tested in the thermolysin assay and the results demonstrate that mutations can influence the conformational state of c-Src.

Because thermolysin assay assesses the conformation based on SH3 domain affinity, we were curious as to the availability of the SH2-domains in these conformations and whether or not this could be correlated with an open/closed conformation. We utilized a fluorescence polarization assay to look at the SH2-domain. A c-Src SH2 optimal peptide was synthesized and a FITC fluorophore was appended to be used as our reporter molecule to assess K_d values. A higher affinity for the FITC-SH2 peptide should indicate better accessibility of the SH2-domain, correlating to an open conformation, whereas a decrease in affinity signified poor accessibility, indicating a closed conformation.

We decided to look at a select few open/apo/closed mutations. Surprisingly, it appears that outside of some exceptions, the K_d of the FITC-SH2 peptide are arguably all the same regardless of the half-lives/conformational state. These results lead us to conclude that the FP assay using the FITC-SH2 peptide cannot be used to identify conformational states. A plausible explanation is that the global conformation of c-Src isn't affecting SH2 domain accessibility. The SH2 domain is in a configuration that allows the pocket to be accessed, regardless of the conformation.

To further characterize these mutations, we decided to explore the catalytic activity and binding affinities to ATP and substrate peptide. According to the activity assay data collected from all active mutations, there does not appear to be any that are over-active as none surpassed the activity of pY419 wt-Src. Also, there

was unfortunately no correlation between conformational states and activity. Since pY419 is an open state and fully active and pY530 is closed but inactive it was hypothesized conformations were correlated to the catalytic activity of c-Src. Therefore, mutations that stabilized an open conformation was thought to be more active compared to mutations stabilizing a closed conformation. We reasoned that this could be due to the individual mutations effecting catalytic activity more than the conformational state.

Next, we explored, specifically, how these conformational states affected c-Src function. What exactly do changes in conformational states disrupt? The most intriguing question is whether or not conformational states could affect phosphorylation states. We took an open conformation D120N-Y530F, apo Y530F, and a closed T341R-Y530F and looked at autophosphorylation rates at Y419. Gratifyingly, T341R-Y530F autophosphorylation is slower than Y530F and D120N-Y530F.

Whether or not the faster phosphorylation rates are due to open conformations or activation loop conformations dictated by the mutation stabilized conformational state is an experiment we would like to look further into in the future. It is possible that depending on the conformational changes, the activation loop might be in conformations that does not make Y419 available for phosphorylation similar to c-Abl's activation loop tyrosine phosphorylation studies done by Lamontanara et. al. We would propose expressing a kinase dead mutation along with an open and closed mutation such as K298R-R163W-Y530F and K298R-T341R-Y530F and using kinase domain c-Src to investigate activation loop phosphorylation accessibility. It would also be of interest to do this with inhibitors as well. These additional experiments could enable us to study activation loop dynamics and to take a look at whether or not c-Src's activation loop acts similarly to c-Abl.

Taken together, it appears there is a strong case that these clinical mutations can disrupt c-Src regulation by influencing the native conformational c-Src state and changing the rate of autophosphorylation at Y419. The next steps would be to assess whether or not these effects can lead to cancer progression. CRISPR would be

needed to introduce these mutations into healthy cell lines such as NIH 3T3 cells to see if over time, these mutations are transformative. Overall phosphorylation states should be measured as well cell viability, which would be clues as to these mutant c-Src's involvement in oncogenesis.

Chapter 3 describes the design and reasoning behind the development of the first dual HDAC/c-Src inhibitor. Panobinostat, an HDAC inhibitor was found to have synergy with the selective inhibition of c-Src. We decided to combine a pyrazolo-pyrimidine scaffold, **3.1**, which would serve as the c-Src pharmacophore, and a previously published HDAC inhibitor, **3.10** which could be used in its entirety as the HDAC pharmacophore on the same molecule to create a dual c-Src/HDAC inhibitor. After SAR optimization, compound **3.4** was found to be the most potent against HDAC1 and c-Src. We ascertained that both pharmacophores needed to be on the same scaffold for the dual inhibition to be efficacious, which we attributed to decrease in toxicity and that synergistic effects of inhibiting both HDAC and c-Src were maintained. Interestingly, the chimeric inhibitor **3.4** was more potent against HDAC1 than c-Src which lead us to believe that most cellular activity seen could be due to potent HDAC1 inhibition. In an attempt to improve upon this dual inhibitor, dasatinib versions of the HDAC/c-Src inhibitor were synthesized, **3.11** and **3.12**. This would allow us to greatly increase inhibition to c-Src as well as maintain HDAC potency, which both **3.11** and **3.12** has demonstrated. This will need to be tested *in cellulo* to see if synergy is retained and whether or not the increase inhibition of c-Src could help increase overall efficacy. Similar to the pyrazolopyrimidine version of the dual HDAC/c-Src inhibitor, the das-HDAC should be assessed to evaluate whether or not there is any benefits to having a dual acting inhibitor on the same scaffold.

Chapter 4 takes on a similar story as Chapter 3, but instead of a rationally designed dual HDAC/c-Src inhibitor, we serendipitously found a dual p38 β /c-Src inhibitor, **4.1** in an attempt to improve dasatinib c-Src inhibition in triple negative breast cancer. In an interest to improve the pharmacokinetics of this dual p38 β /c-Src inhibitor, we decided to rationally design a dasatinib/BIRB-796 (Das-BIRB) hybrid molecule, **4.4**. Due to the BIRB-796 piece, inhibition against p38 should be

maintained if not improved while hopefully decreasing binding to cytochrome P450 in an attempt to bolster metabolic stability.

This strategy worked and metabolic stability was increased, as found in mouse liver microsome LC/MS/MS assay (**4.4** half-life = 42min from **4.1** half-life = 3min), which prompted us to send **4.4** to Luceome to assess kinase selectivity against 137 kinases to compare against the original p38 β /c-Src inhibitor, **4.1** as well as **4.2**. Selectivity was relatively similar. Luceome, however, did not carry p38 β which will need to be tested later at DiscoverX, but due to the **4.4** being able to inhibit p38 α , one would assume that p38 β is also inhibited. Unfortunately, the Das-BIRB inhibitor is poor against MDA-MB-231 cell lines (546 nM) compared to the original **4.1** (6 nM) so despite the improved metabolic stability, the decrease in *in cellulo* potency was not acceptable. This result might throw into doubt whether or not p38 β and c-Src dual inhibition is responsible for the parent p38 β /c-Src inhibitor's success, compared to dasatinib, against MDA-MB-231 cell, and if it is actually another unknown kinase or non-kinase target that is needed for efficacy. A full kinome scan against all 518 kinases is warranted to further explore all possible kinase targets as the previous kinome scan was only a panel of 137 kinases.

Appendix A

A.1 Introduction: Developing a Truly Selective c-Src Inhibitor

Most kinase drug discovery efforts are involved in targeting the ATP pocket of the catalytic domain and in fact, greater than 99% of all previously reported kinase inhibitors are ATP-competitive.^{1,2} The ATP binding site, specifically the pocket where adenine resides (A-pocket) with its well defined recessed hydrophobic cavity, is an attractive target site that has yielded potent inhibition which has been translated into therapeutic drugs for cancer. However, despite these successes, difficulties exist with this approach. First, the highly conserved nature of the A-pocket throughout not only kinases but other enzymes that require ATP is a problem.³ The ATP-competitive inhibitors are designed to mainly mimic the adenine portion of ATP which has been described as a highly recognized template as nearly similar binding contacts are retained, such as the H-bonding between the kinase ‘hinge’ and the adenine ring which greatly reduces selectivity.^{2,4} This can decrease the therapeutic value of the drug, due to undesired side effects caused from off-target binding, as well as limiting its usefulness as a biological probe in studying signal transduction pathways.^{3,5,6} Second, ATP-competitive inhibitors have to compete with ATP, which has a low micromolar binding affinity to kinases and present oftentimes in saturating concentrations as high as 10 mM in cancer cells.⁷ Therefore, to achieve potent binding in the ATP pocket *in cellulo* requires high affinity inhibitors with low nanomolar to picomolar range.^{3,8}

To address these limitations, different strategies have evolved in an effort to improve upon selectivity while retaining potency.⁶ An approach we have taken is to design an inhibitor, wherein a portion of the compound still resides within the A-pocket as an anchor that binding while the other portion is devised to increase selectivity by sampling interactions that are immediately outside of the adenine

binding domain. As our laboratory is interested in studying the signal transduction pathways affected by the PTK c-Src, an exclusive biological probe is crucial and could hopefully be obtained from this approach. Discovered in 1978, c-Src, was the first identified PTK which was later implicated as a proto-oncogene. c-Src is believed to associate with a number of receptor tyrosine kinases (RTK) such as EGFR and PDGF, which serves in part as their regulator and also as a cotransducer of their originating signals.⁹ This activation of c-Src results in the phosphorylation of downstream targets such as focal adhesion kinase (FAK), Ras, Stat3, and phosphoinositide 3-kinase (PI3K) which play an integral role in cell proliferation, division, and survival, as well as cell motility and adhesion as shown in Figure 1.^{9,10} As such, the dysregulation of c-Src has been implicated in cancers including breast, colon, pancreatic, and lung cancer and consequently, multiple studies conducted have validated c-Src as a target for the treatment of such cancers.⁹ Our goal is to design selective inhibitors of c-Src that can be used as biological probes.

As an initial gauge for c-Src inhibitor selectivity, c-Abl, also a PTK, was selected based upon high sequence similarity (68%) and nearly identical ATP-binding pockets. Selectivity between c-Src and c-Abl has been difficult to achieve and at present, there are no reported clinical or preclinical inhibitors of c-Src that do not also inhibit c-Abl.¹¹ Furthermore, recent studies suggest that c-Abl activity corresponds to tumor suppression in solid cancers and accordingly, it is desirable to avoid the inhibition of c-Abl while targeting c-Src.¹²

Our lab recently developed compound **A1** for the inhibition of c-Src using a strategy that involves not only targeting the A-pocket but also the adjacent P-loop pocket.¹³ **1** shown in Figure 1 was found to have a selective inhibition for c-Src ($K_i = 64$ nM) over c-Abl ($> 125,000$ nM). **A1** was also subjected to an in vitro ATP-site competition binding assay (KINOMEScan) against 200 kinases at a concentration of 10 μ M.¹⁴ The results, shown in Figure A2 demonstrate impressive selectivity and stands in stark contrast alongside **PP2**, which was previously classified in the literature as a highly selective c-Src inhibitor.¹⁵

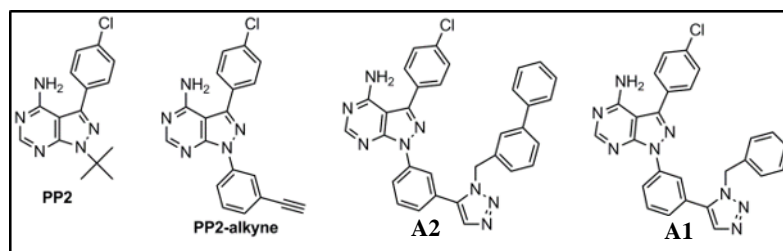


Figure A1: PP2, PP2-alkyne, A2, and A1.

The remarkable selectivity of compound **A1** is believed to be due to the compound interaction within the P-loop. Unfortunately, **A1** still targets c-Raf, and B-Raf which remains the last remaining hurdle to an otherwise perfectly selective inhibitor in this panel. In developing **A1** as a biological probe exclusively for c-Src, it will be necessary to exclude the residual binding from c-Raf and B-Raf. As such, we will explore the following: 1.) Validating a possible key interaction located within the P-loop pocket that is shown in a docking model of **A1** in c-Src for a possible approach in improving selective inhibition. 2.) SAR studies probing the P-loop pocket using analogs of **A1** and its benzyl analog **A2** (shown in Figure 1). 3.) Utilizing a recently developed BRAF binding assay to assess improved analogs.

A.2 Probing the Validity of the Docking Model of Compound A1

Developing an inhibitor that binds to two different sites within the ATP pocket, A-pocket and the adjacent P-loop pocket, also known as the glycine-rich loop, could retain potency while improving upon selectivity. Usually occupied by

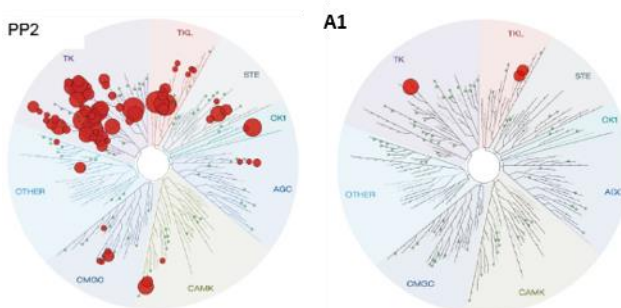


Figure A2: KINOMEScan of **PP2** and **A1**. The red circles represent the kinase inhibited and the larger the radius of the circle correlates with increasing potency. (Taken from Brandvold et. al)¹

the phosphate groups of ATP, the P-loop has been underutilized in regards to inhibition and to our knowledge, there have been no attempts to build into this region to improve selectivity. Recent reports, have cited the impact that the P-loop has on ligand-protein interactions and it has been shown that mutations in the P-loop are responsible for imatinib resistance to c-Abl.¹⁶ Studies resulting from this observation have also suggested that the conformational variability of the P-loop across PTKs might be a promising alternative in exploring specific binding.^{16,17} From our initial modeling analysis, c-Src appears to exhibit a wider P-loop opening compared to c-Abl (shown in Figure A3) and therefore this slight difference in conformation could be exploited to achieve selectivity. If the strategy proves successful for c-Src, it could also be applied in other PTK inhibitor blueprint as well.

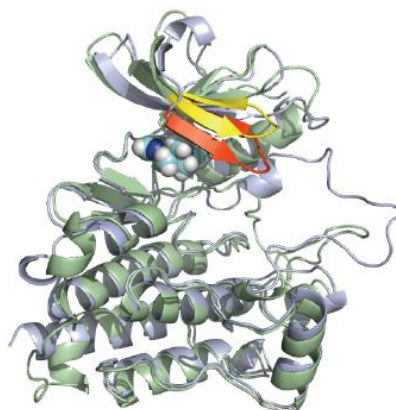


Figure A3: c-Src is colored light green with P-loop of c-Src highlighted yellow. c-Abl is colored light blue with P-loop of c-Abl highlighted red. (Taken from Brandvold et.al)¹

The docking model in Figure A4 is of **A1** in an optimized conformation within the binding site of c-Src. The **PP2-alkyne** portion of the inhibitor occupies the A-pocket as predicted. The phenyl group is situated right at the juncture between the A-pocket and the P-loop pocket and is where the ribose of ATP usually resides. Within the P-loop itself sits the triazole and biphenyl ring, which is currently orientated to maximize van der Waals contacts within the pocket. Upon further inspection, the short methylene linker between the triazole and biphenyl ring serves as the first logical option from which to probe the validity of the docking model

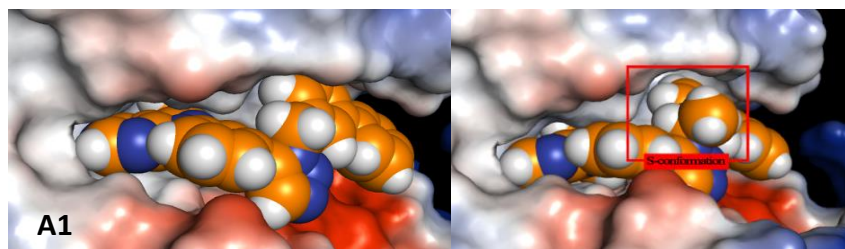
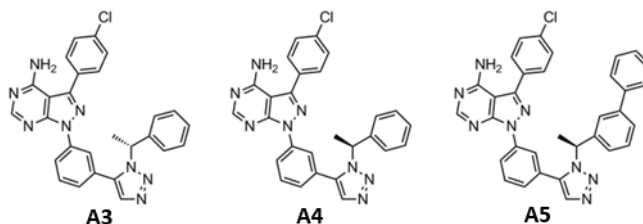


Figure A4: Left is compound **A1** docking model in c-Src. Right is docking model of compound **A1** showing the *S* conformation. Note in the picture on the right, compound is not in optimized conformation.

while possibly improving upon selectivity. By introducing a chiral center upon insertion of a methyl group directly on the linker (Figure A5), we can assess, through biochemical assay, whether the triazole and biphenyl groups are positioned correctly in the docking model. According to the model in Figure A4, the **A3** would be weakly binding/not bind due to unfavorable steric clash with the P-loop pocket whereas the **A4** would bind more favorably.



Cpd #	c-Src Ki (nM)
A1	64
A2	139
A3	1733
A4	409
A5	373

Figure A5: Biochemical assay and chemical structure of compounds **A1-A5** in c-Src

A.3 SAR of Compound **A1** and **A2**

SAR will be performed around the second biphenyl ring of compound **A1** and benzyl ring of **A2**. These analogs can be biochemically assayed as a method to probe the P-loop pocket for favorable interactions while further optimizing potency and selectivity of the initial compounds. Electron withdrawing groups (F, CF₃) and

electron donating group (Me, O-Me) were added around the phenyl rings as a first round assessment and from there improved in a second round assessment if need be. Also, if the compound (in Figure A5) proves potent, SAR results from Figure A7 and A8 can be pooled together to create a derivative using the best combination of substituents.

A.4 Results and Discussion

In order to assess whether or not the previous SAR analogs of compound **A1** and **A2** eliminate BRAF and c-RAF binding, TR-FRET Eu binding assay for BRAF will be employed to assess the best inhibitors of c-Src and determine whether or not they bind to BRAF.¹⁸ BRAF will be GST-tagged, whereupon Eu labeled anti-GST labeled and an Alexa Fluor 647 labeled substrate will serve as the two FRET pairs. When the substrate is bound to BRAF, this brings the substrate linked fluorophore in relatively close proximity to the Eu labeled anti-GST thereby inducing FRET and increase of fluorescence is observed. Upon inhibitor binding, FRET can no longer occur and a decrease in fluorescence is monitored and a binding curve can be plotted.

Cpd #	BRAF IC50 (uM)
A1	0.55
A4	4.6
A5	0.33
A18	10

Figure A6: BRAF binding assay of compounds **1**, **A4**, **A5**, and **A18** (3-OMe)

To validate the possible key interactions shown in a docking model of **A1** both **A3** and **A4** were prepared from the **PP2-alkyne** scaffold via ruthenium catalyzed click chemistry. The results of the assay are shown in Table A6. We were encouraged to see that the biochemical data agreed with our docking model as **A3** has high K_i of 1733 nM vs. the **A4** with $K_i = 409$ nM. When **A4** is compared to **A2** ($K_i = 139$ nM), the potency is slightly worse. In the hopes of improving potency, a phenyl substituent was added **A5**, which is a similar modification previously done to further optimize the binding of **A2** into **A1**. Compared to its benzyl predecessor **A4**, the K_i of the biphenyl **A5** is slightly improved, however, when contrasted against

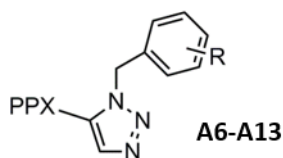
A1 ($K_i = 64$ nM) the addition of the phenyl ring doesn't seem to impart additional favorable interactions.

However, the 4-fold difference in potency between the two benzyl isomers **A3** and **A5**, which should in theory translate to the biphenyl **A5** as well, could be exploited for selectivity against other kinases, especially BRAF, one of the remaining kinases we want to rid of inhibition. As such, we employ a recently developed BRAF binding assay and the initial results are shown in Table A6.¹⁸ An IC_{50} of 4.6 μ M was obtained for **A4** compared to $IC_{50} = 0.55$ μ M of **1**, which is an 8-fold decrease in inhibition. Unfortunately, **A5** ($IC_{50} = 0.33$ μ M) displays similar IC_{50} to **1** which is not beneficial in our case. However, this might suggest that the extra phenyl ring in **A1** compared to the benzyl **A2** not only augmented binding to c-Src but either introduced/improved BRAF inhibition as well. This suggest, the methyl isomer might therefore not be the reason of selectivity of **A4** between c-Src and BRAF. This could also partly explain why the further optimization of the scaffold **PP2**, which only moderately inhibit BRAF, towards specific binding of only c-Src abolished nearly all other kinase inhibition, but surprisingly introduced BRAF inhibition.

SAR around the benzyl ring of compound **A2** was generated (shown in Table A7) from a collection of benzyl azides previously synthesized. These substituted azides were appended to **PP2-alkyne** through ruthenium mediated click chemistry. From the collection of compounds synthesized (**A6-A13**) only **A6** (4-F, $K_i = 143$ nM) showed 2-fold improvement over the parent compound **A2**. To evaluate if additional potency could be conferred by the addition of the phenyl substituent, **A28** (4-F, Ph) was synthesized and unfortunately, no appreciable increase in binding was observed.

The biphenyl ring in **A1** was also subjected to a round of SAR using substituted biphenyl azides made through Suzuki coupling (Table A8). In general, any group in the ortho position or possessing the electronegative CF_3 group was not as favorable for c-Src inhibition as parent compound **A1**. It was revealed that **A16** (4-Me) and **A20** (3-Me) only had slightly decreased binding affinity compared to

the parent biphenyl compound **A1**. We hypothesized that since these functionalities are being extended

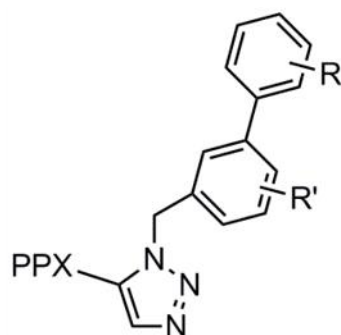


Cpd #	R	c-Src K_i (nM)
A1	N/A	64
A2	N/A	139
A6	4-F	143
A7	3-Me	337.5
A8	3-OMe	257.5
A9	2-Me	277
A10	2-F, 3-CF ₃	340
A11	4-F, 3-CF ₃	363
A12	3-COOMe	545
A13	4-OMe	High

Figure A7: Biochemical assay of compounds **A6-A13** in c-Src

towards a broader opening of the P-loop pocket, a slightly larger hydrophobic group such as an isopropyl may be more advantageous for binding due to increased surface area contact. Unfortunately, these new modifications do not bind as well and have a K_i in the low single digit μ M range (Table A8).

It was promising to see that one compound, **A18** (3-OMe) has comparable K_i to the parent biphenyl **A1**. The introduction of any substituents leading to new interactions within the P-loop pocket, that could either improve or retain similar binding affinities to the parent biphenyl **A1**, could concede additional selectivity for c-Src and hopefully decrease its viability for BRAF. **A18** (3-OMe), along with **A16** (4-Me) and **A20** (3-Me) were analyzed in an initial BRAF binding assay whereupon only **A18** (3-OMe) exhibited decreased BRAF potency with an $IC_{50} = 10 \mu$ M compared to the parent biphenyl **A1**, $IC_{50} = 0.55 \mu$ M. This infers that the extra 3-OMe, does interfere with BRAF binding thereby **A18** (3-OMe) could be a suitable alternative to **A1**. A profiling of **A18** will be performed in the near future.



Cmpd #	R	c-Src Ki (nM)
A13	4F	222
A14	4-OMe	503
A15	4-CF3	3087
A16	4-Me	123
A17	3-F	876
A18	3-OMe	162
A19	3-CF3	1743
A20	3-Me	151
A21	2-Me	425
A22	2-F	284
A23	2-OMe	705
A24	2-CF3	High
A25	3-iPr	1102
A26	4-iPr	2526
A27	4-OiPr	High

Figure A8: Biochemical assay of compounds **13-28** in c-Src and parent biphenyl compound **1**.

A.5 Introduction: Gatekeeper c-Src Inhibitors and DFG-out Conformation

Our next project goal focuses on c-Src itself, namely exploring an important structural conformation termed the DFG-flip. The DFG refers to the aspartic acid, phenylalanine, and glycine residues on the activation loop. DFG-out/in (Figure A10A) refers to the position of the phenylalanine, which moves almost 10 Å and rotates nearly 180° to reside either in the hydrophobic pocket (an active DFG-in,

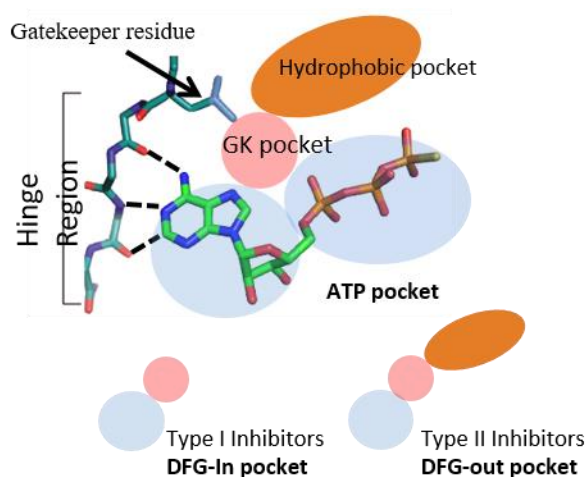


Figure A9: A simplified cartoon with ATP bound depicting the most common binding pockets of Type I and Type II inhibitors.

FigureA9) or a solvent exposed region adjacent to the ATP pocket in a flipped out (an inactive DFG-out) conformation.¹⁹ This structural feature has been widely studied in a variety of kinases and has only recently become a popular topic to pursue due to the accidental discovery of the DFG-out conformation discovered between imatinib (Gleevec) binding to c-Abl kinase.²⁰

Due to its dynamic and highly flexible nature of the DFG, it has been difficult to examine its kinetics. Therefore, it is unknown if the DFG-out is stable enough to exist in sufficient numbers without any ligands. As such, this conformation can be compound dependent; as how or where the compounds bind can stabilize or force the kinase into either the DFG-in (Type I binding) or DFG-out conformation (Type II binding). Unfortunately, efforts to design small molecules to explore SAR of the binding pocket of the DFG-out conformation are troublesome and tedious. As a result, there aren't many known Type II inhibitors for c-Src as just a small change in SAR can cause small shifts in the conformation of the pocket of interest leading to a completely different binding mode than its parent compound. It is even possible the compound will no longer bind to the DFG-out, but such conclusions cannot be drawn without a crystal structure.

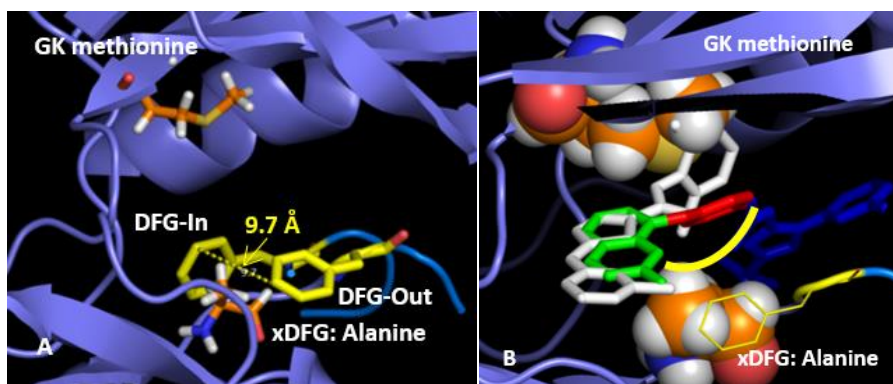


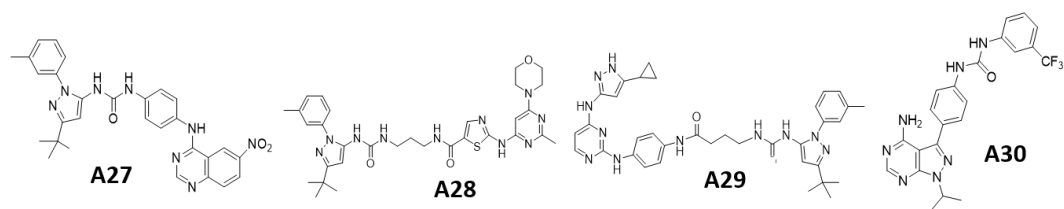
Figure A10: **A:** Crystal structure of T341M c-Src, DFG-out (PDB: 3F3W) aligned with wt-Src DFG-in (PDB: 3G5D) demonstrating the DFG-flip, shown in yellow. The orange residues show the GK methionine and the xDFG residue, alanine. **B:** Same crystal structure as above instead Compound A27 (T341M) and Dasatinib (wt-Src) are shown. Compound A27 is split into three different colors signifying the binding pockets. Green = ATP pocket, red = GK pocket, blue = hydrophobic pocket. Dasatinib is shown in white and visualizes how a bulky GK can prevent access into the hydrophobic pocket and GK pocket. The yellow curved line demonstrates one design strategy to evade the GK by avoiding binding directly through the GK pocket (as shown by the phenyl ring of Dasatinib and red portion of compound A27) which all current Type II binding follows.

Less than 10% of kinases have been found to adopt the DFG-out conformation.²¹ Whether this is due to the lack of an appropriate ligand that can favorably force the DFG-out remains to be seen, however, it has been observed that certain amino acid residues can disfavor this conformation. DFG-out inducing ligands, Type II inhibitors, can be physically blocked from binding by a bulky gatekeeper (GK) residue, which allows access to a back hydrophobic pocket, which is the characteristic cavity to which all type II inhibitors bind. Another possible residue is the one preceding the DFG moiety. This particular residue is also located at the juncture right before the hydrophobic pocket (Figure A10B). It may not have an effect in Type II binding alone but in conjunction with a bulky GK we hypothesized it could prevent the DFG-out conformation altogether. We observed this situation in some MAP kinases, as they are unable to adopt the DFG-out conformation. These MAP kinases consist of a bulky methionine GK and a serine residue at the xDFG position, compared to c-Src (GK = threonine and xDFG = alanine) which can assume the DFG-out conformation.

A.6 Results and Discussion

Therefore, to investigate if these two residues can prevent kinases from adopting a DFG-out we questioned if it was possible to turn a known kinase that can adopt DFG-out into a kinase that cannot adopt DFG-out through the mutation of those two residues simultaneously. We believe this can yield some insight into how certain residues can affect the DFG-out inactive conformation and also how these residues contribute to ligand binding. Depending on results obtained, this mutation can be incorporated onto other kinases and used as a simple test to identify between Type I (binding only in ATP pocket) vs. Type II compounds. Presently, the only method to conclusively categorize compound binding is to obtain a crystal structure.

A double point mutation was applied to c-Src, T341M (GK) and A406S (xDFG) and was evaluated against known Type II inhibitors. As controls, T341M c-Src and A406S c-Src was also tested to eliminate these single point mutations as the reason for decreased inhibitor binding. Known Type I inhibitors were also included as these compounds should bind c-Src regardless of its conformation. The results of the study are summarized in Figure A11 (red indicates the commercially available compounds). Unfortunately, there were no known commercially available inhibitors of T341M for c-Src. We also found that even a literature conceived compound (resynthesized here) purported to inhibit T341M was actually a weaker than expected binder of T341M c-Src (Compound **A27**). Therefore, it was not possible to validate T341M, A406S model accurately as we concluded that a Type II inhibitor that binds T341M, A406S, and wild type (wt) c-Src equipotent was ideal. It was reasoned that difficulties in obtaining such a compound would lie in the inhibition of T341M c-Src, as the extremely bulky GK itself can sterically exclude any Type II binding. Based upon several devised strategies to evade the GK, 31 compounds were synthesized. The results of the lead compounds are shown in Figure A11. Eventually, it was found that literature compound **A30**, which was never tested against T341M, afforded equipotent binding to T341M ($K_i = 19$ nM), A406S ($K_i = 17$ nM), and wt-Src ($K_i = 28$ nM), and demonstrated a 6-fold shift in potency for the T341M-A406S mutant ($K_i = 114$ nM). While these results suggested that using the



Compound, Ki (nM)	wt-Src	T341M	A406S	T341M-A406S	Confirmed Binding mode
Dasatinib	< 0.02	1936	-	4572	DFG-in
Ponatinib	11	414	18	1682	DFG-out
DCC-2036	50	221		773	DFG-out
Tozasertib	500	539		434	DFG-in
DSA7	4.1	439.5			DFG-out
GP19	0.1	46		6341	
A27	133	505			DFG-out, from literature
A28	1	308			
A29	201	194	-	190	
A30	28	19	17	114	DFG-out, from literature

Figure A11: Lead compounds of the 37 compounds tested are shown. Compounds marked in red are commercially available. Compounds in blue were provided by Prof. Dustin Maly, and compounds in black were synthesized. Out of the synthesized compounds **A28** was the most potent against wt-Src.

T341M-A406S mutant could aid in the identification of Type II inhibitors, these two residues, at least in c-Src, were not able to prevent a DFG-out conformation.

During the course of this study, several other compounds demonstrated interesting results, most notably compound **A29**. Devised to evade the GK by building around the GK pocket (a strategy in which there is no literature precedent, shown in Figure A10B by the yellow line), **A29** demonstrated equipotent binding to wt-Src, T341M, A406S, as well as T341M-A406S. Based on the data collected, even if the Type II inhibitors bound potently to wt-Src but less potently to T341M, there was still an observable decreased shift in binding affinity against T341M-A406S. These findings thereby might implicate **A29** as a Type I binder despite its structural similarities to all Type II inhibitors (a urea moiety is usually indicative of Type II binding). Further SAR of **A29** was explored in an effort to tease out the binding mode. Unfortunately, none of the data were conclusive about the mode of binding. Inevitably, a crystal structure would have to be obtained to assess the binding mode of **A29** and whether or not its GK evading strategy would be useful for future design of other GK evading Type II binders.

In this regard, current efforts are underway in developing NMR as an alternative approach in identifying DFG-out binders. There are only a few literature precedents in using NMR to identify Type I vs. Type II.²² However, the system developed appears tedious, a possible reason as to why it is not widely adopted, involving the expression of more than several different forms of ¹⁵N labeled kinase of interest. These strategies involve the ¹⁵N labeling of backbone amides of the kinase, as well as the selective individual ¹⁵N labeling of certain amino acids in order to identify each amino acid signal through 2D TROSY, as well as comparing to known crystal structures to ascertain which signal belonged to the phenylalanine of the DFG. Therefore, monitoring the absence (DFG-in) or presence (DFG-out) of the phenylalanine signal would allow the identification of Type I vs. Type II binders.²² Instead, we propose to directly monitor the DFG flip by mutating the phenylalanine to a tryptophan (F408W) (which shares similar properties, and therefore shouldn't affect the kinetics of the DFG flip) and use it as a reporter in NMR studies.

A F408W c-Src mutant has already been expressed and determined to be fully active. The single mutation on the DFG allows the ability to directly monitor the kinetics of the DFG flip by being able to selectively replace any tryptophan residues, including the tryptophan of the DWG with a ¹⁵N indole or cheaper fluoro-indole reporter. There is literature precedent for the relatively easy incorporation of ¹⁵N indole or fluoro-indoles into both wt-Src and F408W Src, as the protein expression system can easily replace any tryptophans with any indole of choice.²³ There are only 8 tryptophans in wt-Src and therefore comparing labeled wt-Src with labeled F408W should allow the ease of distinguishing the tryptophan signal of the DWG. The absence or presence of the ¹⁵N or fluorine signal of the DWG should enable the determination of Type I vs. Type II compounds using the library of compounds that have already been synthesized. With the success of this developed method, we envision the general application towards other kinases in determining the mode of compound inhibition as well as further developing these NMR techniques in studying the dynamics of the DFG flip.

A.7: References

- (1) Garber, K. *Nat Biotech* **2006**, 24 (2), 127.
- (2) Zhang, J.; Yang, P. L.; Gray, N. S. *Nat Rev Cancer* **2009**, 9 (1), 28.
- (3) Scapin, G. *Drug Discov. Today* **2002**, 7 (11), 601.
- (4) Lawrence, D. S.; Niu, J. *Pharmacol. Ther.* **1998**, 77 (2), 81.
- (5) Morphy, R. *J. Med. Chem.* **2010**, 53 (4), 1413.
- (6) Knight, Z. A.; Shokat, K. M. *Chem. Biol.* **2005**, 12 (6), 621.
- (7) Cohen, P. *Nat. Rev. Drug Discov.* **2002**, 4, 309.
- (8) Lawrence, D. S.; Niu, J. *Pharmacol. Ther.* **1998**, 77 (2), 81.
- (9) Biscardi, J. S.; Tice, D. A.; Parsons, S. J. In *Advances in Cancer Research*; 1999; Vol. 76, pp 61–119.
- (10) Roskoski Jr., R. *Biochem. Biophys. Res. Commun.* **2005**, 331 (1), 1.
- (11) Metz, J. T.; Johnson, E. F.; Soni, N. B.; Merta, P. J.; Kifle, L.; Hajduk, P. J. *Nat. Chem. Biol.* **2011**, 7 (4), 200.
- (12) Allington, T. M.; Galliher-Beckley, A. J.; Schiemann, W. P. *FASEB J.* **2009**, 23 (12), 4231.
- (13) Brandvold, R.; Ste, M. E.; Fox, C. C.; Soellner, M. B. *ACS Chem. Biol.* **2012**, 7, 1393.
- (14) Fabian, M. A.; Biggs, W. H.; Treiber, D. K.; Atteridge, C. E.; Azimioara, M. D.; Benedetti, M. G.; Carter, T. A.; Ciceri, P.; Edeen, P. T.; Floyd, M.; Ford, J. M.; Galvin, M.; Gerlach, J. L.; Grotzfeld, R. M.; Herrgard, S.; Insko, D. E.; Insko, M. A.; Lai, A. G.; Lelias, J.-M.; Mehta, S. A.; Milanov, Z. V.; Velasco, A. M.; Wodicka, L. M.; Patel, H. K.; Zarrinkar, P. P.; Lockhart, D. J. *Nat Biotech* **2005**, 23 (3), 329.
- (15) Hanke, J. H.; Gardner, J. P.; Dow, R. L.; Changelian, P. S.; Brissette, W. H.; Weringer, E. J.; Pollok, B. A.; Connelly, P. A. *J. Biol. Chem.* **1996**, 271 (2), 695.
- (16) Patel, R. Y.; Doerksen, R. J. *J. Proteome Res.* **2010**, 9 (9), 4433.
- (17) Guimaraes, C. R. W.; Rai, B. K.; Munchhof, M. J.; Liu, S.; Wang, J.; Bhattacharya, S. K.; Buckbinder, L. *Journal of chemical information and modeling*. United States June 2011, pp 1199–1204.
- (18) Lebakken, C. S.; Riddle, S. M.; Singh, U.; Frazee, W. J.; Eliason, H. C.; Gao, Y.; Reichling, L. J.; Marks, B. D.; Vogel, K. W. *J. Biomol. Screen.* **2009**, 14 (8), 924.
- (19) Seeliger, M. A.; Nagar, B.; Frank, F.; Cao, X.; Henderson, M. N.; Kuriyan, J. *Structure* **2007**, 15 (3), 299.
- (20) Schindler, T.; Bornmann, W.; Pellicena, P.; Miller, W. T.; Clarkson, B.; Kuriyan, J. *Sci.* **2000**, 289 (5486), 1938.
- (21) Zuccotto, F.; Ardini, E.; Casale, E.; Angiolini, M. *J. Med. Chem.* **2010**, 53 (7), 2681.
- (22) Langer, T.; Vogtherr, M.; Elshorst, B.; Betz, M.; Schieberr, U.; Saxena, K.; Schwalbe, H. *ChemBioChem* **2004**, 5 (11), 1508.
- (23) Crowley, P. B.; Kyne, C.; Monteith, W. B. *Chem. Commun. (Camb)*. **2012**, 48 (86), 10681.